Vol. 119 nos. 1-6

March-April 1958

PROCEEDINGS OF THE ACADEMY OF SCIENCES

OF THE USSR

(DOKLADY AKADEMII NAUK SSSR)

Physical Chemistry Section

A publication of the Academy of Sciences of the USSR

IN ENGLISH TRANSLATION

Year and issue of first translation:
vol. 112, nos. 1-6   Jan.-Feb. 1957

Annual subscription	*$160.00*
Single issue	*35.00*

CONSULTANTS BUREAU INC.
227 W. 17th ST., NEW YORK 11, N. Y.

Printed in the United States

PROCEEDINGS OF THE ACADEMY OF SCIENCES OF THE USSR

Physical Chemistry Section

Volume 119, Numbers 1-6 March-April 1958

CONTENTS

CONTENTS (continued)

CONTENTS (continued)

KINETICS OF THE POLYMERIZATION OF ISOBUTYLENE IN THE PRESENCE OF THE ADDITION COMPOUND OF BORON TRIFLUORIDE WITH ETHER

M. I. Vinnik, G. B. Manelis, G. V. Epple, and N. M. Chirkov

(Presented by Academician V. N. Kondrat'ev, August 7, 1957)

This paper is concerned with an investigation of the kinetics of the polymerization of isobutylene in the presence of the diethyl ether-boron trifluoride complex — $(C_2H_5)_2O \cdot BF_3$. To avoid diffusion difficulties, the experiments were carried out with the $(C_2H_5)_2O \cdot BF_3$ catalyst in the form of a thin adsorbed film on the surface of small fused quartz tubes.

Before experiments, the reactor, with its packing of quartz tubes (free volume 0.34 liter; surface of packing ~ 0.5 m^2), was evacuated to a pressure of 10^{-4} to 10^{-5} mm Hg. Ether vapor was admitted first to the requisite pressure, and then boron trifluoride was added. The quantity of BF_3 added to the reactor was determined by the loss from a flask of known volume. The equilibrium pressures of the etherate (P^g_{e-t}), boron trifluoride ($P^g_{BF_3}$) and ether (P^g_{eth}) in the gas phase, and the quantity of etherate condensed on the surface (P^l_{e-t}) were determined in each experiment. The following information was required to calculate these values: the equilibrium constant for the dissociation of the etherate in the gas phase $K_p = \frac{P^g_{BF_3} \cdot P^g_{eth}}{P^g_{e-t}} = 92.5$ (at t = 70°) from the data of Brown and Adams [1], the total pressure (P_{tot}) in the reactor after the addition of boron trifluoride and ether, and the balancing equation for P_{BF_3} and P_{eth}.

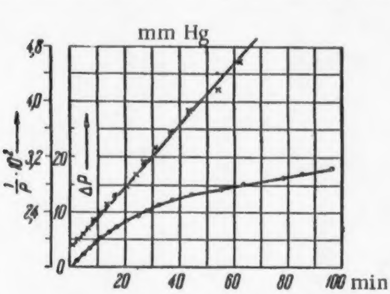

Fig. 1. Kinetic curve (and its inverted form) for the polymerization of iC_4H_8 in the presence of the etherate of boron trifluoride. t = 70°, $P^g_{BF_3} = 74.2$, $P^g_{eth} = 4.8$ and $P_{i-C_4H_8} = 52$ mm Hg. $V_{reactor} = 0.34$ liter.

Special attention was paid to the preparation of pure reagents, free from traces of moisture. Boron trifluoride was prepared and purified by a previously described method [2]. Diethyl ether was redistilled up a fractionating column from metallic sodium and was stored over sodium. Isobutylene was fractionated up a high efficiency vacuum column and was dried by bubbling through a liquid Na-K alloy.

The rate of the reaction was expressed as the decrease in pressure of isobutylene (mm Hg per minute in a reactor of volume 1 liter), ascribed to 1 mole of adsorbed etherate. Figure 1 shows the kinetic curve and its inverted form for the polymerization of $i-C_4H_8$ in the presence of the etherate $(C_2H_5)_2O \cdot BF_3$. At t = 70° and small values of $P_{i-C_4H_8}$ (up to 100-150 mm Hg), the kinetic curve is well represented by an equation of the second order up to 40-50% conversion, and the velocity constant K_1 determined from it does not depend on the initial pressure of $i-C_4H_8$.

The effect of the pressures of BF_3 and ether in the gas phase on the catalytic activity of the etherate was investigated for a range of $P_{i\text{-}C_4H_8}$ from 30 to 110 mm Hg. Ether and boron trifluoride were connected by the equilibrium $BF_3(C_2H_5)_2O \rightleftarrows BF_3 + (C_2H_5)_2O$; to simplify the treatment of the results, the experiments were carried out under conditions such that the vapor pressure of the etherate was equal, or nearly equal, to its saturation pressure, i.e., at constant thermodynamic activity of the etherate. It was found that, when P_{eth} was increased from 1.8 to 72 mm Hg, the catalytic velocity constant, K_1, decreased by a factor of more than 40 (Fig. 2, and Table 1). In view of the lack of data on the partial pressures of $(C_2H_5)_2O$ and BF_3 over solutions of $(C_2H_5)_2O$ in the etherate, we can give no precise figures for the concentration of ether in the liquid phase which corresponds to a given value of P^g_{eth}. But Raoult's law may be applied when the mole fraction of ether in the solution is small (~ 0.03). The effect of ether on the catalytic activity of $(C_2H_5)_2O \cdot BF_3$ is similar to the effect of water on the acidity of mineral acids (phophoric, sulfuric, etc.). This powerful effect of ether, even at low concentrations, can only be explained by its basic properties.

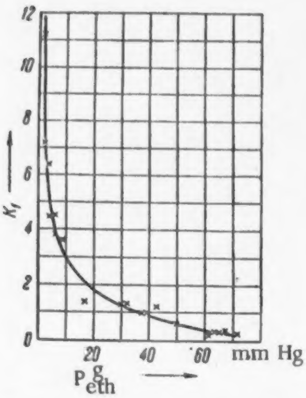

Fig. 2. Dependence of the velocity constant of the polymerization of $i\text{-}C_4H_8$, in the presence of the etherate of boron trifluoride, on the pressure of ether in the gas phase.

Figure 3 and Table 1 show the dependence of the velocity constant of the polymerization, K_1, on the equilibrium pressure of boron trifluoride in the gas phase. At relatively low pressures of BF_3 there was a linear relation between K_1 and $P^g_{BF_3}$. As $P^g_{BF_3}$ was raised to 100-200 mm Hg this linear relation broke down, and the value of K_1 increased more slowly than before. Judging from Experiments Nos. 21, 22 and 23, where $P^g_{BF_3}$ varies from 215 to 290 mm Hg, it may be concluded that at large pressures of boron trifluoride the velocity constant does not alter (within the limits of experimental error).

TABLE 1

No.	$P^0_{BF_3}$	P^0_{eth}	P_{tot}	$P^g_{BF_3}$	P^g_{eth}	P^g_{e-t}	P^l_{e-t}	$P^g_{BF_3} : P^g_{eth}$	$P_{i\text{-}C_4H_8}$ mm Hg	K_1
	mm Hg									
1	13,5	80	81	5,25	71,7	4,0	4,25	$7{,}3\cdot10^{-}$[illegible]	82	0,24
2	19,0	80	76	5,5	66,5	4,0	9,5	$8{,}3\cdot10^{-}$[illegible]	110	0,32
3	21,8	60	67,5	11,5	49,8	6,2	4,0	0,23	108	0,58
4	24,6	80	78	8,4	63,8	5,8	10,4	0,13	157	0,27
5	24,5	81	78,5	8,3	64,7	5,7	10,6	0,13	174,5	0,26
6	25,2	79,7	76,8	8,3	62,6	5,7	11,2	0,13	39	0,21
7	25,0	80	76,5	8,0	63,0	5,5	11,5	0,13	33	0,26
8	24,0	60	64	11,1	47,2	5,7	7,2	0,23	106	1,2
9	33,8	60,5	57,5	12,5	39,2	5,8	15,5	0,32	112	0,99
10	36	60,2	58,8	14,4	38,6	5,8	15,8	0,37	62	1,02
11	47	61	55,0	17,5	31,5	6,1	23,5	0,55	106	1,3
12	47,7	61	53,5	17,25	30,5	5,7	24,7	0,56	64	1,3
13	60	60,5	50,2	22,0	19,5	5,7	32,3	1,1	64	1,6
14	60,5	51,0	50,5	27,1	17,6	5,8	27,5	1,5	62	1,4
15	59,6	20,5	61,5	48	9,0	4,6	7,0	5,3	58	3,6
16	80,4	11	83	74,2	4,8	3,9	2,2	15,5	53	4,5
17	80,6	15,5	84	71,9	6,8	5,3	3,3	10,5	53	3,9
18	82,3	18,0	82,5	71,1	6,3	4,9	6,6	11,3	58	4,5
19	109	20,5	103	92,8	4,3	4,9	10,3	21,6	58	6,4
20	109	20,0	101,5	93,0	4,1	4,3	11,4	22,6	56	
21	—	—	—	253	2,1	5,8	7,1	120	33	7,2
22	—	—	—	290	1,8	5,8	6,4	160	33	11,3
23	—	—	—	215	2,5	5,8	4,7	86	33	12,2

Footnote. $P^0_{BF_3}$ and P^0_{eth} are the original pressures of BF_3 and ether in the reactor; $P^g_{BF_3}$ and P^g_{eth} are the equilibrium pressures of BF_3 and ether in the reactor; P_{tot} is the total pressure in the reactor after the addition of BF_3 and ether; P^g_{e-t} is the equilibrium pressure of etherate in the gas phase; P^l_{e-t} is the quantity of etherate adsorbed on the surface of the quartz; K_1 is the bimolecular constant expressed in terms of the decrease in pressure of $i\text{-}C_4H_8$ in a reactor of volume 1 liter with 1 mole of adsorbed etherate.

At t = 70° and $P_{i-C_4H_8}$ > 100-150 mm Hg, the reaction diverged from the bimolecular in the same way as with phosphoric and sulfuric acid catalysts [3, 4]. The nature of this divergence was as follows: with a rise in $P_{i-C_4H_8}$ there was a decrease in the bimolecular velocity constant K_1, and the degree of conversion fell below the value corresponding to a kinetic curve of the second order. The experimental data for the relation between the rate of polymerization, W, and $P_{i-C_4H_8}$ could be expressed satisfactorily by an empirical equation of the same type as for sulfuric and phosphoric acid catalysts:

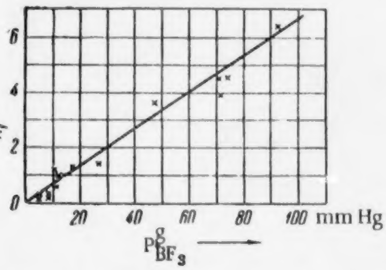

Fig. 3. Dependence of the velocity constant of the polymerization of i-C_4H_8 in the presence of the etherate of boron trifluoride, on the pressure of boron trifluoride in the gas phase.

$$W = \frac{Aa^2 P_{iC_4H_8}}{(1 + aP_{iC_4H_8})^2},$$

where A and a are parameters.

For instance, with a catalyst characterized by $P^g_{BF_3}$ = = 16 mm Hg and P^g_{eth} = 15 mm Hg, a change in $P_{i-C_4H_8}$ from 50 to 390 mm Hg produced a tenfold decrease in the bimolecular velocity constant.

It is evident, from the data in Table 1, that the etherate of boron trifluoride is an effective catalyst for the polymerization of i-C_4H_8. An etherate, characterized by $P^g_{BF_3}$ = 67 mm Hg and P^g_{eth} = 5.5 mm Hg at 70°, showed the same catalytic activity as 70% sulfuric acid with an acidity function of − 6.05.

Judging by its catalytic activity, the etherate must have the properties of a strong acid. Wichterle [5] showed that, in 100% etherate as medium, the indicator benzalacetophenone ($pK_B = -5.6$) was ionized to a considerable extent. We used the following indicators: o-nitroaniline, 5-chloro-2-nitroaniline, 2,4-dichloro-6-nitroaniline and 2,4-dinitroaniline, to determine the acidity functions of etherate-ether systems.

For 100% etherate, the value of $\log \frac{C_{BH^+}}{C_B}$ for the indicator 2,4-dinitroaniline was equal to 1.8. If we follow Wichterle in assuming that, for concentrations of etherate near 100%, pK_B for the indicator is the same as in aqueous solution, then H_0 for 100% etherate must be − 6.2.

Meerwein [6] and Greenwood and Martin [7] considered that the etherate dissociated to form the $C_2H_5^+$ ion. If this were so, the products of polymerization of i-C_4H_8 should contain transformation products of the ions $C_2H_5^+$ and $C_2H_5OBF_3^-$ (C_6H_{12}, $C_4H_9OC_2H_5$). But these substances could not be detected by mass-spectrography in the polymerization products of i-C_4H_8 in an etherate medium. We conclude that the etherate ionizes by means of a C−H linkage. Isobutylene ionizes in an etherate medium as follows: $(C_2H_5)_2OBF_3 + i\text{-}C_4H_9 \rightleftharpoons i\text{-}C_4H_9^+ + C_4H_9OBF_3^-$, and further transformation procedes by the usual acid mechanism.

LITERATURE CITED

[1] H. C. Brown and B. M. Adams, J. Am. Chem. Soc. 64, 2557 (1942).

[2] M. I. Vinnik, G. B. Manelis, et al., J. Inorg. Chem. 1, 628 (1956).

[3] N. M. Chirkov and M. I. Vinnik, Proc. Acad. Sci. USSR 99, 823 (1954).

[4] N. M. Chirkov and M. I. Vinnik, Proc. Acad. Sci. USSR 105, 766 (1955).

[5] O. Wichterle, Z. Laita, and M. Pazlar, Chem. Listy 49, 1612 (1955).

[6] H. Meerwein, Angew. Chem. 64, 374 (1955).

[7] N. N. Greenwood, R. L. Martin, and H. J. Emelens, J. Chem. Soc. (1950), 3030.

Institute of Chemical Physics of the
Academy of Sciences of the USSR

Received August 1, 1957.

PHYSICOCHEMICAL INVESTIGATION OF SOME SYSTEMS CONTAINING TRIETHYLALUMINUM AND ITS DERIVATIVES

A. I. Graevskii, Sh. S. Shchegol', and Z. S. Smolian

(Submitted by Academician A. V. Topchiev, August 5, 1957)

Triethylaluminum and titanium tetrachloride can be used as catalysts for the low pressure polymerization of ethylene, propylene and other alkenes [1, 2]. Depending on its method of preparation [3-5], triethylaluminum usually contains considerable quantities of products of oxidation and decomposition (hydride and ethoxide) and also halogen derivatives. In view of the differences in behavior of these products in the polymerization process, it was of interest to make a quantitative study of the composition of a sample of triethylaluminum synthetized from ethyl bromide, and to investigate its use as a catalyst for the preparation of polyethylene and polypropylene. For this purpose we made use of the capacity of many organic compounds of aluminum to form complexes, at the expense of the unfilled 3p electron level of the central aluminum atom, with nucleophilic reagents containing atoms of nitrogen, oxygen or fluorine [6-8].

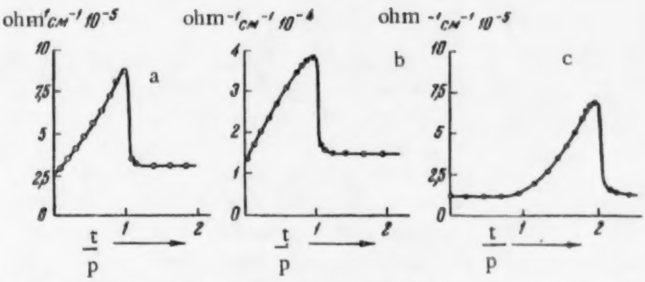

Fig. 1. Conductimetric titrations with quinoline in cyclohexane solution: a) $Al(C_2H_5)_3$, b) $Al(C_2H_5)_2Br$, c) $Al(C_2H_5)_2H$. Here and in the following curves, t/p is the mole ratio of quinoline, added in the titration, to aluminum, contained in the sample being titrated.

Pure triethylaluminum, diethylaluminum hydride, diethylaluminum bromide and diethylaluminum ethoxide, synthetized by known methods [3, 4, 9], were dissolved in cyclohexane and titrated with quinoline, either potentiometrically in a cell with silver and platinum electrodes, or conductimetrically in a cell with unplatinized plate electrodes. The titrations were done in an inert gas atmosphere. A PL-5 potentiometer was used for measuring electrode potentials in the potentiometric titrations; direct current was used for the conductimetric titrations, and the voltage could be varied from 1.5 to 30 volts;* the current was measured with a mirror galvanometer, type M-21, or a microammeter.

The conductimetric titration curves for individual substances (Fig. 1) showed that quinoline forms with triethylaluminum an electrically conducting complex $Al(C_2H_5)_3 \cdot C_9H_7N$ with diethylaluminum bromide a conducting complex $Al(C_2H_5)_2Br \cdot C_9H_7N$ and with diethylaluminum hydride a nonconducting complex $Al(C_2H_5)_2H \cdot C_9H_7N$ and a complex $Al(C_2H_5)_2H \cdot 2C_9H_7N$ which is a good conductor. Diethylaluminum ethoxide does not form complexes with quinoline.

* In view of the high internal resistance of the cell (0.1-1 meg), the current was very small and polarization of the electrodes could be neglected.

The previously unknown complex $Al(C_2H_5)_2Br \cdot C_9H_7N$ was isolated during the course of the investigation; it crystallized from cyclohexane in the form of colorless crystals of m. p. 45°.

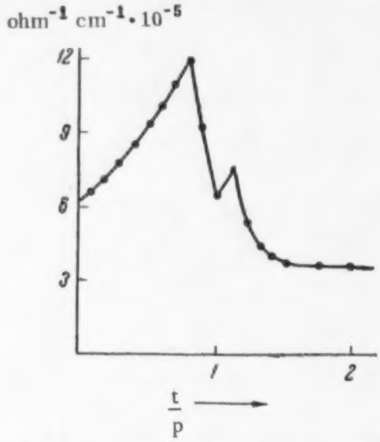

Fig. 2. Conductimetric titration of a mixture containing $Al(C_2H_5)_3$, $Al(C_2H_5)_2Br$, $Al(C_2H_5)_2H$, $Al(C_2H_5)_2OC_2H_5$.

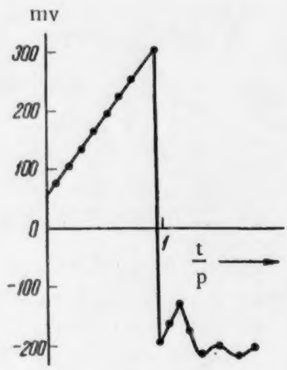

Fig. 3. Potentiometric titration of a mixture containing $Al(C_2H_5)_3$, $Al(C_2H_5)_2Br$, $Al(C_2H_5)_2H$, $Al(C_2H_5)_2OC_2H_5$.

The potentiometric titrations confirmed the conductimetric results, and the changes in electrode potential at the turning points were considerably more distinct than the conductivity maxima.

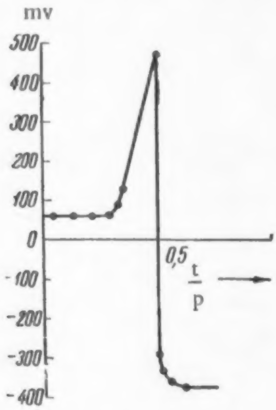

Fig. 4. Potentiometric titration of the equimolecular mixture $Al(C_2H_5)_2Cl + AlC_2H_5Cl_2$.

Figures 2 and 3 show the curves for the conductimetric and potentiometric titration of mixtures containing $Al(C_2H_5)_3$, $Al(C_2H_5)_2Br$, $Al(C_2H_5)_2H$, and $Al(C_2H_5)_2OC_2H_5$. These curves may be interpreted as follows. The growth in conductivity from its original value to the first maximum (Fig. 2) can be explained by the formation of well conducting complexes between quinoline and triethylaluminum or diethylaluminum bromide. At these first maxima $Al(C_2H_5)_3$ and $Al(C_2H_5)_2Br$ are completely titrated. The subsequent decrease in conductivity is due to the formation of the nonconducting complex $Al(C_2H_5)_2H \cdot C_9H_7N$ which, on the addition of excess of quinoline, is converted into the complex $Al(C_2H_5)_2H \cdot 2C_9H_7N$, and the conductivity of the system rises again. The position of the second maximum corresponds to the complete conversion of the hydride into a bimolecular complex with quinoline. On further addition of quinoline the conductivity of the mixture falls, since quinoline is a nonconductor, and aluminum ethoxide does not form a complex with quinoline.

Interesting results were obtained by the titration of an equimolecular mixture of $Al(C_2H_5)_2Cl$ and $Al(C_2H_5)Cl_2$ ("sesquichloride"). This mixture could not be investigated conductimetrically, because titration with quinoline in cyclohexane gave a crystalline precipitate, probably an insoluble complex of quinoline with ethylaluminum dichloride. The formation of this precipitate caused a sharp drop in the current through the conductimetric cell because of a marked increase in the resistance between the electrodes. At the point of the potentiometric curve (Fig. 4), corresponding to a mole ratio of quinoline to aluminum equal to 0.5, there was a sharp change in potential, supporting the suggestion that a complex was formed.

Our work is also of practical interest, as it provides a rapid and reliable method of determining active triethylaluminum for estimating the relation between catalyst and cocatalyst in the production of polyalkenes.

LITERATURE CITED

[1] K. Ziegler, U. Gellert, and W. Lehmkuhl, Angew. Chem. 67, 425 (1955).

[2] K. Ziegler, Angew. Chem. 67, 541 (1955).

[3] A. Grosse and J. Mavity, J. Org. Chem. 5, 106 (1940).

[4] K. Ziegler, Angew. Chem. 64, 323 (1952).

[5] K. Ziegler, Angew. Chem. 68, 721 (1956).

[6] K. Ziegler and H. Lehmkuhl, Z. anorg. u. allgem. Chem. 283, 414 (1956).

[7] E. Krause and B. Wendt, Ber. 56, 466 (1923).

[8] E. Bonitz, Chem. Ber. 88, 742 (1955).

[9] R. S. Brokaw and R. N. Pease, J. Amer. Chem. Soc. 72, 3237 (1950).

Received August 5, 1957.

A COPPER CATALYST FOR THE OXIDATION OF PROPYLENE TO ACROLEIN

O. V. Isaev, M. Ia. Kushnerev, and L. Ia. Margolis

(Submitted by Academician V. N. Kondrat'ev, August 6, 1957)

Investigation of the oxidation of propylene to acrolein on a series of metallic oxides [1] showed that, with cuprous oxide, oxygen could be introduced into the hydrocarbon molecule without removing the double bond, leading to the formation of the unsaturated aldehyde, acrolein.

It is known that cuprous oxide is a typical defect-type semiconductor, whose electrical conductivity in the temperature region of 0 to 250° varies from 10^{-9} to 10^{2} ohm^{-1} cm^{-1} depending on its oxygen content [2]. A comparison of the electrical properties of cuprous oxide with its adsorptive capacity for propylene showed that, the less oxygen there was in the catalyst, the greater was the sorption of propylene. It was probable that the catalytic activity of cuprous oxide would also change with a change in its oxygen content.

A number of foreign patents [3, 4] gave data on the preparation of active catalysts for this process, based on cuprous and cupric oxides. In one of these patents [4] it was stated that cupric oxide is inactive for the above reaction. But the more recent patents recommended the use of cupric oxide supported on different carriers. It was not made clear what was the phase composition of the copper catalyst, what occurred on the catalyst at the time of reaction and which of the oxides was catalytically active.

Three series of experiments were carried out to elucidate these questions, using as catalysts: 1) cupric oxide CuO, 2) cuprous oxide Cu_2O and 3) metallic copper, supported on pumice.

Cupric oxide was prepared by saturating pumice with a solution of $Cu(NO_3)_2$ and calcining at 500° C. Cuprous oxide, prepared by the method of D. N. Finkel'shtein [5], was washed and applied to pumice from its aqueous suspension. Metallic copper was obtained by reducing the oxide supported on pumice in a stream of hydrogen at 300-350° C.

The phase compositions of the catalysts, before and after use, were investigated by x-ray diffraction. The diffraction patterns were photographed with a Debye camera 57.3 mm in diameter, using the iron K_α frequency.

The catalysts were tested by the flow method at atmospheric pressure, using a mixture of propylene and air containing 10-12% of propylene and about 20% of oxygen, in the temperature range 300-400°, for periods of 40 minutes.

Figure 1 shows the x-ray diffraction results obtained with the three catalysts; the abscissa represents <u>d</u>, the distance between the planes of the crystal lattice, and the ordinate represents the intensity of the line, determined visually.

Treatment of cupric oxide with a propylene-air mixture at 300° C did not alter the phase composition of the catalyst. But raising the temperature to 400° caused reduction to cuprous oxide and to the metal. Under the same conditions, cuprous oxide was always partially reduced to metal. When the propylene-air mixture was passed over copper at 300° there was partial oxidation to Cu_2O.

Further investigation of these catalysts by electron diffraction showed that, after treatment with the propylene-air mixture, the surfaces of all the samples were covered with a layer of cuprous oxide.

Thus, in the presence of the propylene-air mixture, cupric oxide was reduced to $Cu_2O + Cu$, and metallic copper was oxidized to cuprous oxide. The oxidation of propylene to acrolein took place in the presence of cuprous oxide. The appearance of the metallic phase in this system can be explained by the reduction of Cu_2O to metal. Analysis of the outgoing gas, after the oxidation of the propylene, showed almost complete absence

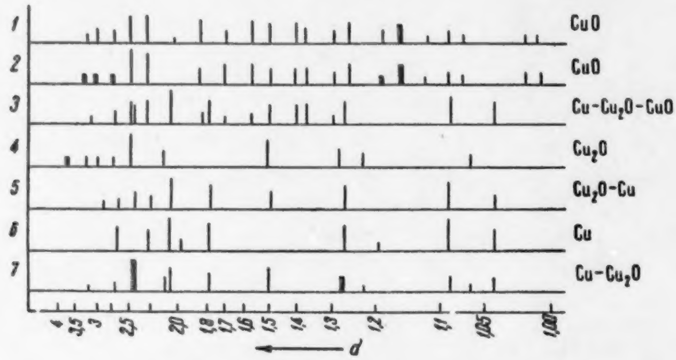

Fig. 1. Changes in the phase composition of copper catalysts during the oxidation of propylene with atmospheric oxygen.
1) Original cupric oxide; 2) cupric oxide after reaction at 300°; 3) cupric oxide after reaction at 400°; 4) original cuprous oxide; 5) cuprous oxide after reaction at 350°; 6) original metallic copper; 7) copper after reaction at 300°.

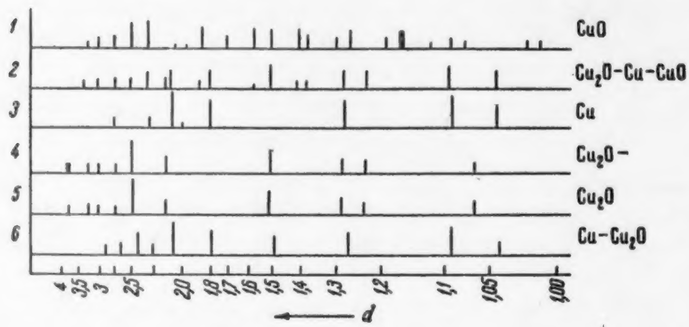

Fig. 2. Changes in the composition of copper oxide catalysts after reduction with a mixture of propylene and nitrogen.
1) Original cupric oxide; 2) cupric oxide after reduction at 300°; 3) cupric oxide after reduction at 400°; 4) original cuprous oxide; 5) cuprous oxide after reduction at 200°; 6) cuprous oxide after reduction at 350°.

of oxygen. Thus, during the reaction, the catalyst was working in a reducing atmosphere, so that the conversion $Cu_2O \rightarrow Cu$ could occur. To investigate this phase change, the catalyst was treated with a mixture of propylene and nitrogen, containing 10% of propylene and less than 1% of oxygen, at 200-400°. The x-ray diffraction results are shown in Fig. 2. Considerable reduction of cuprous oxide to copper was found at 350°. When the mixture was passed over cupric oxide at 300°, there was partial reduction of the oxide to metal. When the temperature was raised to 400°, the cupric oxide was rapidly and completely reduced to copper. The introduction of oxygen into the mixture, as described above (see Fig. 1) again led to partial oxidation of the metallic copper to cuprous oxide. Cupric oxide was not observed in this diffraction photograph.

Thus, depending on the proportion of propylene, the addition of oxygen to the reaction mixture should either depress or enhance the reduction of cuprous oxide.

From what has been said above, it is clear that the composition of the catalyst is self-regulating by the reversible processes of reduction of Cu_2O to Cu and of oxidation of Cu to Cu_2O. Depending on the composition of the reaction mixture and the temperature conditions of the catalytic process, the phase composition of the catalyst changes, and there is either an enrichment of cuprous oxide or the oxygen content of the cuprous oxide increases. In either case there is a change in catalytic activity with respect to the oxidation of propylene to acrolein. The introduction of oxygen in one case, and of propylene in the other, leads to an increase in the activity of the catalyst, which is in agreement with the data of the patents [6-8], where it is recommended that the catalyst be regenerated by stopping the supply of propylene or oxygen.

LITERATURE CITED

[1] L. Ia. Margolis, S. Z. Roginskii, and T. A. Gracheva, J. Gen. Chem. 26, 1368 (1956).*

[2] A. F. Ioffe, "Semi-conductors in contemporary physics" Bull. Acad. Sci. USSR (1954).

[3] British Patent 658,179, March 10, 1951; C. A. 46, 4562 (1952).

[4] British Patent 640,383, July 19, 1950; C. A. 45, 1619 (1951).

[5] Iu. V. Kariakin and I. I. Angelov, Pure Chemical Reagents, (Moscow, 1955).**

[6] British Patent 668,867, March 26, 1952; C. A. 47, 1729 (1953).

[7] U. S. Patent 2,608,585, August 26, 1952; C. A. 47, 800 (1953).

[8] British Patent 671,123, April 30, 1952; C. A. 46, 8845 (1952).

Institute of Physical Chemistry of the
Academy of Sciences of the USSR

Received July 25, 1957.

* Original Russian pagination. See C. B. Translation.

** In Russian.

LIQUID RISE IN CAPILLARIES OF VARIABLE CROSS SECTION AND CAPILLARY HYSTERESIS

M. M. Kusakov and D. N. Nekrasov

(Submitted by Academician A. V. Topchiev, August 8, 1957)

For capillary tubes of circular cross section, the height, h, of capillary rise of a nonviscous liquid can be found from the condition

$$\frac{\partial U}{\partial h} = 0, \tag{1}$$

where U, the potential energy of the wetting liquid in the capillary is given by

$$U = \pi\rho g \int_0^h r^2 h\, dh - 2\pi\sigma \int_0^h r\, dh, \tag{2}$$

where ρ is the density of the liquid, g is the acceleration due to gravity, r is the radius of the capillary and σ is the surface tension of the liquid at its boundary with the saturated vapor. Equation (2) is correct provided that the meniscus has a spherical form and that the liquid wets the capillary. In this expression the function $r = f(h)$ determines the form of the capillary (representing a surface of revolution about an axis conciding with the axis of the capillary); for a cylindrical capillary $r = r_0$, where r_0 is the radius of the capillary; for conical capillaries $r = a + bh$, where a and b are constants; for a periodic contraction and expansion (for example, according to a sinusoidal law) of the capillary $r = \alpha + \beta \sin \gamma h$, where α, β, and γ are constants, etc. The real positive roots $h_1, h_2, \ldots, h_i, \ldots$, of Equation (1) for $\left(\frac{\partial^2 U}{\partial h^2}\right)_{h=h_i} > 0$ are the heights corresponding to unstable equilibrium.* Liquid rise occurs in the capillary over the range of values of h from 0 to h_1, or from h_i to h_{i+1}, if over this range $\frac{\partial U}{\partial h} < 0$; but, for values corresponding to the range for which $\frac{\partial U}{\partial h} > 0$, liquid rise can only be accomplished at the expense of external work. For cylindrical and conically diverging capillaries there exists one height of capillary rise, for conically converging (open) capillaries two heights [2], and for periodically contracting and expanding capillaries several heights. In the last case the number of heights is always limited, determined by the number of positive real roots of Equation (1), i.e., on the form of the capillary or the nature of the function $r = f(h)$.

The heights of capillary rise of a liquid in a capillary of variable cross section can also be found by the simultaneous solution (for example, graphically) of the obvious pair of equations

$$\left.\begin{aligned} h\rho g &= \frac{2\sigma}{r} \\ r &= f(h) \end{aligned}\right\} \tag{3}$$

* Mention is made in [1] of the possible existence of several positions of equilibrium for liquids in capillaries of variable cross section.

It is interesting to note that, for a capillary whose form is given by the equation $r = \frac{2\sigma}{h\rho g}$ (the internal form of the capillary is obtained by rotation of the hyperbola $rh = \frac{2\sigma}{\rho g}$ about a vertical axis), any height will be found to be in equilibrium.

Obviously this circumstance is connected with the nonreproducible heights of capillary rise sometimes observed experimentally with certain liquids. In many cases cylindrical capillaries are found to have a variable cross section, and, if the shape of the capillary and the values of σ and ρ for the liquid are such that the condition $rh = \frac{2\sigma}{\rho g}$ is even approximately fulfilled, non-reproducible results will be found for the height of capillary rise.

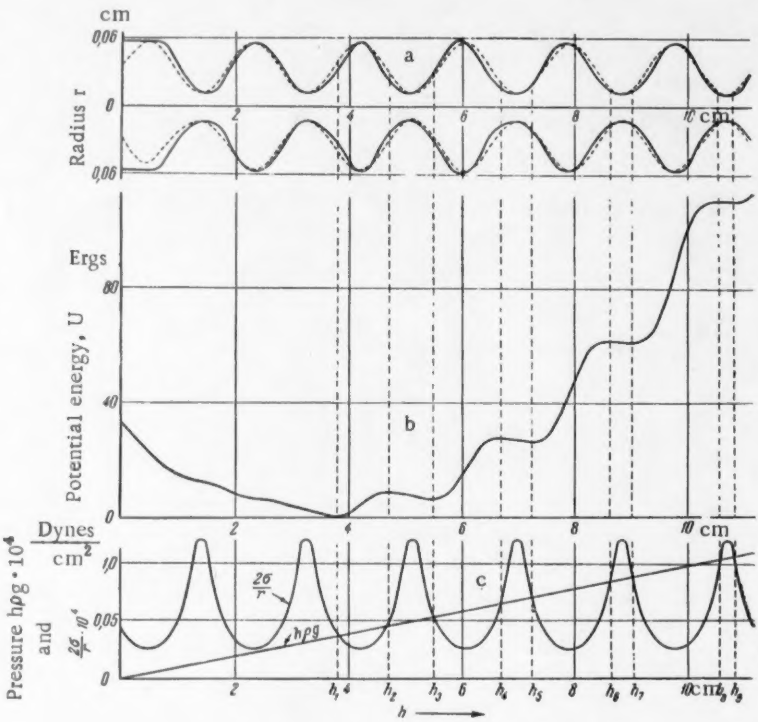

Fig. 1. a) Capillary profile: experimental (continuous line) and calculated (dotted line); b) dependence of the potential energy of the gravitational and capillary forces, acting on the liquid in the capillary, on the height; c) dependence of hydrostatic and capillary pressures on the height [graphical solution of Equations (3)].

Experimental confirmation of the above considerations was obtained from the capillary rise of water in a converging conical capillary, and also in a specially made glass capillary which periodically converged and diverged in accordance with a sinusoidal law. As an example, for the sinusoidal capillary, we show graphically $U = f(h)$;* $h\rho g = f(h)$ and $\frac{2\sigma}{r} = f(h)$. In Fig. 1, a the continuous line shows the actual profile of one of the capillaries (obtained by measurement of the internal diameter under the microscope after grinding away half

* In the graph of $U = f(h)$ the value $U = 0$ is conditionally combined with the observed value of the energy.

the capillary) and the dotted line shows the profile calculated from the equation $r = \alpha + \beta \sin\gamma h$, where the constants α, β and γ were found by combining the results of measuring 2r for different values of h. For the capillary under consideration $\alpha = 0.034$, $\beta = 0.022$, and $\gamma = 3.38$. It is clear from the graphs of $U = f(h)$ (Fig. 1, b), $h\rho g = f(h)$ and $\frac{2\sigma}{r} = f(h)$ (Fig. 1, c) that, for the given capillary with water, there should be nine heights of capillary rise, of which five (h_1, h_3, h_5, h_7, and h_9) correspond to stable equilibrium, and four (h_2, h_4, h_6 and h_8) to unstable equilibrium. Experimentally (both with raising and lowering of the liquid) all five heights were observed, and their values practically coincided with those calculated from Equations (1) or (3). The most stable height in this case was the first of the stable heights, which is in accordance with the graph of $U = f(h)$.

Thus, conclusions as to the existence of several heights of capillary rise in capillaries of variable cross section, a phenomenon known as capillary hysteresis, can be obtained from consideration of the general conditions of equilibrium of liquids in capillaries.

LITERATURE CITED

[1] A. Iu. Davidov, Theory of Capillary Phenomena* (Moscow, 1851**), p. 201.

[2] H. Bouasse, Capillarite, phenomenes superficiels (Paris, 1924), p. 189.

Received July 29, 1957.

* In Russian.

** As in original — Publisher's note.

THE MECHANISM OF THE ANODIC FORMATION OF BICHROMIC ACID

A. I. Levin and S. S. Savel'ev

(Submitted by Academician A. N. Frumkin, July 22, 1957)

The direct electrochemical method for obtaining bichromic acid makes use of the equilibrium established between chromate anions in the absence of an electric current [1]:

$$2CrO_4^{2-} + 2H^+ \rightleftarrows 2HCrO_4^- \rightleftarrows Cr_2O_7^{2-} + H_2O.$$

Experiment shows [2] that, with a decrease in pH and with an increase in the concentration of the electrolyte containing chromic anhydride, the above equilibrium is displaced to the right, that is in the direction of the formation of $Cr_2O_7^{2-}$.

It would be expected that the desired change in ionic equilibrium would be subject to a definite kinetic law. Indeed, from consideration of the electrode processes in a chromium bath [3], it follows that, when high enough potentials are created at the anode during electrolysis, there is a very marked shift of the pH of the anolyte toward the acid region. If we take an aqueous solution of sodium bichromate, then at high current densities in consequence of the considerable polarization, the predominant anodic process must be the reaction of the formation of isopolychromic acids of the type – $H_2O(Cr_2O_3)_n$, i.e., $H_2Cr_2O_7$, $H_2Cr_3O_{10}$, $H_2Cr_4O_{13}$ – with the formation of chromic anhydride, which concentrates in the layer around the anode in the form of bichromic acid and its analogs.

For practical investigation of the reaction, the anodic processes were studied in a bath resembling the mercury electrolytic cell used for the manufacture of chlorine and alkali:

$$Hg^- \mid H_2O,\ NaOH \parallel H_2O,\ Na_2Cr_2O_7,\ H_2Cr_2O_7 \mid PbO_2^+.$$

The anodic and cathodic compartments were separated by a diaphragm, and the anode was made of lead peroxide. On electrolysis, alkali was formed in the catholyte, while in the anolyte there was formed a polychromate solution containing sodium bichromate and bichromic acid, whose concentration increased during the electrolysis.

Investigation of the possible anodic processes at a lead peroxide electrode has shown that the discharge of hydroxyl ions is accompanied by a high polarization [4]. At a high enough anode current density there is finally an increase in the concentration of $Cr_2O_7^{2-}$ ions and an increase in the acidity of the electrolyte. In this case the activity of the OH^- ion drops considerably and its discharge potential becomes very high. It is because the anodic oxidation of hydroxyl ions is greatly retarded in strongly acid solutions that conditions are reached for other possible processes to occur. It may be presumed that one of the following processes will take place at the anode:

$$2H_2O - 4e \rightarrow O_2 + 4H^+ \qquad \varphi_1 = \varphi_1^0 + \frac{0{,}0002\,T}{Z}\log\frac{[H^+]^4[O_2]}{[H_2O]^2}; \tag{1}$$

$$2H_2O - 2e \rightarrow H_2O_2 + 2H^+ \qquad \varphi_2 = \varphi_2^0 + \frac{0{,}0002\,T}{Z}\log\frac{[H^+]^2[H_2O_2]}{[H_2O]^2}; \tag{2}$$

$$H_2O - 2e \rightarrow O + 2H^+ \qquad \varphi_3 = \varphi_{3}^{0} + \frac{0{,}0002\,T}{Z}\log\frac{[H^+]^2[O]}{[H_2O]}, \tag{3}$$

in which it is known [5] that φ_1, φ_2, and φ_3, calculated from the free energies of the Reactions (1), (2), and (3) are 1.229, 1.776, and 2.42 volts, respectively. The high value of the equilibrium potential of Reaction (3) shows that the formation of atomic oxygen according to Equation (3), in the presence of $Cr_2O_7^{2-}$ ions, is only possible when the oxidation of bichromate anions is taking place at high overvoltage. However, Fig. 1 shows that the value of the anodic potential, φ_a, in a bath containing sodium bichromate, did not reach φ_3, even at large current densities.

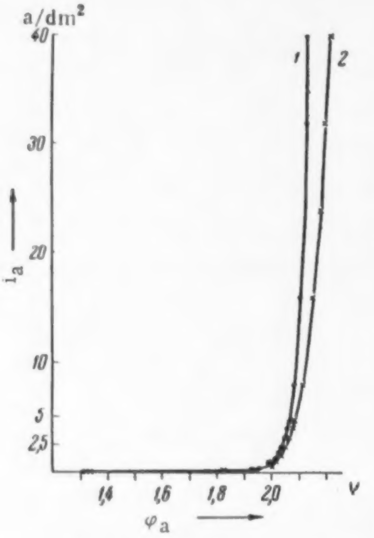

Fig. 1. Change of anodic potential, φ_a, with increasing current density, i_a, for a solution of $Na_2Cr_2O_7$. 1) 500 g/liter; 2) 700 g/liter.

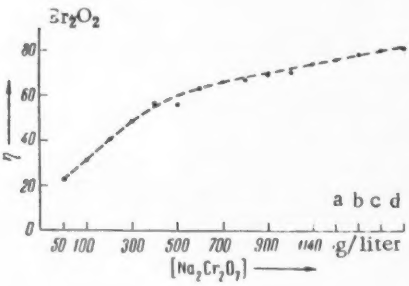

Fig. 2. Dependence of the yield of $H_2Cr_2O_7$ per unit current on the initial concentration of $Na_2Cr_2O_7$. a) Saturated at 30°, b) at 35°, c) at 40°, d) at 45°.

It may be concluded that the anodic oxidation of water procedes with the formation of molecular oxygen [Reaction (1)] and not by Reaction (3) to give atomic oxygen.

According to Glesston [6] all the irreversible processes of anodic oxidation take place with the intermediate formation of hydrogen peroxide, i.e., by Scheme (2). According to this hypothesis the formation of bichromic acid should also pass through a primary stage of the formation of H_2O_2 at the anode. But such a discharge mechanism is unlikely for the conditions under consideration. At the very high concentration of bichromate anions and the low activity of H_2O in the neighborhood of the anode the rate of formation of H_2O_2 must be quite insignificant. Because of this the potential φ_2 of the reaction of formation of hydrogen peroxide, shifts toward the positive side. When it is considered further that, in the absence of a depolarizer, hydrogen peroxide would be rapidly decomposed (into water and oxygen), it is reasonable to adopt the view that the inconsiderable quantity of H_2O_2 produced cannot play any significant part in the oxidizing action. Thus, the influence of hydrogen peroxide on the kinetics of the formation of bichromic acid can be disregarded.

It is also found that, in the electrolysis of sodium bichromate solution, there is a loss of water from the anolyte which is due to decomposition. This obviously takes place by Reaction (1) which, however, procedes more slowly than with the above-mentioned content of sodium bichromate in the original solution. This observation supports the view that the optimum condition for the electrolysis of sodium bichromate is with a high concentration of $Na_2Cr_2O_7$ in the electrolyte. The predominating anodic process is then the reaction of the formation of free bichromic acid and its analogs – the isopolyacids – at the expense of the direct participation of the $Cr_2O_7^{2-}$ anion in the anodic process.

From consideration of the anode process, it is not diffi- difficult to see that the high activity of the $Cr_2O_7^{2-}$ anion favors the course of the reaction producing bichromic acid and retards all the remaining processes. This view is supported by the fact that the yield of chromic anhydride per unit current (Fig. 2) markedly increased with the concentration of sodium bichromate, with which it forms the compound $Na_2O(CrO_3)_n$.

Lead is almost the only electrode material suitable for carrying out the process for the production of the free acid, since the formation of peroxide on the surface occurs more rapidly than the discharge of OH^- or H_2O at their prevailing concentrations. Lead acts as a catalyst for the discharge of the $Cr_2O_7^{2-}$ anion; this is linked with the formation on its surface of lead peroxide, which plays the part of a specific oxygen carrier [7]. The

electrochemical process for the formation of bichromic acid cannot be carried out successfully if its rate is low. It is therefore necessary to ensure that the volume of electrolyte, determining the concentration of the solution, and the current loading of the bath are strictly in the correct ratio.

Hydrolysis does not occur in the short period of time in which a large quantity of bichromic acid is formed. For this reason, the yield per unit current markedly increases at high current densities per unit volume and with rapid removal of the acid formed in the anolyte. Side reactions, reducing the yield of bichromic acid per unit current, are best prevented by reducing the quantity of anolyte in the space between the diaphragm and the anode. The anolyte should be in the form of a thin layer which is continuously circulating. Circulation is also necessary so that the bichromic acid, formed in large quantities, is immediately removed from the anolyte.

The direct electrolytic production of bichromic and polychromic acids in solution is of practical interest, since from such electrolytes it is subsequently possible to obtain compact cathodic deposits of chromium.

LITERATURE CITED

[1] A. I. Levin and A. I. Falicheva, J. Phys. Chem. 28, 1952 (1954); 29, 91 (1955).

[2] N. Hackerman and A. Powers, J. Phys. Chem. 57, 2, 139 (1953).

[3] A. I. Levin and A. I. Falicheva, J. Appl. Chem. 29, 1673 (1956).*

[4] A. I. Levin, Trans. Ural Ind. Inst., Coll. 27, Sverdlovsk (1947).

[5] W. M. Latimer, The Oxidation States of the Elements and Their Potentials in Aqueous Solutions, (New York, 1938), 72.

[6] S. Glesston, Introduction to Electrochemistry (IL, 1951).

[7] V. G. Khomiakov, V. P. Mashovets, and L. L. Kuz'min, Technology of Electrochemical Products** (1949), p. 405.

S. M. Kirov Ural Polytechnic Institute.

Received July 21, 1957.

* Original Russian pagination. See C. B. Translation.

** In Russian.

SCHEME FOR CALCULATING THE PHYSICOCHEMICAL PROPERTIES OF DERIVATIVES OF PARAFFIN HYDROCARBONS

Iu. A. Pentin

(Submitted by Academician B. A. Kazanskii, August 2, 1957)

Rules, governing a number of physicochemical properties of different types of hydrocarbons, can readily be formulated with the aid of V. M. Tatevskii's conception of types and subtypes of carbon-carbon and carbon-hydrogen bonds [1]. A scheme, based on this conception, for calculating the physicochemical characteristics of hydrocarbons [2] gives good agreement with experimental results, and it is also possible to deduce the characteristics of substances which have not been investigated and even of substances which have never been produced, but the possibility of whose existence is predicted by the theory of chemical structure.

There is great theoretical and practical interest in the possibility of extending the use of this conception to calculate the physicochemical properties of other classes of organic compounds (besides hydrocarbons). In this paper we consider, as an example, derivatives of paraffin hydrocarbons of the general formula

$$C_nH_{2n+2-m}X_m, \qquad (1)$$

where X is a univalent substituent group.

Applying the conception of subtypes of chemical bonds* to compounds of this structure, we suppose that the properties of a bond as with hydrocarbons, are determined mainly by the atoms forming the bond and by atoms directly linked to these. There are the following general forms of subtype of bond for C−C, C−H, and C−X in compounds of structure (1):

$$C_i^k - C_j^l, \quad C_i^k - H, \quad C_i^k - X, \qquad (2)$$

where $\underline{i}$ and $\underline{j}$ show whether the carbon atom is primary, secondary, tertiary, or quaternary (i, j = 1, 2, 3, 4) and the indices $\underline{k}$ and l show how directly X is linked to the particular carbon atom (k, l = 0, 1, 2, 3). Bond subtypes characteristic of ethane and methane derivatives cannot be taken into account, as they do not appear in higher homologs.

We now set out to express some physicochemical property P (molecular volume, refraction, energy of formation from atoms, etc.) of substance (1) in terms of the corresponding partial properties p_{ij}^{kl}, p_i^k (H), p_i^k (X) of the different chemical subtypes of bond, the numbers of each subtype being given by the coefficients n_{ij}^{kl}, n_i^k (H), and n_i^k (X); then

$$P_{C_nH_{2n+2-m}X_m} = \sum_{ij}^{kl} n_{ij}^{kl} p_{ij}^{kl} + \sum_i^k n_i^k(H)\, p_i^k(H) + \sum_i^k n_i^k(X)\, p_i^k(X). \qquad (3)$$

* The types of bond in these compounds are

$$\gt C - C \lt, \quad \gt C - H, \quad \gt C - X.$$

It turns out, however, that the coefficients n_i^k (H) and n_i^k (X) depend on the coefficients n_{ij}^{kl} and can be obtained by a linear combination of the following:

$$
\begin{aligned}
n_1^0(\mathrm{H}) &= 3\,(n_{12}^{00} + n_{12}^{01} + n_{12}^{02} + n_{13}^{00} + n_{13}^{01} + n_{14}^{00}),\\
n_1^1(\mathrm{H}) &= 2\,(n_{12}^{10} + n_{12}^{11} + n_{12}^{12} + n_{13}^{10} + n_{13}^{11} + n_{14}^{10}),\\
n_1^2(\mathrm{H}) &= n_{12}^{20} + n_{12}^{21} + n_{12}^{22} + n_{13}^{20} + n_{13}^{21} + n_{14}^{20},\\
n_2^0(\mathrm{H}) &= n_{12}^{00} + n_{12}^{10} + n_{12}^{20} + n_{12}^{30} + 2n_{22}^{00} + n_{22}^{01} + n_{22}^{02} + n_{23}^{00} + n_{23}^{01} + n_{24}^{00},\\
n_2^1(\mathrm{H}) &= {}^1/_2\,(n_{12}^{01} + n_{12}^{11} + n_{12}^{21} + n_{12}^{31} + n_{22}^{01} + 2n_{22}^{11} + n_{22}^{12} + n_{23}^{10} + n_{23}^{11} + n_{24}^{10}),\\
n_3^0(\mathrm{H}) &= {}^1/_3\,(n_{13}^{00} + n_{13}^{10} + n_{13}^{20} + n_{13}^{30} + n_{23}^{00} + n_{23}^{10} + n_{23}^{20} + 2n_{33}^{00} + n_{33}^{10} + n_{34}^{00}),\\
n_1^1(\mathrm{X}) &= n_{12}^{10} + n_{12}^{11} + n_{12}^{12} + n_{13}^{10} + n_{13}^{11} + n_{14}^{10},\\
n_1^2(\mathrm{X}) &= 2\,(n_{12}^{20} + n_{12}^{21} + n_{12}^{22} + n_{13}^{20} + n_{13}^{21} + n_{14}^{20}),\\
n_1^3(\mathrm{X}) &= 3\,(n_{12}^{30} + n_{12}^{31} + n_{12}^{32} + n_{13}^{30} + n_{13}^{31} + n_{14}^{30}),\\
n_2^1(\mathrm{X}) &= {}^1/_2\,(n_{12}^{01} + n_{12}^{11} + n_{12}^{21} + n_{12}^{31} + n_{22}^{01} + 2n_{22}^{11} + n_{22}^{12} + n_{23}^{10} + n_{23}^{11} + n_{24}^{10}),\\
n_2^2(\mathrm{X}) &= n_{12}^{02} + n_{12}^{12} + n_{12}^{22} + n_{12}^{32} + n_{22}^{02} + n_{22}^{12} + 2n_{22}^{22} + n_{23}^{20} + n_{23}^{21} + n_{24}^{20},\\
n_3^1(\mathrm{X}) &= {}^1/_3\,(n_{13}^{01} + n_{13}^{11} + n_{13}^{21} + n_{13}^{31} + n_{23}^{01} + n_{23}^{11} + n_{23}^{21} + n_{33}^{01} + 2n_{33}^{11} + n_{34}^{10}).
\end{aligned}
\tag{4}
$$

If the expressions given by (4) for n_i^k (H) and n_i^k(X) in terms of n_{ij}^{kl} are substituted in (3), and the corresponding terms are grouped, we obtain for the physicochemical property P, the equation

$$
P_{\mathrm{C}_n\mathrm{H}_{2n+2-m}\mathrm{X}_m} = \sum_{ij}^{kl} n_{ij}^{kl} P_{ij}^{kl}, \tag{5}
$$

which does not contain terms with coefficients n_i^k. The new constants P_{ij}^{kl} are combinations of the partial properties p_{ij}^{kl}, p_i^k (H), and p_i^k (X), arising from the above subtypes of the C−C, C−H, and C−X bonds; the expressions for P_{ij}^{kl} are not reproduced so as to avoid encumbering the text.

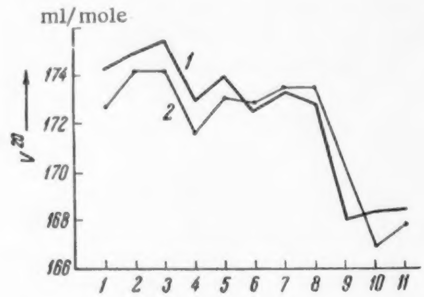

Fig. 1. Experimental (1) and calculated (2) values of the molecular volume, V^{20}, in ml/mole of some alcohols $C_9H_{19}OH$.

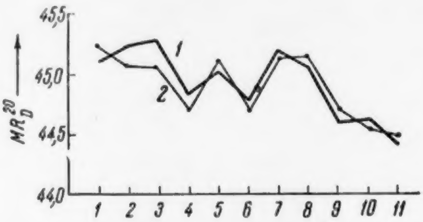

Fig. 2. Experimental (1) and calculated (2) values of the molecular refraction, MR_D^{20}, in ml/mole of some alcohols $C_9H_{19}OH$.

Thus, the physicochemical property, P, of a substance is represented in the final calculation by the the number of C−C chemical bonds of the various subtypes and some values of P_{ij}^{kl} which, according to the scheme of evaluation, must remain relatively constant for all the compounds of a given class. These constants cannot yet be calculated theoretically. Verification of the usefulness of Equation (5) and, hence, of the above conception, can be obtained, either by comparing P_{ij}^{kl} values calculated from experimental values of a physicochemical property, P, for different compounds of the type (1) with a given substituent X, or by determining P_{ij}^{kl} values for one group of compounds of this type and using these values to calculate P for comparison with experimental results for another group of compounds.

So far the scheme has only been tested by calculating some physicochemical properties of monohydric alcohols (X = OH). The precision of these calculations is illustrated in Figs. 1 and 2 by curves showing the experimental and calculated values of the molecular volumes and refractions of some alcohols. The points on the x-axis correspond to different isomers of the alcohol $C_9H_{19}OH$: 1) nonan-1-ol, 2) nonan-3-ol, 3) nonan-5-ol, 4) 3-methyloctan-4-ol, 5) 2,5-dimethylheptan-5-ol, 6) 2,5-dimethylheptan-4-ol, 7) 2,2,4-trimethylhexan-4-ol, 8) 3,5,5-trimethylhexan-3-ol, 9) 2,4-dimethyl-3-ethylpentan-3-ol, 10) 2,2-dimethyl-3-ethylpentan-3-ol, 11) 2,2,3,4-tetramethylpentan-3-ol.

The thick lines on the figures show the experimental data, the thin lines show the calculated results. The coincidence of these lines is satisfactory; the general shapes of the curves agree well. Without the use of the conception of subtypes of bond in this case (isomers with the same molecular weight) we should obtain constant values of the physicochemical characteristics, which would be contrary to the experimental results.

TABLE 1

Values of the Constants P_{ij}^{kl} in ml/mole for Calculating the Molecular Volumes and Refractions of Monohydric Alcohols

P_{ij}^{kl}	V^{20}	MR_D^{20}	P_{ij}^{kl}	V^{20}	MR_D^{20}
P_{12}^{10}	35,32	9,404	P_{23}^{10}	2,37	3,806
P_{12}^{01}	38,57	8,806	P_{23}^{01}	4,77	3,921
P_{13}^{10}	26.67	8,191	P_{24}^{10} *	(−3,81)	(3,454)
P_{13}^{01}	31,50	7,347	P_{33}^{01}	−5,91	2.528
P_{14}^{10}	—	—	P_{34}^{10}	−15,61	1.590
P_{22}^{01}	13,74	5,262			

* The value of this constant was obtained from only one equation.

The values of the constants P_{ij}^{kl} for calculating the molecular volumes and refractions of monohydric alcohols, shown in Table 1, were obtained by the method of least squares from the experimental values of these characteristics for 54 alcohols (for which there was data in the literature on d_4^{20} and n_D^{20}). The values of the constants P_{ij}^{kl} (k and l = 0), for the C−C bond isolated from the hydroxyl group, are the same as the corresponding values for the alkanes calculated by Tatevskii and his co-workers, and may be obtained from [2]. Recently the scheme has also been used for calculating the magnetic susceptibilities of some alcohols [3], and the agreement between experimental and calculated results was again fully satisfactory.

It would be very interesting to test the application of the scheme to calculating the properties of compounds of other types (X = F, Cl, Br, I, NH_2, etc.). But it is already clear that possibilities of explaining and predicting values of the physicochemical constants of organic compounds based, in particular, on such conceptions of the theory of chemical structure as the valency state of the atom and type and subtype of chemical bond, have a wider application than was shown previously [2], both in respect to the groups of substances and properties which can be included.

LITERATURE CITED

[1] V. M. Tatevskii, Proc. Acad. Sci. USSR 74, 2 (1950); 75, 6 (1950).

[2] V. M. Tatevskii, Chemical Structure of Hydrocarbons and Regularities in Their Physicochemical Properties *(Moscow, 1953).

[3] V. A. Ziborov, Iu. A. Pentin, and V. M. Tatevskii, J. Phys. Chem. 32, Part 3 (1958).

Received November 17, 1956.

* Original Russian pagination. See C. B. Translation.

INVESTIGATION OF THE RADIOLYSIS OF HYDROCARBONS BY A SPECTRAL METHOD

L. S. Polak, Academician A. V. Topchiev,
N. Ia. Cherniak and I. Ia. Kachkurova

The greatest difficulty in investigating the radiolysis of hydrocarbons is the qualitative and quantitative analysis of the liquid products. The determination of the ultraviolet and infrared absorption spectra is an essential aid in this respect.

In the radiolysis of alkanes the basic process is the rupture of the C–H bond, a process of dehydrogenation; hydrogen accumulates in the gas phase, while different liquid products are formed according to whether the original alkane molecules lose hydrogen in the form of atoms or molecules. The loss of an atom of hydrogen leads to the formation of the radical C_7H_{15}, which enters into a further reaction with loss of hydrogen, to give a residue in the liquid phase in the form of heptene; the loss of $2H_2$ with the production of two double bonds must lead to the formation of a diene, which subsequently actively dimerizes and polymerizes.

The ultraviolet absorption spectrum can be used to establish the presence of conjugated dienes in the radiolysis products, and the infrared spectrum to detect compounds with an ethylenic linkage (heptenes, etc.); other individual products of radiolysis can also be detected.

We investigated the radiolysis of alkanes under the action of γ-rays from Co^{60} sources of nominal strength 1400 and 20,000 curies. Irradiation was carried out in glass ampules which had been evacuated and sealed in the absence of oxygen. The gaseous and liquid phases of the radiolysis products were investigated separately after opening the ampules. The main part of the work was done with heptane, but some other available normal alkanes and isooctane and cyclohexane were also irradiated.

The ultraviolet spectra were obtained, with a spectroscope having an attachment for automatic recording, in the Optical Laboratory of the Institute of Organometallic Compounds of the Academy of Sciences of the USSR. The spectra were usually determined over the range $30\text{-}45 \cdot 10^3$ cm^{-1}, and in special cases over the range $25\text{-}45 \cdot 10^3$ cm^{-1}. Figure 1 shows some of the curves obtained; the dose in millions of roentgens and the dilution of the sample are given for each curve. It is clear that irradiated n-hexane, heptane and octane gave similar curves with absorption maxima in the region of $40\text{-}44 \cdot 10^3$ cm^{-1}. The spectrum of irradiated isooctane was similar to that of irradiated octane. In addition to the above band, there was a further band at longer wavelength in the spectrum of irradiated dodecane, and this was even more pronounced in the spectrum of irradiated cetane. The spectrum of irradiated cyclohexane was different from that of hexane and the other normal hydrocarbons, for an equal dosage of $40 \cdot 10^6$ r.

It is well known that saturated hydrocarbons are completely transparent in the region under consideration – $\sim 30\text{-}45 \cdot 10^3$ cm^{-1} (the absorption curves of the nonirradiated hydrocarbons correspond to the base line in Fig. 1), and that isolated ethylene bonds absorb at a considerably shorter wavelength.

On the other hand, the absorption of the conjugated dienes is very strong and has a maximum ($\epsilon \sim 20,000$) in the range $\sim 42\text{-}46 \cdot 10^3$ cm^{-1}, which is precisely in the region where we found maxima.

Thus, the absorption shown by the irradiated alkanes in the region stated is in accordance with the formation of conjugated dienes (and polyenes).

There is no doubt that aromatics were formed in irradiated cyclohexane. Their presence was also shown in the usual way – a positive formalite reaction with irradiated cyclohexane (nonirradiated material gave a negative reaction).

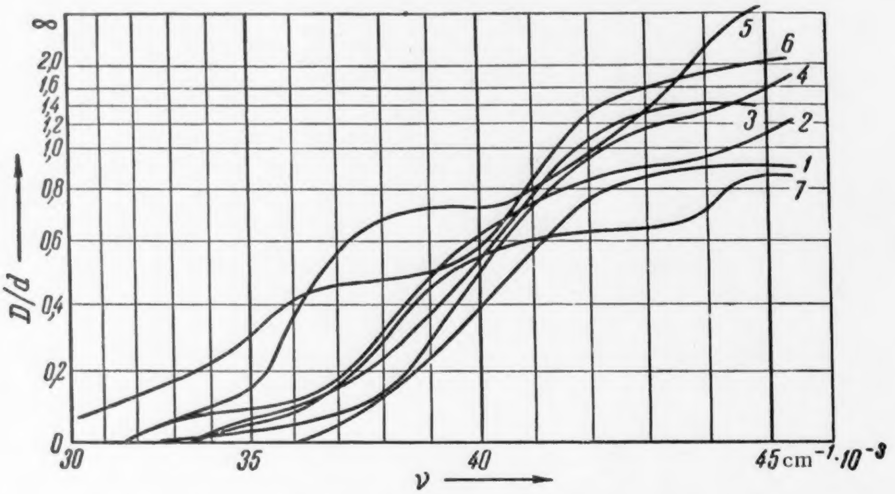

Fig. 1. Ultraviolet absorption spectra of irradiated hydrocarbons. 1) n-Heptane, dose $99 \cdot 10^6$ r, dilution 1:10; 2) isooctane, dose $40 \cdot 10^6$ r, dilution 1:5; 3) n-octane, dose $40 \cdot 10^6$ r, dilution 1:5; 4) n-hexane, dose $34 \cdot 10^6$ r, dilution 1:5; 5) n-dodecane, dose $40 \cdot 10^6$ r, dilution 1:10; 6) n-cetane, dose $40 \cdot 10^6$ r, dilution 1:5; 7) cyclohexane, dose $40 \cdot 10^6$ r, dilution 1:20.

Ten times as much methane was formed by irradiation from isooctane as from n-octane, and there was a corresponding decrease in the amount of hydrogen formed, which must have been accompanied by a decrease in the formation of dienes. In practice we found:

	Integrated absorption in the region $38 \cdot 10^3$ - $45 \cdot 10^3$ cm^{-1}
n-octane	25.50
isooctane	20.45

Figure 2 shows the ultraviolet absorption curves of three fractions, obtained by fractionating irradiated heptane (without heating). Fraction I was the most volatile, IV was the heavy yellow residue with a molecular weight ~ 200; the spectrum of fraction III coincided with that of the original heptane, and is not reproduced. Consideration of the curves shows that the absorption of the two volatile fractions is characterized by a boundary on the long wavelength side and a decrease in the range $42.5\text{-}45.5 \cdot 10^3$ cm^{-1} (the curves differ from each other only in the intensity of absorption; the dilution for fraction I was 1:40 and for II was 1:10). The absorption found can only be due to the presence of dienes (probably mainly heptadiene, which has a volatility very close to that of heptane).

Consideration of Fig. 2 supports the view that in the radiolysis of heptane, together with other conversions, dehydrocyclization can occur with formation of toluene. This possibility will be examined by us carefully in a subsequent experimental investigation.

The absorption curve of the heavy residue (which, after separation from the original heptane, fluoresced strongly in ultraviolet light) showed a continuous increase in absorption from $35 \cdot 10^3$ to $45 \cdot 10^3$ cm^{-1} (the high dilution of 1:100 was required). Here, it is clear that absorption was due to polyenes as well as to conjugated dienes, and probably also to all the possible dimers and polymers obtained as the result of secondary reactions between dienes and polyenes.

Thus, the results obtained from the fractionation of irradiated heptane confirm and make more precise the results of Fig. 1.

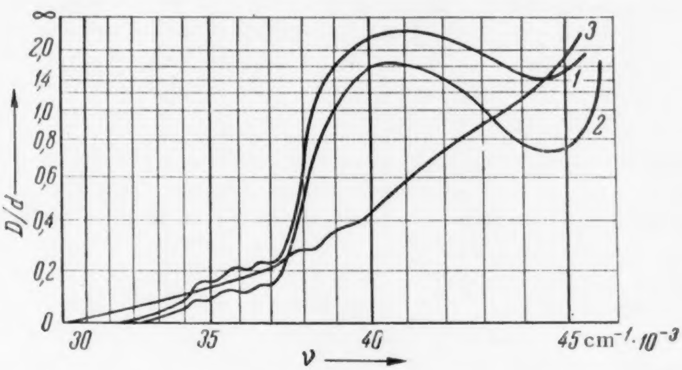

Fig. 2. Ultraviolet absorption spectra of fractions of irradiated heptane (dose $137 \cdot 10^6$ r). 1) Fraction I, dilution 1 :40; 2) Fraction II, dilution 1 :10; 3) Fraction IV (residue), dilution 1 :100.

The dependence of the intensity of absorption in the range $38 \cdot 10^3$ - $42 \cdot 10^3$ cm^{-1} on the molecular weight of the alkane used is shown in Fig. 3, a. The abscissa shows the number of carbon atoms in the molecule of different liquid alkanes, the ordinate shows the intensity of absorption $E_{42} = \frac{D}{d} \times$ dilution at a frequency of $42 \cdot 10^3$ cm^{-1} ($D = \log \frac{I_0}{I_{trans}}$; d is the cell thickness; dilution of the irradiated product was necessary to avoid absorption of all the incident light) and also S_i, the area bounded by the absorption curve, the ordinates at $38 \cdot 10^3$ and $44 \cdot 10^3$ cm^{-1} and the abscissa, which is the line of full transmission (the zero line of the original nonirradiated alkane).

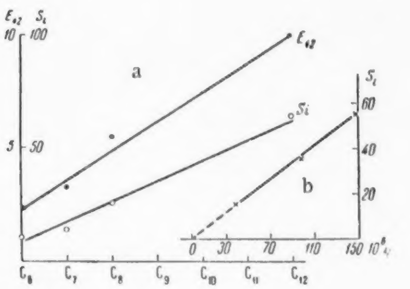

Fig. 3. a) The dependence of the intensity of absorption on the molecular composition of the irradiated hydrocarbon, and b) the dependence of the intensity of absorption of irradiated heptane on the dose.

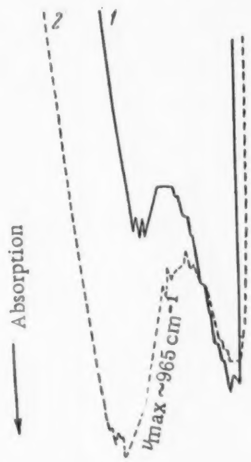

Fig. 4. Infrared absorption spectra 1) of original and 2) of irradiated ($158 \cdot 10^6$ r) n-heptane.

Both the functions characterizing the absorption of the dienes formed by the irradiation of different alkanes can be represented by straight lines, to which the experimental points well approximate. Thus, in the range C_6 to C_{12}, the absorption of the dienes increases with the number of CH_2 groups in the alkane molecule. Since the formation of a diene involves the loss of four hydrogen atoms, it is reasonable to suppose that the probability of such a reaction would increase with the number of CH_2 groups.

Figure 3, b shows the relation between the intensity of ultraviolet absorption of irradiated heptane and the radiation dose. Although only three points have been determined, a straight line can be drawn through them with some confidence, since, up to $150 \cdot 10^6$ r all the indices characterizing the change of heptane under irradiation show a linear increase, and the points on the graph lie close to the straight line. Since, as we showed above, the ultraviolet absorption in this particular region is caused by dienes (or polyenes), the straight line shows that there is a linear increase in the quantity of dienes with dosage from 40 to 150 million r. At lower doses the relation is almost sure to be linear. Further experimental work would be necessary to be certain of what happens at higher dosage.

The infrared absorption spectra of the original and of irradiated (dose $158 \cdot 10^6$ r) heptane, in the region 900-1000 cm^{-1} are shown in Fig. 4. The rest of the infrared spectra, which were recorded with an IKS-11 instrument, are not reproduced as no difference between the two spectra could be observed. The measurements were made twice with slits of 0.270 and 0.235 mm. It is clear from a comparison of the curves in Fig. 4 that irradiated heptane has a distinct band with $\nu_{max} \sim 965$ cm^{-1} (different from the original heptane). It is known that this band corresponds to the $-CH{=}CH-$ bond with a trans configuration. Although it is possible that other olefins might be formed by the radiolysis of heptane, the formation of trans-heptene is the most probable process. The production of this heptene is accompanied by the formation of a molecule of hydrogen in the gaseous products of radiolysis, i.e., this is one of the primary processes of dehydrogenation by radiolysis. Similar results using infrared spectra were obtained in [2].

We express our deep gratitude to Corresponding Member of the Academy of Sciences of the USSR, I. V. Obreimov for making it possible to record the ultraviolet absorption spectra and to Professors S. R. Sergienko and M. P. Teterina for recording the infrared spectra.

LITERATURE CITED

[1] A. Gillam and E. Stern, Electronic Absorption Spectra of Organic Compounds (IL, 1957).*

[2] N. A. Slovokhotova and V. L. Karpov, Collection of Papers on Radiation Chemistry, Bull. Acad. Sci. USSR (1955), p. 206.

Institute of Petroleum of the
Academy of Sciences of the USSR

Received October 8, 1957.

* Russian translation.

KINETICS OF THE PROCESS OF FORMATION OF OXIDE FILMS ON TUNGSTEN AND MOLYBDENUM

V. A. Arslambekov and K. M. Gorbunova

(Submitted by Academician P. A. Rebinder, October 4, 1957)

During an investigation of the kinetics of processes of oxidation of tungsten and molybdenum, using a method capable of detecting changes in weight to a high accuracy, together with the results characterizing the oxidation of these metals, some facts were discovered whose consideration is of interest for the interpretation of data on the kinetics of oxidation of any metals.

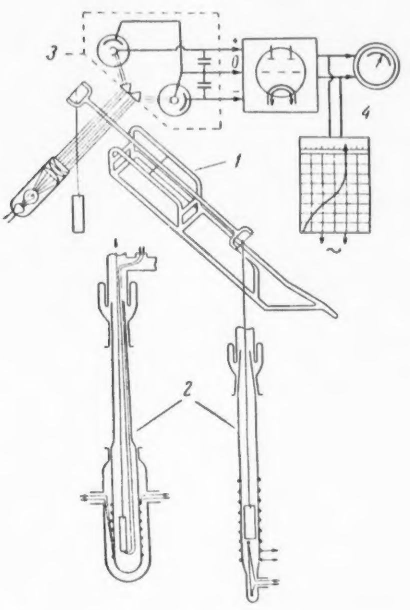

Fig. 1. Diagram of apparatus. 1) Balance; 2) tube furnace; 3) measuring equipment; 4) recording galvanometer.

The apparatus used made it possible to carry out continuous observation of the growth of the oxide film over a wide range of oxygen pressure and temperature by a weighing method. Weighing was accomplished with the aid of a specially constructed vacuum quartz microbalance of the beam type (Fig. 1). The sensitivity of the balance was $5 \cdot 10^{-7}$ g for a division of the microscale (equal to 0.001 mm) for a load of 7 g. The time of swinging of the balance was 5 seconds. Together with visual observation, an automatic record could be obtained of the change in weight, using suitable electronic equipment and a recording galvanometer.

The sample, attached by a long platinum wire to the beam of the balance, was heated by a tube furnace, constructed in one of two ways: with a vacuum jacket for high temperatures, and without one for medium temperatures. With this type of construction the furnace reached a temperature of 1050° with a vacuum of $1 \cdot 10^{-7}$ mm Hg (a bifilar winding was used). The temperature was measured with a thermocouple situated in the immediate neighborhood of the sample (1-2 mm away), and was maintained constant with with an accuracy of ± 2°. The oxygen was obtained by the decomposition of pure potassium permanganate and was purified by passage through granules of pure KOH and a trap cooled by liquid oxygen. The sample was prepared from tungsten or molybdenum foil, of purity 99.95% with a surface of 8 to 30 cm^2 and a weight of 5 g, and was subjected to various preliminary treatments. The samples of the first series were ground and immediately degreased by treatment with a solution of KOH. The samples of the second series were ground, subjected to electrolytic polishing and finally washed carefully with distilled water. The samples of the third series were oxidized after receiving the above treatment and the oxide formed was either reduced with hydrogen at a temperature of 600° and P_{H_2} = 20 mm Hg, or completely evaporated in vacuo (~ 10^{-7} mm Hg) at temperatures of 600 and 1050° for molybdenum and tungsten, respectively.

The method described for the preparation of the surface and the high sensitivity of the balance enabled us, for the first time, to follow the oxidation of tungsten and molybdenum at temperatures close to room temperature (Fig. 2), which was not achieved previously even in such careful work as that of Gulbransen and Wysong [1]; the latter did not detect the formation of an oxide film on Mo at room temperature.

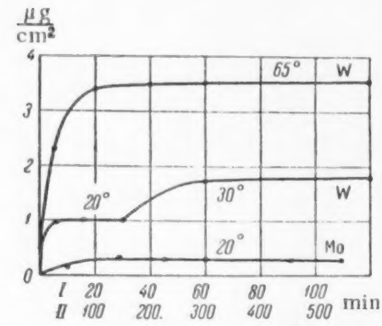

Fig. 2. Oxidation of tungsten and molybdenum at P_{O_2} = 100 mm Hg. I) W; II) Mo.

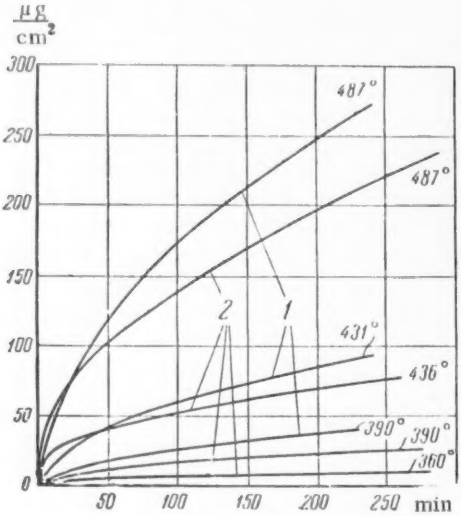

Fig. 3. Oxidation of tungsten at P_{O_2} = = 24 mm Hg. 1) Ground; 2) polished electrolytically.

At higher temperatures, the quantity of oxygen reacting both with molybdenum and tungsten increased noticeably, and there was a considerable rise in the rate of growth of the oxide film on these metals. At temperatures above 300° the growth of the oxide film on both tungsten and molybdenum could be expressed by an equation of the parabolic type – $X^2 = kt + C$.

It was found experimentally that the value of $\underline{k}$, the oxidation velocity constant, depended very little on the size of the original (specific) surface in the case of oxide films of significant thickness. Thus, for samples of molybdenum with the same apparent surface, but with very different true surfaces (one sample after electrolytic polishing, the other after reduction in hydrogen of the previously formed MoO_2 film), the velocity constants at a given temperature were found to be equal, but the values of the constant C in the equation differed considerably. For polished samples C was practically zero, and for reduced samples C was nearly equal to the quantity of oxygen used in the preliminary formation of the oxide film.

Though the increase of the specific surface, due to roughening of the surface layers of metal by reduction of oxide, hardly affected the velocity constant, $\underline{k}$, yet the difference in the surface state of samples, subjected only to grinding or to grinding followed by electrolytic polishing, had a great effect on the value of $\underline{k}$ and even of the activation energy, but not on the value of the constant C. The effects of this difference in surface treatment on the course of the kinetic curves are well illustrated in Fig. 3.

The variations with temperature of the velocity constants of oxidation of tungsten and molybdenum, for samples with different surface pretreatments, are shown in Fig. 4. Values of the activation energy are shown in Table 1.

A probable explanation of the differences in activation energies of samples of tungsten, subjected to grinding and electrolytic polishing, is that the grinding produces severe mechanical distortion of the surface layers which leaves permanent strains. In the case of samples subsequently subjected to electrolytic polishing, the strained surface layer is dissolved. Indeed, electron diffraction by the latter gave a clear pattern, characteristic of rolled tungsten with a structural axis [001]. The activation energy for the oxidation of the ground samples is reduced, obviously because of the strains caused by grinding.

Both for tungsten and molybdenum, the slope of the line relating log k and 1/T is different below 360°; the slope shows that, in this temperature region, the process is proceding with a lower energy of activation, and, indeed, that the activation energy is half that prevailing at higher temperatures.

Kinetic measurements, made when a particular sample was oxidized with successive changes from one temperature region to another (carried out with a number of samples at different conditions and temperatures),

showed that the velocity constant was greatly affected by the thickness of the oxide film. The velocity constant was greatest for a small film thickness, and decreased several fold with increasing film thickness at the same temperature. These relationships are evident from the data of Fig. 4.

TABLE 1

Experimental conditions	Temperature range in ° C.	E in kcal/mole
	Tungsten	
Electrolytic polishing, P_{O_2} = 24 mm	360-500	46.5
Grinding, P_{O_2} = 24 mm	390-500	41.0
Grinding, P_{O_2} = 100 mm	360-550	43
Grinding, P_{O_2} = 100 mm, thin film	200-360	22
	Molybdenum	
Grinding, P_{O_2} = 100 mm	360-500	36.0
Grinding, P_{O_2} = 100 mm, thin film	320-360	25

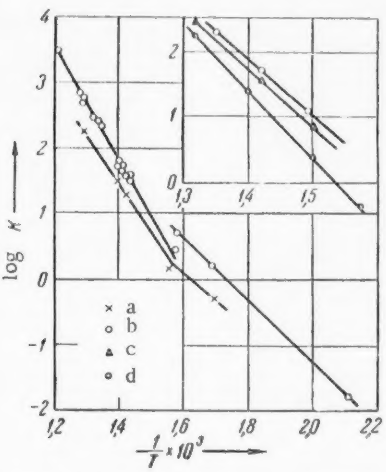

Fig. 4. Relation between velocity constant and temperature for the oxidation of tungsten and molybdenum. a) Molybdenum; b) tungsten, ground, P_{O_2} = 100 mm Hg; c) tungsten, ground, P_{O_2} = 24 mm Hg; d) tungsten, polished electrolytically, P_{O_2} = 24 mm Hg.

An obvious explanation of this dependence of the velocity constant on the thickness of the oxide film is that the growth of the oxide controls the diffusion of components through the film, a process which is known to occur along the grain boundaries and within the crystal lattice. At lower temperatures the oxidation process is slow, and the oxide film does not become very thick and is commensurable with the dimensions of the crystallites composing it, so that the decisive role in the transfer of reacting components must be played by diffusion along the grain boundaries (or of blockages, forming in the separate grains in consequence of irregular development and growth of nascent oxide), characterized by a low energy of activation. With an increase of film thickness to a value somewhat exceeding the dimensions of the individual oxide grains, the rate of oxidation begins to be controlled by diffusion of components throughout the crystal lattice, which is associated with a higher activation energy. The role of temperature in this is taken to be its effect on the rate of transfer from the region of small thickness of oxide (with the process controlled by diffusion between crystallites) to the region of thick oxide, with control by diffusion through the whole volume.

LITERATURE CITED

[1] E. Gulbransen and W. Wysong, Metals Technol. 14, 6, Techn. Publ. 2224, 2226 (1947).

Institute of Physical Chemistry,
Academy of Sciences of the USSR

Received September 27, 1957.

EFFECT OF THE DEHYDRATION OF THE SURFACE OF SILICA GEL ON THE ADSORPTION OF VAPORS OF BENZENE AND HEXANE

L. D. Beliakova and A. V. Kiselev

(Submitted by Academician M. M. Dubinin, August 10, 1957)

Investigation of the dehydration of the surface of adsorbents, which are proton acids, is of interest because the presence of surface hydroxyl groups increases the energy of adsorption of substances having electron donor properties [1, 2]. This does not only apply to adsorbates capable of forming hydrogen bonds, but also to unsaturated and aromatic hydrocarbons, capable in some cases of forming molecular π-complexes with proton acids. Thus, baking silica gel in air so as to dehydrate the surface, decreases the adsorption of benzene vapor as well as of methanol [3]. With an increase of the hydration of a silica surface, obtained by combustion of a silico-organic compound, there is a rise in the adsorption and heat of adsorption of benzene vapor, whereas the corresponding values for hexane remain practically unaltered [4].

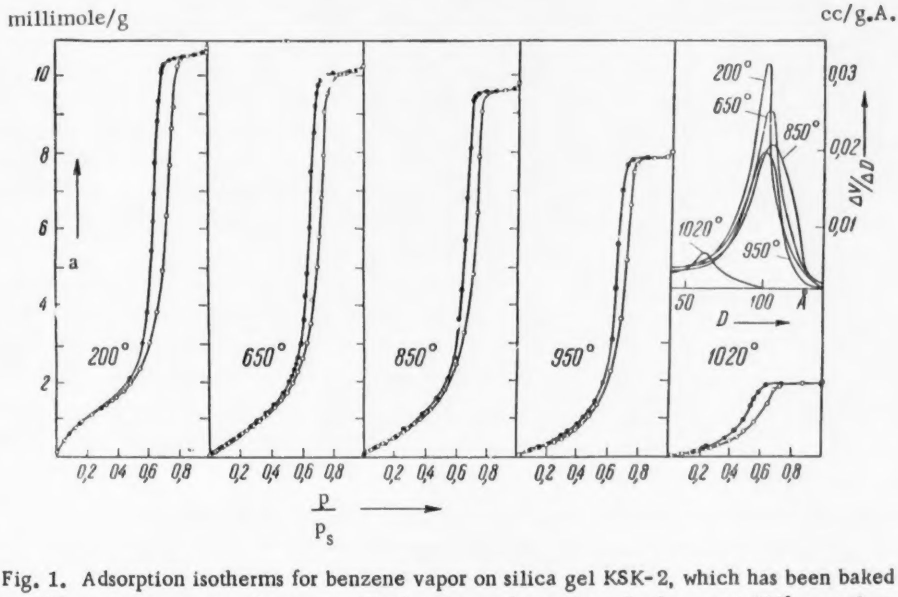

Fig. 1. Adsorption isotherms for benzene vapor on silica gel KSK-2, which has been baked at different temperatures in vacuo. Black points — desorption. Isotherms at 200° are taken from [8]. Top right — curves for the distribution of pore size, calculated from the isotherms.

In this paper we have investigated the dependence of the adsorption of benzene and hexane vapors on the concentration of hydroxyl groups in the surface of large pore silica gel KSK-2,* the changes in the gel being

* This sample of silica gel was investigated in [5 and 6].

produced by dehydration in vacuo. This was done by placing the sample (about 3 g) in the quartz cartridge of a vacuum apparatus, and baking at temperatures of 200, 400, 500, 650, 850, 950, and 1020°. At 200 and 400° evacuation was continued for about 100 hours, and at higher temperatures for 25 to 60 hours. The criterion for the termination of baking was the practical cessation of the evolution of water at the given temperature.* The liberated water was absorbed by magnesium perchlorate and weighed on a quartz spring balance [7]. The accuracy of this determination was $5 \cdot 10^{-6}$ g of water for 1 g of silica gel. After dehydration at each of the stated temperatures, adsorption isotherms were measured for nitrogen at − 195° (to determine the specific surface of the sample) and for benzene and hexane vapors at 20°. These two hydrocarbons with the same number of carbon atoms in the molecule are adsorbed differently by acid adsorbents, and a comparison of their behavior provides a means of estimating the condition of the surface of the adsorbent. Adsorption and desorption isotherms of benzene vapor were measured up to the pressure ratio $p/p_s = 1$. Adsorption isotherms of hexane vapor were measured up to $p/p_s \approx 0.4$.

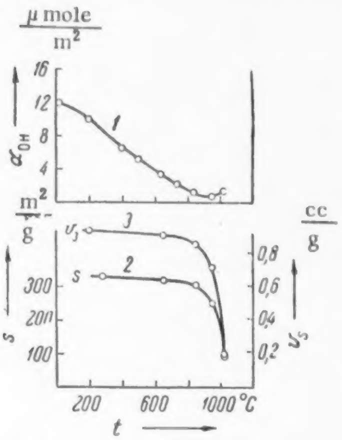

Fig. 2. Changes in 1) surface concentration of hydroxyl groups α_{OH}, 2) specific surface s and 3) total volume of pores v_s, as functions of the temperature of baking of silica gel KSK-2 in vacuo.

Figure 1 shows the adsorption and desorption isotherms of benzene vapor. It is evident from this figure that the adsorption of benzene vapor, in the region of monomolecular coverage, strongly decreases with increasing temperature of baking of the silica gel, and that there is also a change in the shape of the isotherm from convex to concave. Figure 2 shows the effect of the temperature of baking in vacuo on the specific surface s, the pore volume v_s, and the concentration of hydroxyl groups α_{OH} in the surface of the silica gel. On heating the silica gel to 850° both the surface of the sample s and the pore volume v_s decreased by 9%, and, on heating to 950°, by 20%. However, from the distribution curves of pore size, in effect diameter (Fig. 1), it is obvious that the pore size did not alter. Significant contraction of the pores only occurred on heating to a higher temperature. Thus, after baking at 1020° the mean pore diameter decreased from 100 to 62 A, and, as is evident from the distribution curves, the narrower pores came to occupy a considerable proportion of the pore space. Thus, baking a large pore silica gel in vacuo [9, 10] produced no significant change of structure, and heating to approximately 900° did not alter its surface appreciably.** From Fig. 2 it is clear that the concentration of hydroxyl groups in the surface of silica gel suffered a more than tenfold reduction as the result of baking the sample at 950°.*** The total quantity of gas evolved between 400 and 1020° amounted to about 4 μ moles per g, i.e., considerably less than in [13].

Thus, in investigating the adsorption of hydrocarbons on wide pore samples, baked at temperatures from 200 to 950°, we were using silica gels of the same pore structure, but with different degrees of hydration of the surface, which enabled us to study the dependence of the adsorption of benzene and hexane vapors on the single factor of the variation of the concentration of hydroxyl groups in the surface of the gel.

The left hand side of Fig. 3 shows absolute adsorption isotherms of benzene vapor in the monomolecular region, obtained from the experimental isotherms of Fig. 1 by calculation to unit surface, determined from the adsorption of nitrogen. The absolute adsorption isotherms for hexane vapor are shown on the right of Fig. 3.

The adsorption isotherms of hexane vapor on hydrated silica gel are nearly linear, and are very similar in character to those for hexane vapor on liquid water [14]. While the adsorption of hexane vapor is practically

* In the last 12 hours evacuation liberated about $3 \cdot 10^{-4}$ g of water from 1 g of silica gel.

** Baking in air [11] and in water vapor [10] causes a considerable reduction in surface at lower temperatures.

*** The slight rise in the curve at a temperature of 1020° is probably associated with the occurrence of part of the "structural water" of silica gel within the primary particles of the skeleton, and its evolution at high temperatures. It cannot be attributed to the surface, but its quantity is small, as is also shown by experiments on deuterium exchange [12].

unaffected by a tenfold change in the hydration of surface, the adsorption of benzene vapor decreases by a factor of 3.5 (at $p/p_s = 0.1$, curves for KSK-2 at 200 and 950°).

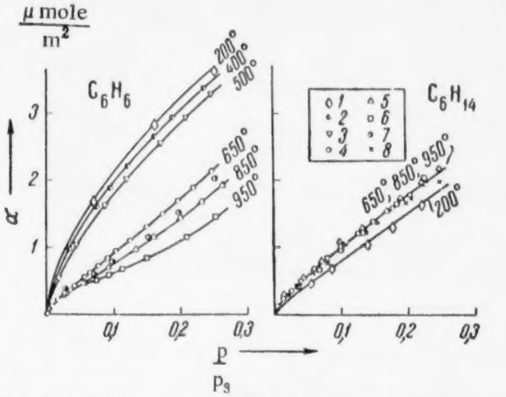

Fig. 3. Absolute adsorption isotherms of benzene (left) and hexane (right) vapors on the surface of silica gel KSK-2 which has been baked in vacuo at 1) 200°, 2) 400°, 3) 500°, 4) 650°, 5) 850°, 6) 950°, and 7) 1020°. 8) represents data for quartz.

In the case of the adsorption of hexane on silica gel there is a Van der Waals interaction with the participation, not only of the surface atoms of the adsorbent, but also of atoms within the particles of the skeleton, so that changes in the electrical and magnetic properties of the surface, caused by dehydration, do not significantly alter the energy of adsorption of saturated hydrocarbons. Van der Waals forces also have an important role in the adsorption of benzene, but the adsorption energy of benzene by purely Van der Waals adsorption [15] is less than the adsorption energy of hexane. As opposed to adsorption on graphite [15], it is evident from Fig. 3 that the adsorption of benzene vapor on the hydrated surface of silica gel considerably exceeds that of hexane, and the heat of adsorption of benzene vapor on the hydrated surface of silica is greater than that of hexane [8]. This shows that, in the adsorption of benzene on the hydrated surface of silica, there is an additional interaction of the π complex type [1, 2, 8, 16, 17] in addition to the Van der Waals interaction. Unlike hexane, benzene vapor shows a marked decrease in adsorption with a fall in the concentration of OH groups in the surface of the gel, because there is a decrease in the possibility of this additional interaction between benzene molecules and OH groups in the surface. With removal of hydroxyl groups from the surface there is a reduction in the additional specific interaction, which is characteristic of the adsorption of benzene on the hydrated surface of silica gel. While on a hydrated surface the absolute value of the adsorption of benzene vapor, at a pressure ratio $p/p_s = 0.1$, is more than 2.5 times that for hexane (Fig. 3), on a dehydrated surface the absolute values of the adsorptions of benzene and hexane vapors are always similar, because on the dehydrated surface the molecules of both benzene and hexane are only held by Van der Waals interaction. Since the polarizability of hexane is greater than that of benzene, the adsorption of hexane vapor on the dehydrated surface of silica gel, as also on the surface of graphitized soot [15], is somewhat greater than that of benzene vapor. Thus, at $p/p_s = 0.1$, the adsorption of hexane on silica gel KSK-2 at 950° is 1.7 times that of benzene.*

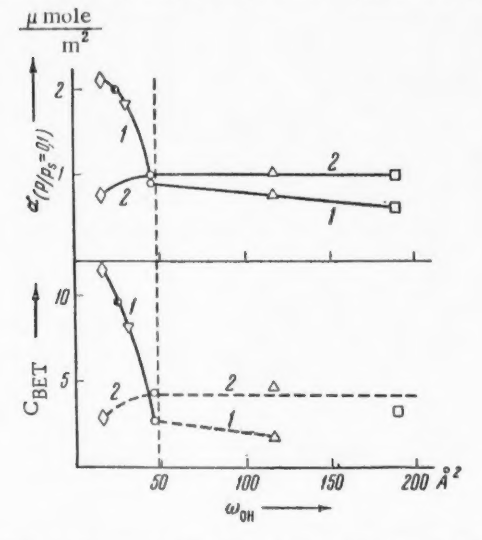

Fig. 4. Dependence of the absolute value of the adsorption at $p/p_s = 0.1$ and of the constant C in the BET equation on the area, ω_{OH}, available per hydroxyl group, 1) for benzene and 2) for hexane. The designations of the points are the same as in Fig. 3. The vertical dotted line shows the value of $\omega_{C_6H_6}$.

Figure 4 shows the dependence of the absolute value of the adsorption at $p/p_s = 0.1$, and of the constant C in the BET equation, on the area, ω_{OH}, available per OH group, for both benzene and hexane.** It is clear from this figure that the main fall in adsorption and energy of adsorption for benzene vapor occurs over a relatively narrow range of α_{OH}, approximately from 3.5 to 5.5 μmole/m², which corresponds to a change of ω_{OH} from 30 to 45 A². Since the

* It is evident from Fig. 3 that adsorption of hexane vapor on silica gel, baked at 650° or above, coincides with adsorption on quartz [18]. The adsorption isotherms of benzene vapor on samples baked at 1020° lie above those on samples baked at 850 and 950° (Fig. 3), showing that there is an increase in adsorption potential in the narrow pores [16], which occupy a large part of the total pore space in samples baked at 1020°.

** See footnote on following page.

benzene molecule occupies about 49 A^2 [8, 16], when adsorbed on the surface of silica gel as a compact monolayer, the rapid fall in the adsorption of benzene in this region is obviously associated with the inability of benzene molecules to interact simultaneously with hydroxyl groups in the surface.

LITERATURE CITED

[1] A. V. Kiselev, Proc. Acad. Sci. USSR 106, 1046 (1956).***

[2] A. V. Kiselev in Coll. "Surface Chemical Compounds and their Role in Adsorption Phenomena,"**** (Moscow, 1957), pp. 90, 199.

[3] A. V. Kiselev, K. G. Krasil'nikov, and L. N. Soboleva, Proc. Acad. Sci. USSR 94, 85 (1954).

[4] A. A. Isirikian and A. V. Kiselev, Proc. Acad. Sci. USSR 115, 343 (1957).***

[5] A. A. Isirikian and A. V. Kiselev, Proc. Acad. Sci. USSR 110, 1009 (1956). ***

[6] L. D. Beliakova, O. M. Dzhigit, and A. V. Kiselev, J. Phys. Chem. 31, 1577 (1957).

[7] M. A. Kaliko, in Coll. "Surface Chemical Compounds and Their Role in Adsorption Phenomena,"**** (Moscow, 1957), p. 155.

[8] A. A. Isirikian and A. V. Kiselev, J. Phys. Chem. 31, 2127 (1957).

[9] R. A. Van Nordstrand, N. E. Kreger, and H. E. Ries, J. Phys. Coll. Chem. 55, 621 (1951).

[10] G. Rice, Coll. Papers on Catalysis, "Catalysis of Organic Reactions," ***** (IL, 1955), p. 37.

[11] G. K. Boreskov, M. S. Borisovan et al., Proc. Acad. Sci. USSR 62, 649 (1948).

[12] R. G. Haldeman and P. H. Emmett, J. Amer. Chem. Soc. 78, 2117 (1956).

[13] W. Stöber, Koll. Zs. 145, 17 (1956).

[14] D. C. Jones and R. H. Ottewill, J. Chem. Soc. (1955), p. 4076.

[15] N. N. Avgul', G. I. Berezin, A. V. Kiselev, and I. A. Lygina, Bull. Acad. Sci. USSR, Div. Chem. Sci. 1304 (1956). ***

[16] A. V. Kiselev, Prog. Chem. 25, 705 (1956).

[17] A. N. Terenin, in Coll. "Surface Chemical Compounds and Their Role in Adsorption Phenomena,"**** (Moscow, 1957), p. 206.

[18] Iu. A. El'tekov, Dissertation, MGU, Chem. Fac. 1956.

M. V. Lomonosov Moscow State University.

Received June 26, 1957

** The BET equation is well satisfied by the adsorption isotherms of benzene vapor on silica gel baked at 200, 400, and 500°; the range of application of the equation narrows for samples baked at 650 and 850°. In all cases the adsorption isotherms of hexane vapor are less well expressed by this equation [16], but there is no doubt about the consistency of the values of the constant C.

*** Original Russian pagination. See C. B. Translation.

**** In Russian.

***** Russian translation.

CATALYTIC ACTIVITY OF GERMANIUM WITH RESPECT TO THE REACTION OF ISOTOPIC EXCHANGE BETWEEN HYDROGEN AND DEUTERIUM

G. K. Boreskov and V. L. Kuchaev

(Submitted by Academician A. A. Balandin, October 9, 1957)

The object of our work was to compare the specific catalytic activity of the semiconductor element germanium with the activity of transition metals having unfilled d-levels, with respect to the reaction of isotopic exchange between hydrogen and deuterium.

Tamaru and Boudart [1] investigated the course of this reaction at 302° on a film of germanium, obtained on glass by the thermal decomposition of GeH_4. The adsorption of hydrogen was investigated as well as the hydrogen-deuterium exchange. The authors inclined to the view that adsorption of hydrogen on germanium occurred with dissociation into atoms. The activation energy of adsorption at small coverages was 14.6 kcal/mole the heat of adsorption 23.5 kcal/mole. The authors supposed that hydrogen atoms were linked to the germanium surface by covalent forces and that their mobility along the surface was considerably less than in the case of adsorption on metals.

EXPERIMENTAL METHODS

Apparatus. We investigated the catalytic activity of germanium by a static method with circulation. The content of HD in the hydrogen-deuterium mixture was determined by a thermal conductivity method. A detailed description of the apparatus is given in [2].

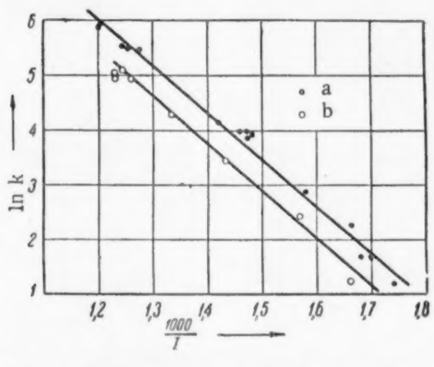

Fig. 1. Variation of the activities of the two samples of germanium with the reciprocal of the absolute temperature. a) Sample No. 1, S = 200 cm²; b) sample No. 2, S = 100 cm².

The reaction was carried out in a quartz reactor in the temperature range 300 to 550°, at pressures from 40 to 190 mm Hg, with an equimolecular mixture of hydrogen and deuterium. The reactor was separated from the rest of the system by two traps at liquid nitrogen temperature, to protect the catalyst from the action of mercury vapor, vacuum grease, etc.

Catalyst. The catalyst used was monocrystalline germanium of the electron conductor type, with a specific electrical resistance of 6 ohm·cm. The germanium was crushed in an agate mortar to a particle size of 10^{-1} mm. The surface was determined from the particle size. Two samples of germanium were investigated, with surfaces of 200 cm^2 (weight 2.8 g) and 100 cm^2 (weight 1.8 g). Owing to uncertainty as to the roughness, the actual value of the surface may have been somewhat greater. Before its catalytic activity was studied, the germanium was usually reduced at 650° by circulating the hydrogen-deuterium mixture for 6 hours.

Preparation of hydrogen and deuterium. The gases used were prepared electrolytically. To remove possible traces of oxygen and nitrogen, both the hydrogen and deuterium were passed successively through a furnace containing a palladium catalyst, silica gel as drying agent and charcoal granules cooled by liquid nitrogen. The hydrogen was also passed through a nickel chromium catalyst at 300° to establish a high temperature equilibrium between ortho and para hydrogen.

Heavy water containing 99.6% D_2O was used to prepare the deuterium.

RESULTS

The specific catalytic activity of germanium was calculated from the formula

$$k = \frac{n}{St} \ln \frac{C'_{HD} - C^0_{HD}}{C'_{HD} - C_{HD}},$$

where n is the number of moles of gas in the apparatus; S is the surface of the catalyst; C'_{HD}, C^0_{HD}, and C_{HD} are concentrations at equilibrium, initial and after reaction for time t.

TABLE 1

Pressure in mm Hg	Degree of conversion	Quantity of HD in moles (x 10^3)
189	0.49	2.8
130	0.50	1.9
40	0.50	0.5

This formula is correct for any mechanism of exchange between hydrogen and deuterium [2].

The variations of the catalytic activities kS of both samples of germanium with the reciprocal of the temperature, determined at a mixture pressure of 40 mm Hg, are shown in Fig. 1. The activation energy of the reaction is 17 kcal/mole. The specific catalytic activity of both samples of germanium at 330° was about $3 \cdot 10^{-10}$ mole/cm^2·second. The catalytic activity, determined before reduction of the sample at 650°, was somewhat higher.

The order of the reaction was investigated for the first sample of germanium at 480°. Table 1 shows the number of moles of hydrodeuterium formed after 24 minutes and the corresponding degree of conversion, for different pressures. The same degree of conversion obtained for different pressure shows that the reaction is of the first order.

DISCUSSION OF RESULTS

Table 2 shows the specific catalytic activities of germanium and some metals with respect to the reaction of hydrogen-deuterium exchange, at a temperature of 300°, and a mixture pressure of 40 mm Hg.

TABLE 2

Catalyst	Ge (film on glass)	Ge (mono-crystalline)	Fe	Co	Ni	Cu	Au
Sp. cat. activity mole/cm^2·sec	$1 \cdot 10^{-10}$	$1.5 \cdot 10^{-10}$	$1.5 \cdot 10^{-10}$	$2.4 \cdot 10^{-9}$	$3.5 \cdot 10^{-7}$	$0.65 \cdot 10^{-11}$	$5.9 \cdot 10^{-9}$
Activation energy of exchange kcal/mole	–	17	8.1	7.9	8.0	16	7.0

The specific catalytic activity of the germanium film, obtained by the thermal decomposition of GeH_4, was taken from the paper quoted [1]. It is clear from Table 2 that this activity is of the same order of magnitude as that of monocrystalline germanium in our experiments. Then, since the reaction is of the first order, and its activation energy (17 kcal/mole) is close to the activation energy of adsorption of hydrogen on germanium (14.6 kcal/mole) obtained in [1], it appears that, under the conditions of our experiments, the exchange takes place by an adsorption-desorption mechanism at small degrees of coverage of the germanium surface by gas atoms, and the limiting stage of the reaction is adsorption. On changing to a greater degree of coverage of the surface, the activation energy of the reaction must evidently increase, approaching the activation energy of hydrogen desorption (about 41 kcal/mole) at a degree of coverage close to unity.

The values of the specific catalytic activity of the metals Fe, Co, Ni, Cu, and Au in Table 2 are calculated from published data [2] on the assumption of a first order reaction. It is obvious from the table that the activities of the metals of the fourth period increase with increasing atomic number and reach their maximum with nickel.

On moving from nickel to copper, an element with a filled d-level, the catalytic activity falls sharply. It can be seen from Table 2 that at 300° the activity of germanium is of the order of 10^{-3} times that of nickel, and is close to that of iron. On moving to lower temperatures the catalytic activity of germanium must become very much less than that of the transition elements, owing to the high value of the activation energy.

The catalytic activity of copper is an order of magnitude less than that of germanium. This is clearly because the type of interaction of hydrogen with germanium is different from that with metals, and is not associated with electrons of the d-level.

LITERATURE CITED

[1] K. Tamaru and M. Boudart, Adv. in Catal. 9 (1957).

[2] M. A. Avdeenko, G. K. Boreskov, and M. G. Slin'ko, "Problems of Kinetics and Catalysis, * 9, "Isotopes in Catalysis," (1957), p. 61.

The L. Ia. Karpova Scientific Research
Physicochemical Institute.

Received October 1, 1957.

* In Russian.

A NEW METHOD OF INTERPRETING THE MAGNETIC SUSCEPTIBILITY OF DIAMAGNETIC ORGANIC COMPOUNDS

Ia. G. Dorfman

(Presented by Academician N. N. Semenov, November 13, 1957)

According to quantum mechanical theory the magnetic susceptibility κ of a diamagnetic molecule is made up from two terms, the classical Langevin diamagnetism κ_d and the quantum mechanical Van Vleck paramagnetism κ_p [1]:

$$\chi = \chi_d + \chi_p = -\frac{Ne^2}{mc^2}\sum_i^k \overline{r_i^2} + N\sum \frac{|(n|\mu_z|0)|^2}{W_n - W_0}, \tag{1}$$

where N is the Avogadro number, r_i^2 is the mean value of the square of the distance of the i-th electron from the axis of procession, $(n\,|\mu_z|\,0)$ are the diagonal matrix elements of the orbital magnetic moments of the unexcited state, $W_n - W_0$ are the energy differences between the excited and unexcited state.

On the other hand, according to the empirical magnetochemical scheme of Pascal [2]:

$$\chi = \sum \chi_A + \sum \lambda_s, \tag{2}$$

where κ_A are negative constants representing the individual atoms composing the molecule, and λ_s are supplementary constants (positive or negative) characterizing deviations from additivity due to the influence of various structural features.

There is no obvious correspondence between Formulas (1) and (2). In other words there is no simple physical interpretation of Pascal's empirical constants κ_A and λ_s from the present theoretical point of view. We set ourselves the problem of examining the magnetochemistry of diamagnetic organic molecules on the basis of Equation (1).

It is not possible to split up κ into κ_d and κ_p experimentally, so the following method was adopted. The Langevin diamagnetism of the molecule, which is less sensitive to structural features than κ_p, was calculated from the approximate formula of Kirkwood [3]:

$$\chi_d = -\frac{Ne^2 a_0^{1/2}}{4mc^2}\sqrt{k\alpha} = -3{,}11\cdot 10^6\sqrt{k\alpha}, \tag{3}$$

where $a_0 = \frac{\hbar^2}{mc^2}$ is the so-called Bohr radius, $\underline{k}$ is the total number of electrons in the molecule and α is the experimentally determined polarizability.

Analysis of the Kirkwood formula and comparison of calculated and experimental values of the susceptibility for compounds for which it is reasonable to suppose that $\kappa_p \sim 0$, show definitely that the approximate Formula (3) well represents the Langevin diamagnetism of the molecule.

A comparison of κ_d calculated from (3) with the experimental value of κ made it possible to determine κ_p for a large number of aliphatic and alicyclic compounds. Consideration of these results revealed a series of regularities.

In the first place, it was established that the specific carriers of the paramagnetism κ_p – "magnetoforms" – are certain groups of atoms, shown in Table 1 together with the approximate values of their individual paramagnetic susceptibilities κ_p'.

TABLE 1

	$>C=C<$	$-C\equiv C-$	$>C=O$	$C\begin{smallmatrix}\nearrow O\\ \searrow H\end{smallmatrix}$	$C\begin{smallmatrix}\nearrow O\\ \searrow OH\end{smallmatrix}$	OH	$C\begin{smallmatrix}\nearrow O\\ \searrow NH_2\end{smallmatrix}$	$-N\begin{smallmatrix}\nearrow O\\ \searrow O\end{smallmatrix}$	$C\equiv N$	$-C\begin{smallmatrix}\nearrow O\\ \searrow O-\end{smallmatrix}$
$+\chi'_p \cdot 10^6$	~ 8	~ 3	~ 11	~ 11	8,2	~ 1	~ 7	15,8	~ 3	~ 9

Secondly, it was shown that the molecules as a whole show a relatively small general molecular paramagnetism κ_p'', dependent on the symmetry of the molecule, and decreasing with an increase in the branching of isomers. Thus:

$$\chi_p = \sum \chi_p' + \chi_p''. \tag{4}$$

The summation of the paramagnetisms of the individual magnetoform groups can only be carried out in full measure when the groups are situated far apart from each other in the molecule (e.g. diallyl).

Thirdly, it was shown that an additive scheme can be used for the diamagnetic components of the susceptibility κ_d. Thus, it was found that individual atoms can contribute atomic diamagnetic components :

$$\chi_{dC}' = -8\cdot 10^{-6},\ \chi_{dH}' = -2\cdot 10^{-6},\ \chi_{dO} = -9\cdot 10^{-6},\ \chi_{dN}' = -7\cdot 10^{-6},\ \chi_{dCl}' = -19\cdot 10^{-6}$$

etc. The presence of double and triple bonds, C = C, C ≡ C and others, causes a small surplus diamagnetism, analogous to the exaltation of refraction: $\chi_{dC=C}' \simeq -1{,}6\cdot 10^{-6}$, $\chi_{dC\equiv C}' \simeq -1{,}8\cdot 10^{-6}$ etc. All these atomic and group constants have a definite physical meaning, which essentially distinguishes them from the empirical constants of Pascal. Thus, a new magnetochemical scheme has been developed, which conforms with Formula (1). The practical application of this scheme, to determine the structural formula of an organic compound, does not require the laborious calculation of the diamagnetic component κ_d by the additive method described. For this problem (in the case of aliphatic and alicyclic compounds) it is permissible to use Kirkwood's Formula (3). The susceptibility of the compound can then be calculated as follows:

$$\chi = -3{,}11\cdot 10^{6}\sqrt{k\alpha} + \sum \chi_d' + \sum \chi_p' + \chi_p'', \tag{5}$$

where α is measured experimentally, $\underline{k}$ is directly determined from the composition and κ_p' is obtained from Table 1.

TABLE 2

	$-\kappa\cdot 10^6$ calc. by our scheme*	$-\kappa\cdot 10^6$ exp.	$-\kappa\cdot 10^6$ calc. by new Pascal scheme
Glycol	38.5–39.5	38.7;39.0	37.4
Allyl alcohol	36.2–36.7	36.7	34.0
Oleic acid	210.3	208.0;209.5	208.3

* κ_p'' for oleic acid was extrapolated to 14 CH_2 groups; for the others it was taken from experiment for one CH_2 group.

Table 2 shows as examples the values of the susceptibility of a few compounds, calculated by our scheme [4] found experimentally and calculated by the new Pascal scheme. Comparison shows that our scheme, as well

as being physically simple, is not inferior to the Pascal scheme in other respects. The additive scheme for diamagnetic components may be of use for calculating intramolecular fields; this is discussed in another paper [4].

LITERATURE CITED

[1] J. H. Van-Vleck, The Theory of Electric and Magnetic Susceptibilities, (Oxford, 1948).

[2] P. Pascal, Comptes rend. 156, 323 (1913); J. Hoareau, A. Pacault, and P. Pascal, Cahiers de Phys. 74, 30 (1956).

[3] J. G. Kirkwood, Phys. Zs. 73, 57 (1932).

[4] Ia. G. Dorfman, Proc. Acad. Sci. USSR 119, 3 (1958).*

* Original Russian pagination. See C. B. Translation.

RADIOLYSIS OF HEPTANE AND SOME OTHER ALKANES

L. S. Polak, Academician A. V. Topchiev, and N. Ia. Cherniak

The present communication is the first of a planned series of papers, dealing with investigation of the basic principles and the mechanism of the radiolysis of individual paraffin hydrocarbons, in the liquid and solid states, under irradiation with γ-rays.

Co^{60} sources with nominal strengths of 1400 and 20,000 curies were used as sources of γ-radiation. The main work was carried out with n-heptane, but other individual hydrocarbons were also investigated. The purified hydrocarbons were quite transparent to ultraviolet light, and their specific gravities and indices of refraction (with the exception of cetane) did not differ from the values given in the literature.

The hydrocarbons were carefully deoxygenated in ampules of molybdenum glass, which were then sealed and irradiated.

When the ampules were opened, after exposure to the requisite dose of radiation, the quantity of gas in the products was determined. The gas was then analyzed for its content of H_2, CH_4 and other gaseous hydrocarbons by chromatographic separation on charcoal and silica gel. The accuracy of the determination of the total yield of gas was ± 5%. The specific gravity, the index of refraction, the molecular weight (cryoscopic method) and the iodine number (method of Margoshes) were determined for the liquid products. Ultraviolet and infrared spectra were also recorded, and the products were distilled and sulfonated.

Change of temperature within the range − 30 to + 200° did not affect the yield or character of the gaseous products of radiolysis. Special experiments showed that formation of gas ceased at the moment that irradiation was stopped, but continued as before when irradiation was restarted.

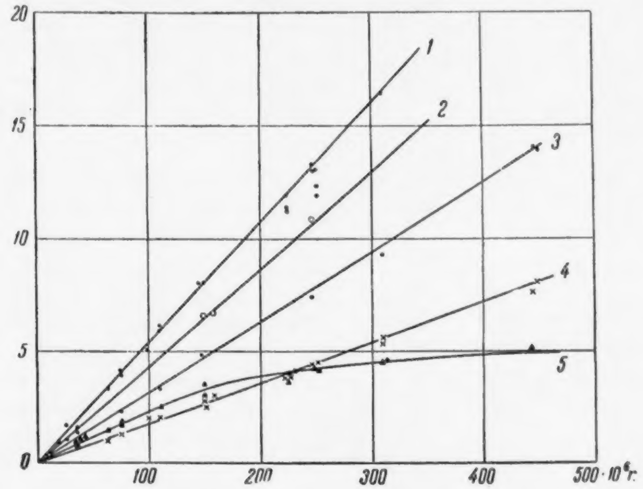

Fig. 1. 1) Yield of gas in cc (N.T.P.) from 1 cc of original n-heptane; 2) change in molecular weight of the liquid; 3) change in specific gravity of the liquid ($\Delta d_4^{20} \cdot 10^3$); 4) change in refractive index of the liquid ($\Delta n_D^{20} \cdot 10^3$); 5) iodine number of the liquid.

The curves of Fig. 1 show the changes in the characteristics of the liquid products, and the total quantity of gas formed, as functions of the γ-ray dosage applied to the samples. For doses in the range 0 to $500 \cdot 10^6$ roentgens, the quantity of gas formed and the increases in the molecular weight, specific gravity and index of refraction of the liquid phase showed a linear variation with exposure. The iodine number of the liquid phase showed a linear variation up to a dose of approximately $150 \cdot 10^6$ roentgens, but subsequently varied little over a wide range of dosage.

We considered the question of the effect of the number of CH_2 groups, and the relative content of CH_3 groups, on the results of radiolysis (Table 1). The quantity of methane increased, depending on the relative quantity of CH_3 groups in the molecule, from 0 for cyclohexane to 37% for isooctane. The relative rise in density and index of refraction of irradiated normal alkanes increased linearly from C_6 to C_{12}; but the C_{16} hydrocarbon did not conform to this linear increase and there was a marked fall in the effect.* All the results for isooctane were lower than for n-octane.

TABLE 1

Hydrocarbon	Ratio $\frac{CH_3}{CH}$	Composition of gas (methane hydrogen fraction) %		$\frac{\Delta d}{d_{init}}$ in %	$\frac{\Delta n}{n_{init}}$ in %
		H_2	CH_4	at constant dose $250 \cdot 10^6$ roentgens	
Cyclohexane	0	100	0	12,0	3,5
n-Cetane	0,059	98,5	1,5	7,8	2,7
n-Dodecane	0,077	—	—	11,5	5,8
n-Octane	0,111	97,5	2,5	10,1	3,6
n-Heptane	0,125	97,0	3,0	9,6	3,25
n-Hexane	0,143	96,8	3,2	8,4	3,1
Isooctane	0,278	63,0	37,0	8,8	2,8

The irradiated heptane was subjected to vacuum distillation at approximately 0.5 mm Hg, when the first fraction came off while cooling with ice, and distillation was continued at room temperature to leave a constant weight of a heavy residual fraction. The fractions were condensed in a trap cooled by liquid air. In all cases the light fractions had a molecular weight approximately 100, and an iodine number varying with dosage from 2 to 3. Distilling with heptane were the light products of radiolysis, heptene, heptadiene and their analogs.

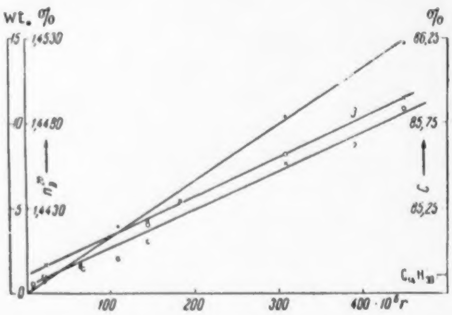

Fig. 2. Changes in the heavy residue as functions of the dosage: 1) weight %, 2) index of refraction n_D^{20} and 3) elementary composition % C.

From the curves of Fig. 2 it is obvious that, with increasing dosage, the weight percent of heavy residue and its index of refraction increased proportionally to the dose. The molecular weight of the heavy residue varied within the limits 175 to 218 over eight determinations, with an average of approximately 200. The specific gravity of this residue was 0.76 to 0.800.

At the beginning of radiolysis at relatively small doses, the formation of polymers could be practically disregarded, and the elementary composition of the heavy residue coincided with that of tetradecane. The percentage of carbon increased linearly with dosage, and at approximately $400 \cdot 10^6$ roentgens the composition corresponded to that of a saturated homolog of the alkane series with an increasing content of unsaturateds and their polymers. The heavy residue was sulfonated. For a dosage of $309 \cdot 10^6$ roentgens it showed 19% of unsaturateds and 81% of saturateds.

* It is interesting to note that, as shown in [1], the yield of hydrogen from fatty acids (arachidic, behenic, mellissic) increased linearly with the number of C atoms in the molecule up to C_{16} and then decreased.

In addition to the above results, it is necessary to consider also the following experimental facts: 1) the liquid products of irradiation contain trans-heptene, as was shown by the infrared spectrum [2]; 2) they also contain dienes and polyenes, as was shown by the infrared absorption spectrum [2].

It was shown in [3], with the aid of liquid chromatography, that considerable quantities of saturated and unsaturated dimers are produced by radiolysis (the dosage was of the same order as that used by us).

On the basis of the experimental results, and of well known ideas of the character of a reaction [4-9] occurring under the influence of ionizing radiations, the following may be considered as possible primary reactions in the radiolysis of heptane:

$$1\quad \left.\begin{array}{l} C_7H_{16} + e \\ C_7H_{16}^{+} + e \end{array}\right\rangle C_7H_{15}^{\cdot} + H \quad C_7H_{16} \rightsquigarrow C_7H_{16}^{\bullet} \rightarrow C_7H_{15}^{\cdot} + H^{\bullet}$$

$$1'\quad H^{\bullet} + RH \rightarrow H_2 + R\cdot \quad C_7H_{15}^{\cdot} + C_7H_{15}^{\cdot} \rightarrow C_{14}H_{30},\ H + H \xrightarrow{+M} H_2$$

$$2\quad \left.\begin{array}{l} C_7H_{16}^{+} + e \\ C_7H_{16} + e \end{array}\right\rangle C_7H_{16}^{\bullet} \rightarrow C_7H_{14} + H_2 \quad 3\quad C_7H_{16}^{\bullet} \rightarrow C_7H_{12} + 2H_2$$

$$4\quad \left.\begin{array}{l} C_7H_{16} + e \\ C_7H_{16}^{+} + e \end{array}\right\rangle C_6H_{13}^{\cdot} + CH_3^{\cdot},\quad 4'\quad \begin{array}{l} CH_3^{\cdot} + RH \rightarrow CH_4 + R\cdot \\ C_6H_{13}^{\cdot} + RH \rightarrow C_6H_{14} + R\cdot \end{array}$$

$$5\quad C_7H_{16}^{\bullet} + C_7H_{16}^{\bullet} \rightarrow C_{14}H_{30} + H_2,\ C_7H_{16}^{\bullet} + C_7H_{16} \rightarrow C_7H_{15}^{\cdot} + C_7H_{15}^{\cdot} + H_2 \rightarrow C_{14}H_{30} + H_2$$

Judging by the amount of methane in the gas, Reaction 4 is considerably less probable than reactions leading to the formation of hydrogen.

Our use of the paramagnetic resonance spectrum to demonstrate the presence of the heptyl radical and of atomic hydrogen in irradiated frozen heptane shows that Reaction 5, if it occurs at all, at any rate does not play an important role.

Further development of the process takes place as follows. Interaction of the radical C_7H_{15} with a molecule of the original hydrocarbon does not lead to the formation of any new radical or molecular product, so that the most probable further transformation is the recombination of two C_7H_{15} radicals to form tetradecane (1'). Recombination of the radical C_7H_{15} with the radical C_6H_{13}, formed by Reaction 4, is less probable, since the quantity of C_6H_{13} is small in comparison with that of C_7H_{15}. For the same reason there is little probability of the formation of dodecane by the recombination of C_6H_{13} radicals [the C_6H_{13} radical can sooner give a hexane molecule by interaction with a molecule of the original hydrocarbon (4')]. Among the secondary reactions there is the polymerization of the dienes produced by Reaction 3.

Thus, for any possible variant of the reaction leading to the formation of hydrogen molecules in the gas phase, the sum of the unsaturateds and saturateds (dimers of heptane) in the liquid phase must be equal to the number of molecules of hydrogen, maintaining a balance for small doses (while the polymerization of unsaturateds can be ignored). We found that for a hydrogen yield of 4.5 ± 10%, the yields of unsaturateds and saturateds were respectively, 1.5 and 2.5 moles per 100 equivalents.

Thus, the sum of the saturateds and unsaturateds was approximately 11% less than the hydrogen, which is within the limits of accuracy of the determinations.

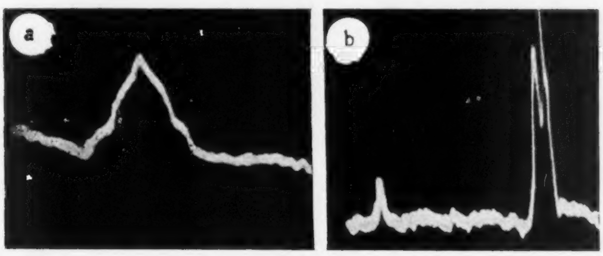

Fig. 3. Paramagnetic resonance spectra: a) heptyl radicals, b) heptyl radicals and atomic hydrogen.

In order to establish the existence of free radical mechanisms in the complex radiolysis reaction, it was necessary to obtain direct evidence of the formation of free radicals by radiolysis. This evidence was obtained by stabilizing the radicals at low temperature. Heptane was irradiated in the frozen state at 77° K (in liquid nitrogen). The paramagnetic resonance spectrum was then recorded while the material was kept at this temperature. We express our deep gratitude to Profresor V. V. Voevodskii, with whose apparatus the spectra were recorded in the Institute of Chemical Physics of the Academy of Sciences of the USSR. Spectra were obtained with a characteristic fine structure. They showed the presence, in the irradiated frozen heptane, of free alkyl radicals and also of smaller quantities of free hydrogen atoms (Fig. 3). When the irradiated frozen heptane was melted, the radicals recombined, as was clearly shown by the gradual disappearance of their paramagnetic resonance spectra.

Thus, together with the evidence for free radical mechanisms in some of the reactions in the radiolysis of alkanes, it was shown that alkyl radicals can accumulate in irradiated hydrocarbons in the frozen state at 77° K, and that even hydrogen atoms can partially persist at this temperature for a very long time, facts which open up new possibilities in hydrocarbon chemistry.

We express our thanks to the workers in the Radiation Source Group of the L. Ia. Karpov Physicochemical Institute and particularly to L. Kh. Breger and V. B. Osipov for their assistance in this work.

LITERATURE CITED

[1] V. Uaitkhed, K. Gudmen, and I. Breger,* Coll. "Radiation Chemistry," (IL, 1953), p. 286.

[2] L. S. Polak, A. V. Topchiev, N. Ia. Cherniak, and I. Ia. Kachkurova, Proc. Acad. Sci. USSR 119, 1 (1957).**

[3] H. A. Dewhurst and E. H. Winslow, J. Chem. Phys. 26, 4, 969 (1957).

[4] S. Ia. Pshezhetskii and M. T. Dmitriev, Prog. Chem. 26, part 7, 725 (1957).

[5] F. W. Spiers, Disc. Farad. Soc. 12, 13 (1952).

[6] F. S. Dainton, Ann. Rev. Nucl. Sci. 5, 213 (1955).

[7] D. Zh. Magi and M. Barton,* Coll. "Radiation Chemistry," (IL, 1953), p. 18.

[8] A. Prevost-Bernas, A. Chapiro, et al. Disc. Farad. Soc. 12, 98 (1952).

[9] M. H. J. Wijnen, J. Chem. Phys. 24, 851 (1956).

Institute of Petroleum of the
Academy of Sciences of the USSR

Received August 8, 1957.

* These names have been transliterated from the Russian, since the original work was not available. — Publisher's note.

** Original Russian pagination. See C. B. Translation.

CHANGES IN MICROHETEROGENEITIES OF ALLOYS UNDER THE INFLUENCE OF HEATING

Z. A. Sviderskaia, M. E. Drits, and E. S. Kadaner

(Presented by Academician I. P. Bardin, August 7, 1957)

It is usually accepted that the maintenance of an alloy for a long enough time at high temperature produces a more uniform distribution of components, i.e., a disappearance of the microheterogeneities formed in the process of crystallization. According to this view, thanks to the increased diffusion of mobile elements on heating, there is an evening out of concentration in the microspaces of the solid solution, and also a solution and coagulation of phases which removes the primary heterogeneities of the cast structure. But the application of autoradiographic methods to the study of the structure of alloys has shown clearly that a high degree of uniformity cannot be obtained for all alloys, nor with all conditions of annealing.

We showed in a previous paper [1] that homogenizing annealing of some nickel base alloys lead to an increase in the nonequilibrium distribution of certain elements, i.e., in essence, to an increased hetrogeneity in the structure of these alloys. Similar results were found in an investigation of the kinetics of the redistribution of components during the annealing of some light alloys based on aluminum and magnesium. Using quantitative estimates of the degree of micro-nonuniformity, based on the statistical treatment of photometric autograph data, and applying the coefficients of micro-nonuniformity, K and C *, introduced by us, we showed graphically how the micro-nonuniformity of alloys depended on different annealing conditions [2].

The curves of Fig. 1 show the changes in the coefficients of micro-nonuniformity of the binary alloys Al—Fe and Al—Ca with increasing time of annealing, at a temperature 50° below the solidus line.

The curves are of the same shape for both alloys, but in the case of the Al—Ca system the change in the slope of the curves occurs after a shorter period of annealing. It is clear from the curves that the use of a relatively short soaking time in annealing produces a fall in the coefficients of micro-nonuniformity, i.e., to an evening out of the structure of the alloys. But, with an increase in the heating period, there is either a definite rise in the degree of micro-nonuniformity or a noticeable tendency in that direction.

It should be noted that in both the above alloys we are concerned with binary systems showing almost complete absence of solubility in the solid state, i.e., for the given range of alloying, there is a considerable quantity of a second phase in the structure of these alloys. In conformity with this, the processes of evening out the structure consist, in principle, of changes in the distribution and form of particles of secondary segregations. Comparison of the curves obtained with micro-autoradiograms, and also with the normal microstructures of alloys annealed for different times, shows a correspondence between the observed changes in the structure of the alloys and the coefficients of micro-nonuniformity. As we have noted previously [3], in the autoradiographic

---

* The coefficient $K = \frac{100 - n}{100}$ (where 100 is the total number of microspaces in which the content of an element was determined, and n is the value of the maximum on the distribution curve) allows for the total number of departures of the concentration of the element from its mean content in the alloy, for the part of the structure investigated. The coefficient $C = \frac{C_{max}}{C_{min}}$ defines the possible variations of concentration in different microspaces of the alloy.

investigation of alloys of aluminum and iron, the heterogeneity of cast structures of similar alloys is always high and firmly persists under the influence of temperature. With an increase in the period of annealing there is, at first, some erosion of the dendrites at the expense of the redistribution of iron and calcium in the structure. This explains the decrease in the degree of micro-nonuniformity of the alloys (Fig. 1). Later, a longer period

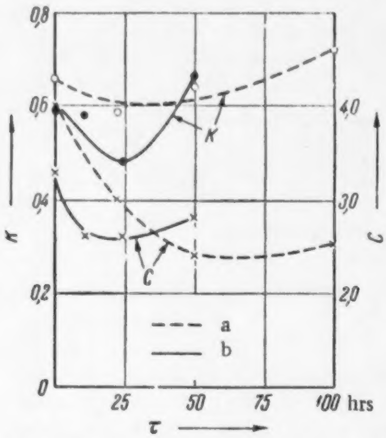

Fig. 1. Effect of time of annealing on the micro-nonuniformity of alloys: a) alloy of Al with 0.19% Fe, b) alloy of Al with 0.4% Ca.

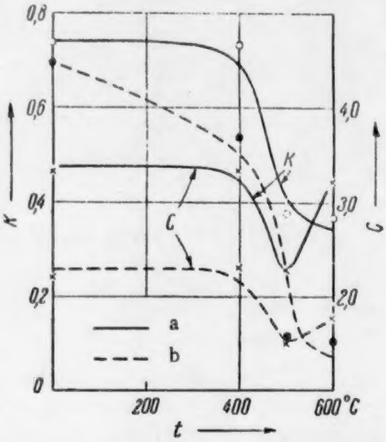

Fig. 2. Effect of temperature of annealing on the micro-nonuniformity of alloys: a) alloy of Mg–Mn–Al–Ca (0.2% Ca), b) alloy of Mg with 0.17% Ca.

of annealing produces an enlargement of the dendrites and individual agglomerates of alloying components at the expense of coagulation, which also leads in general to the formation of a coarser structural nonuniformity. The change in the character of the distribution of the alloying elements with increased annealing time is illustrated by the example of alloys of aluminum with calcium (Fig. 3). The dark parts of the micro-autoradiograms shown correspond to positions where radioactive calcium (Ca^{45}) is concentrated.

An increase in the micro-nonuniformity of the structure of alloys under the action of heating was also found with alloys of magnesium and calcium, which, within the concentration range investigated (up to 0.2% Ca), proved to be essentially solid solutions. The existence of a second phase was shown only at high magnification and in very limited amounts.

The curves of Fig. 2 show the changes in the coefficients of micro-nonuniformity with increasing temperature of annealing (24 hours) for the alloys Mg–Ca and Mg–Mn–Al–Ca.

In both cases heating the alloy to 500° produced a marked fall in the micro-nonuniformity of the distribution of calcium, which shows the high intensity of the processes of redistribution occurring at this temperature. It is evident from the micro-radiogram (Fig. 4, b) that, in the case of the binary alloy of magnesium and calcium, complete leveling out of the composition of the alloy took place with respect to calcium, i.e., intra-dendritic segregation did not occur at all. When the annealing temperature was raised to 600° there was a considerable increase in the values of the coefficient C for both the alloys (Fig. 2), while the values of the coefficient K remained practically constant. Clearly, in this case also, some heterogenization of structure took place. At such high annealing temperatures coagulation processes occur very intensively, and fairly coarse aggregates of calcium form in the alloy structure, causing peaks to appear on the photometric blackening curves. This depends particularly on the size of the coefficient C, which determines the scale of possible variations in concentration in the part of the structure investigated, and less on the value of the coefficient K, which characterizes the total number of deviations from the mean composition of the alloy. The formation of concentrated aggregates in the structure of the Mg–Ca alloy at a high annealing temperature is well shown in the micro-radiogram (Fig. 4, c).

Thus, by controlling the annealing conditions, it is clearly possible to produce a "secondary heterogenization" of the alloy structure, i.e., an increase in its micro-nonuniformity. The development of a similar heterogenization will depend on the nature and interaction of the alloy components, and also on the original micro-

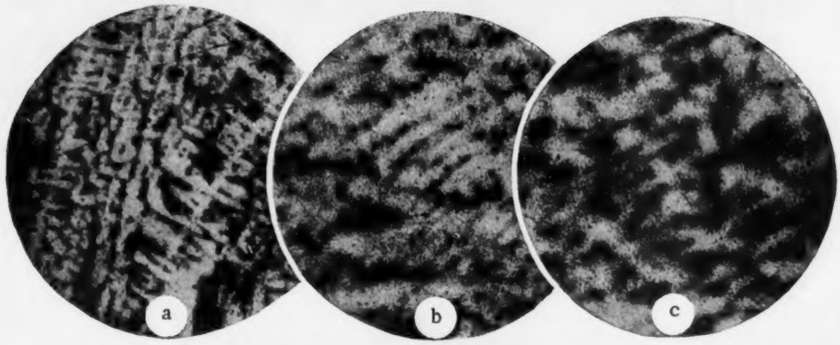

Fig. 3. Micro-radiograms of the alloy Al – 0.4% Ca; × 25. a) Cast; b) annealed at 570° for 24 hours; c) annealed at 570° for 50 hours.

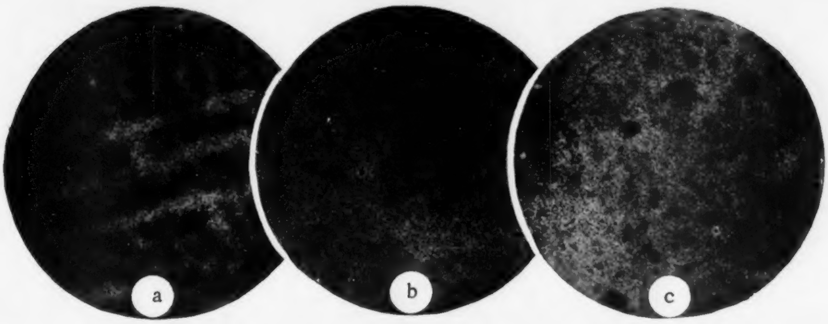

Fig. 4. Micro-radiograms of the alloy Mg – 0.17% Ca; × 25. Annealed for 24 hours: a) at 400°, b) at 500°, c) at 600°.

nonuniformity of the alloy and on the relative rates of the processes of solution and coagulation for the given temperature-time conditions of heating. With alloys of the solid solution type heterogenization of structure on annealing depends on the formation of definite particles with increased concentration of alloying element, but, with alloys containing a considerable amount of a second phase, micro-nonuniformity of structure may increase at the expense of changes in the dimensions and shapes of the structural components. In either case, an increase in the degree of heterogeneity of structure under definite conditions of heating cannot be predicted from the properties of an alloy, and requires further more fundamental investigation.

LITERATURE CITED

[1] S. T. Kishkin and S. Z. Bokshtein, Coll. Uses of Isotopes in Technology, Biology and Agriculture,* Acad. Sci. USSR Press (1955).

[2] Z. A. Sviderskaia, M. E. Drits, and E. S. Kadaner, Metal Working and Processing, 5 (1957).

[3] M. E. Drits, E. S. Kadaner, Z. A. Sviderskaia, and E. L. Shcherbinina, Bull. Acad. Sci. USSR, Div. Tech. Sci. 6 (1957).

A. A. Baikov Institute of Metallurgy of the Academy of Sciences of the USSR

Received August 6, 1957.

* In Russian.

THE CLASSICAL THEORY OF STRONG ELECTROLYTES

V. V. Tolmachev and S. V. Tiablikov

(Submitted by Academician N. N. Bogoliubov, August 19, 1957)

The basic problem of the theory of strong electrolytes is the calculation of the correction ΔF to the free energy, arising from the mutual interaction of the ions. The essential step in this field was made by Debye, who treated correctly the electrostatic interaction of ions, and obtained for ΔF the expression:

$$\Delta F = -\frac{N\theta}{12\pi}\frac{v}{r_d^3}, \tag{1}$$

where N is the number of ions, $\theta = kT$, $\underline{v}$ is the volume for one ion, and r_d is the Debye radius given by:

$$r_d^2 = D\theta v\,(4\pi \sum_{(a)} n_a e_a^2)^{-1}; \quad n_a = \frac{N_a}{N}, \tag{2}$$

where N_a and e_a are the number of ions of type $\underline{a}$ and the charge on each, and D is the dielectric constant of the solvent.

Debye and Hückel [1] applied a correction to (1) for the ultimate radius of the ion r_0:

$$\Delta F = -\frac{N\theta}{12\pi}\frac{v}{r_d^3}\left(1 - \frac{3}{4}\frac{r_0}{r_d} + \ldots\right). \tag{3}$$

By comparison of (3) with experimental data, values of r_0 were obtained which agreed well with other estimates of r_0 for large values of the ionic radius. In the case of small ions agreement was lacking.

Bjerrum [2] introduced another correction into (1) which, for small concentrations of pairs of ions of opposite sign occurring close to each other, has the form:

$$\Delta F = -\frac{1}{2}N\theta\alpha - \frac{N\theta}{12\pi}\frac{v}{r_d^3}(1-\alpha)^{3/2}, \tag{4}$$

where $\frac{N\alpha}{2}$ is the number of pairs of ions of opposite sign occurring at a separation from each other of less than $q = \frac{e^2}{D\theta}$;

$$\alpha = \frac{1}{2v}\int_{r_0}^{q} e^{e^2/D\theta r}\, 4\pi r^2 dr. \tag{5}$$

The basis of this correction is that, according to Bjerrum, the Debye theory can only apply to ions which are sufficiently far apart from each other. Pairs of ions of opposite sign should be considered more as neutral molecules rather than as they are treated in the Debye theory. It should be noted that in Bjerrum's expression for ΔF there is a correction term of the Debye-Hückel type, which has been omitted in (4).

In this paper we investigate the question of the statistical bases of the Debye-Hückel and Bjerrum expressions, using the correlation functions methods of N. N. Bogoliubov [3]*.

The series of equations for the correlation functions has the form [3]:

$$\frac{\partial F_{a_1 \ldots a_s}}{\partial q_1^\alpha} + \frac{F_{a_1 \ldots a_s}}{\theta} \frac{\partial U_{a_1 \ldots a_s}}{\partial q_1^\alpha} + $$
$$+ \frac{1}{\theta v} \int \sum_{(1 < a_{s+1} < M)} F_{a_1 \ldots a_{s+1}} n_{a_{s+1}} \frac{\partial \Phi_{a_1 a_{s+1}}(|q_1 - q_{s+1}|)}{\partial q_1^\alpha} dq_{s+1} = 0 \tag{6}$$

$$U_{a_1 \ldots a_s} = \sum_{(1 \leqslant i < j \leqslant s)} \Phi_{a_i a_j}(|q_i - q_j|). \tag{7}$$

Then, as in [3] it is assumed that $\sum\limits_{(1 \leqslant a \leqslant M)} e_a n_a = 0$, and $\sum\limits_{(1 \leqslant a \leqslant M)} n_a = 1$. Following the basic methods of [4], (6) is solved in the form

$$F_{a_1 \ldots a_s} = C_{a_1 \ldots a_s} \exp\left\{-\frac{1}{\theta} \overline{U}_{a_1 \ldots a_s}\right\}, \tag{8}$$

$$\overline{U}_{a_1 \ldots a_s} = \sum_{(1 \leqslant i < j \leqslant s)} \overline{\Phi}_{a_i a_j}(|q_i - q_j|). \tag{9}$$

We introduce the new correlation functions $g_{a_1 \ldots a_s}$ instead of $C_{a_1 \ldots a_s}$:

$$C_{a_1} = g_{a_1}, \tag{10}$$
$$C_{a_1 a_2} = g_{a_1} g_{a_2} + v g_{a_1 a_2},$$
$$C_{a_1 a_2 a_3} = g_{a_1} g_{a_2} g_{a_3} + v(g_{a_1} g_{a_2 a_3} + g_{a_2} g_{a_1 a_3} + g_{a_3} g_{a_1 a_2}) + v^2 g_{a_1 a_2 a_3}$$

and make the substitutions $\frac{1}{\theta}\Phi = v\psi$; $\frac{1}{\theta}\overline{\Phi} = v\overline{\psi}$. Then, expressing $g_{a_1 \ldots a_s}$ in the form of a series in powers of $\underline{v}$,

$$g_{a_1 \ldots a_s} = g^0_{a_1 \ldots a_s} + v g^1_{a_1 \ldots a_s} + \ldots, \tag{11}$$

we obtain the following equation for g^0_{ab}:

$$g^0_{ab}(|q|) + \psi_{ab}(|q|) - \overline{\psi}_{ab}(|q|) +$$
$$+ \sum_{(1 \leqslant c \leqslant M)} n_c \int \psi_{ac}(|q - q'|) \{g^0_{bc}(|q'|) - \overline{\psi}_{bc}(|q'|\} dq' = 0 \tag{12}$$

(for a uniform spatial distribution of field $g_{a_1} = 1$).

By putting g^0_{ab} equal to zero, Equation (12) can be used to find $\overline{\psi}_{ab}(|q|)$ for a known $\psi_{ab}(|q|)$. In the case when a single radius r_0 is ascribed to the ions, we obtain for the binary correlation function:

$$F_{ab}(|q|) \cong \begin{cases} \exp\left\{-\frac{e_a e_b}{\theta} \frac{1}{|q|} e^{-|q|/r_d}\right\}, & |q| > r_0; \\ 0, & |q| \leqslant r_0 \end{cases} \tag{13}$$

* See also [7, 8] for the question of the statistical basis of the Debye theory.

(correct to terms of the first order for the plazmen* parameter inclusively). An expression for F_{ab} of such a form was naturally to be expected.

For the part of the free energy ΔF arising from the interaction of ions we use the general formula [5]

$$\Delta F = \frac{N}{2\gamma} \sum_{(1 \leq a,b \leq M)} n_a n_b \int\limits_V \int\limits_0^1 \Phi_{ab}(|q|) F_{ab}(|q|; \tau\Phi)\, dq d\tau. \tag{14}$$

Substituting (13) in (14), we have:

$$\Delta F = N \frac{2\pi}{vD} \sum_{(1 < a,b < M)} n_a n_b e_a e_b \int\limits_{r_0}^{\infty} \int\limits_0^1 \left(\exp\left\{ -\frac{\tau e_a e_b}{D\theta r} e^{-\frac{r}{r_d}\sqrt{\tau}} \right\} - 1 \right) r dr d\tau. \tag{15}$$

In the case when the ionic radius is large enough, i.e.,

$$r_0 \gg \max_{(a,b)} \left| \frac{e_a e_b}{D\theta} \right| = q, \tag{16}$$

the exponent in the unintegrated Expression (15), there are at least small concentrations of pairs of ions of opposite sign close to each other, the Bjerrum correction. For simplicity we will consider the special case of an electrolyte composed of two sorts of ion with the same absolute value of charge. In this case Formula (15) attains the simpler form:

$$\begin{aligned} \Delta F = {} & N \frac{e^2}{D} \frac{\pi}{v} \int\limits_{r_0}^{q} \int\limits_0^1 \exp\left\{ -\tau \frac{e^2}{D\theta r} e^{-\frac{r}{r_d}\sqrt{\tau}} \right\} r dr d\tau - \\ & - N \frac{e^2}{D} \frac{\pi}{v} \int\limits_{r_0}^{q} \int\limits_0^1 \exp\left\{ \tau \frac{e^2}{D\theta r} e^{-\frac{r}{r_d}\sqrt{\tau}} \right\} r dr d\tau + \\ & + N \frac{e^2}{D} \frac{\pi}{v} \int\limits_q^{\infty} \int\limits_0^1 \left(\exp\left\{ -\tau \frac{e^2}{D\theta r} {}^{-\frac{r}{r_d}\sqrt{\tau}} \right\} - 1 \right) r dr d\tau - \\ & - N \frac{e^2}{D} \frac{\pi}{v} \int\limits_q^{\infty} \int\limits_0^1 \left(\exp\left\{ \tau \frac{e^2}{D\theta r} e^{-\frac{r}{r_d}\sqrt{\tau}} \right\} - 1 \right) r dr d\tau, \end{aligned} \tag{17}$$

where, for convenience of consideration, the integral with respect to r is divided into two parts, from r_0 to q and from q to ∞.

Replacement of the exponent in the first term of (17) by unity shows that it will be less than $N\theta$ multiplied by the square of the plazmen parameter $\frac{v}{r_d^3}$. With the second factor, we split up the exponential factor which occurs in the exponent of the unintegrated equation, then

$$\begin{aligned} \int\limits_{r_0}^{q} \int\limits_0^1 \exp\left\{ \frac{\tau e^2}{D\theta r} e^{-\frac{r}{r_d}\sqrt{\tau}} \right\} r dr d\tau = {} & \int\limits_{r_0}^{q} \int\limits_0^1 \exp\left\{ \frac{\tau e^2}{D\theta r} \right\} r dr d\tau - \\ & - \frac{e^2}{D\theta r_d} \int\limits_{r_0}^{q} \int\limits_0^1 \exp\left\{ \frac{\tau e^2}{D\theta r} \right\} \tau^{3/2} r dr d\tau + \ldots \end{aligned}$$

In the case of electrolytes the value of $\frac{e}{D\theta\, r_0}$ cannot be reckoned as small in comparison with unity, so that the main contribution to the integral with respect to r is given by the region where $r \sim r_0$. Hence, for the integrations with respect to τ, all that is required is an asymptotic approach to them for $r \sim r_0$, and this is easily carried out seeing that

* Transliteration of Russian – Publisher's note.

$$\int_0^1 e^{\tau\beta}\, d\tau \cong \frac{e^\beta}{\beta}; \quad \int_0^1 e^{\tau\beta}\tau^{3/2} d\tau \cong \frac{e^\beta}{\beta} \quad (\beta \gg 1).$$

Thus

$$-N \frac{e^2}{D}\frac{\pi}{v}\int_{r_0}^{q}\int_0^1 \exp\left\{\frac{\tau e^2}{D\theta r} e^{-\frac{r}{r_d}\sqrt{\tau}}\right\} r\,dr\,d\tau = -\frac{1}{2} N\theta\alpha +$$

$$+\frac{1}{8\pi} N\theta\alpha \frac{v}{r_d^3} + N\theta\alpha O\left(\left[\frac{v}{r_d^3}\right]^2\right),$$

where α is defined by Formula (5).

The third and fourth terms of (17) are easily evaluated by splitting up the exponent in the unintegrated equation, which gives

$$-\frac{1}{12\pi} N\theta \frac{v}{r_d^3}\left(1 - \frac{3}{4}\frac{q}{r_d} + \ldots\right).$$

Omitting terms involving the square of the plazmen parameter, we finally obtain:

$$\Delta F = -\frac{1}{2} N\theta\alpha - \frac{1}{12\pi} N\theta \frac{v}{r_d^3} + \frac{1}{8\pi} N\theta\alpha \frac{v}{r_d^3}, \qquad (18)$$

which for small values of α is the same as Expression (4) derived from Bjerrum's theory.

A more detailed comparison of Expression (17) with the corresponding expression from Bjerrum's theory can only be made after a numerical evaluation of the integrals.

Doubts are repeatedly expressed about the basis of Bjerrum's theory (see, for example the discussion of this problem in [6]). It appears to us that our results clarify, to a satisfactory degree, the basic points of Bjerrum's theory.

In conclusion the authors take this opportunity of thanking Academician N. N. Bogoliubov for his interest in the work.

LITERATURE CITED

[1] P. Debye and E. Hückel, Phys. Zs. 24, 185 (1923).

[2] N. Bjerrum, Kgl. Danske Vid. Selsk. Math.-fys. Medd., 7, 9 (1926).

[3] N. N. Bogoliubov, "Dynamic Problems in Statistical Physics," (M.-L., 1946). *

[4] S. V. Tiablikov and V. V. Tolmachev, Proc. Acad. Sci. USSR 114, 6 (1957).**

[5] N. N. Bogoliubov, S. V. Tiablikov, D. N. Zubarev, and V. V. Tolmachev, Text of the proceedings of the Conference on Many Body Problems, New Jersey, U.S.A., January, 1957.

[6] R. Fowler and E. Guggenheim, "Statistical Thermodynamics,"*** Chapter 9, (IL, 1949); G. Falkenhagen, "Electrolytes," *** (L, 1935).

[7] R. H. Fowler, Proc. Cambr. Phil. Soc. 22, 861 (1925); Trans. Farad. Soc. 23, 434 (1927).

[8] H. A. Kramers, Proc. Koninkl. nederl. akad. wet., Amsterdam 30, 145 (1927).

V. A. Steklov Mathematical Institute of the
Academy of Sciences of the USSR.

Received August 12, 1957.

* In Russian.

** Original Russian pagination. See C. B. Translation.

*** Russian translation.

THE STOICHIOMETRIC NUMBER OF THE REACTION OF ELECTROCHEMICAL DESORPTION OF HYDROGEN

Academician A. N. Frumkin

There have recently been repeated discussions in the literature [1-7] on the question of the applicability of the criterion, first proposed in another form by Horiuti and Ikushima [8] for explaining the mechanism and the nature of the slow stage of the reaction of conversion of hydrogen ions into molecular hydrogen $2H^+ + 2e^- \rightleftharpoons H_2$. The authors quoted proceded from the relation

$$\vec{i}/\overleftarrow{i} = f(\eta) = e^{\lambda\eta}, \tag{1}$$

where $\vec{i}$ and $\overleftarrow{i}$ are respectively the rates of transfer of hydrogen from solution to the gas phase and the reverse process, for 1 cm^2 of surface (in electrical units); η is the cathodic overvoltage divided by RT/F; and λ is a number characterizing the process.

Nowadays, it is customary to use as criterion the stoichiometric number ν, equal to $2/\lambda$. This number expresses how many times the slowest stage must be repeated for a single occurrence of the total process. It follows from (1) that

$$\nu = 2\,(\partial\eta/\partial i)_{\eta=0}\, i_0 = 2/f'(0), \tag{2}$$

where i is the total current of the reaction of cathodic liberation of H_2 and i_0 is the exchange current when $\eta = 0$. The values of ν used, obtained with the aid of Equation (2), in a number of cases lead to doubtful results, particularly on the assumption that the liberation of hydrogen takes place by an electrochemical desorption mechanism. In this case [9]

$$i = v_1 - v_2 + v_3 - v_4 = 2\,(v_1 - v_2) = 2\,(v_3 - v_4), \tag{3}$$

where v_1 and v_2, respectively, are the rates of the forward and reverse reaction of the discharge stage – ionized $H^+ + e^- \rightleftharpoons H_{ads}$, and v_3 and v_4 are the rates of the forward and corresponding reverse reaction of the stage of electrochemical desorption – adsorbed $H_{ads} + H^+ + e^- \rightleftharpoons H_2$.

If it is assumed that the surface of the electrode is uniform, and that the transfer of H_{ads} on it is not associated with an appreciable activation energy, the values of v can be expressed by the equations (repulsive forces between adsorbed particles and the so-called ψ_1 effects are not taken into account):

$$v_1 = k_1\,(1-\theta) = k_1^0 e^{\alpha_1\eta}\,(1-\theta); \tag{4a}$$

$$v_2 = k_2\theta = k_2^0 e^{-\beta_1\eta}\theta; \tag{4b}$$

$$v_3 = k_3\theta = k_3^0 e^{\alpha_2\eta}\theta; \tag{4c}$$

$$v_4 = k_4\,(1-\theta) = k_4^0 e^{-\beta_2\eta}\,(1-\theta), \tag{4d}$$

where $\alpha_1 + \beta_1 = \alpha_2 + \beta_2 = 1$; θ is the degree of coverage of the surface by atomic hydrogen; k_1^0, k_2^0, k_3^0, and k_4^0 are constants for a solution of defined composition, and are connected by the relation

$$k_2^0 k_4^0 = k_1^0 k_3^0. \tag{5}$$

Since the differences between α_1 and α_2 must be small, in order to simplify the calculations, we will from now on put $\alpha_1 = \alpha_2 = \alpha$ and $\beta_1 = \beta_2 = \beta$. According to Bockris and others [4, 7], $\nu = 1$ for electrochemical desorption. According to Lukovtsev [1], ν lies between 1 and 2.* Vetter [5], considering only the case when θ is small, concludes that the value $\nu = 1$ only follows from the electrochemical kinetic equation if the current, i_{0I} of the reversible stage discharge-ionization is small in comparison with the current, i_{0II}, of the reversible stage desorption-adsorption. Because of these divergent views it seemed desirable to submit the question to further examination. Reference will first be made to some previously established relations [9].

From the condition of the constancy of θ with time it follows, according to (4) that:

$$\theta = (k_1+k_4)/(k_1+k_2+k_3+k_4). \tag{6}$$

Further:

$$i_{0I} = k_1^0 k_2^0/(k_1^0+k_2^0), \quad i_{0II} = k_1^0 k_3^0/(k_1^0+k_2^0). \tag{7}$$

The ratio $\frac{k_2^0}{k_3^0} = \frac{i_{0I}}{i_{0II}}$ may be denoted by γ. An expression can now be determined for $f(\eta)$. As has been shown in [1, 3]:

$$\vec{i} = v_1 v_3 (v_2+v_3)^{-1} + v_3; \quad \overleftarrow{i} = v_2 v_4 (v_2+v_3)^{-1} + v_4; \tag{8}$$

$$f(\eta) = \vec{i}/\overleftarrow{i} = (v_1 v_3 + v_2 v_3 + v_3^2)/(2v_2 v_4 + v_3 v_4). \tag{9}$$

If the values of $\underline{v}$ from (4a) to (4d) are inserted in (9), and θ is expressed in terms of the values of k^0 in accordance with (6) and (4), then, making use of (5), after a simple rearrangement** it can be shown that:

$$f(\eta) = (2\gamma e^{\eta}+1)/(2\gamma e^{-\eta}+1), \quad f'(0) = 4\gamma/(1+2\gamma). \tag{10}$$

From (10) and (2) it follows that:

$$\nu = 1 + 1/2\gamma = 1 + i_{0I}/2i_{0II}. \tag{11}$$

Thus, ν only equals 1 when $i_{0I} \ll i_{0II}$; if $i_{0I} \gg i_{0II}$, ν can be as large as required. This result must not be be considered surprising. Indeed, it follows from (8) that:

$$i_0 = i_{0I}\cdot i_{0II}/(i_{0I}+i_{0II}) + i_{0II} = i_{0II}\cdot(1+2\gamma)/(1+\gamma) = i_{0I}\cdot(1+2\gamma)/\gamma(1+\gamma) \tag{12}$$

If $\gamma \gg 1$, then $i_0 = 2i_{0II}$; but if $\gamma \ll 1$, then $i_0 = i_{0II} = \gamma^{-1} i_{0I}$.

From (2), making use of (10) and (12), we find that:

$$(\partial\eta/\partial i)_{\eta=0} = (1+\gamma)/4\gamma i_{0II} = (1+\gamma)/4i_{0I} = {}^1/_4(1/i_{0I} + 1/i_{0II}). \tag{13}$$

In accordance with (12) and (13), the existence of a considerable exchange current for the second stage, i_{0II}, with a small i_{0I}, ensures a high value of the total exchange current, but with little polarization of the electrode. Equation (13) was obtained previously [5] for the case of small coverage θ.

The calculation given here of the value of ν does not, however, give a true representation of the values of the magnitude of ν presented in the literature. The fact is that, although in principle a direct experimental determination of the value of i_0 is possible *** with the aid of hydrogen isotopes, yet, in practice, in the determination of ν, it is customary to make use of not the true, but the "extrapolated" value of the exchange current. The procedure is to look for a straight section of the $\eta - \log i$ curve, and then, assuming that the value

---

* As opposed to the other references quoted, in [1, 3], electrochemical desorption is considered with a nonuniform surface, characterized by a logarithmic adsorption isotherm.

** A relation equivalent to (10) was first given in [3].

*** However, the latter cannot be very precise, since the use of the data obtained requires a knowledge of the isotope factor, which is determined from the values of the partition coefficients at considerable cathodic overvoltages, i.e., under conditions very different from those of the determination of i_0.

of $\overleftarrow{i}$ can be neglected in comparison with that of $\overrightarrow{i}$ for values of η within this section, to find i_0 by extrapolating the $\eta - \log i$ curve to $\eta = 0$. The possibility of a difference between the "true" and "extrapolated" exchange currents was first discussed in [2, 3]. An experimental comparison of these values has, apparently, only been made once, and not with very great accuracy [10].

We will now consider what the magnitude of ν will be, using the extrapolated value of the exchange current $(i_0)_e$. The designation ν' is used to distinguish it from the values considered previously, then:

$$\nu' = 2\,(\partial\eta/\partial i)_{\eta=0}\,(i_0)_e. \tag{14}$$

The magnitude of $(i_0)_e$ depends essentially on at what speeds v can be neglected, over the range of values of η for which there is a linear relation between η and $\log i$. Suppose first that $\gamma \gg 1$ (retarded desorption). Then, according to (4), $k_4^0 \ll k_1^0$, and according to (4a) and (4d), $k_4 \ll k_1$. When η is not too large ($\eta \ll \log \gamma$), from the condition that $\gamma \gg 1$, i.e., that $k_3^0 \ll k_2^0$, it follows also that $k_3 \ll k_2$. For the same range of values of of η Equation (6) can be transformed into:

$$\theta = k_1/(k_1 + k_2) = k_1^0 e^{\eta} \,/\, (k_1^0 e^{\eta} + k_2^0), \tag{15}$$

hence, according to (3), (4c), (4d), and (5),

$$i = 2\,(v_3 - v_4) = 2k_1^0 k_3^0 \cdot (e^{(1+\alpha)\eta} - e^{-\beta\eta})/(k_1^0 e^{\eta} + k_2^0). \tag{16}$$

When $\eta \gg 1$, it follows from (16) that

$$i = 2k_1^0 k_3^0 \cdot e^{(1+\alpha)\eta}/(k_1^0 e^{\eta} + k_2^0), \quad (i_0)_e = 2i_{0\text{II}} = i_0. \tag{17}$$

From (17) and (13), when $\gamma \gg 1$, it follows that

$$\nu' = 2\,(\partial\eta/\partial i)_{\eta=0}\,(i_0)_e = 1. \tag{18}$$

If it is supposed that $\gamma \ll 1$ (retarded discharge), then by the same reasoning as above, it is found that, when η is not too large ($\eta \ll \log \gamma^{-1}$), k_2 can be neglected in comparison with k_3 and k_1 in comparison with k_4, and, consequently, in accordance with (6), (5), (3), (4a), (4b), (7), and (12):

$$\theta = k_4/(k_3 + k_4) = k_1^0 \,/\, (k_1^0 + k_2^0 e^{\eta}), \tag{19}$$

$$i = 2\,(v_1 - v_2) = 2k_1^0 k_2^0 \cdot (e^{(1+\alpha)\eta} - e^{-\beta\eta}) \,/\, (k_1^0 + k_2^0 e^{\beta\eta}), \quad (i_0)_e = 2i_{0\text{I}} = 2\gamma i_0. \tag{20}$$

It follows from (20) that, in contrast to the case considered earlier, when $\gamma \ll 1$, the extrapolated exchange current is not equal to the true current. From (20), (14), and (13), it follows that, when $\gamma \ll 1$, $\nu' = 1$.

Thus, if the speeds of the first and second stages differ by an order of magnitude, and if a part of the $\eta - \log i$ curve is used for extrapolation for which the condition $\eta \ll |\log \gamma|$ is fulfilled, the value ν' found for the extrapolated exchange current is equal to 1. The same value of ν' is obtained if the anodic instead of the cathodic branch of the $\eta - \log i$ curve is used for extrapolation. It should be noted that, in order that the expressions on the right hand sides of Equation (16) and (20) for $\eta \gg 1$ should correspond to the linear relation between η and $\log i$, which is normally used as a basis for extrapolation, it is necessary that the first term in the denominator should be considerably less or considerably greater than the second. But this condition breaks down if a nonuniform surface is considered with a logarithmic adsorption isotherm.

Suppose now that γ is nearly equal to 1, i.e., that k_2^0 and k_3^0 are of the same order of magnitude.* According to (5) k_1^0 and k_4^0 must also be of the same order of magnitude. In this case, according to (4), when $\eta \gg 1$, $k_4 \ll k_1$ and $k_2 \ll k_3$, so that:

$$\theta = k_1/(k_1 + k_3) = k_1^0/\,(k_1^0 + k_3^0)\,; \tag{21}$$

$$i = v_1 + v_3 = e^{\alpha\eta} \cdot 2k_1^0 k_3^0/\,(k_1^0 + k_3^0); \quad (i_0)_e = 2k_1^0 k_3^0/\,(k_1^0 + k_3^0). \tag{22}$$

* This assumption should not be regarded as artificial. Actually, it follows, from some approximate calculations published elsewhere [11], that the activation energies of the processes of ionization and electrochemical desorption of H_{ads} at equilibrium potential must be nearly equal, if $\alpha = 0.5$.

From (22), (14), (13), and (7):

$$\nu' = (1 + 1/\gamma)(k_1^0 + k_2^0)/(k_1^0 + k_3^0). \qquad (23)$$

In the special case $k_2^0 = k_3^0$, i.e., $\gamma = 1$, $\nu' = 2$.

If the anodic branch of the $\eta - \log i$ curve is used for extrapolation, the expression for ν' differs from (23) in that $k_1^0 + k_3^0$ is replaced by $k_2^0 + k_4^0$.

If η is large enough, namely if $\eta \gg |\log \gamma|$, the values of k_2 and k_4 in (6) may always drop, which leads in the general case to Equations (22) and (23), as was shown previously in [12]. The possibility of obtaining two different values of $(i_0)_e$ (and consequently two values of ν'), by extrapolating different parts of the cathodic branch of the $\eta - \log i$ curve, was shown previously in (5).

Note added in proof. After this paper had been sent to the printer, an article appeared by Makrides [13], who also, but from a different viewpoint, discusses the question of the value of the stoichiometric number in the case of electrochemical desorption. His conclusions on the dependence of this number on γ agree with our own with respect to the value of ν'. He does not point out the difference between ν' and ν, so that, on the basis of the above treatment, it may be presumed that his conclusions as to the value of ν may not always be correct.

LITERATURE CITED

[1] P. D. Lukovtsev, J. Phys. Chem. 21, 589 (1947).

[2] P. D. Lukovtsev and S. D. Levina, J. Phys. Chem. 21, 599 (1947).

[3] P. D. Lukovtsev, Dissertation, L. Ia. Karpov Phys.-Chem. Inst. (1940).

[4] J. O' M. Bockris, Modern Aspects of Electrochemistry (London, 1954), p. 209; J. O. M. Bockris and E. Potter, J. Res. Inst. Catalysis 4, 50 (1956); 4, 256 (1957); N. Pentland, J. O' M. Bockris, and E. Sheldon, J. Electrochem. Soc. 104, 182 (1957).

[5] K. Vetter, Zs. Elektrochem. 59, 435 (1955).

[6] J. Horiuti, J. Res. Inst. Catalysis 5, 1 (1957); J. Horiuti, T. Nakamura Zs. Phys. Chem. (N.F.) 11, 358 (1957); J. Horiuti, H. Sugawara, J. Res. Inst. Catalysis 4, 1 (1956).

[7] R. Parsons, Trans. Farad. Soc. 47, 1332 (1951).

[8] J. Horiuti and M. Ikusima, Proc. Imp. Acad. Tokyo, 15, 39 (1939).

[9] A. N. Frumkin, J. Phys. Chem. 31, 1875 (1957).

[10] S. D. Levina, Acta Physicochim. USSR 14, 294 (1941).

[11] A. N. Frumkin, Trans. of 4th Conf. on Electrochem. (Discussion).

[12] A. N. Frumkin, J. Phys. Chem. 10, 568 (1937); Acta Physicochim, USSR 7, 475 (1937).

[13] A. Makrides, J. Electrochem. Soc. 104, 677 (1957).

Received December 24, 1957.

THE ATMOSPHERIC CORROSION OF IRRADIATED METALS

A. V. Bialobzheskii

(Presented by Academician A. N. Frumkin, October 16, 1957)

Up to the present time, no works have been published on the study of the influence of radiation on the atmospheric corrosion of metals. Allen [1] points out that corrosion in gases under the influence of ionizing radiations has not been made the subject of study, and points to the well-known fact that no corrosion is observed in the exit windows of cathode ray tubes and cyclotrons, in spite of the powerful radiation passing through them. It might seem that this fact provides evidence that radiation shows no noticeable influence on the corrosion of metals in atmospheric conditions. Our studies have shown, however, that in a number of cases ionizing radiation considerably accelerates the processes of atmospheric corrosion.

The experiments were carried out in a closed glass vessel at a relative humidity of 98%. A cathode ray tube, a BFV-70 x-ray tube and a specimen of Co^{60} were used as radiation sources.

TABLE 1
The Influence of Radiation on the Corrosion of Various Metals in an Atmosphere of Air at a Relative Humidity of 98% (Duration of Irradiation 16 Hours, Temperature, 25°)

Radiation source	Metal being irradiated	External appearance of metal after irradiation	Increase in wt. in g/specimen
Cathode ray tube 800 kv, 4.1 μamp	Iron	Covered with compact reddish-brown corrosion products	0.0247
Ditto	Copper	Olive-colored rim around the edge, brick-red corrosion products in the center	0.0120
Ditto	Aluminum	Isolated white patches of corrosion	0.0023
Ditto	IX18N9T Steel	Brilliant, with no visible signs of corrosion	0
Cathode ray tube 4.1 μamp, 400 kv	Zinc	Covered with white corrosion products	0.0053

Notes: 1. For all the metals tested, control corrosion experiments were carried out in parallel under the same conditions, but without the radiation. In all cases the metals retained their initial appearance and showed no change in weight. 2. The rate of corrosion was calculated for the iron specimen and was found to be equal to 1 mm/year.

It was established (see Table 1) that the corrosion of iron, copper and zinc is sharply accelerated, while that of aluminum is accelerated to a much lesser extent, by the action of ionizing radiation in a moist atmosphere (the metals are listed in decreasing order of effect of radiation action). In our experiments, radiation showed absolutely no intensifying action on the corrosion of stainless steel. Under atmospheric conditions, therefore, the least effect of the action of radiation is shown by those metals which are able to form stable oxide films on their surface.

Figure 1 shows photographs of iron specimens after irradiation. A photograph of a specimen which has not been irradiated is given for comparison.

It was also established that in a dry atmosphere (dried with phosphorus pentoxide) no corrosion takes place under any irradiation conditions. This provides evidence that with irradiation in atmospheric conditions, corrosion takes place under a film of moisture which is formed on the metal surface as a result of condensation or adsorption of water vapor upon it, and is consequently of an electrochemical character, as in the case of ordinary atmospheric corrosion. The data in Table 2 show that increase in the intensity of the irradiation increases the rate of corrosion of iron.

TABLE 2
The Influence of Radiation Intensity On The Corrosion of Armco Iron In An Atmosphere of 98% Relative Humidity (Duration of Irradiation 10 hours, Temperature 25°)

Radiation source	Cuttent in μamp	Position of specimen in apparatus	Energy absorbed in ev/cc•sec	Increase in wt. of specimen, g/specimen
Cathode ray tube	4.1	above	$1.9 \cdot 10^{19}$	0
		below	$6.8 \cdot 10^{17}$	0.0133
	1.0	above	$4.7 \cdot 10^{18}$	0.0060
		below	$1.7 \cdot 10^{17}$	0.0061
	0.4	above	$1.9 \cdot 10^{18}$	0.0043
		below	$6.8 \cdot 10^{16}$	0.0021
X-ray tube BFV-70, 50 kv	200	above	$2.7 \cdot 10^{18}$	0.0050
		below	$5.3 \cdot 10^{16}$	0.0018
	50	above	$6.8 \cdot 10^{17}$	0.0006
		below	$1.3 \cdot 10^{16}$	0

The fact, unexpected at first sight, that the upper specimen irradiated with an electron stream of 4.1 μamp and absorbing the maximum amount of energy shows absolutely no corrosion, is , as our experiments have shown, the result of the influence of a secondary factor — the heating of the specimen as a result of the absorption of a large amount of energy, which leads to the removal from the metal surface of the moisture film necessary for the atmospheric corrosion process to take place, as has been shown above. When the upper specimen was cooled with water or air, an immediate increase in the corrosion of its irradiated surface was observed. The intensifying action of the radiation can be seen very clearly from the experiments illustrated in Figs. 2 and 3, — in both cases the metal which has been protected from direct radiation is not corroded at all.

The intensification of the corrosion process under irradiation may be the result of a change in the state of the corrosion medium or of a change in the state of the metal surface layer. In order to resolve this question, we carried out the following experiment: two specimens were placed in position with a 5-millimeter thick lead plate between them. The upper specimen of the pair absorbed $2.8 \cdot 10^{16}$ ev/sec. In the lower, the value of the absorbed energy equalled zero (neglecting the extremely small effect of the scattered radiation). In spite of this difference, both specimens were corroded to the same extent. This shows that the products of radiation changes in the atmosphere, and not metal surface activation, play the chief role in intensifying corrosion under the influence of radiation.

We have carried out a cycle of experiments designed to examine the parts played by the most important constituents of the atmosphere — oxygen and nitrogen; the results are given in Table 3.

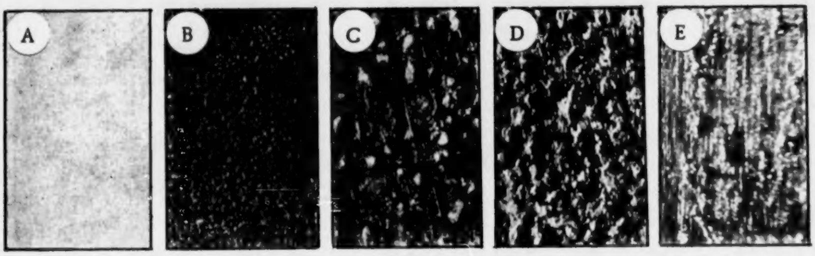

Fig. 1. Photographs of iron specimens after corrosion tests in an atmosphere of 98% relative humidity. A) Without irradiation (10 hours); B and C) after irradiation with x-rays (10 hours); D) after irradiation with electron stream of 3 μamp (15 hours); E) after irradiation with a cobalt source (70 hours). A and B) 2 × ; C, D, and E) 30 × .

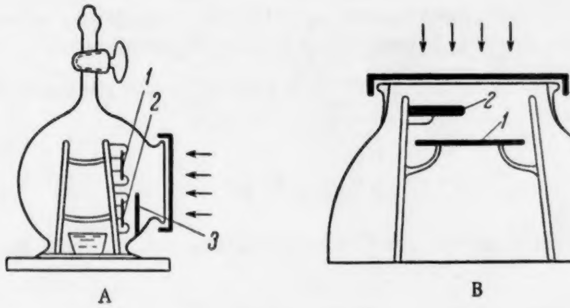

Fig. 2. Diagram of the apparatus used in experiments on the influence of the direct action of a beam of x-rays (A) and an electron beam (B) on the corrosion of an iron specimen. Diagram A: 1) unprotected specimen, 2) protected by 5-millimeter thick lead plate, 3) Diagram B: 1) specimen; 2) lead half-disc, 5 mm thick.

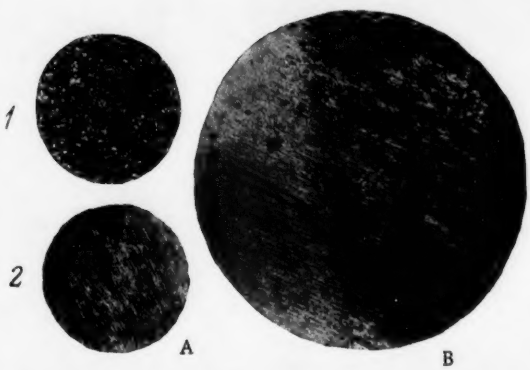

Fig. 3. The influence of the direct action of an x-ray beam (A) and a beam of electrons (B) on the corrosion of an iron specimen. A1) unprotected specimen, 2×; A2) specimen behind 5-millimeter thick lead plate, 2×; B) exposed part on the right, part protected by lead on the left.

TABLE 3

The Corrosion of Armco Iron After 10 Hours in Various Gas Mixtures at 98% Relative Humidity With Irradiation From A Cathode Ray Tube (2.0 μamp; 800 kv)

Atmosphere	Upper specimen, energy absorbed $0.8 \cdot 10^{19}$ ev/cc·sec	Lower specimen, energy absorbed $3 \cdot 10^{17}$ ev/cc·sec
	Increase in wt. in g/specimen	
Pure oxygen	0.0031	0.0019
Nitrogen 80%, oxygen 20%	0.0059	0.0079
Argon 80%, oxygen 20%	0.0010	0.0024
Pure nitrogen	0.0001	0.0002

The data given show that nitrogen, which is inert under normal conditions, becomes actively corrosive under the influence of radiation. The activation of nitrogen

takes place only in the presence of oxygen and may consequently be attributed to the formation of its oxygen products, the most important of which is N_2O_5.

As early as 1911, V. G. Khlopin established that ozone, hydrogen peroxide and nitrous anhydride are formed in moist air under the influence of ultraviolet light [2]. The analyses which we carried out on the atmosphere from the reaction vessel after irradiation showed that the greatest amount of ozone (from the 4.1 μamp, 800 kv electron beam) amounted to 0.4% in air and to 0.5% in pure oxygen. The quantity of oxides of nitrogen, calculated as NO_3', amounted to approximately 0.08%. Hydrogen peroxide was not detected quantitatively in our experiments. It is evidently formed in insignificant amounts. All these long-lived products of irradiation of the atmosphere undoubtedly have an intensifying action on the processes of corrosion. The action of the short-lived radiation products (OH and OH_2 radicals, O atoms, compounds of the type NO_3, etc.) is even more intense, as is shown by the experiments referred to in Figs. 2 and 3.

It is interesting that the extent of the corrosion in pure oxygen is not markedly greater than in the argon—oxygen mixture. This is evidently the result of the passivating action of the strongly oxidizing medium created in oxygen during irradiation.

According to our ideas, the intensification of the process of atmospheric corrosion results from the fact that the radiation products formed intensify the corrosion current of the microcells by acting as energetic cathodic depolarizers. This theory of ours is at present being checked experimentally.

In conclusion I express my gratitude to Professor N. D. Tomashov for much valuable counsel during the discussion of the present work.

LITERATURE CITED

[1] A. Allen, Collection, The Scientific and Technical Fundamentals of Atomic Energy, edited by K. Gudmen , 2, (Foreign Lit. Press, 1950), p. 224.

[2] V. G. Khlopin, J. Russ. Phys.-Chem. Soc. 43, 554 (1911).

Institute of Physical Chemistry,
USSR Academy of Sciences.

Received October 11, 1957.

MAGNETOCHEMISTRY OF ORGANIC COMPOUNDS AND "CHEMICAL" SHIFTS OF NUCLEAR MAGNETIC RESONANCE

Ia. G. Dorfman

(Presented by Academician N. N. Semenov, November 13, 1957)

It is known that "chemical" shifts of nuclear magnetic resonance are caused by intramolecular magnetic fields, acting on the given nucleus, and depend on the chemical bond of the given atom in the molecule. Calculation of these fields is closely connected with the orientation of the magnetic moments in the molecules, induced by an external field [1]. Attempts at the theoretical calculation of these moments and the chemical shifts produced by them [2] met with very great difficulties in most cases, similar to attempts at the theoretical calculation of susceptibilities.

Recently, we were able to devise a magnetochemical scheme of organic compounds. This allowed us to evaluate the diamagnetic and paramagnetic components of the magnetism of aliphatic and alicyclic compounds and to find the fraction of the susceptibilities arising from separate atoms and groups of atoms [3]. It is natural to attempt to apply these results of magnetochemistry to the consideration and calculation of chemical shifts of nuclear magnetic resonance.

First of all, let us consider the case when protons are present in a group of atoms, connected by only single bonds, for example: $CH_3—C\lessdot$, NH_2, $CH_3—N<$, $CH_2—$ in alicyclic compounds. As the observed shifts are related to the shift in H_2O, it is necessary to consider the OH group also. It is assumed that the resonance is observed at some fixed frequency. Let us assume that for this an external field H_0 is required for resonance of a proton in an isolated hydrogen atom.

As magnetochemical data show [3], the atoms C, N, and O in the groups given, display diamagnetism (for 1 mole): $\chi_{dC} \cong 8 \cdot 10^{6}$, $\chi_{dN} \cong 7 \cdot 10^{-6}$, $\chi_{dO} \cong -9 \cdot 10^{-6}$. The paramagnetism of these atoms in the groups given is practically zero.

TABLE 1

	$CH_3—C\lessdot$	NH_2	$CH_3—N<$	CH_2 in alicyclic compounds
$10^5\delta$ cal	−0,42	−0,41	−0,32	−0,31
$10^5\delta$ exp	−0,40	−0,36	−0,25	−0,36

An external field, acting on these atoms, induces moments which are oriented antiparallel to the external field. At the location of the proton these induced moments form a field, oriented parallel to the external field, i.e., augmenting it. Thus, for resonance of a proton in H_2O it is necessary that the field $H_r = H_0 - k_{OH}H_r$, and for resonance of a proton in any of the given groups it is necessary that the field $H_{gr} = H_0 - k_{gr}H_{gr}$, where k_{OH} is a constant peculiar to OH and k_{gr} is a constant associated with the particular group.

As is known, the shift, relative to water, may be designated by the value

$$\delta_{gr} = \frac{H_r - H_{gr}}{H_r} = \frac{-k_{OH}H_r + k_{gr}H_{gr}}{H_r}.$$

Since H_{gr} differs from H_r by an insignificant fraction of a percent, we may consider that $H_{gr}/H_r \cong 1$ and $\delta_{gr} = - k_{OH} + k_{gr}$. The constants k_{OH} and k_{gr} are the values of the fields produced at the location of the proton by its diamagnetic neighbors with an external field equal to 1. Thus

$$k_{OH} = \frac{\chi_{dO}}{d^3_{OH}N}; \quad k_{gr} = \frac{1}{N}\sum \frac{\chi_{dA}}{d^3_{AH}},$$

where d_{OH} is the separation between the proton and the O nucleus in OH; N is Avogadro's number; κ_{dA} is the susceptibility of one of the surrounding atoms; d_{AH} is the separation between the nucleus A of the given atom and the proton investigated. Considering that $d_{OH} = 0.96 \cdot 10^{-8}$ cm, $d_{CH} = 1.09 \cdot 10^{-8}$ cm, $d_{NH} = 1.01 \cdot 10^{-8}$ cm and $d_{C-C} = 1.54 \cdot 10^{-8}$ cm, we obtain the results given in Table 1; thus, $k_{OH} = 1.54 \cdot 10^{-5}$. The good agreement between the calculated and the experimental values of the shifts confirms the accuracy of the considerations on which the calculations were based.

For groups of atoms containing double or triple bonds, for example $=CH_2$ or $\equiv CH$, the paramagnetic component of the susceptibility is considerably increased, as ensues from magnetochemical considerations. If this paramagnetism was only caused directly by the carbon atoms connected to each other by double or triple bonds, then the effect that we noted above of diamagnetic carbon atoms on protons, would be weaker in the presence of double or triple bonds. In this case, the field required for resonance of protons in $=CH_2$ and in $\equiv CH$ would be greater than in $-CH_3$. Experiment (4) shows, on the contrary, that $\delta_{=CH_2} = +0.05 \cdot 10^{-5}$ to $0.02 \cdot 10^{-5}$, i.e., close to zero, and $\delta_{\equiv CH} = -0.25 \cdot 10^{-5}$, i.e., considerably less than δ_{CH_3}. On the other hand, experiments carried out on the resonance of C^{13} nuclei [5] show that the paramagnetism of a double bond also reduces to the value of the field required for resonance of the carbon nuclei. Thus, the paramagnetism of double and triple bonds, augmenting the external field, acts in the same direction both at the carbon nucleus and at the protons nearest to them. This apparently indicates that this paramagnetism is produced by electrons, "encircling" both the C atoms and the H atoms directly connected to them.

The considerations and calculations presented make it possible to establish a connection between nuclear magnetic resonance investigations and magnetostatic susceptibility (magnetochemistry). One may hope that the combination of these two fields of investigation will prove very useful in the study of molecular structure.

LITERATURE CITED

[1] N. F. Ramsey, Phys. Rev. 78, 699 (1950); 83, 540 (1951); 86, 243 (1952).

[2] J. A. Pople, Proc. Roy. Soc. London A 239, 541 (1957).

[3] Ia. G. Dorfman, Proc. Acad. Sci. USSR 119, 2 (1958).*

[4] L. H. Meyer, A. Saika, and H. S. Gutowsky, J. Am. Chem. Soc. 75, 4567 (1953).

[5] P. C. Lauterbur, J. Chem. Phys. 26, 217 (1957).

Leningrad Hydrometeorological Institute

Received November 11, 1957.

* Original Russian pagination. See C. B. Translation.

A NEGATIVE TEMPERATURE COEFFICIENT IN HYDROCARBON OXIDATION

N. S. Enikolopian

(Presented by Academician V. N. Kondrat'ev, September 14, 1957)

A characteristic property of hydrocarbon oxidation is the presence of a so-called negative temperature coefficient in a certain temperature range [1-11]. Figure 1 shows a curve of reaction rate against temperature, typical of hydrocarbon oxidation. The temperature range between the two extremes is called the region of "negative temperature coefficient." The maximum usually lies in the range 350-400° and the minimum 450-500°. Depending on the nature of the hydrocarbons, the pressure, the mixture composition, the state of the surface and other factors, the temperature limits of the region may vary.

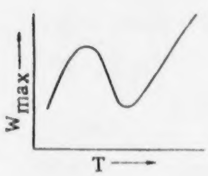

Fig. 1.

The existence of a region of a negative temperature coefficient strongly affects the kinetics of slow oxidation, the position of the limits and the character of hydrocarbon self-ignition. However, until recently this phenomenon was not explained rationally. A detailed examination showed that the existing theories [6, 12-14] do not, in fact, explain the phenomenon of a negative temperature coefficient.

On the basis of N. N. Semenov's theory [15] on degenerate branching, in this work we considered the phenomenon of a negative temperature coefficient as a result of competing elementary processes that participate in a complex chain reaction.

It is accepted that at low temperatures hydrocarbons are oxidized through peroxide radicals, formed by the reaction

$$\dot{R} + O_2 \rightarrow RO\dot{O}. \qquad (1)$$

This process is characterized by a low steric factor (10^{-3} to 10^{-4}) and a low activation energy (2-4 kcal/mole). The elementary process of degenerate branching, according to B. Lewis and G. Elbe [13] and V. V. Voevodskii and V. I. Vedeneev [16], may be considered as the result of a peroxide radical interacting with a stable intermediate product, for example, with an aldehyde

$$RO\dot{O} + R'CHO \rightarrow R\dot{O} + \dot{O}H + R'\dot{C}O. \qquad (2)$$

As a result of this reaction, three new active centers are formed from one radical. The endothermal heat of this process is about 10 kilocalories per mole [16].

Besides Reaction (2) which results in branching, the peroxide radical $RO\dot{O}$ may also enter the propagation Reaction (17)

$$RO\dot{O} \rightarrow R'CHO + R''\dot{O}. \qquad (3)$$

Reaction (3) proceeds by first isomerizing the peroxide radical and therefore it has a high activation energy (20 kcal/mole) [18].

The competition between Reactions (2) and (3) leads to the appearance of a maximum on the curve in Fig. 1. In fact, at low temperatures the peroxide radical should react by the bimolecular Reaction (2), which

proceeds with a lower activation energy (10-12 kcal/mole). The rate of this process increases with an increase in temperature and this leads to an increase in the rate of hydrocarbon oxidation. At a certain temperature (corresponding to the maximum rate on the curve in Fig. 1), the monomolecular propagation Reaction (3), which proceeds with a high activation energy, starts to predominate over the branching Reaction (2) and this results in a decrease in the oxidation rate. At these temperatures the oxidation rate is determined, not by process (3) as occurred at lower temperatures, but by the formation of the peroxide radical (1), as the latter reaction is characterized by a low steric factor, although it does have a low activation energy. As Reaction (1) becomes the limiting stage in the process, the destruction of active centers is mainly determined by the destruction of radicals R. Thus, with an increase in temperature, due to the competition between the two parallel peroxide radical reactions, (2) and (3), on the one hand, the possibility of branching decreases and, on the other, the stationary concentration of $RO\dot{O}$ radicals decreases, as Reaction (1) becomes the limiting process. Due to this, the rate of hydrocarbon oxidation falls sharply with an increase in temperature.

The decrease in the oxidation rate will proceed up to a definite temperature (corresponding to the minimum in the curve in Fig. 1). With a further increase in temperature the reaction rate again starts to grow, as it comes under the effect of degenerate branching of another type [19]

$$RCHO + O_2 \rightarrow R\dot{C}O + H\dot{O}_2. \quad (4)$$

N. N. Semenov [15] proposed this type of degenerate branching and we applied it in considering the mechanism of methane oxidation [17]. The elementary process (4) is strongly endothermal and it should therefore be considered only at relatively high temperatures (after the rate minimum on the curve in Fig. 1).

The appearance of a region of negative temperature coefficient in hydrocarbon oxidation may be considered qualitatively.

Starting from such a simplified scheme for hydrocarbon oxidation and considering that the branching rate is less than the rate of chain propagation, we obtain the following expression for the reaction rate:

$$W = \frac{W_0 a_3}{g_1 + \frac{g_2}{a_1} a_3 - 2a_2}, \quad (5)$$

where W is the rate of hydrocarbon oxidation, W_0 is the rate of active center formation, g_1 is the constant of $RO\dot{O}$ radical destruction, g_2 is the constant of $\dot{R}$ radical destruction, $a_1 = K_1[O_2]$; $a_2 = K_2[X]$; $a_3 = K_3$; $[X]$ is the concentration of the intermediate product, responsible for degenerate branching (aldehyde).

It follows from Equation (5) that under the given conditions the reaction rate is determined by the aldehyde concentration [X], whose maximum corresponds to the maximum rate. The maximum concentration of X is, in its turn, a complex function of temperature [20].

Assuming that the total activation energy of Reaction (2) is less than the activation energy of Reaction (3), it is readily shown by using Equation (5) that the rate of hydrocarbon oxidation passes through a maximum with increasing temperature. For this, Equation (5) is rewritten in dimensionless coordinates:

$$\theta = \frac{1}{1 + \alpha - \beta}, \quad (6)$$

where $\theta = W \cdot g_1/W_0 a_3$ is the dimensionless reaction rate; $\alpha = g_2 a_3/g_1 a_1$ is the dimensionless parameter, which takes into account the relative rates of processes (3) and (1); $\beta = 2a_2/g_1$ is the dimensionless branching parameter.

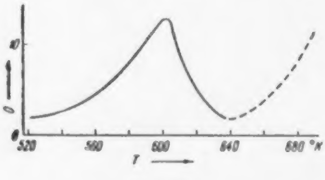

Fig. 2.

Figure 2 gives the curve of reaction rate against temperature, calculated by Equation (6). For this calculation we assumed that $\alpha = 4 \cdot 10^6 e^{-1800/RT}$; $\beta = 9 \cdot 10^4 e^{-10000/RT}$.

We also solved the reverse problem. Assigning the necessary values to the ratio of the pre-exponentials and the difference in activation energy of the elementary reactions, in Equation (6), we calculated the value of the steric factor for Reaction (1) with a normal

pre-exponential (10^{13}) for Reaction (3), so that the maximum of the reaction rate would appear at 400°. The calculations showed that if the difference in activation energy of Reactions (3) and (2) was taken as 10 kcal/mole, then the steric factor for Reaction (1) would be of the order of 10^{-3}.

Thus, the simplified scheme proposed for hydrocarbon oxidation, taking into account the competition between Reactions (3) and (2), results in the appearance of a maximum in the reaction rate against temperature curve. Apparently, with a further increase in temperature, consideration of Reaction (4) will result in an increase in the reaction rate.

LITERATURE CITED

[1] R. N. Pease, J. Am. Chem. Soc. 51, 1839 (1929); 60, 2244 (1938).

[2] R. N. Pease and W. K. Munroe, J. Am. Chem. Soc. 56, 2054 (1934).

[3] D. W. Newitt and L. S. Thornes, J. Chem. Soc. (1938), 1669.

[4] H. A. Beatty and G. J. Edgar, J. Am. Chem. Soc. 56, 102 (1934).

[5] G. H. N. Chamberlain and A. D. Walsh, 3rd Symposium on Combustion (Baltimore, 1949).

[6] M. B. Neiman and B. V. Aivazov, Nature 135, 655 (1935).

[7] B. V. Aivazov and M. B. Neiman, J. Phys. Chem. 8, 88 (1936).

[8] J. Barwell and C. N. Hinshelwood, Proc. Roy. Soc. A 205, 375 (1951).

[9] N. M. Chirkov and S. G. Entelis, Coll. Kinetics of Chain Oxidation Reactions* (Acad. Sci. USSR Press, 1950), p. 118.

[10] N. C. W. Shu and J. Bardwell, Canad. J. Chem. 33, 1415 (1955).

[11] V. Ia. Shtern, Coll. Chain Reactionsof Hydrocarbon Oxidation in the Gas Phase* (Acad. Sci. USSR Press, 1955), p. 37.

[12] A. K. Ubbelohde, Proc. Roy. Soc. A 152, 354 (1935).

[13] B. Lewis and G. Elbe, Combustion, Flames and Explosions in Gases (Foreign Lit. Press, 1948) [Russian Translation].

[14] V. Jost, Explosions and Combustion in Gases (Foreign Lit. Press, 1952) [Russian Translation].

[15] N. N. Semenov, Chain Reactions* (1934).

[16] V. V. Voevodskii and V. I. Vedeneev, Proc. Acad. Sci. USSR 106, 4, 679 (1956). **

[17] L. V. Karmilova, N. S. Enikolopian and A. B. Nalbandian, J. Phys. Chem. 30, 4, 798 (1956).

[18] N. N. Semenov, Some Problems of Chemical Kinetics and Reactivity* (Acad. Sci. USSR Press, 1954).

[19] N. S. Enikolopian, J. Phys. Chem. 30, 4, 769 (1956).

[20] N. S. Enikolopian, G. V. Korolev and G. P. Savushkina, J. Phys. Chem. 31, 4, 865 (1957).

Institute of Chemical Physics of the
Academy of Sciences of the USSR

Received September 11, 1957.

* In Russian.

** Original Russian pagination. See C. B. translation.

THE THERMODYNAMICS OF THE CHLORINATION OF RARE EARTH METAL OXIDES WITH GASEOUS CHLORINE

I. S. Morozov and B. G. Korshunov

(Presented by Academician I. I. Cherniaev, November 16, 1957)

The present work is a continuation of our studies on the thermodynamics and chemistry of the interaction of rare metal oxides with gaseous chlorine [1, 2]. A study has been made of the equilibria in reactions of the type $4MCl_3 (s) + 3O_2 (g) \rightleftharpoons 2M_2O_3 (s) + 6Cl_2 (g)$, where M denotes Sc, La, Nd, and Sm. The studies were carried out in conditions where the equilibrium state was approached from either direction, i.e., from the chloride– oxygen side and the oxide– chlorine side. The chlorides of the metals were prepared from specimens made available to us by I. N. Zaozerskii, according to the method described in the textbook [3]. The equilibrium composition of the gases was determined by a static method, by which a specimen of the gases was removed through a capillary from the reaction space above the mixture of oxide and chloride after equilibrium had been established in the system.

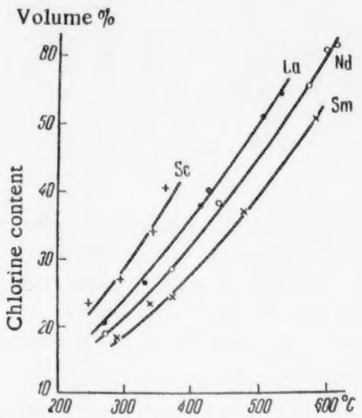

Fig. 1. Dependence of the Cl_2 content in the equilibrium gas composition on temperature.

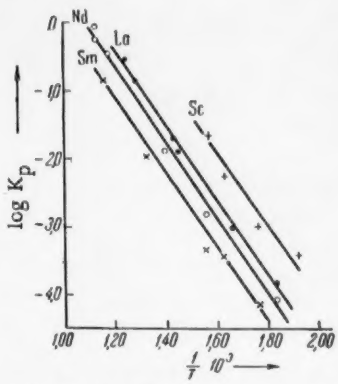

Fig. 2. Dependence of log K_p on 1/T.

The analysis was carried out in a gas buret placed in a thermostat, concentrated sulfuric acid saturated with chlorine being used as sealing liquid. The chlorine was absorbed from the mixture of gases with 20% caustic soda solution while the oxygen was determined as the difference between the volume of gas taken for analysis and the volume of gas absorbed.

The "flow" method used in the works mentioned above was not applicable to the oxides under examination, in view of the extremely low rates of establishment of equilibrium in the reactions, particularly at low temperatures. We established that the equilibrium state in the oxide– chlorine system is not reached even after 10 days (at 350°). The data concerning the composition of the gas phase above the $Nd_2O_3-Cl_2$ and $La_2O_3-Cl_2$

systems in the work [2], therefore, do not evidently correspond to the equilibrium condition, in contrast to the data for the chloride–oxygen system, in which equilibrium is established much more rapidly.

TABLE 1

Results Obtained from Study of the Equilibria in the Systems $4MCl_3 (s) + 3O_2 (g) \rightleftharpoons 2M_2O_3 (s) + 6Cl_2 (g)$

Temperature, °C	Equilibrium composition of the gas phase % by volume		K_p	ΔZ, cal	ΔH, cal
	Cl_2	O_2			
Reaction $4ScCl_3 (s) + 3O_2 (g) \rightleftarrows 2Sc_2O_3 (s) + 6Cl_2 (g)$					
250	23,5	76,5	$3,762 \cdot 10^{-4}$	8190	+24580
295	27,2	72,8	$1,051 \cdot 10^{-3}$	7740	
340	34,2	65,8	$8,747 \cdot 10^{-3}$	6310	
364	40,6	59,4	$2,136 \cdot 10^{-2}$	4860	
Reaction $4LaCl_3 (s) + 3O_2 (g) \rightleftarrows 2La_2O_3 (s) + 6Cl_2 (g)$					
274	20,5	79,5	$1,478 \cdot 10^{-4}$	8450	+25230
330	26,7	73,3	$9,198 \cdot 10^{-4}$	8380	
415	38,0	62,0	$1,264 \cdot 10^{-2}$	5980	
425	40,2	59,8	$1,972 \cdot 10^{-2}$	5440	
505	50,6	49,4	$1,393 \cdot 10^{-1}$	3050	
533	54,4	45,6	$2,733 \cdot 10^{-1}$	2070	
Reaction $4NdCl_3 (s) + 3O_2 (g) \rightleftarrows 2Nd_2O_3 (s) + 6Cl_2 (g)$					
270	19,0	81,0	$8,857 \cdot 10^{-5}$	10070	+25700
368	28,6	71,4	$1,504 \cdot 10^{-3}$	8270	
440	38,3	61,7	$1,344 \cdot 10^{-2}$	6100	
575	55,7	44,3	$3,438 \cdot 10^{-1}$	1800	
600	60,5	39,5	$7,962 \cdot 10^{-1}$	395	
615	61,4	38,6	$9,319 \cdot 10^{-1}$	120	
Reaction $4SmCl_3 (s) + 3O_2 (g) \rightleftarrows 2Sm_2O_3 (s) + 6Cl_2 (g)$					
290	18,5	81,5	$7,406 \cdot 10^{-5}$	10630	+25520
340	23,5	76,5	$3,762 \cdot 10^{-4}$	9600	
372	24,3	75,7	$4,597 \cdot 10^{-4}$	9750	
480	37,2	62,8	$1,069 \cdot 10^{-2}$	6785	
585	50,6	49,4	$1,393 \cdot 10^{-1}$	3360	

Taking this into consideration in the study of the equilibrium from the oxide–chlorine side, and in order to have an excess of the latter in the gas phase (compared with the equilibrium composition), we used the method described in the work [4]. The chloride, placed in the furnace in an atmosphere of oxygen, was heated to 50-80° above the temperature of the experiment, and when constant pressure had been established in the system the temperature was rapidly lowered to the required value. Equilibrium in the chloride–oxygen system was reached in 3-5 days, according to the temperature of the experiment.

Chlorination of the oxides and oxidation of the chlorides of the metals proceeds without the formation of intermediate products. Thus, analysis of the oxides of Sc, La, Nd, and Sm, chlorinated at 400°, showed in the products the chlorides of composition $ScCl_3$, $LaCl_3$, $NdCl_3$ and $SmCl_3$ (M :3Cl ratio 0.421; 1.30; 1.32; 1.40; respectively; according to theory 0.424; 1.30; 1.36; and 1.42).

In accordance with the equation for the Law of Mass Action, the equilibrium constants for the reactions $4MCl_3 (s) + 3O_2 (g) \rightleftharpoons 2M_2O_3 (s) + 6 Cl_2 (g)$ were calculated as follows:

$$K_p = P^6_{Cl_2} / P^3_{O_2},$$

where P_{Cl_2} and P_{O_2} – the equilibrium partial pressures of the chlorine and oxygen; and

$$P_{Cl_2} = \frac{P_{syst}}{760} \frac{A}{100}, \quad P_{O_2} = \frac{P_{syst}}{760} \frac{100 - A}{100},$$

where A – percentage concentration of chlorine in the gas phase, $P_{syst.}$ – pressure in the system, corresponding to equilibrium (see Table 1).

The free energy changes for the reactions, calculated in accordance with the well-known expression

$$\Delta Z = -RT \ln K$$

are also given in Table 1.

The mean values for the heat effects in the reactions, according to the reaction isochore equation

$$\log K_{T_2} - \log K_{T_1} = \frac{\Delta H}{2{,}303 R}\left(\frac{1}{T_1} - \frac{1}{T_2}\right),$$

amounted to + 24,580; + 25,230; + 25,700; + 25,520 cal. respectively in the temperature ranges indicated. Figure 1 shows the equilibrium composition of the gas phase. Figure 2 shows the relationship between log K_p and 1/T. As can be seen from Fig. 2, the values for log $K_p = f(1/T)$ fall satisfactorily on straight lines.

The results obtained show that the close physical and chemical properties of the elements under examination result in a similarity in thermodynamic properties.

LITERATURE CITED

[1] I. S. Morozov and B. G. Korshunov, The Chemistry of the Rare Elements 2, 102 (1955). *

[2] I. S. Morozov and B. G. Korshunov, J. Inorg. Chem. 1, 2606 (1956).

[3] Textbook of Preparative Inorganic Chemistry, edited by G. Brauer, (Foreign Lit. Press, 1956). **

[4] V. I. Smirnov and A. I. Tikhonov, Bull. Acad. Sci. USSR, Div. Tech. Sci. 9, 48 (1956).

N. S. Kurnakov Institute of General and Inorganic Chemistry.

Received November 11, 1957.

* In Russian.

** Russian translation.

CALCULATION OF THE RATE OF DECOMPOSITION OF DIATOMIC MOLECULES

E. E. Nikitin

(Presented by Academician V. N. Kondrat'ev, October 24, 1957)

The paper [1] gives the calculation of the rate constant for the thermal decomposition of diatomic molecules and the distribution functions according to the vibrational states on breakdown of the thermal equilibrium distribution. An essential feature of this calculation is the assumption that the vibrational quanta remain approximately constant up to the dissociation limit. In the present work the rate constant for the reaction AB + C → A + + B + C is calculated without this limitation.

Let us assume that on collision in a diatomic molecule, a change may take place only between neighboring vibrational levels, while dissociation of the molecule is possible only from the last discrete level [1]. We shall use $P_{k,k-1}$ to denote the probability of the change from the k level to the $k-1$ level for one collision, and P_{∞} to denote the probability of the change from the last n-th discrete level to the state with a continuous energy spectrum. We shall assume also that the Maxwellian distribution of colliding molecules is observed. This assumption is also extremely well justified when the dissociation energy is greater than kT (the percentage correction of the rate of reaction taking account of the breakdown of the Maxwellian distribution of the order of $kT/25D$ [2]). In this case the probability of the vibrational excitation of the molecule on collision from the $k-1$ level to the k level is related to $P_{k,k-1}$ by the relationship

$$P_{k-1,k} = P_{k,k-1} \exp\left(-\frac{E_{k,k-1}}{kT}\right) \equiv \alpha_k P_{k,k-1}, \tag{1}$$

which follows from the detailed equilibrium principle. In this expression, $E_{k,k-1}$ denotes the energy difference between the k and $k-1$ levels.

If we use $x_k(t)$ to denote the distribution function, i.e., the probability of finding the molecule in the k-th level, then the change in this quantity with time is described by the following system of equations:

$$\frac{dx_k}{dt} = Z\{\alpha_k P_{k,k-1} x_{k-1} - (P_{k,k-1} + \alpha_{k+1} P_{k+1,k}) x_x + P_{k+1,k} x_{k+1}\}, \quad k = 0, 1, \ldots, n, \tag{2}$$

with the limiting conditions $x_{-1} = x_{n+1} = 0$, which signify that the vibrational spectrum of the molecule contains $n+1$ levels. In the system of Equations (2), Z denotes the number of collisions of AB and C in 1 second and the symbol $P_{\infty} = P_{n,n+1}\alpha_{n+1}$ is introduced.

The general solution of the system has the form

$$x_k(t) = \sum_{m=0}^{n} A_k(\mu_m) \exp(-\mu_m t), \tag{3}$$

where μ_m are the particular values of the matrix $\hat{B}$ of the right-hand part of the system (m denotes these particular values in the order of increasing μ).

If $P_{n,\,n+1} = 0$, then the particular values of the corresponding matrix $\hat{B}^{(0)}$ form a series $\mu_m^{(0)}$. The first particular value $\mu_0^{(0)} = 0$ then corresponds to the thermal equilibrium distribution.

If $P_{n,\,n+1} \neq 0$, then in accordance with the general theory of local excitations [3], all the μ_m are shifted relative to $\mu_m^{(0)}$ in one direction, namely $\mu_m > \mu_m^{(0)}$ when $P_{n,\,n+1} > 0$. If $\mu_0 \ll \mu_1$, then for $t \gg 1/\mu_1$ it follows from (3) that there is an exponential damping of the distribution function, which corresponds to decomposition. Calculation shows that the condition $\mu_0 \ll \mu_1$ is fulfilled for most reactions (for example, for T = 1000°, D = 100 kcal/mole, $\mu_0 \sim \mu_1 \cdot 10^{-8}$). For the same condition, the lowest particular value of the matrix may be found by reducing its determinant $D(\hat{B} - \mu\hat{1})$ to zero by steps of μ and confining ourselves to the linear term.

Calculation gives

$$\mu_0 = Z \Big/ \Big[\sum_{j=0}^{n} \exp\Big(-\frac{E_j}{kT}\Big) \sum_{s=j}^{n+1} \exp\Big(\frac{E_s}{kT}\Big) \Big/ P_{s,s-1}\Big], \tag{4}$$

where summation is carried out at all discrete levels. In the Expression (4), the second sum in brackets is slightly dependent on the lower limit of summation, since the terms in the sum increase markedly with increase in the index s. They can therefore be taken out from the summation over j and the lower limit of the summation may be taken as unity. The sum to j terms is then simply equal to the vibrational sum of states Q. Since the equilibrium distribution function is determined by the formula

$$x_k^{(0)} = \exp\Big(-\frac{E_k}{kT}\Big) \Big/ Q,$$

the Expression (4) may be rewritten in the simpler form:

$$\mu_0 = Z \Big/ \Big[\frac{1}{x_n^{(0)} P_\infty} + \sum_{k=1}^{n} \frac{1}{x_k^{(0)} P_{k,k-1}}\Big]. \tag{5}$$

In order to calculate μ_0 we note that normally the relationship $x_n^{(0)} P_\infty \gg x_k^{(0)} P_{k,\,k-1}$ is observed. This leaves only the second term in (5) – the sum of the changes in the discrete spectrum. If we assume that near the dissociation threshold $E_{k,\,k-1} < kT$, while $P_{k,\,k-1}$ is slightly dependent on E_k for low quanta, then the summation may be replaced by an integration, and $P_{k,\,k-1}$ taken out from under the integral sign at the point E = D:

$$\sum_{k=1}^{n} \frac{1}{x_k^{(0)} P_{k,k-1}} \approx \frac{1}{\mathscr{E}} \int_0^D \frac{dE}{x(E)\,P(E)} \approx \frac{kT}{\mathscr{E} P(D)} \exp\Big(\frac{D}{kT}\Big) Q. \tag{6}$$

Here $\mathscr{E}$ denotes a certain average quantum close to the dissociation threshold.

After these transformations the Formula (5) has the form:

$$\mu_0 = Z\Big(\frac{\mathscr{E}}{D}\Big)\Big(\frac{D}{kT}\Big) P(D) \exp\Big(-\frac{D}{kT}\Big) \Big/ Q. \tag{7}$$

The changes between nonneighboring levels may be calculated approximately if we sum the values of μ_0, determined by Formula (7), along all the "parallel routes" of the decomposition. In this case $\mathscr{E} P(D)$ in (7) should be replaced by $\sum_n \mathscr{E}_n P_n(D)$, where the index n corresponds to changes to a neighboring level via 1, 2, etc. levels. The probability $P_n(D)$ is slightly dependent on the transferred energy $\mathscr{E}_n$, when the collision time τ is small compared with the characteristic time of the change $\hbar/\mathscr{E}_n$. If τ is large compared with $\hbar/\mathscr{E}_n$, then $P_n(D)$ decreases rapidly (exponentially) with increase in $\mathscr{E}_n$ (adiabatic collisions [4]). The minimum value $\mathscr{E}_N$, at which $P_n(D)$ begins to decrease sharply, may be found from the condition

$$\mathscr{E}_N \tau / h \sim 1. \tag{8}$$

The collision time τ is determined by the expression $\tau = \rho/v$, where ρ = radius of action close to the operating (exchange) forces, while v is the mean relative rate of the colliding molecules. As follows from experiments on ultrasonic dispersion, the value of ρ is approximately the same for all molecules and is equal to 0.2 - 0.3 A.

Taking account of the normalizing condition $\sum_n P_n = 1$ and the fact that P_n (D) is slightly dependent on $\mathcal{E}_n$ when $\mathcal{E}_n < \mathcal{E}_N$, we obtain

$$\sum_n \mathcal{E}_n P_n(D) \approx \frac{\mathcal{E}_N}{2} \sim \frac{\hbar}{\rho} \sqrt{\frac{2kT}{\pi m}}.$$

Here m is the reduced mass of the colliding molecules.

Thus, taking into account nonneighboring changes, Formula (7) has the form:

$$\mu_0 \sim Z \frac{\hbar}{\rho} \sqrt{\frac{4}{\pi m D}} \left(\frac{D}{kT}\right)^{1/2} \exp\left(-\frac{D}{kT}\right) / Q. \tag{9}$$

The decomposition rate constant k is equal in magnitude to μ_0, averaged for the rotational states of the molecule AB:

$$k = \int \mu_0(D_{\mathrm{eff}}) \exp\left(-\frac{E_{\mathrm{rot}}}{kT}\right) \frac{dE_{\mathrm{rot}}}{kT}. \tag{10}$$

Here $D_{\mathrm{eff}} = D - \lambda E_{\mathrm{rot}}$ while the factor λ depends in a complex fashion on E_{rot} and lies within the range $0 < \lambda < 1$. The reduction in the effective dissociation energy results from the centrifugal forces and can be calculated for each concrete example.

Since the internal degrees of freedom of the molecule C have not been taken into consideration in the derivation of Formula (7), it is applicable to the case of collisions of diatomic molecules AB with an atom. The decomposition of bromine may be taken as an example of such a reaction: $Br_2 + Ar \rightarrow Br + Br + Ar$,* which has been studied over a wide temperature range (300-2000° K) [5]. The experimental decomposition rate constant is equal to

$$k = 6 \cdot 10^{-2} Z_0 \left(\frac{D}{kT}\right)^{1.97} \exp\left(-\frac{D}{kT}\right), \tag{11}$$

where Z_0 is the gas-kinetic collision number. This formula is accurate for a change in k of a factor of 10^{27}; the relationship between the pre-exponent and the temperature may therefore be taken as established.

Numerical calculation of D_{eff} for Br_2 shows that when $E_{\mathrm{rot}} < D$, the factor λ is slightly dependent on E_{rot} and is equal to approximately 0.9. The integration (10) then gives $k \approx 10\,\mu_0(D)$. For the evaluation of μ_0 in accordance with (9), we observe that in the temperature range 300-2000° K it may be assumed that $Q \approx$ $\approx kT/\hbar\omega$.

Taking into account the fact that the collision number Z for vibrational excitation of a molecule may exceed the gas-kinetic collision number by a factor of 3-4, and that there are two electronic states ($^1\Sigma_g^+$ and $^3\Pi_{1u}$) for the same dissociation energy D, evaluation of the decomposition rate constant in accordance with (9) leads to the expression:

* A calculation of the rate of decomposition of Br_2 was made by Rice [6]. The author did not take into account the breakdown of the equilibrium distribution and rotation, and the increased pre-exponential factor was related to the greater statistical weight of the energy region of the order kT close to the dissociation limit. When the breakdown of the equilibrium distribution is taken into account, as can be seen, for example, from (5), the greater density of the levels close to the dissociation threshold cannot increase the decomposition rate constant. A similar problem was solved by Careri [7] who, however, without justification suggested transfer from lower vibrational levels in the region of the continuous energy spectrum.

$$k \sim 5 \cdot 10^{-2} Z_0 \left(\frac{D}{kT}\right)^{1.5} \exp\left(-\frac{D}{kT}\right). \tag{12}$$

Thus, the calculated and experimental values of the decomposition rate constants are of the same order of magnitude (the quantity $(D/kT)^{1/2}$ varies from 3-7 in the temperature range studied).

In conclusion I have to express my gratitude to Professor N. D. Sokolov for valuable observations and discussion of the present work.

LITERATURE CITED

[1] E. E. Nikitin, Proc. Acad. Sci. 116, 4, 584 (1957). *

[2] J. Prigogin and M. Mahieu, Physica 16, 51 (1950).

[3] I. M. Lifshits, J. Exptl.-Theoret. Phys. 17, 1017 (1947).

[4] N. F. Mott and G. Massey, The Theory of Atomic Collisions, (Foreign Lit. Press, 1951).**

[5] H. B. Palmer and D. F. Hornig, J. Chem. Phys. 26, 98 (1957).

[6] O. K. Rice, J. Chem. Phys. 9, 259 (1941); 21, 750 (1953).

[7] G. Careri, Nuovo Cim. 6, 94 (1949); 7, 155 (1950); J. Chem. Phys. 21, 749 (1953).

Institute of Chemical Physics of the
Academy of Sciences of the USSR

Received September 28, 1957.

* Original Russian pagination. See C. B. Translation.

** Russian translation.

THE ADSORPTION POTENTIAL IN THE NEIGHBORHOOD OF SPHERICAL PARTICLES OF COLLOIDAL DIMENSIONS

L. V. Radushkevich

(Presented by Academician M. M. Dubinin, November 2, 1957)

Disperse systems consisting of extremely small spherical particles are of interest to research workers, since materials of practical importance are found among such systems, for example, "blacks," silica gel, titania gel, etc., which have been shown by electron microscope studies to possess a globular structure, while the dimensions of the particles can often be readily determined with sufficient accuracy. In addition, by studying these systems it is possible to examine certain fundamental questions regarding the theory of adsorption, since the simple geometry facilitates the necessary calculations without introducing any hypothesis concerning the structure of the system. On the basis of the general theories of adsorption potential increase in the splits, pores and cracks of a sorbent, it is often suggested that there is an increase in potential near the point of contact of of spherical particles. It might therefore be assumed that for certain sorbents consisting of nonporous spherical particles, a potential increase of this sort should be reflected in the shape of the vapor adsorption isotherms. This suggestion, however, requires quantitative confirmation, which has not yet been done even approximately.

Let us consider first of all the adsorption field created close to an isolated (single) spherical particle of diameter $\delta = 2r$ at a distance d from its surface. It is most convenient to carry out the calculation by comparing the adsorption potential P of the particle with its value at the same distance from a plane surface, when it is equal to P_∞. It may be confirmed a priori that $P < P_\infty$, the reduction in potential being brought about by two factors: the influence of the curvature of the surface and the finite dimensions of the particle. The calculation which we propose relates to particles whose diameters lie within the range 100-2000 A, which corresponds to the dimensions most frequently encountered in silica gel, blacks, etc. In order to take account of the possible formation of polymolecular layers, the value of the potential was calculated at distances from the surface equal to 3-7 times the radii of the molecules being adsorbed. Under these conditions the distance d is several times greater than the distance between the adsorbent molecules and in the calculation of the adsorption potential it is possible to employ integration instead of summation without appreciable error.

The volume element of the adsorbing particle, expressed as the differential of the volume of a spherical segment, is equal to

$$dv = \pi R\left(2R - r - d + \frac{r^2 - R^2}{r + d}\right) dR .$$

The adsorption potential at a point situated at a distance d from the surface can therefore be expressed as

$$P = \pi N \int_{d}^{2r+d} f(R)\, R\left(2R - r - d + \frac{r^2 - R^2}{r + d}\right) dR , \tag{1}$$

where $f(R)$ is the potential of the interaction of the adsorbent molecule with the molecule being adsorbed. Without going into a discussion of the nature of this interaction, it is possible in any case to represent this function in the general form [1]:

$$U = f(R) = -\left(\frac{B}{R^6} + \frac{C}{R^8}\right) + De^{-R/\rho} \tag{2}$$

or

$$f(R) = f_1 + f_2 + f_3.$$

Here, the first two terms of the sum characterize the attraction and the last term the repulsion. For a plane surface, as is well known [2]:

$$P_\infty = 2\pi N \int_d^\infty f(R)\, R(R-d)\, dR.$$

From this, using the Expression (2), we find that

$$P_\infty = P'_\infty + P''_\infty + P'''_\infty,$$

where

$$P'_\infty = -{}^1/_6\pi BNd^{-3}; \quad P''_\infty = -{}^1/_{15}\pi CNd^{-5}; \quad P'''_\infty = 2\pi DN\rho^3 e^{-x}(2+x)$$

and $x = \frac{d}{\rho}$. For the spherical particle, substitution of the corresponding quantities from (2) in the Formula (1) and integration lead to other relationships which on reduction have the form

$$P = \alpha P'_\infty + \beta P''_\infty + \gamma P'''_\infty,$$

where

$$\alpha = (1+\eta)^{-3}; \quad \beta = \frac{2,5\eta^2 + 2,5\eta + 1}{(1+\eta)^5};$$

$$\gamma = \frac{e^{-y}(y^2 + \eta y^2 + 2\eta y + 4y + 6) - (2\eta y - \eta y^2 - 2y + 6)}{y(2\eta + 1)(2 + \eta y)}.$$

Here $\eta = \frac{d}{\delta}$ and $y = \frac{\delta}{\rho}$. In the last formula, y is very large (for example, for ρ = 0.2-0.5 A, y is equal to 300-2000) and the first term in the numerator is extremely small and may be neglected. Then

$$\gamma = (2\eta + 1)^{-1}\left[1 - \frac{2(\eta y + 3)}{y(\eta y + 2)}\right]$$

or, when $y \cong 10^3$, more simply:

$$\gamma \cong (2\eta + 1)^{-1}.$$

Finally, therefore:

$$P = (1+\eta)^{-3} P'_\infty + \frac{2,5\eta^2 + 2,5\eta + 1}{(1+\eta)^5} P''_\infty + (2\eta + 1)^{-1} P'''_\infty.$$

It can be readily seen that all the quantities α, β, and γ are never greater than unity, while they reach their maximum values when $2r \to \infty$ or $\eta \to 0$, i.e., over a plane surface. From this it follows that

$$P < P_\infty.$$

Table 1 gives the values of the coefficients α, β, and γ for different values of η, found from the formulas.

These results show that in the range of particle dimensions and distances d indicated, when the values of η lie within the range from 0.005 to 0.10, the coefficients α, β, and γ differ considerably from unity, which corresponds to a plane surface. Evidently, however, the contributions of the quadrupole term and the repulsion

component are small compared with the contribution of the dipole term and may be neglected. But in any case, it may be expected that above a single particle at a distance of from 2-3 molecular layers, we have to take account of a reduction of adsorption potential of 10-20% compared with the value over a plane surface at the same distance.

TABLE 1

η	α	β	γ	
			$y=100$	$y=1000$
0	1	1	1	1
0,005	0,985	0,990	0,962	0,987
0,01	0,971	0,975	0,953	0,978
0,02	0,942	0,953	0,938	0,959
0,05	0,864	0,888	0,888	0,908
0,10	0,751	0,792	0,814	0,831
0,30	0,455	0,532	0,612	0,624
0,50	0,296	0,377	0,490	0,500
1,00	0,125	0,188	0,327	0,333

On going to particles in contact, and limiting ourselves for the sake of simplicity to particles of equal dimensions, we observe that close to such systems the potentials from the separate particles are added to one another. Thus, for a pair of particles in contact, at points lying on a common tangent and situated at equal distances from both particles, the potential is simply doubled. Consequently, we have in this case:

$$P_{1,2} = 2P = 2(\alpha P'_{\infty} + \beta P''_{\infty} + \gamma P'''_{\infty}).$$

For large particles with diameters of approximately 1000 A and above, we may take $P_{1,2} = 2P_{\infty}$, since in this case $\alpha = \beta = \gamma = 1$. This corresponds to the maximum increase in adsorption potential in the space between two particles. Similar calculations by de Boer and Custers [3], and also by Moelwyn-Hughes [4], for a concave hemisphere at its center, gave $P = 4P_{\infty}$. In the case of a cylindrical pit with a hemisphere at the foot, we have at its center $P \cong 6P_{\infty}$, and for a space enclosed on all sides we have $P = 8P_{\infty}$. It may therefore be said that in the space between particles in contact the increase in potential is relatively small even for the largest colloidal particles and becomes still smaller when the particles are small; for example, for the smallest we have $P_{1,2} \cong 1.5\,P_{\infty}$.

In the center of a group of 3 particles such as is formed in closest packing, which is situated at $\eta = 0.106$ from each particle, the adsorption potential is equal to $P_{1,2,3} = 3\,P$ or, for small particles, $P_{1,2,3} \cong 3 \cdot 0.75\,P'_{\infty} \cong 2.25\,P'_{\infty}$.

In experimental studies, large quantities of spherical particles are always dealt with. For loosely packed systems, on the basis of the above calculations, we might expect a slight increase in the potential at a small number of contact points, which would be practically compensated by the reduction in potential over the free surface of the particles, so that the adsorption isotherm should correspond closely to the isotherm for particles not in contact, other conditions being equal.

I have to express my gratitude to Academician M. M. Dubinin for his interest in the present work.

LITERATURE CITED

[1] R. Fowler and E. Guggenheim, Statistical Thermodynamics *(Foreign Lit. Press, 1949), p. 346.

[2] F. London, Zs. Phys. Chem. (B) 11, 222 (1930).

[3] J. H. de Boer and J. F. H. Custers, Zs. Phys. Chem. (B) 25, 225 (1934).

[4] E. A. Moelwyn-Hughes, J. Coll. Sci. 11, 4-5, 501 (1956).

Institute of Physical Chemistry,
USSR Academy of Sciences

Received October 25, 1957

* Russian translation.

THE PROBLEM OF CARBONIUM ION FORMATION IN ADDITION REACTIONS OF OLEFINS

A. E. Shilov, R. D. Sabirova, and V. I. Gorshkov

(Presented by Academician N. N. Semenov, October 9, 1957)

Heterolytic reactions of additions at multiple bonds proceed by a stepwise donor-acceptor mechanism (see for example [1]). In the first stage intermediate active compounds are formed and subsequent reactions of these lead to the formation of the product. In particular, in acid-catalyzed processes (hydrohalogenation, hydration and the addition of acids) the reaction proceeds via the formation of a protonized form of the olefin. For example:

$$C_2H_4 + H^+ \rightleftarrows (C_2H_4 \cdot H)^+ \xrightarrow{HA} C_2H_5A + H^+.$$

The presence of an established acid-base equilibrium in the first stage is shown by the linear dependence of the rate constant on the acidity of the medium [2]. The nature of the ion formed in the first stage is the subject of wide discussion at the present time. In many papers the authors suggest that the reaction proceeds via a carbonium ion:

$$C_2H_4 + H^+ \rightleftarrows \begin{matrix} H \diagdown \\ H - \\ H \diagup \end{matrix} C - \overset{+}{C} \begin{matrix} \diagup H \\ \\ \diagdown H \end{matrix}. \qquad (1)$$

On the other hand, beginning with Dewer [3], it has often been assumed that the ion formed has the structure of a π-complex in which the π-bond of the olefin is not completely converted into a σ-bond, C—H:

$$C_2H_4 + H^+ \rightleftarrows \underset{\substack{\downarrow \\ H}}{CH_2 = CH_2}. \qquad (2)$$

For an experimental test of one or the other hypothesis it is possible to make use of the fact that in the π-complex the nature of the bond formed with the proton must be different from the nature of the other C—H bonds, i.e., the H atom added must be nonequivalent to the other atoms. In a carbonium ion, the H atoms of the CH_3 group must be equivalent. Therefore, if we take an acid with labeled hydrogen (for example D_2SO_4) then in the case of Reaction (1) we should observe a rapid exchange of deuterium between the sulfuric acid and the olefin and in the case of Reaction (2), the exchange must not occur.

The prevailing opinion on the facile exchange of olefins with acids [4, 5], it would seem, confirms the carbonium ion mechanism. However, a more careful examination shows that we cannot assume such an unequivocal course from the data on exchange. In particular, the exchange of ethylene with deuterosulfuric acid was studied under conditions [10], when the reaction rate of the reverse, empirical Reaction (3) was not very small:

$$C_2H_4 + D_2SO_4 \rightleftarrows C_2H_4DOSO_3D. \qquad (3)$$

Naturally in this case exchange must be observed, regardless of the nature of the intermediate ion, as without doubt the H atoms of the CH_3 group in ethylsulfuric acid are equivalent.

We studied the absorption of ethylene in D_2SO_4 under conditions of almost complete absence of decomposition of ethylsulfuric acid. For this, the reaction was performed with an increased ethylene pressure (about 4 atmos) at room temperature. The reaction vessel was an inverted glass U-tube. Into one of its limbs was placed deuterosulfuric acid and ethylene was frozen down into the other with the vessel connected to a vacuum system. After this, the whole tube was sealed off in vacuum and the ethylene began to be adsorbed in the sulfuric acid while the vessel was shaken mechanically. To maintain the required ethylene pressure, the limb of the vessel, containing liquid ethylene was cooled in a cooling mixture at − 75°.

TABLE 1
Mass Spectrum of Ethyl Chloride (electron energy 85 ev, temperature of ionization chamber ~ 200° C)

m/e	C_2H_5Cl	Ethyl chloride from reaction products
69	—	—
68	—	6,3
67	2,3	100
66	100	30,8
65	13	348
64	342	36
63	21	—

To determine the D content of the ethylsulfuric acid formed, the latter was hydrolyzed with water to ethyl alcohol, which was treated with HCl in the presence of zinc chloride [6] to give ethyl chloride. The ethyl chloride obtained in this way was analyzed on an MS-1A mass spectrometer [7].

To determine the isotopic composition of the acid hydrogen, the acid was diluted with a definite amount of water and reacted with CH_3MgI to give methane, which was analyzed for CH_3D content on the mass-spectrometer [9].

In Table 1 we give the distribution of the line intensities in the calibration spectrum of normal ethyl chloride and in the mass spectra of the reaction products analyzed. The intensity values are given as percentages of the intensity taken as a standard in the given mass spectrum.

The compositions of the products formed, calculated from the data in Table 1, are given in Table 2. In the calculation it was assumed that in the first approximation the probability of stripping of each H and D atom in dissociation ionization in a mass spectrometer is the same.

TABLE 2

Expt. No.	Conc. of sulfuric acid in %	$\frac{(D_2SO_4)+(H_2SO_4)}{(C_2H_4)}$ absorbed	D in original sulfuric acid (%)	D in acid H of mixture formed (%)	Isotopic composition of ethyl chloride (%)			
					C_2H_5Cl	C_2H_4DCl	$C_2H_3D_2Cl$	remaining poly-deuterides
1	99,9	1,1	100	—	9,3	89	2,4	0,5
2	99,9	2	100	—	5,8	91	3,6	0,1
3	94,5	3,4	74	77	40	59	0,07	0,01
4	99,7	4,7	26	—	86	14	0,2	0,01

It is obvious that the only deuterium derivative contained in the mixture in any significant amount is monodeuteroethyl chloride. The formation of small amounts of $C_2H_3D_2Cl$ in Experiments 1 and 2 is apparently due to the reversal of Reaction (3). In Experiment 3 is presented the isotopic composition of the acid hydrogen of the original sulfuric acid and the mixture of sulfuric and ethylsulfuric acids formed. It is apparent that the light hydrogen of the ethylene does not enter the acid in the reaction process.

We obtained similar results for the hydration of isobutylene in 4 M and 6 M deuterosulfuric acid. The reaction was performed in sealed ampules at room temperature. The hydroxyl hydrogen was washed out of the trimethyl carbinol formed with light water and the carbinol was analyzed directly on the mass-spectrometer. The deuterosulfuric acid was analyzed for deuterium content before and after the reaction. It was found that in this case the reaction proceeds without significant exchange of the sulfuric acid and the olefin, since the reaction product was almost exclusively the monodeuteroalcohol.

From these results it follows unequivocally that in the addition of sulfuric acid to ethylene and the addition of water to isobutylene, the stage of the reversible formation of a carbonium ion [Reaction (1)] is absent. Apparently, the π-complex hypothesis is thus experimentally confirmed.

It is interesting to note that from the absence of exchange it also follows that not only is a reversible isomerization of the π-complex into a carbonium ion absent, but also the isomerization of the π-complex into an isomeric π-complex.

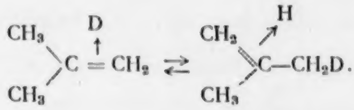

(4)

In addition, at first sight it appears that this reaction must go readily as it is not associated with either energetic or steric difficulties (in particular for isobutylene, where the proton being added is directed to the CH_2 group). We consider that the absence of such exchange confirms the recent proposal of I. I. Moiseev and Ia. K. Syrkin [8], that the π-complex is a formation which includes the whole acid molecule and is close in structure to an ion pair. In this case the isomerization (4) would naturally be hindered.

In the recent paper of Taft and Purlee [11] it was also shown that the hydration of olefins in dilute acids proceeded without exchange of the hydrogen of the water and the olefin. The authors established the absence of exchange by using heavy water for the hydration and analyzing the olefin which did not have time to react. To prove that exchange is absent in this case it is necessary to show that equilibrium is attained between the gaseous and the dissolved olefin. Apparently, this condition was actually fulfilled. Together with the data obtained in the present work, these results show that over a wide range of acid concentrations, the stage of reversible carbonium ion formation is absent.

From the data on the addition of sulfuric acid to ethylene, it is possible to determine the isotope effect of this reaction. From Experiment 4 (Table 2) (performed with a large excess of acid) it follows that

$$\frac{k_H}{k_D} = \frac{[C_2H_5Cl]}{[C_2H_4DCl]}\,\frac{[D^+]}{[H^+]} \sim 2{,}2\,.$$

The ratio k_H/k_D for hydration in dilute acids [11] is close to unity.*

We consider that the insignificant isotope effects in the additions to olefins indicate that the limiting act of the reaction can hardly be irreversible isomerization of the π-complex into a carbonium ion

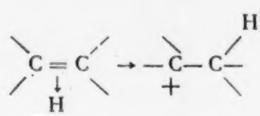

(as was proposed in the papers of Taft and other authors), as such a process must, apparently, proceed with the maximal isotope effect. The accurate interpretation of the isotope effect is, however, made more difficult by the fact that the reaction has many stages.

The authors would like to thank V. L. Tal'roze for consultations on performing mass-spectroscopic analyses.

LITERATURE CITED

[1] E. A. Shilov, Coll. Problems of the Mechanism of Organic Reactions,** (Kiev, 1953), p. 7.

[2] N. M. Chirkov, M. I. Vinnik, S. G. Entelis, and V. I. Tsvetkova, Coll. Problems of Chem. Kinetics, Catalysis and Reactivity,** (Acad. Sci. USSR Press, 1955).

* The values of the isotope effects obtained by Taft, in particular the reverse isotope effect ($k_H/k_D < 1$) for one case, unequivocally indicate the presence of reversible protonization of the olefin in the first stage of the reaction. From this it follows that the proposal of Syrkin and Moiseev [8] on the six-membered transition complex, if correct, cannot in any case replace the idea of an intermediate protonized ion.

** In Russian.

[3] M. Dewar, The Electronic Theory of Organic Reactions (Oxford, 1949), p. 141.

[4] G. P. Miklukhin, Prog. Chem. 17, 663 (1948).

[5] A. I. Brodskii, Chemistry of Isotopes*(Acad. Sci. USSR Press, 1952), p. 208.

[6] J. F. Norris and H. B. Taylor, J. Am. Chem. Soc. 46, 753 (1924).

[7] V. L. Tal'roze, G. D. Tantsyrev, and Ia. A. Iukhvidin, Factory Labs. 21, 1175 (1955).

[8] I. I. Moiseev and Ia. K. Syrkin, Proc. Acad. Sci. 115, 541 (1957).**

[9] M. Orchin, J. Wender, and R. A. Friedel, An. Chem. 21, 1072 (1949).

[10] J. Horiuti and M. Polanyi, Nature 134, 847 (1934).

[11] L. Purlee and R. W. Taft, J. Am. Chem. Soc. 78, 5807 (1956).

Institute of Chemical Physics of the
Academy of Sciences of the USSR

Received October 7, 1957.

* In Russian.

** Original Russian pagination. See C. B. Translation.

ADSORPTION OF AMMONIA ON GRAPHITIZED CARBON BLACK

A. A. Voskresenskii

(Presented by Academician M. M. Dubinin, December 2, 1957)

As is well known, adsorption of water vapor on carbon black adsorbents exhibits a number of specific features which manifest themselves in a characteristic shape of the adsorption isotherm. Systematic investigation of this problem [1] has led to the conclusion that the characteristics mentioned are due to the ability of adsorbed water molecules to form association complexes by virtue of the formation of hydrogen bonds. If this view is correct, it might be expected that other substances,for which, as is the case with water, adsorption energy on carbon black adsorbents is small and forces of interaction in the adsorption layer due to hydrogen bonding may be quite considerable, would be characterized by a similar form of the adsorption isotherm. In connection with this problem, a few years ago we had in this laboratory undertaken the investigation of the adsorption of ammonia vapor on carbon black adsorbents at temperatures near the boiling point of ammonia. Preliminary experiments carried out with graphitized carbon black have enabled us to establish that in this case the adsorption isotherm was bending upwards which confirmed the fundamental correctness of the theory. A paper by Beebe and Dell [2] also led the authors to a similar conclusion. However, whereas the amount of water adsorbed on carbon black adsorbents as well as the shape of the adsorption isotherms depend strongly on the degree of oxidation of the surface of the adsorbents, in conformity with the theories mentioned, it is found that in the case of ammonia reversible upward-bent adsorption isotherms are observed only for carbon blacks which have been heated at a high temperature. Thus, according to Beebe and Dell [2] adsorption of ammonia on Spheron-6 carbon black which has been graphitized at 1000°, is irreversible: over the initial portion of the isotherm the portion corresponding to desorption lies above that corresponding to adsorption. On the other hand adsorption of ammonia on the same carbon black graphitized at 2700° is reversible over the entire range of the corresponding pressures. From what has been said so far it follows that it is not possible to apply our views concerning the adsorption of water vapor directly to the case of the adsorption of ammonia on carbon blacks.

Below, we report our results of measurements of the adsorption of ammonia vapor at a temperature of − 36.3° on Ukhta channel black graphitized for two hours at a temperature of 1700° in a current of hydrogen. The choice of the black and of the conditions of its preliminary heat treatment were governed by our endeavor to prepare a carbon black adsorbent with a relatively uniform surface. The specific surface of the black was determined by low-temperature nitrogen adsorption and was found to be 100 m^2/g. All measurements were carried out on the standard volumetric apparatus adopted in this laboratory. The temperature of the adsorbent was maintained constant within ± 0.1° by means of the cryostat described by G. G. Muttik [3]. Ammonia was prepared by repeated fractionation of a concentrated aqueous solution of ammonia at low temperature, followed by drying over metallic sodium.

In Fig. 1 is shown the adsorption isotherm of ammonia on channel black at a temperature of − 36.3°. In the top left-hand corner of the diagram is illustrated the initial portion of the same isotherm on a larger scale. The adsorption is fully reversible over the entire range of corresponding pressures.

If we assume that the area taken up by a molecule of ammonia is equal to $\omega = 13.1$ A^2, we find the adsorption capacity of a monolayer — $a_m = 1.27$ mM/g. In other words, as we move along the curve up to point A in Fig. 1, adsorption remains, evidently, monomolecular, while point A corresponds approximately to the transition to polymolecular adsorption.

Comparison of the isotherm illustrated in Fig. 1 with well-known adsorption isotherms of water vapor on similar adsorbents leads us to the following conclusions.

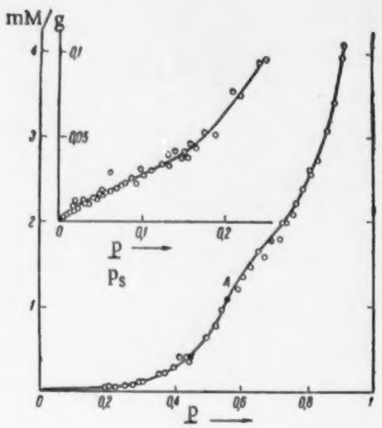

Fig. 1.

Although in both cases the adsorption isotherms are bent upward over the region corresponding to monomolecular adsorption, they show, nevertheless, essential differences in shape. Adsorption isotherms for water exhibit a region of very steep gradient which is absent on adsorption isotherms of ammonia. In the case of water this region of steep rise is displaced in the direction of increasing relative pressure as the degree of oxidation of the surface decreases, and the amounts adsorbed at lower pressures are extremely small. As has already been pointed out, in the case of the adsorption of ammonia on carbon blacks of different degrees of surface oxidation the isotherms are not shifted in the direction of greater relative pressures with decreasing concentration of oxygen complexes on the surface which latter constitute the primary centers of adsorption of water molecules [4]. In addition, as will be seen from Fig. 1, in the case of adsorption of ammonia on carbon blacks the amounts adsorbed at relatively low pressures are still quite considerable. These peculiar features may be explained when we realize that as a result of the greater polarizability of the ammonia molecule, as compared with that of a water molecule, the energy of interaction with the surface of the graphite lattice is greater in the case of ammonia than it is in the case of water, while the energy of the hydrogen bond is greater for water.

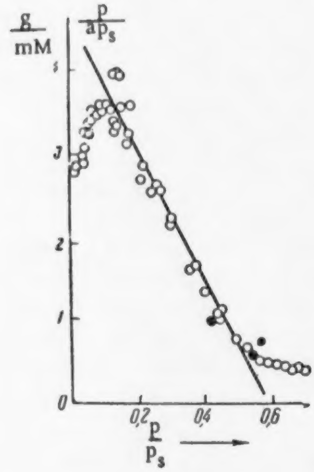

Fig. 2.

As has been shown by Bering and Serpinskii [5] the predominance of forces of attraction at close range within the adsorbed layer will always manifest itself in adsorption isotherms which will be bent upward in the initial portion, and this will be so quite independently of the actual mechanism of interaction between the adsorbed molecules. To describe the upward-bent portion of the adsorption isotherm of water vapor on carbon blacks, Dubinin and Serpinskii [4] have deduced the equation

$$a = \frac{a_0 ch}{1 - ch}, \tag{1}$$

where a is the amount adsorbed, h is the relative pressure of water vapor, and c and a_0 are constants, the latter denoting the number of "primary" adsorption centers constituted by molecules of chemisorbed oxygen.

In Fig. 2 it will be seen that over the relative pressure range from 0.1 to 0.45 our data may be described by an equation of the form of (1), although, as has already been pointed out, adsorption of ammonia on carbon blacks is unaffected by the amount of chemisorbed oxygen. We are therefore going to show below that a relationship between a and h similar to that given by Equation (1) may be arrived at without assuming the existence of any primary adsorption centers on the surface of the adsorbent.

We shall start with the assumption that even on a perfectly uniform surface two-dimensional adsorption complexes of different dimensions are formed within the adsorbed monolayer as a result of hydrogen bonding. In other words, we are assuming that as a result of adsorption individual nonassociated molecules may form complexes composed of two molecules, that such complexes may change into termolecular ones, etc.

Let θ denote the total area covered by the adsorbed substance, and $\theta_1, \theta_2, \theta_3, \ldots,$ the fractional areas covered by complexes of one, two, three, etc., molecules. It is obvious that

$$\theta = \theta_1 + \theta_2 + \theta_3 + \cdots + \theta_n + \cdots \quad (2)$$

Let k'_n denote the velocity constant of formation (through adsorption) of a complex of n molecules, and k''_n the velocity constant of decomposition (through desorption) of such a complex. Let us also assume that $k'_2 = k'_3 = k'_4 = \ldots$, and $k''_2 = k''_3 = k''_4 = \ldots$; from general physical considerations it is evident that $k'_1 \neq k'_2$ and $k''_1 \neq k''_2$.

If we also take it, as is usually done in similar cases, that at equilibrium the rate of adsorption on complexes of (n - 1) molecules is equal to the rate of desorption from complexes of n molecules, we easily obtain the following set of equations:

$$\begin{aligned}
\theta_1 &= \frac{k'_1}{k''_1}(1-\theta)h, \\
\theta_2 &= \frac{k'_n}{k''_n}\theta_1 h = \frac{k'_1}{k''_1}\frac{k'_n}{k''_n}(1-\theta)h^2, \\
\theta_3 &= \frac{k'_n}{k''_n}\theta_2 h = \frac{k'_1}{k''_1}\left(\frac{k'_n}{k''_n}\right)^2(1-\theta)h^3, \\
&\cdots\cdots\cdots\cdots\cdots\cdots \\
\theta_p &= \frac{k'_n}{k''_n}\theta_{n-1} h = \frac{k'_1}{k''_1}\left(\frac{k'_n}{k''_n}\right)^{n-1}(1-\theta)h^n
\end{aligned} \quad (3)$$

Putting, for the sake of brevity, $\frac{k'_1}{k''_1} = c'$ and $\frac{k'_n}{k''_n} = c''$, and adding Equations (3) term by term, we obtain:

$$\theta = \Sigma\theta_i = c'(1-\theta)h[1 + c''h + (c''h)^2 + \cdots + (c''h)^n] \quad (4)$$

On calculating the value of the geometrical progression on the right-hand side of Equation (4) for $n \to \infty$, we obtain the final expression:

$$\theta = \frac{a}{a_m} = \frac{c'h}{1-(c''-c')h}, \quad (5)$$

where a_m is the adsorption capacity of the monolayer. It is evident that Equation (5), deduced without assuming the existence of primary adsorption centers on the surface of the adsorbent, is similar in form to Equation (1).

The author wishes to thank Messrs. V. V. Serpinskii and B. P. Bering for their constant interest and assistance in this investigation.

LITERATURE CITED

[1] M. M. Dubinin, An Investigation of the Adsorption of Gases and Vapors on Carbon Black Adsorbents * (Moscow, 1956).

[2] R. A. Beebe and R. M. Dell, J. Phys. Chem. 59, 754 (1955).

[3] K. V. Chmutov, The Technique of Physico-Chemical Experimentation* (1954), p. 72.

[4] M. M. Dubinin and V. V. Serpinskii, Proc. Acad. Sci. USSR 99, 1034 (1954).

[5] B. P. Bering and V. V. Serpinskii, Problems of Kinetics and Catalysis* (Acad. Sci. USSR Press, 7, 1949), p. 383.

Institute of Physical Chemistry of the
Academy of Sciences of the USSR

Received November 22, 1957.

* In Russian.

ON THE THERMAL IONIZATION OF HYDROGEN AND HYDROCARBONS IN THE PRESENCE OF METALLIC CATALYSTS

P. G. Ivanov and Academician A. A. Balandin

It is well known that gases which are adsorbed by hot metallic surfaces or which pass into solution in metals, undergo ionization and impart to the surface of the metal a constant and reproducible electrochemical potential which is characteristic for the given metal (see, for example, [1]). It has been established that the charge on metallic surfaces may be removed by evacuation of the gas; it may also be removed by means of chemical reactions as, for example, by burning adsorbed hydrogen with oxygen. It has also been established that adsorption and desorption of gases by a metal is accompanied by changes of its electrochemical potential.

The object of our experiments was to detect directly the appearance of charged particles in the gaseous phase in the presence of metallic surfaces possessing catalytic properties (see apparatus in Fig. 1). Disc-shaped electrodes a and a' made of a metal which may serve as a catalyst, were screwed on the ends of two rods b and b' which were sealed into accurately ground caps fitted into the ends of the main glass tube. The ends of the two rods were connected to an electrostatic volt meter v or some other instrument sufficiently sensitive to measure weak currents. The glass tube was 3.8 cm in diameter and 70 cm long. The electrodes inside the tube as well as the gas around them could be heated up to 520° by means of a small electric heating coil c, 8 cm long. When the coil was hot the free ends of the tube remained cool. It was established that no current passed along the walls of the tube since, firstly, the results were unaffected when the length of the cool portion of the tube was varied in different assemblies and, secondly, the strength of the current depended on the nature of the electrodes (see below). The distance between the electrodes was 20 mm. The temperature was measured by means of a molybdenum glass thermometer d reading to 510°, the lower end of the thermometer rested on the upper disc electrode and was attached to the rod b by means of clamps. The use of molybdenum glass made it possible to carry out experiments over the temperature range from 20 to 510°. With quartz glass diffusion of hydrogen ions was observed on heating.

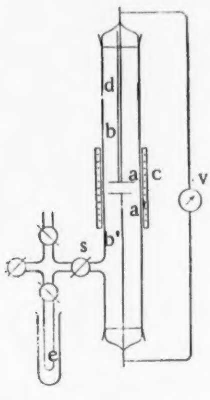

Fig. 1. Diagram of apparatus.

Before each experiment the apparatus was evacuated to a pressure of 10^{-4} mm Hg. In experiments with saturated vapors of organic liquids the latter were placed in glass tube e where they were degassed, followed by freezing for a period during which the apparatus was evacuated. The liquids were then warmed to 25° and their vapors were then conducted into the discharge tube. When the pressure was equalized the discharge tube was closed (stopcock s) and the rate of discharge of the volt meter v (type S-91), connected to the electrodes without an external resistance and charged up to 150 v, was measured as the temperature was gradually raised. The time intervals were determined by means of a good stop watch. From the rate of discharge of the voltmeter it was possible to draw conclusions on the degree of ionization of the gas and vapors contained in the space between the electrodes. Experiments with hydrogen were carried out at a pressure of 1 atmos; the gas used was electrolytic hydrogen suitably purified. The electrodes were of palladium, aluminum, and copper and the surface area of each was 6 cm^2. Palladium was saturated with hydrogen before each experiment. The discharge current was strongest when palladium was saturated with hydrogen.

The experimental results are presented in the form of curves, the axis abscissae referring to time τ - the reciprocal of the rate of discharge of the voltmeter, the axis of ordinates referring to the temperature. The

greater the degree of ionization the closer to the vertical axis and the lower does the curve lie.

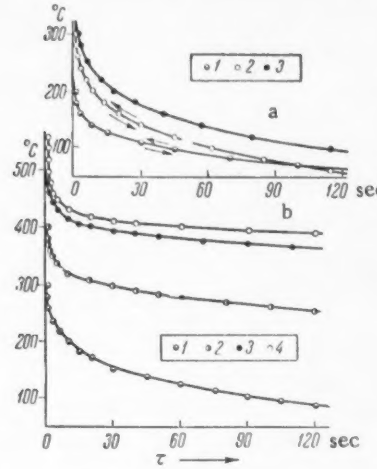

Fig. 2. a) Hydrogen. Electrodes: 1) Pd/Pd, 2) Pd/Al, 3) Cu/Cu, b) Cyclohexane. Electrodes: 1) Pd/Pd, 2) Pd/Al, 3) Al/Al. Benzene. Electrodes: 4) Al/Al.

The results for hydrogen with palladium, aluminum, and copper electrodes are presented in Fig. 2, a from which it will be seen that a marked increase in the concentration of ions begins below 100°. An important fact is that ionization of hydrogen with increasing temperature depends on the electrode material and is always reproducible and reversible, i.e., the curve which corresponds to ionization during the heating-up coincides with the curve corresponding to cooling. The ionizing efficiency may be characterized, for example, by the temperature at which the reciprocal rate of discharge is equal to 60 seconds. The lower this temperature the greater is the ionizing efficiency. With palladium electrodes this temperature is found to be quite low in the case of hydrogen, namely, $t_{60} = 90°$. For a palladium aluminum pair of electrodes, $t_{60} = 100°$; with copper electrodes, $t_{60} = 135°$.

In a similar manner we have investigated the ionization of vapors of some hydrocarbons of different structures: n-heptane, 2,2,4-trimethylpentane, cyclohexane, benzene, dekalin, tetralin, as well as a cyclic ketone – cyclohexanone, using different electrodes (see Figs. 3 and 4). It was found that in all these cases ionization did take place. The experiments with hydrocarbons were always reproducible, except in those cases in which hysteresis was observed (see below). The curves obtained for n-heptane with palladium electrodes were not completely reproducible (see Fig. 3, a and Table 1). In Table 1 are shown the values of t_{60} for all hydrocarbons investigated as well as for hydrogen in those cases where the pressure was higher than 1 atm. The sign ↑ denotes curves obtained during heating, the sign ↓ denotes those

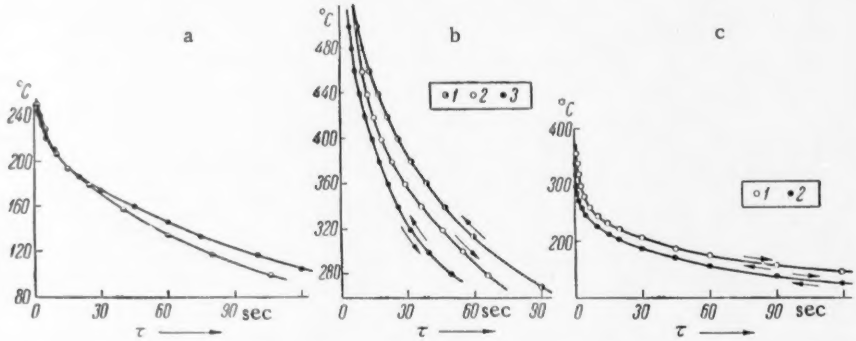

Fig. 3. a) n-Heptane. Repeat experiments. Electrodes: Pd/Pd. b) n-heptane. Electrodes: 1,2) Al/Al, 3) C/Al. c) 1) n-heptane, 2) 2,2,4-trimethylpentane. Electrodes: Cu/Cu.

corresponding to cooling; wherever these signs are not shown the curves corresponding to heating and cooling coincide with each other, in other words, the process is reversible: there is no hysteresis. Most of the curves show no hysteresis. Hysteresis was, however, observed in the case of dekalin and tetralin and in some cases with n-heptane. In the case of n-heptane, using aluminum electrodes, a noticeable, although small, increase in the degree of ionization was observed when the cup of the lower electrode was packed with activated palm-tree charcoal; the corresponding curve is displaced toward the left and the process is reversible. The lower curves in Fig. 4, b with tetralin and Pd were obtained in repeat experiment immediately after the original one; the degree of ionization was found to be greater in the repeat experiment than in the first one. Now, ionization

in a gas, in the presence of metallic surfaces, can be observed already at low temperatures, for example, below 100° in the case of hydrogen. This ionization process is not the same as the thermal ionization of hydrogen in bulk which, as is well known, takes place at high temperatures, since in this case the ionization potential of hydrogen is high.

TABLE 1

Electrode I	Electrode II	Constituent of gaseous phase	t_{60}
Pd	Pd	Hydrogen	90
		n-Heptane	135-145
		Cyclohexane	125
		Dekalin	200↑ - 165↓
		Tetralin	155↑ - 125↓
		Cyclohexanone	95
Pd	Al	Hydrogen	100
		Cyclohexanone	280
Cu	Cu	Hydrogen	135
		n-Heptane	175
		Iso-octane	155
Al	Al	n-Heptane	260
		Cyclohexane	385
		Benzene	400
		Dekalin	260↑ - 200↓
		Cyclohexanone	145

The ionization in question depends strongly on the nature of the electrode material. It follows that the ionization process must be taking place on the surface of the metal. In addition, this type of ionization also depends on the nature of the gas (see Table 1). From this it follows that the process must be taking place within the layer of molecules adsorbed on the metal. The experimental results cannot be explained by the physical surface effects already known, since phenomena like the Richardson effect, thermionic emission, as well as the release of secondary electrons during bombardment of surfaces with charged particles take place at a considerably higher temperature. Also the phenomenon cannot be explained by the type of ionization observed in chemical surface processes and in adsorption phenomena since in this case the degree of ionization should decrease with time and the process should cease when the surface would be completely covered by the adsorbed layer. However, in our case no decrease of the current with time could be observed (in the experiment with hydrogen and Pd-electrodes at 360° the current remained constant over a period of 45 minutes). The fact that the degree of ionization was greater the more saturated the Pd-electrode was with hydrogen, is also evidence against the hypothesis which assumes that ionization in this case is conditioned by adsorption. We are thus confronted by a new effect, namely, the thermal ionization of adsorbed molecules and the release of the ions into the gaseous phase at a low temperature.

The electrons left on the electrode rapidly escape into the bulk of the metal and, consequently, under these conditions of ionization no equilibrium exists. Since the process is a stationary one, the current is determined by the rate of ionization of the adsorbed molecules. The ionization energy barrier in the adsorbed layer will be lower than in the gas since the ionization potential of the molecules in the gas will be reduced by the work function Φ_0. In fact, the observed degree of ionization decreases in the series

$$\mathrm{Pd} > \mathrm{Cu} > \mathrm{C} > \mathrm{Al} \tag{1}$$

(see Table 1 and Experiments with charcoal), and it is also in this order that the value of Φ_0 decreases for these solids; according to Michaelson [2], the values of Φ_0 for Pd, Cu, C, Al are, respectively, 4.82, 4.47, 4.39, and 3.74 v. However, this decrease is still insufficient for an adequate explanation of the effect observed since, for example, for hydrogen $\Phi_0 = 15.4$ v and for Pd it equals 4.82 v; the difference of 10.6 v (i.e., approximately 240 kcal)

is still very large. Since the rates of these processes are determined not only by the value of the energy barrier but also by the entropy factor, it must be concluded that in the case of the processes observed the entropy factor is very large.

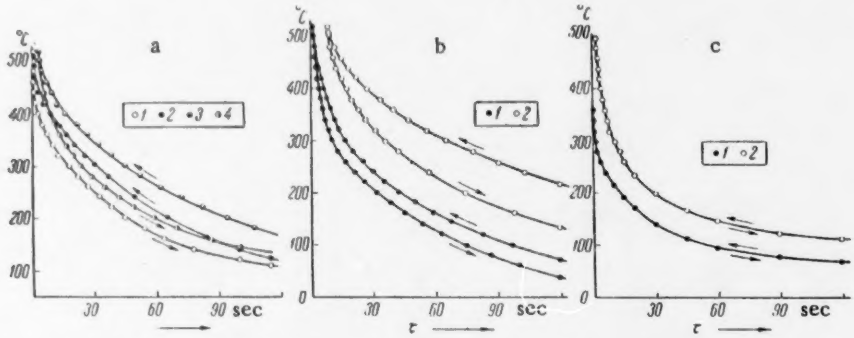

Fig. 4. a) Dekahydronaphthalene. Electrodes: 1,2) Pd/Pd; 3,4) Al/Al.
b) Tetrahydronaphthalene. Electrodes: 1) Pd/Pd; 2) Pd/Pd, repeat experiment.
c) Cyclohexanone. Electrodes: 1) Pd/Pd, 2) Al/Al.

The hysteresis observed in the case of tetralin and dekalin may be due to a stearic factor; owing to the complexity of these molecules the electrons colliding with the ions are not immediately captured in the same positions from which they were originally released and, as a result, recombination is retarded.

It is very important to note that the series (1) runs parallel with the series which characterizes the catalytic activity of metals in hydrogenation and dehydrogenation reactions. The effect observed takes place within the same range of temperatures as the catalytic reactions just mentioned.

This novel effect, the existence of which has been demonstrated by this investigation, is of importance in catalysis. It has not been discussed in existing electronic theories of catalysis, but there is no doubt that it must be taken into account in the theory of catalytic processes.

Further investigations will be undertaken in due course.

LITERATURE CITED

[1] R. C. L. Bosworth and E. K. Rideal, Proc. Roy. Soc. (London) A, 162, 1 (1937).

[2] H. B. Michaelson, J. Appl. Phys. 21, 536 (1950).

M. V. Lomonosov State University,
Moscow

Received December 26, 1957

HEAT OF ADSORPTION OF BENZENE AND HEXANE VAPORS ON QUARTZ

A. A. Isirikian and A. V. Kiselev

(Presented by Academician M. M. Dubinin, August 10, 1957)

The investigation of adsorptive properties of quartz is of interest because of its similarity to a wide class of highly disperse porous adsorbents – the silica gels – with respect to the chemical structure of the surface [1-4]. The investigation of adsorption of benzene and hexane vapors on quartz as well as on other nonporous hydroxides is interesting also because the energy of adsorption of benzene represents, evidently, not only the energy of interaction due to Van der Waals' forces, but also the additional energy due to hydrogen bonding with the hydroxyl groups on the surface; on the other hand, the energy of adsorption of hexane is due to Van der Walls forces only [5-7]. Finally, investigation of adsorption and of heats of adsorption of vapors on quartz is also of interest in connection with the determination of the dependence of the thickness of polymolecular adsorbed films on the relative vapor pressure p/p_s, as well as the dependence of the energy of adsorption on the thickness of the adsorbed film; for investigations of this kind it is necessary to use comparatively coarse nonporous adsorbents in order to avoid complicating the adsorption process by capillary condensation right up to high values of p/p_s.

No direct determinations of heats of adsorption of these hydrocarbons on quartz have been carried out. In papers [8, 9] the isosteric heats of adsorption of benzene vapors on quartz have been calculated. However, the results cannot be easily correlated because of their inaccuracy due to the small specific surface areas of the quartz samples used, as well as due to different conditions of preparation and thermal pre-treatment of the samples.

In the present investigation the authors have determined adsorption isotherms and differential heats of adsorption of benzene and n-hexane vapors on quartz powder right up to saturation point; the apparatus used was the calorimetric adsorption apparatus described in a recent paper [10]. The specific surface area of the quartz powder was 6.0 m^2/g, as determined by nitrogen adsorption [11]. This sample was also used previously in the investigation of heats of adsorption of methanol vapors [12]. In order to remove the products of the reaction of methanol with the surface of quartz the latter was repeatedly washed with water, the wash liquors being decanted, and the wet powder was then dried at 130°. The dry powder was then placed in the calorimetric tube and was evacuated at 200° in the apparatus mentioned. The hydrocarbons were used in the manner described previously [10, 13].

In Fig. 1 are plotted the absolute adsorption isotherms for hexane and benzene vapors, α being the amount adsorbed per unit surface area. In the case of benzene the isotherm was determined right up to saturation point. The isotherms are reversible up to values of p/p_s of $\approx$ 0.9 and possess the S-shape characteristic of adsorption on nonporous adsorbents. At higher values of p/p_s there was obtained a distinctly reproducible hysteresis loop resulting from capillary condensation in the gaps between quartz particles which have coalesced during the drying process and have formed a compact deposit on the discs of the calorimetric tube. The pore volume distribution curve plotted in the upper part of the diagram and calculated from the desorption branch of the isotherm, shows that the majority of the interstices had a diameter varying from 1,000 to 7,000 A. These dimensions approximately correspond to the particle dimensions of the powder, as determined from electron-microphotographs. As the relative pressure p/p_s increases from the onset of hysteresis up to saturation point the surface area of the adsorbed film disappears [14, 15], i.e., an area of $s' \approx$ 4 m^2/g, or about 0.7s. Thus, the reduction s' as a result of the reversible nature of capillary condensation up to the point where hysteresis begins [14, 16], amounts to no more than 0.3 s and adsorption over the middle range of p/p_s may therefore be regarded as uncomplicated by capillary condensation.

In Fig. 1 we have plotted, for comparison, adsorption isotherms of the same vapors on silica gel KSK-2 of uniform wide-pore size [10, 13]. It will be seen that the branch of the curve corresponding to desorption begins to drop steeply around a relative pressure of 0.7. In this region of relative pressure adsorption on quartz is still relatively free from any appreciable complication due to capillary condensation in the interstices between the particles; for this reason the absolute adsorption isotherm of benzene and hexane vapors on quartz may be used to determine the thickness of the adsorbed layers which is necessary in applying corrections in the dimensions of pores of silica gels as given by Thompson's formula [15, 17]. In the case of silica gels of uniform pore size the drop of the desorption branch of the curve takes place over relatively narrow range of p/p_s within which the thickness of the adsorbed film on quartz varies to a negligible extent. Therefore, in order to determine the true dimensions of the orifices of pores of silica gels having the structure of an array of uniform globular particles [16]. It is sufficient to add to the diameter obtained by Thompson's formula for the maximum of the pore volume distribution curve, twice the thickness of the adsorbed film on quartz determined from the isotherms of Fig. 1 at the corresponding value of p/p_s [15].

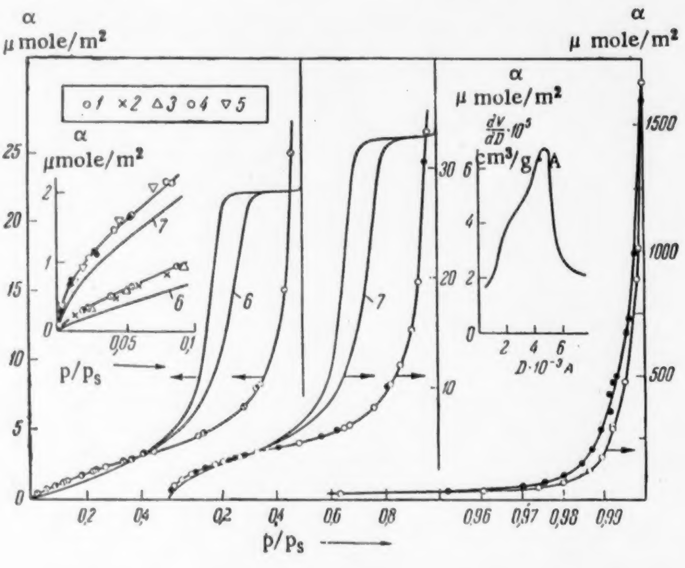

Fig. 1. Absolute adsorption isotherm of n-hexane vapors on quartz (1), silica gel KSK-2 at 650° (2) and mineral silica (3), and of benzene on quartz (4) and mineral silica (5). The dots denote desorption. Isotherms on which no experimental points are shown are those for hexane (6) and benzene (7) on silica-gel KSK-2 at 200°. Top right-hand corner: pore volume distribution curve in quartz powder in relation to pore diameter.

In the initial region of the completion of a monomolecular film adsorption on quartz is greater than on silica gel KSK-2 which has been heated at 200° [13], an effect which is, in the main, due to the lesser compactness of the structure of such a silica gel. From Fig. 1 it will be seen that after heat treating this silica gel at 650° [7] the amount of hexane adsorbed on it is very close to that adsorbed by quartz, and the same applies to silica obtained by ignition of organosilicon compounds [6]. Adsorption of benzene also depends strongly on the degree of hydration of the surface of silica [6, 7]. From Fig. 1 it will be seen that adsorption of benzene on ignited silica obtained from organosilicon compounds approaches very closely adsorption on quartz when the surface of such silica powder has been hydrated [6]. The adsorption isotherm of benzene vapor on quartz is well expressed by the BET equation which gives the volume of the compact monolayer as $\alpha_m = 3.35\,\mu$ mole/m², which corresponds to an area $\omega_0 = 1/\alpha_m = 49$ A² for the area occupied by a benzene molecule, a value also obtained from adsorption on silica gel [10, 7].

In Fig. 2 is illustrated the dependence of the heat of adsorption of benzene vapors, Q_a, on the absolute adsorption, α, on quartz. From the diagram it will be seen that when the first two layers are complete the heat of adsorption exceeds the heat of condensation by only 3% while after the adsorption of another two layers the excess amounts to 1%. The further decrease of the heat of adsorption is very gradual; this is due to the decrease in the energy of adsorption with increasing distance from the surface of the adsorbent (increasing thickness of adsorbed film) and to some unavoidable diminution of the surface of the film at the points of contact between quartz particles. In the case of the bare smooth surface of quartz the heat of adsorption can only be less than the values indicated in Fig. 2 over the range stated.

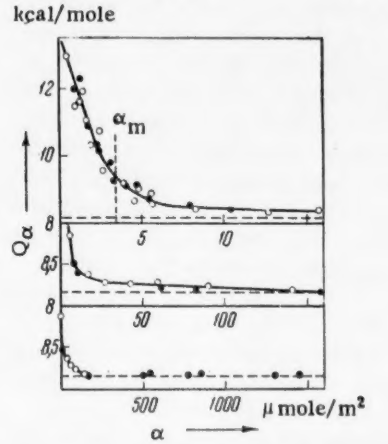

Fig. 2. Dependence of the heat of adsorption of benzene vapor on quartz on the degree of surface coverage. The dots denote desorption. The horizontal broken line gives the latent heat of condenstion L. The vertical broken line gives the monolayer adsorption capacity α_m.

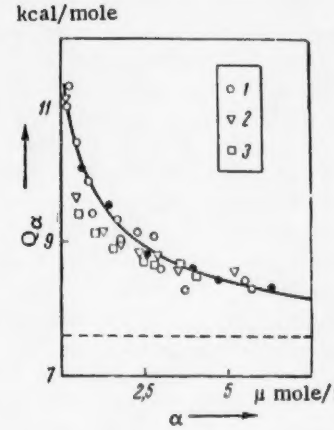

Fig. 3. Dependence of the heat of adsorption of vapors of n-hexane on the amount adsorbed on quartz (1) and on silica (2) and (3). The dots denote desorption, the broken line indicates the latent heat of condensation.

In Fig. 3 is illustrated the dependence of the heat of adsorption of n-hexane on quartz on the absolute adsorption. In this case we again observe a gradual decrease in the heat of adsorption. The heat of adsorption of hexane on silica obtained by ignition of organosilicon compounds [6] is close to the value obtained on quartz.

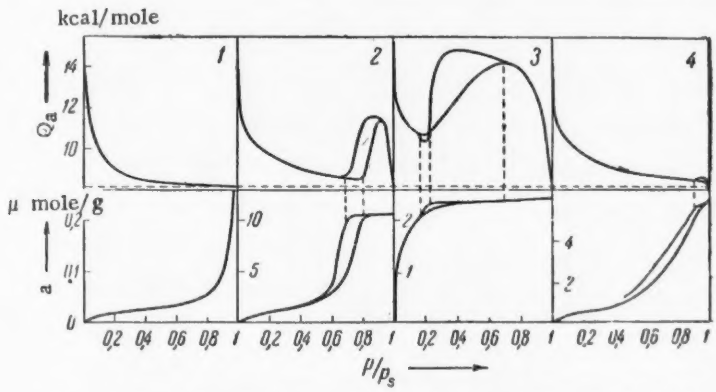

Fig. 4. Dependence of heats of adsorption (upper diagrams) and desorption (lower diagrams) of benzene vapors on the relative pressure on quartz (1), wide-pore silica gel (2), fine-pore silica gel (3) and silica of nonuniform pore size (4). The horizontal broken line indicates the heat of condensation.

A more accurate and detailed investigation of the dependence of the heat of adsorption on monomolecular coverage, using the constant heat transfer colorimeter [10], is difficult with powders with a surface area of less than 10 m^2/g. It is hoped that a more detailed investigation of this region of adsorbent coverage of quartz will be carried out later.

Integration of the curve expressing the dependence of the actual heat of adsorption of benzene vapors, $Q_a - L$, on α gives a value of 50-90 erg/cm^2.* If to this value we add the full surface energy of benzene, 68 erg/cm^2, we obtain for the heat of wetting of quartz by benzene a value of 120-160 erg/cm^2, which is no more than 1.1 to 1.5 times larger than the heat of wetting of silica gel [13].**

From Fig. 2 it will be also seen that the curve representing the differential heat of adsorption on quartz unlike similar curves obtained for silica gels of uniform pore size [10, 13, 18], has no maximum since the adsorption isotherm rises continuously and because the adsorbed liquid is not affected by capillary forces and its properties approach those of the normal liquid in a gradual manner. The differences in the heats of adsorption on approaching saturation are clearly seen in Fig. 4 in the case of adsorbents of all four structural types [15]. In this figure the dependence of differential heats of adsorption, Q_a, and of the amounts adsorbed, $\underline{a}$, on the relative pressure p/p_s are juxtaposed for convenience of comparison. In the case of simple polymolecular adsorption on an adsorbent of the first structural type, such as nonporous quartz, the heat of adsorption approaches asymptotically the heat of condensation. In the case of an adsorbent of the second structural type, a wide pore silica gel, there occurs maxima representing heats of compression of the capillary-condensed liquid resulting from the action of menisci at the orifices of the pores [10, 13, 18]. In the case of adsorbents of the third structural type, such as a fine-pore silica gel, the maxima corresponding to the heats of adsorption and desorption are particularly pronounced as a result of the greater curvature of the menisci enclosing the liquids within the pores [10, 13, 18]. Finally, in the case of adsorbents of the fourth structural type such as silica powder of nonuniform pore size, the heat of compression of the liquid within the pores becomes gradually superposed on the heat of disappearance of the adsorbed film within the pores, and the heat of adsorption is distinctly larger than the heat of condensation over the whole range of film thickness. In this case, however, the maxima are not well-defined [6].

LITERATURE CITED

[1] W. Stober, Koll. Zs. 145, 17 (1956).

[2] L. Miller, Koll. Zs. 142, 117 (1955).

[3] P. F. Holt and D. T. King, J. Chem. Soc. (1955), p. 773.

[4] S. P. Zhdanov and A. V. Kiselev, J. Phys. Chem. 31, 2213 (1957).

[5] A. V. Kiselev, Proc. Acad. Sci. USSR 100, 1046 (1956).

[6] A. A. Isirikian and A. V. Kiselev, Proc. Acad. Sci. USSR 115, 343 (1957).***

[7] L. D. Beliakova and A. V. Kiselev, Proc. Acad. Sci. USSR 119, 2 (1957). ***

[8] W. G. Palmer, Proc. Roy. Soc. (London) A 168, 190 (1938).

[9] A. I. Sarakhov, Bull. Acad. Sci. USSR, Div. Chem. Sci. (1956), p. 150. ***

[10] A. A. Isirikian and A. V. Kiselev, J. Phys. Chem. 31, 2127 (1957).

[11] A. P. Karnaukhov, A. V. Kiselev, and E. V. Khrapova, Proc. Acad. Sci. USSR 94, 91 (1954).

[12] N. N. Avgul' and O. I. Dzhigit et al., Proc. Acad. Sci. USSR 77, 625 (1951).

* Integration at higher values of α introduces errors in the calculation.

** It is possible that the value obtained for the heat of wetting of quartz may, in fact, be somewhat high as a result of the liberation of heat during the disappearance of part of the surface of the adsorbed film.

*** Original Russian pagination. See C. B. Translation.

[13] A. A. Isirikian and A. V. Kiselev, J. Phys. Chem. 32, 3 (1958).

[14] N. N. Avgul', G. I. Berezin et al., J. Phys. Chem. 31, 1111 (1957).

[15] A. V. Kiselev, Methods of Investigation of the Structure of Highly Disperse and Porous Substances * (Acad. Sci. USSR Press, 1953), p. 86.

[16] A. V. Kiselev, Proc. Acad. Sci. USSR 98, 427 (1954).

[17] M. M. Dubinin, J. Phys. Chem. 30, 1632 (1956).

[18] A. A. Isirikian and A. V. Kiselev, Proc. Acad. Sci. USSR 110, 1009 (1956). **

M. V. Lomonosov State University,
Moscow.

Received June 27, 1957.

* In Russian.

** Original Russian pagination. See C. B. Translation.

INVESTIGATION OF HEAT EXCHANGE BETWEEN VIBRATING HEATING ELEMENTS AND VISCOUS LIQUIDS

N. V. Kalashnikov and V. I. Chernikin

(Presented by Academician P. A. Rebinder, July 2, 1957)

Heat transfer from fixed heating elements to liquids contained in vessels takes place by free convection which in the case of viscous liquids is very slow. One of the most effective methods of increasing the rate of heating of liquids is the application of vibrating heating elements in which case heat transfer is mainly effected by forced convection.

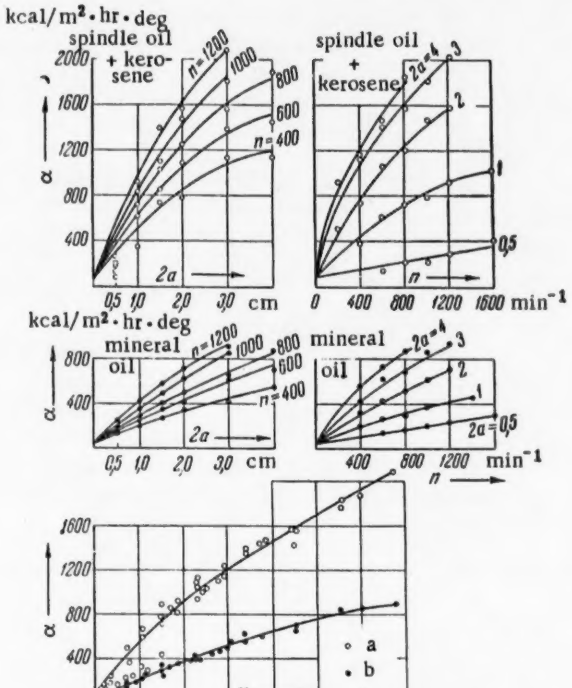

Fig. 1. Dependence of heat transfer coefficient α on vibration conditions: a) Spindle oil + kerosene; b) mineral oil 100.

We have investigated the effect of vibration of heating elements on heat transfer in viscous liquids using an electric vertical vibrator provided with a horizontal cylindrical electric heater 1.98 cm in diameter and having an effective heating length of 28.2 cm. The amplitude of vibrations was varied within the limits of from

$2a = 1$ to 4 cm, the frequency $\underline{n}$ from 100 to 1600 min^{-1}, and the mean square vibration velocity, $\bar{v} = \frac{\omega a}{\sqrt{2}} = \frac{2\pi na}{\sqrt{2}}$, from 4 to 134 cm/sec. The following liquids were investigated: a high-viscosity mineral oil 100 ($\nu_{20} = 66.2$ cm²/sec), automobile lubricating oil 18 ($\nu_{20} = 13.0$ cm²/sec), spindle oil ($\nu_{20} = 1.28$ cm²/sec), and a mixture of spindle oil and kerosene having a viscosity very close to that of diesel oil ($\nu_{20} = 0.17$ cm²/sec). The following results were obtained (Fig. 1):

1. In the absence of vibration ($n = 0$) the heat transfer coefficient α in the case of the mineral oil lies within the limits of 40 to 45 kcal/m²·hr·deg at a temperature of $t_{mean} = 42°$. When the vibration regime is such that $2a \cdot n = 3 \cdot 1200$ ($\bar{v} = 134$ cm/sec) α increases to 900 kcal/m²·hr·deg, i.e., approximately 20 fold. In the case of the mixture of spindle oil with kerosene under these conditions α increases from 80-85 kcal/m²·hr·deg to 2080 kcal/m²·hr·deg, i.e., approximately 24 fold. It is obvious, therefore, that causing heating elements to vibrate is a powerful means of intensifying heat transfer.

2. Increasing 2a, $\underline{n}$ being kept constant, or increasing $\underline{n}$, for 2a = const, leads to a considerable increase of α; consequently, α increases with increasing vibration velocity $\bar{v}$.

3. In the case of liquids of low viscosity the rate at which α increases for $\bar{v}$ = const, depends to a greater extent on the amplitude than on the frequency of vibration. As the viscosity of the liquid increases the dominant role of the amplitude becomes less and less and is practically insignificant in the case of liquids of high viscosity.

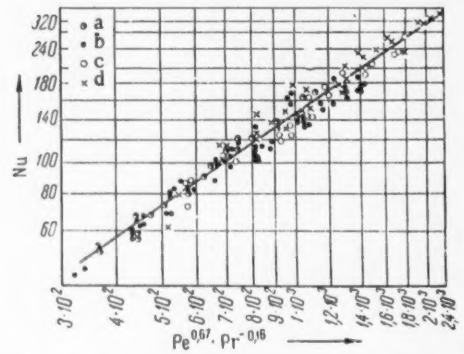

Fig. 2. Parameter Nu as a function of $Pe^{0.67} \cdot Pr^{-0.16}$ (experimental results and theoretical straight line). a) Mineral oil 100; b) automobile lubricating oil 18; c) spindle oil; d) spindle oil + kerosene.

At a vibration velocity of 20 cm/sec and above free convection has practically no effect on the intensity of heat transfer from a vibrating heating element to viscous liquids and heat transfer is effected entirely by forced convection.

The evaluation of the experimental results in terms of parameters defining forced convection [1] led to the following formula (Fig. 2):

$$Nu = 0,146 \; Pe^{0,67} \cdot Pr^{-0,16} \tag{1}$$

The reference temperature in Equation (1) is $t_{mean} = 0.5 (t_{heater} + t_{liq})_{mean}$; t_{heater} denotes the surface temperature of the heating element; t_{liq} is the temperature of the liquid and the reference dimension is the diameter of the heater tube $\underline{d}$. Parameter Pe is calculated from the mean square vibration velocity $\bar{v}$. Formula (1) can be applied to horizontal cylindrical heating elements vibrating vertically with an amplitude of $2a = 1$ to 4 cm and with a velocity $\bar{v} = 20$ to 134 cm/sec, the values of the parameters Pe and Pr being (1.6 to 40) 10^4 and $1.4 \cdot 10^2$ to $1.5 \cdot 10^4$, respectively.

The resistance R of the heating element vibrating in a liquid is determined by the following parameters:

for $0.5 < Re < 2$, $\quad Eu = 63 \; Re^{-2}$

for $2 < Re < 7$, $\quad Eu = 28 \; Re^{-0.82}$

for $7 < Re < 100$, $\quad Eu = 11.5 \; Re^{-0.36}$

where $Eu = \frac{R}{v^2 \rho F}$, $F = dl$, l is the length of the heating element.

LITERATURE CITED

[1] M. A. Mikheev, Fundamentals of Heat Transfer, 1956 [In Russian].

I. M. Gubkin Petroleum Institute, Moscow

Received July 2, 1957

KINETICS AND MECHANISM OF OXIDATION OF ALCOHOLS AND ALDEHYDES BY ACTIVE CHLORINE

I. K. Kozinenko and Academician E. A. Shilov (Acad. Sci. Ukr. SSR)

Up to the present all investigations of the kinetics of oxidation by active chlorine have been concerned with cases in which the direct oxidation of an alcoholic or aldehydic group could become complicated by side reactions with neighboring functional groups, including enolization. This applies to acetaldehyde [1], glycollic aldehyde and glucose [2], lactic and other hydroxy acids [3]. In this investigation the authors have used m-sulfobenzyl alcohol and m-sulfobenzaldehyde (sodium salts), both these compounds being of the type which facilitates observation of the oxidation of an alcoholic or aldehydic group by active chlorine in aqueous solutions without the complicating effects of any side reactions.

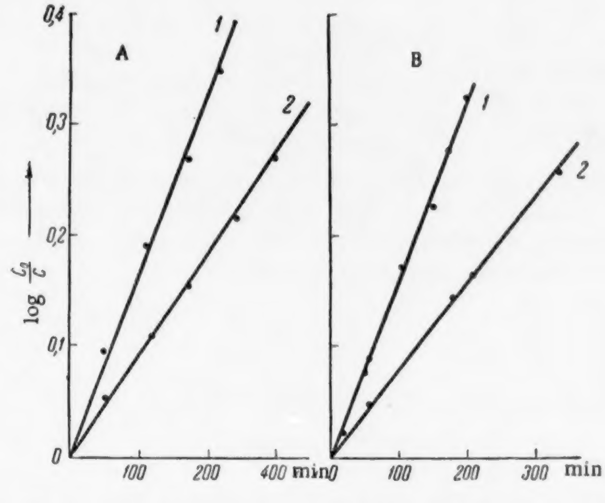

Fig. 1. A) Oxidation of m-sulfobenzyl alcohol. 1) A = 0.2 M, C_0 = 0.00697 M, pH 7.02; 2) A = 0.1 M, C_0 = 0.00697 M, pH 7.05. B) Oxidation of m-sulfobenzaldehyde. 1) A = 0.1 M, C_0 = 0.00516 M, pH 10.75; 2) A = 0.05 M, C_0 = 0.00505 M, pH 10.80.

Oxidation of m-sulfobenzyl alcohol. In preliminary experiments it was established that in the presence of a large excess of the sulfo-alcohol the negligible amount of active chlorine used up in the secondary oxidation of the aldehyde formed could be left out of consideration.

At constant pH and in the presence of a large excess of m-sulfobenzyl alcohol the decrease in the titer of active chlorine (C), in buffered solution, can be expressed by the kinetic equation for unimolecular reactions, as is illustrated by the straight lines in Fig. 1, A. On the other hand, the rate of reaction is found to be almost exactly proportional to sulfo-alcohol concentration and at constant pH can be expressed by the equation:

$$-\frac{dC}{dt} = k_2 AC \qquad (1)$$

where A is the alcohol concentration and C the concentration of active chlorine.

The dependence of the rate of reaction on pH may be studied from Fig. 2 where values of $\tau/2$, i.e., the times necessary for the concentration of active chlorine to drop to half its initial value, are plotted against pH. Values of $\tau/2$ have been calculated for experimentally determined values of k_2 using the formula: $\tau/2 = 0.693/k_2$.

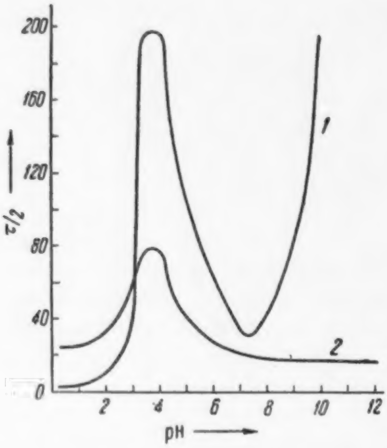

Fig. 2. Dependence of the rate of oxidation of m-sulfobenzyl alcohol (1) and m-sulfobenzaldehyde (2) on pH.

The maxima and the minima of this curve are, above all, conditioned by the composition of the solutions of active chlorine used. The reaction rate maximum over the pH range of 0-2, in the presence of different amounts of hydrochloric acid, is related to the existence of active chlorine in the molecular form (Cl_2). Using the velocity constant of hydrolysis of active chlorine, it can be found that already in a 0.1 molar solution of hydrochloric acid the concentration of free HOCl is very small and further increase in concentration of HCl hardly affects the concentration of Cl_2. As a result, $\tau/2$ also remains constant at pH < 1. There is therefore no doubt that in strongly acid solutions molecular chlorine is the active oxidizing agent for m-sulfobenzyl alcohol.

At pH values greater than 2.5 the rate of reaction decreases rapidly with increasing pH and passes through a minimum at a pH of about 4. The exact minimum corresponds approximately to the existence of active chlorine in the form of free HOCl. The relatively low activity of this oxidizing agent is well-known also in the case of other reactions with active chlorine [2-4].

With further increase of pH the rate of oxidation of m-sulfobenzyl alcohol increases, reaches a second maximum at a pH of about 7.5 and subsequently drops again becoming very slow at pH values greater than 10. Now, the concentration of HOCl in solutions of active chlorine continuously decreases as the pH increases beyond 5, the HOCl molecules dissociating into OCl^- ions [5] in accordance with the formula

$$[\mathrm{HOCl}] = \frac{[\mathrm{H}^+]\,C}{[\mathrm{H}^+] + K_{ac}},$$

where K_{ac} is the electrolytic dissociation constant of HOCl, equal to $4.1 \cdot 10^{-8}$ [2].

The hypochlorite ion is, evidently, incapable of oxidizing the sulfo-alcohol since no oxidation takes place in strongly alkaline solution. Consequently, it must be hypochlorous acid which is the primary or intermediate oxidizing agent at moderate pH values. Parallel with this conclusion it must also be assumed that hydroxyl ions and anions of buffer salts have a catalytic effect on the reaction of HOCl with sulfobenzyl alcohol.

If the velocity constants are related to the concentration of free hypochlorous acid and combined with the activity coefficient of the OH ion, a_{OH^-}, and the concentration of the anion of the buffer salt [An], the velocity of the reaction over the pH range from 4 to 10 may be expressed by the equation:

$$-\frac{dC}{dt} = k_4^0\, A\,[\mathrm{HOCl}] + k_4^{\mathrm{An}} A\,[\mathrm{HOCl}]\cdot[\mathrm{An}] + k_4^{\mathrm{OH}}\, A\,[\mathrm{HOCl}]\, a_{\mathrm{OH}^-}^{0.75}, \qquad (2)$$

where $k_4^0 = 2.2 \cdot 10^{-3}$; $k_4^{An} = 0.0234$ for the acetate ion, 0.245 for the hydrogen phosphate ion and approximately zero for the carbonate ion, and $k_4^{OH} = 1.3 \cdot 10^3$, all in moles per liter per minute.

The experimental results are summerized in Table 1 which gives values of k_2 actually measured and those calculated using the constants k_4 of Equation (2). It will be seen that agreement between experimental and calculated constants is satisfactory over a fairly wide pH range.

The most probable mechanism of the reaction under consideration appears to be that proposed previously by Shilov and Iasnikov [3] for the oxidation of hydroxy compounds. We suggest that oxidation of the alcohol proceeds through a stage involving the formation of an ester of hypochlorous acid:

$$\mathrm{Ar-CH_2OH + HOCl \rightleftarrows Ar-CH_2OCl + H_2O} \quad \text{(I)}$$

$$\mathrm{Ar-CH_2OCl + OH^- \rightarrow Ar\cdot CHO + H_2O + Cl^-} \quad \text{(IIa)}$$

$$\mathrm{Ar-CH_2OCl + An^- \rightarrow Ar\ CHO + HAn + Cl^-} \quad \text{(IIb)}$$

The rates of both reactions are commensurate. At low pH values formation of the ester is rapid and the rate of reaction is limited by the rate of decomposition of the ester which increases with increasing concentration of the base. At high pH values the rate of oxidation is determined by the rate of formation of the alkyl hypochlorite. Superposition of the rates of steps (I) and (II) is responsible for the reaction rate maximum at a pH of about 7.5.

TABLE 1

pH	$10^{[illegible]}$ C mole/g	A mole/g	$10^{[illegible]}$ [An] mole/g	$10^{[illegible]}$ k_2 exp	$10^{[illegible]}$ k_3	$10^{[illegible]}$ k_2 calc
m-Sulfobenzyl alcohol; 30°						
4,05	4,17	0,2	Ac 5	3,5	3,5	3,4
4,70	4,14	0,2	Ac 15	6,0	6,0	5,9
5,52	4,10	0,2	Ac 22,5	8,0	8,0	8,3
6,55	3,84	0,1	Ph 3	13,0	14,9	13,0
7,02	6,97	0,2	Ph 6	18,3	26,2	20,3
7,05	6,97	0,1	Ph 6	20,0	30,2	20,4
7,51	3,09	0,1	Ph 8	23,0	53,6	21,6
7,51	1,50	0,1	Ph 8	23,0	53,6	21,6
8,91	4,64	0,1	Ca 1	9,5	$3{,}3\cdot10^{2}$	9,4
9,85	4,25	0,088	Ca 10	5,9	$17\cdot10^{3}$	5,6
12,85	4,11	0,2	—	1,1	$3{,}2\cdot10^{5}$	1,0
m-Sulfobenzaldehyde, 30°						
4,04	4,87	0,1	Ac 5	9,1	9,1	9,7
4,88	5,03	0,1	Ac 16	17	17	15,9
5,2	4,81	0,1	Ac 20	16	16	18
6,55	6,31	0,1	Ph 4	24,6	28,4	25
7,0	5,30	0,1	Ph 6	33	46,5	33,5
7,45	5,20	0,1	Ph 4	30	64,8	30
8,9	5,50	0,1	Ca 1	37	$1{,}2\cdot10^{3}$	35
9,9	4,80	0,05	Ca 5	37	$12\cdot10^{3}$	35
10,75	5,16	0,1	Ca 9	36	$83\cdot10^{3}$	35
10,8	5,05	0,05	Ca 9	36	$94\cdot10^{3}$	36
12,85	5,60	0,05	—	34	$1\cdot10^{7}$	34

Note. [An] is the concentration of buffer salt; Ac is the acetate ion; Ph is the hydrogen phosphate ion; Ca is the carbonate ion; k_2 is the velocity constant in Equation (1); k_3 is the same constant referred to the concentration of HOCl.

Since mathematical treatment of the results is difficult this discussion of the reaction mechanism must remain a qualitative one. However, in support of the hypothesis proposed it may be mentioned that there is an analogy between this reaction and the oxidation of alcohols by other oxidizing agents, for example, chromic acid and persulfates, in which case esters of the corresponding acids are also formed as intermediate products of reaction [6, 7].

Oxidation of m-sulfobenzaldehyde. The rate of oxidation of m-sulfobenzaldehyde at constant pH and in the presence of excess aldehyde can be expressed by the kinetic equation for unimolecular reaction (see Fig. 1, B).

The variation of the rate of oxidation with pH, in buffered solution, is plotted in Fig. 2 (curve 2). It will be seen that in the acidic range of pH – from 0 to 5 – the curve follows a similar pattern as in the case of m-sulfobenzyl alcohol. In strongly acid solution oxidation is effected by molecular chlorine, whereas the oxidizing power of hypochlorous acid is low. Beginning at a pH of about 4 the rate of reaction increases at first, but, unlike the oxidation of sulfobenzyl alcohol, it does not pass through a maximum, but reaches a constant value at a pH of 8 and remains unchanged right up to pH 13. As in the case of m-sulfobenzyl alcohol, anions of the buffer mixture catalyze the reaction.

The general kinetic equation of the reaction may be written in the form:

$$-\frac{dC}{dt} = k_4^0 A\,[\mathrm{HOCl}] + k_4^{\mathrm{An}} A\,[\mathrm{HOCl}]\,[\mathrm{An}] + k_4^{\mathrm{OH}} A\,[\mathrm{HOCl}]\,a_{\mathrm{OH}}. \quad (3)$$

where $k_4^0 = 7\cdot10^{-3}$; $k_4^{An} = 0.053$ for the acetate, 0.25 for the phthalate and 0.43 for the hydrogen phosphate ion, and $k_4^{OH} = 7.6\cdot10^4$, all units being in moles per liter per minute (see Table 1).

Equation (3) and the curve expressing the dependence of the rate of reaction on pH may be interpreted on the assumption that the reaction takes place according to the following mechanism:

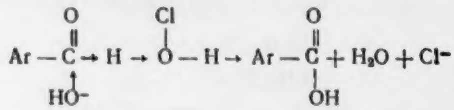

The OH ion may be substituted by the water molecule or by the anion of weak acids. The mechanism involving the hydroxyl ion has an analogy in the Cannizzaro reaction, the only difference being that in this case the hypochlorous acid molecule is the proton acceptor.

In the case of the oxidation of para- and ortho-sulfobenzaldehyde the kinetic features are the same as in the case the meta isomer. Under the same experimental conditions the rate of oxidation of the para isomer is 1.2 times faster and that of the ortho isomer between 5 and 7 times slower than the rate of oxidation of m-sulfobenzaldehyde.

EXPERIMENTAL RESULTS

m-Sulfobenzyl alcohol was prepared by reduction of sodium m-sulfobenzaldehyde with hydrogen over a platinum catalyst [8]. m-Sulfobenzaldehyde was prepared by sulfonation of benzaldehyde with oleum [9]. The sodium salts of the sulfonic acids obtained were purified by repeated recrystallization from water and alcohol.

Solutions of active chlorine were made up in a blackened flask into which reagent solutions, warmed to $30 \pm 0.05°$ in a thermostat, were transferred by means of pipettes. Samples were withdrawn by means of a constant level pipette [2]. Active chlorine was determined iodometrically, the pH was measured potentiometrically with an accuracy of 0.05, using a glass electrode. Reactions in acid solution were carried out in a special apparatus which prevented the escape of chlorine. The correction for spontaneous decomposition of hypochlorite was omitted because it is very small [2].

LITERATURE CITED

[1] J. Groh, Zs. Phys. Chem. 81, 695 (1913).

[2] E. A. Shilov and A. A. Iasnikov, Ukr. Khim. Zhur. 18, 595 (1952).

[3] E. A. Shilov and A. A. Iasnikov, Ukr. Khim. Zhur. 18, 611 (1952).

[4] E. A. Shilov and A. A. Iasnikov, Textile Industry 11, 35 (1950).

[5] E. A. Shilov, A. I. Sliadnev, and G. V. Kupinskaia, J. Gen. Chem. 22, 1497 (1952). *

[6] F. Holloway, M. Cohen, and F. Westheimer, J. Am. Chem. Soc. 73, 65 (1951).

[7] L. Levitt and E. Malinowski, J. Am. Chem. Soc. 77, 4517 (1955).

[8] E. A. Shilov and G. I. Kudriavtsev, Proc. Acad. Sci. USSR 63, 681 (1948).

[9] O. Wallach and M. Wüsten, Ber. 16, 150 (1883).

Kiev Polytechnical Institute,
Institute of Organic Chemistry,
Academy of Sciences of the Ukrainian SSR.

Received November 10, 1957.

* Original Russian pagination. See C. B. Translation.

THE INFLUENCE OF STRUCTURAL FEATURES AND SURFACE PROPERTIES ON THE EXTRACTION BY FROTH FLOTATION OF LEAD MINERALS DIFFICULT TO FLOAT

E. A. Anfimova, V. A. Glembotskii,
Corresponding Member AS USSR I. N. Plaksin, and A. S. Shcheveleva

Of the large number of oxidized lead minerals found in nature which are of importance industrially, several [cerussite $PbCO_3$, anglesite $PbSO_4$, wulfenite $PbMoO_4$ and to a certain extent vanadinite $Pb_5(VO_4)_3Cl$] are comparatively easily extracted by froth flotation.

There are no satisfactory methods in contemporary ore dressing practice, however, for the extraction of a number of oxidized lead minerals of complex composition, such as pyromorphite $Pb_5(PO_4)_3Cl$, mimetesite $Pb_5(ASO_4)_3Cl$, beudantite $PbFe_3(ASO_4)(SO_4)(OH)_6$ and plumbojarosite $PbFe_6(SO_4)_4(OH)_{12}$.

Systematic incomplete extraction of oxidized lead minerals in ore dressing plants leads to considerable losses of lead in the process of concentrating mixed and oxidized lead ores.

The complex chemical composition and structure of the minerals mentioned distinguishes them sharply from the minerals which respond readily to treatment with the flotation and extraction reagents normally employed on the industrial scale.

In this connection we have made an attempt to explain the unsatisfactory results obtained in the extraction of pyromorphite, mimetesite, beudantite and plumbojarosite on the basis of an examination of the features of their crystal chemistry and surface behavior toward water and a number of flotation reagents, so that as a result of such investigations it may be possible to find the most efficient methods for extracting the minerals in question.

We first of all calculated the crystal lattice energies of the lead minerals under study (by Fersman's method).* As can be seen from the data given in Table 1, the values of the crystal lattice energy for cerussite, anglesite and wulfenite (Group I) differ comparatively little from one another.

TABLE 1

Group	Mineral	Crystal lattice energy, kcal	
		total	related to unit cation valence
I	Cerussite	622.32	311.16
	Anglesite	596.71	298.36
	Wulfenite	571.10	285.55
II	Vanadinite	3290.80	329.08
	Mimetesite	3352.35	335.23
	Pyromorphite	3329.30	332.93
III	Beudantite	5513.83	501.80
	Plumbojarosite	10169.73	508.49

* We have related the value of the crystal lattice energy to unit cation valence.

The minerals of Group II, which may be taken to include mimetesite, pyromorphite, and vanadinite, are distinguished by high lattice energy values.

The highest values for the crystal lattice energies are shown by beudantite, mimetesite, plumbojarosite, and pyromorphite. The data given already provide a guide to the evaluation of the flotation properties in relation to the ability of all the minerals listed to interact with the reagents.

Our studies have shown that the flotation properties of the minerals in question and their tendency to interact with reagents correspond with the calculated values of the crystal lattice energies. Thus, for example, it has been established that the efficiency of the treatment of oxidized lead minerals with sodium sulfide decreases on going from minerals of Group I to minerals of Groups II and III. Plumbojarosite shows the highest crystal lattice energy value.

This feature of plumbojarosite corresponds to the fact that it is completely unaffected by sodium sulfide, and no sulfidization takes place even at increased temperature. Under similar conditions cerussite and anglesite show a very active interaction with sodium sulfide.

We have established the particular features of the interaction with sodium sulfide and xanthates and the corresponding suitability for flotation treatment for cerussite and all the other oxidized lead minerals under study, using the radioactive isotope method, a method involving the measurement of the time of adhesion of an air bubble with an electronic apparatus constructed by one of the authors [1], and also, in almost all cases, by direct experimental flotation of the minerals under various conditions. It was established in all these experiments that the efficiency of the sulfidization of the lead minerals studied and of the process of rendering their surfaces hydrophobic by the action of xanthates (both in the case of the independent use of the latter and also in combination with preliminary sulfidization), in almost all the experimental series studied, decreased in the following order: cerussite, anglesite, wulfenite, pyromorphite, mimetesite, beudantite, plumbojarosite, i.e., changes practically in accordance with the increase in the value of the crystal lattice energy.

This relationship between the flotation and sulfidization properties on the one hand and the value of the crystal lattice energy on the other shows that as it increases there is an increase in the energy of the bond between the surface of the mineral and the dipoles of the water together with an increase in the stability of the hydrate layers covering the surface of the mineral particles with the collectors which prevent interaction between the mineral and the flotation reagents. The essential data for estimating the adsorption and flotation activity of the minerals being studied may be obtained on the basis of an examination of the crystallochemical and structural features of these minerals. Thus, for example, the cerussite lattice [2] has mainly a planar structure while the bonds are directed parallel to one another in the absence of a three-dimensional configuration.

These features of the cerussite lattice create favorable conditions for replacement of the ions of the lattice by other ions and for the introduction into the lattice of ions of the flotation reagents. This is all in good agreement with the adsorption and flotation features of cerussite. The distinct cleavage along the (110) and (021) planes and the very poor cleavage along the (010) and (012) planes indicates that when the cerussite is crushed a considerable number of lead ions, which are active toward the flotation reagents, are exposed. Anglesite is characterized [2] by a more compact packing of the atoms and has to a greater extent a three-dimensional rather than a planar configuration; this results in less favorable conditions for interaction with flotation reagents (as is observed in practice).

In the series of anions CO_3^{--}, SO_4^{--}, and MoO_4^{--}, the ionic radii increase from CO_3^{--} to MoO_4^{--}. It is known that for ions with the same charge, the polarizability of the ions increases with increase in the ionic radius, when the ions as it were approach one another and bunch together, which leads to an increase in the stability of the crystal lattice and explains the reduction in the extent of the interaction with flotation collectors in the series from cerussite to wulfenite (together with the other crystallochemical features of these minerals described above).

The minerals of Group II are characterized by a crystal lattice structure of the apatite type [3]. Besides the high lattice energy values already referred to, these minerals have close-packed atoms and a high coordination number (the number of nearest neighbors is six) so that the lead in this case is firmly bound to neighboring atoms; the cleavage is poor.

All this explains the low tendency of the minerals of Group II to interact with flotation reagents.

The crystal structure of plumbojarosite has been insufficiently studied, but on the basis of the data available in the literature it can be seen that the structure of this mineral shows the presence of very short stable bonds, which together with the exceptionally high crystal lattice energy values for the mineral result in a very marked inertness toward flotation reagents and collectors.

Flotation experiments, and experiments using radioactive isotopes, have established that the alkalinity of the pulp has a considerable influence on the flotation properties of the minerals under study, evidently by influencing the hydration properties of the surface.

A change in the alkalinity of the medium causes a change in the strength of the forces holding the flotation reagent to the sulfidized surface of the mineral.

An alkaline medium is the optimum medium for cerussite (pH 8.5 - 9.5) and wulfenite (pH 8.0 - 8.5). For anglesite a weakly alkaline medium is preferable. A neutral medium is best for pyromorphite and vanadinite. Mimetesite and beudantite are floated in a weakly acid medium (pH 5.5 - 6.0). Thus, the alkalinity of the pulp in the flotation of oxidized lead minerals which have been subjected to a sulfidizing process should be adjusted in accordance with their mineralogical composition.

All the minerals indicated require different sulfidization conditions, the duration of the sulfidizing treatment increasing on going from minerals of Group I to minerals of Group III. Plumbojarosite cannot be sulfidized. Experiments have established, however, that phosphothene* can be used for the flotation of plumbojarosite.

The following materials may be used as new and efficient flotation reagents for the flotation of oxidized lead minerals which are difficult to concentrate: phosphothene, petroleum, motor oil and semi-asphalt, together with xanthates.

The authors wish to express their gratitude to Academician N. V. Belov and Professor G. B. Bokii for their valuable advice, which has proved of assistance in the present work.

LITERATURE CITED

[1] V. A. Glembotskii, Bull. Acad. Sci. USSR, Div. Tech. Sci. 11 (1953).

[2] B. F. Ormont, The Structure of Inorganic Substances,** (1950).

[3] A. G. Betekhtin, Mineralogy, (1950).

Received December 18, 1957

* Phosphothene is a naphthene derivative of an alkali dithiophosphate.

** In Russian.

A STUDY OF THE CHANGES IN THE TRANSFERENCE NUMBERS OF IONS AND THE SUSPENSION EFFECT IN LIQUID SUSPENSOID SYSTEMS

O. N. Grigorov and Iu. M. Chernoberezhskii

(Presented by Academician P. A. Rebinder, November 25, 1957)

The change in the transference numbers of ions in various capillary systems, including those with a rigid skeleton and also powder systems composed of separate particles in contact with one another, has been observed and studied by many workers [1]. This phenomenon may be explained by the existence of an electrical double ionic layer at the boundary separating the phases and the participation of the ions entering the layer in the process of current transfer across the capillary system. A similar phenomenon has been observed for solutions of high-molecular compounds and, in particular, A. I. Iurzhenko [2] has shown that in the case of gelatin, the transference numbers of the chloride ion in gelatin remain practically constant, irrespective of whether the gelatin is in the form of a gel or a sol (in the molten state). This indicates that the method by which the structure in the solution is established — whether by mobile particles (large molecules in the case of gelatin) or by an immobile compact skeleton — may have no essential part in determining the change in the transference numbers.

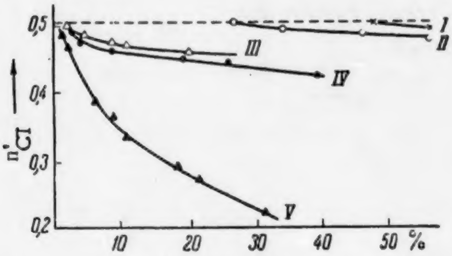

Fig. 1. The relationship between the change in the transference numbers in quartz and bentonite suspensions and the quantity of disperse phase. I - IV) Quartz, with particle sizes: I) 6-10 μ; II) 3-6 μ; III) 1-3 μ; IV) < 1 μ; V) bentonite.

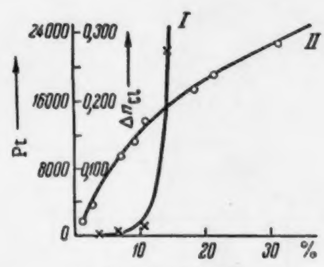

Fig. 2. Curves showing how the structural viscosity and the transference number for bentonite suspensions varies with the quantity of disperse phase. I) Pt: (P is pressure in millimeters of water, t is time in seconds); II) Δn_{Cl}.

It follows from this that in suspensions of irreversible colloids (suspensoids) the change in the transference numbers of the ions may also take place in the case of a stable suspension of appreciable concentration. We may also regard the space between the particles as a system of pores, albeit a mobile system.

The suspension effect, which was discovered and studied first of all by Wiegner and Pallman [3], has attracted the attention of many workers, particularly in recent years [4-9]. The essential feature of this phenomenon is that the pH of a suspension is not in general the same as that of the ultrafiltrate or centrifugate separated from it. The difference in the pH values increases with increase in the concentration of the suspension, and the direction of this change depends on the sign of the charge on the particles of the solid phase. When the particles have a negative charge, the pH of the suspension is less than that of the ultrafiltrate; when the particles are positively charged the opposite is true. Although there are different points of view

regarding the nature of this phenomenon, the majority of authors explain the observed facts on the basis of a Donnan equilibrium, by which it is possible to explain satisfactorily the chief results of the measurements. Another point of view has been put forward in explanation of the cause of the suspension effect by Jenny, Nielsen, Coleman, and others [5]; they consider that the cause of the suspension effect is the high diffusion potential which arises in the measurement of the activity of ions (in particular, pH) at the boundary between the KCl salt bridge and and the suspension.

Overbeek [10] has made a comparison of the Donnan EMF and the suspension effect, and says that they are identical. He reaches the conclusion that the Donnan potential measured experimentally is made up of the difference in the potentials between the suspension and the solution, i.e., a membrane potential and two diffusion potentials, and that the classical equation for the Donnan EMF is incorrect, if the mobility of the counter ions is influenced by the suspended particles. This error is probably real in those cases where the particles have no appreciable charge. The aim of the present work was to examine the relationship between the change in the transference numbers of ions with liquid suspensoid diaphragms on the one hand and the quantity of disperse phase in the suspension and the degree of dispersion of its component particles on the other, and then to find the connection between the changes in the transference numbers of the ions and the observed magnitudes of the suspension effects. The materials chosen for study were bentonite from the Oglavlinskii deposit and quartz powder graded according to size by elutriation into a number of fractions. The results of the experiments on the measurement of the transference numbers of ions* in bentonite and quartz suspensions in 0.01 N KCl solutions are given in Fig. 1.

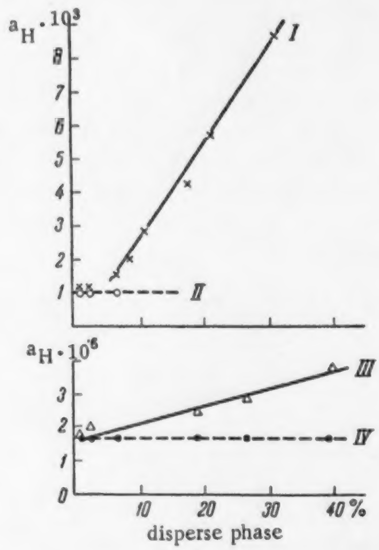

Fig. 3. The influence of the concentration of bentonite and quartz suspension on the magnitude of the suspension effect (a_H): I) for the bentonite suspension; II) for the bentonite centrifugate; III) for the quartz suspension (< 1 μ); IV) for the quartz centrifugate.

It can be seen from Fig. 1 that with increase in the concentration of the disperse phase the transference numbers of the Cl ion in the suspension is decreased, i.e., in other words, the transference number of the K^+ cations is increased, which is in accordance with the negative sign of the charge on these particles.

TABLE 1

Suspension Effect For Quartz Suspensions of Varying Particle Size

Disperse phase, %	pH of the suspensions	pH of the centrifugate
Particles smaller than 1 μ		
1,2	5,80	5,80
2,3	5,70	5,80
8,8	—	5,80
19,7	—	5,80
26,0	5,56	5,80
40,0	5,44	5,80
Particles 1-3 μ		
2,1	5,48	5,46
8,3	5,38	5,48
20,0	—	5,46
32,0	5,24	5,46
Particles 3-6 μ		
27,0	5,32	5,36
34,5	—	5,36
67,0	5,30	—
Particles 6-10 μ		
61,0	5,76	5,76

* The measurements of the transference numbers of the Cl ion were carried out analytically using a method which has been employed in a number of studies in the Leningrad State University Department of Colloid Chemistry [1], with an apparatus of slightly modified construction adapted for measuring the effect in liquid media.

Increase in the degree of dispersion of the particles also leads to a reduction in the transference numbers of the Cl ion. The bentonite suspension, with finer particles than the quartz fraction, but with a φ-potential of the same order as that of the quartz, gave a considerably larger transference number change.

In order to examine the influence of structure-formation in the suspension on the transference number change, the structural viscosity was measured, and the results of these measurements for bentonite are given in Fig. 2. The shape of the curves shows that in this case the structure is not a determining factor in the change of the Cl ion transference numbers, since otherwise the shape of the curves would be identical.

Figure 3 gives data from measurements of the H-ion activity a_H using a glass electrode in suspensions and centrifugates for bentonite and quartz (the fraction with particle size less than 1μ). For quartz and bentonite a linear relationship is observed between the increase in the H-ion activity of the suspension and the increase in the percentage of disperse phase, as has been observed earlier by other authors.

Data showing the influence of the concentration of the disperse phase and particle size on the suspension effect are given in Table 1.

It can be seen from the table that for the quartz fraction with particle diameter 3-6 μ, practically no suspension effect is observed, even at a disperse phase concentration of 67%, whereas for quartz with particle diameter $< 1\ \mu$ at a concentration of 40% the effect amounts to approximately 0.4 pH units.

The data presented thus show that fine suspensoid systems may change considerably the transference numbers of ions, and that this change, which increases with increase in the concentration, is directly related to the suspension effect.

LITERATURE CITED

[1] Coll. The Electrokinetic Properties of Capillary Systems* Izd. AN SSSR, (1956), p. 130.

[2] A. I. Iurzhenko, Bull. Mendeleev All-Union Chem. Soc. 8-9 (1951).

[3] G. Wiegner, Koll. Zs. 51, 49 (1930); H. Pallman, Kolloidchem. Beih. 30, 334 (1930).

[4] A. I. Rabinovich, P. S. Vasil'ev, and T. V. Gotovskaia, Proc. Acad. Sci. 3, 109 (1935).

[5] H. Jenny, Science 112, 164 (1950).

[6] C. E. Marshall, Science 113, 43 (1951).

[7] E. Eriksson, Science 113, 418 (1951).

[8] K. J. Mysels, Science 114, 424 (1951).

[9] C. E. Marshall, Science 115, 361 (1952).

[10] J. Th. G. Overbeek, J. Coll. Sci. 8, 6 (1953).

A. A. Zhdanov State University, Leningrad

Received November 18, 1957

* In Russian.

CONDUCTING A TOPOCHEMICAL DIFFUSION PROCESS AT A CONSTANT RATE

D. P. Dobychin

(Presented by Academician A. N. Terenin, November 23, 1957)

The chemical decomposition of solids, accompanied by the formation of a porous layer of solid products on their surface, is frequently retarded by diffusion of the reacting substances through this layer into the reaction zone. Among such processes can be included the oxidation of a number of metals, the burning of a high-ash fuel, the burning out of coke from aluminosilicate cracking catalysts, the leaching out of melts, the obtaining of porous glass by the action of acids on soda-borosilicate glass, and a number of others. In those cases, where the determining stage of the process is diffusion in a porous layer, the concentrations of reacting substances in bulk (solution, gas) and at the external surface of the porous layer manage to become equal and do not differ between themselves.

We will introduce the terms: D is the effective diffusion coefficient of a reactant in the porous layer of products; $\underline{h}$ is the thickness of the porous layer of products; $\underline{x}$ is the flow coordinate along the thickness of the porous layer ($0 < x < h$); dc/dx is the concentration gradient of the diffusing substance; dm/dt is the reaction rate; $\underline{t}$ is the time; M is the stoichiometric coefficient, equal to the amount of reactant consumed in the formation of 1 cm^3 of porous layer; $\underline{k}$ is the velocity constant of the chemical reaction; c_h is the effective concentration of reactant at the boundary porous layer— unreacted layer; and c_0 is the bulk concentration of reactant in the gas (or liquid) phase at the external boundary of the porous layer.

According to Fick's second law

$$\frac{dc}{dt} = D\frac{d^2c}{dx^2} \tag{1}$$

limiting conditions:

$$x = 0, \quad c_{0,t} = f(t); \tag{2}$$

$$x = h, \quad c_h \simeq 0. \tag{3}$$

Under the conditions of the established process the value of the diffusion stream of reactant through the porous layer toward the reaction zone is equal to the reaction rate:

$$-D\frac{dc}{dx} = \frac{dm}{dt} = M\frac{dh}{dt} = kf(c_h). \tag{4}$$

An exact solution of the problem for the case $c_{0,t}$ = const, given by L. A. Vulis [1], can in many cases be replaced by an approximate solution under the limiting conditions. A quasi-stationary process usually exists at $c_{0,t}$ = const

$$-\frac{dc}{dx} = \frac{c_{0,t} - c_{h,t}}{h} \simeq \frac{c_0}{h}. \tag{5}$$

A quasi-stationary condition means that although c_0/h decreases with increase in $\underline{h}$, the dc/dx gradient is practically constant at any given moment along the whole layer. Hence, considering (4) and (5),

$$-D\ \frac{dc}{dx} = C\ \frac{c_0}{h} = M\frac{dh}{dt}. \tag{6}$$

The so-called "quadratic" (or "parabolic") rule, discovered by Tammann [2], follows from (6)

$$h^2 = \frac{2c_0D}{M}\ t. \tag{7}$$

The rate of the process varies. As the thickness of the layer increases the concentration gradient decreases, and consequently so does the effective concentration, being the result of establishing a mobile equilibrium in the reaction zone at the boundary of unreacted solid. As a result, with a constant concentration of the reactant in bulk, its effective concentration in the reaction sphere during the process will fall and the chemical conditions for forming a porous layer of products will change. This situation, not attracting attention, appears in the schistose structure of porous glasses [3, 4], externally having an appearance reminiscent of Liesegang rings. Hence, the problem arises of how to assure a constancy of reactant concentration in the reaction zone during the process, which should automatically lead to its progressing at a constant rate, not changing as the porous layer grows. The problem consists in finding such an equation for expressing changes in the concentration of the reactant in bulk (gas or solution) as a function of time f(t) as will assure fulfillment of these conditions.

An exact solution is associated with a number of difficulties and its derivation seems impractical after the problem has been solved by the method of approximate solution and experimental verification.

We will now return to the approximate solution. According to the condition

$$\frac{dh}{dt} = A = \text{const}, \tag{8}$$

from which

$$h = A\ t. \tag{9}$$

Substituting (5), (8), and (9) in the limiting conditions (2) and (4), we find the sought function:

$$c_{0,\,t} = \frac{MA^2}{D}\ t = Bt. \tag{10}$$

Thus, the condition for a constancy of the rate of the process and of the effective concentration in the reaction zone is a linear increase in the bulk concentration of reactant during the process.

From (10) it can be seen that the rate at which the porous layer is formed ($A = dh/dt$) increases proportionally to the square root of the rate of increase in the bulk concentration (B) of the reactant. The obtained result is associated with the following basic assumptions: a quasi-stationary status of the process and a linear distribution of the reactant concentration in the porous layer, and also an independence of the porous structure of the layer of products and its thickness, or, more accurately, a practical constancy of the effective coefficient of diffusion through the thickness of the porous layer also during the time of the process. It should be especially emphasized that these same assumptions also lie at the base of the "parabolic" rule, compliance with which by a large number of processes is convincing proof that these conditions are actually fulfilled experimentally.

As follows from the "parabolic" rule, the time required to establish diffusion equilibrium and a quasi-stationary regime is a value of the order of h^2/D. The distance in which the concentration equalizes in a given length of time will have a value of the order of $\sqrt{Dt}$ and should be large in comparison to the distance $h = At$, through which the reactant should diffuse, from which

$$t < \frac{D}{A^2} = \frac{M}{B}. \tag{11}$$

On reaching this time, the found simple rule (10) should no longer be obeyed.

From (10) and (11) it follows that the maximum permissible bulk concentration ($C_{0,\,t} = Bt$) of reactant should be less than the mass stoichiometric coefficient M, the maximum permissible rate of increase in concentration B less than the quotient of M divided by the complete time of the process <u>t</u>, during which a porous

layer of thickness h manages to form on the solid, while the maximum thickness of the porous layer is

$$h = At = A\frac{c_{0,t}}{B} < \frac{AM}{B} = \frac{D}{A^2}. \tag{12}$$

A convenient subject for experimentally verifying the validity of the obtained results was the preparation of porous glass by the leaching of soda-borosilicate glass Na = 7/23 (composition in mole %: Na_2O 7, B_2O_3 23, SiO_2 70) in acid.

TABLE 1

<table>
<tr><th rowspan="2">Expt. No.</th><th rowspan="2">B $\frac{\text{equiv}}{\text{cm}^3\cdot\text{hr}}\cdot 10^4$</th><th rowspan="2">$t_{lin}$, hr</th><th rowspan="2">h_{lin}, cm</th><th rowspan="2">A_{lin}, cm/hr</th><th rowspan="2">D, cm^2/hr</th><th rowspan="2">$\sqrt{\frac{B_1}{B_2}}$</th><th rowspan="2">$\frac{A_{1\,lin}}{A_{2\,lin}}$</th><th colspan="2">$\frac{h_{2\,lin}}{h_{1\,lin}}$</th></tr>
<tr><th>exptl.</th><th>calc.</th></tr>
<tr><td>1</td><td>1,07</td><td>4—4,5</td><td>0,045—
—0,50</td><td>0,0112</td><td>0,0055</td><td rowspan="2">1,44</td><td rowspan="2">1,54</td><td rowspan="2">1,20–1,33</td><td rowspan="2">1,37</td></tr>
<tr><td>2</td><td>0,516</td><td>8,5</td><td>0,060</td><td>0,0074</td><td>0,0050</td></tr>
</table>

The values of D, needed for preparing the experiments, were calculated according to Equation (7) from the data of the experiments performed by O. S. Molchanova, Z. G. Slavianskii, and A. V. Kruglova on the kinetics of the growth of a porous layer on glass Na = 7/23 in its leaching in acid solutions of a constant concentration. For temperatures of 24 and 25° and sulfuric and hydrochloric acid solutions ranging from 0.1 to 3N the values of D varied from 0.00013 to 0.008 cm^2/hour. From the composition of the original glass and the porous glass we calculated $M = 4.71\cdot 10^{-3}$ equiv/cm^3/hr.

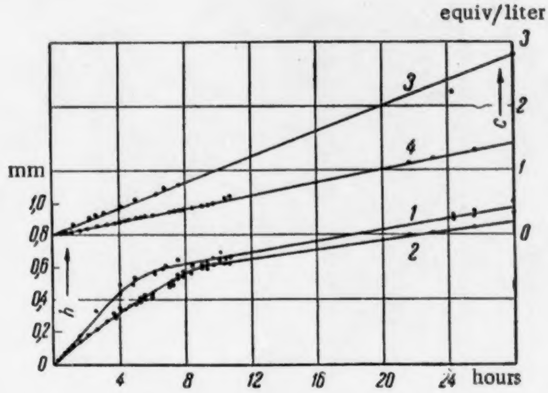

Fig. 1. Kinetics curves of the experiments progressing by a linear regime. 1) h(t), Expt. 1; 2) h(t), Expt. 2; 3) c_0(t), Expt. 1; 4) c_0(t), Expt. 2.

Starting with all of the obtained values of D (from 0.000038 to 0.114 cm^2/hr) and with the values of A (from 0.005 to 0.04 cm/hr) derived from the experimental data, we calculated with the aid of Equation (10) the necessary values of the rate of increase in the concentration of acid B (from 0.000012 to 0.70 equiv/cm^3·hour). Assigning different times for the length of experiment (from 5 to 72 hours), we determined that the limiting permissible values of B range from 0.000065 to 0.00094 equiv/cm^3·hr.

For the experiments at room temperature with sulfuric acid, on the assumption D = 0.001 - 0.005 cm^2/hr and A = 0.01 cm/hr., we obtain B = 0.000094 - 0.00047 equiv/cm^3·hr and h < 0.1 - 0.5 cm.

The experiments were run at room temperatures on polished specimens of glass Na = 7/23. A calibrated microscope was used to measure the thickness of the porous layer during the leaching process. A linear increase

in the acid concentration was achieved by the continuous dropwise addition of concentrated sulfuric acid from a pressure regulated graduated cylinder into various amounts of vigorously stirred distilled water. The results of two such experiments are given in Table 1. As can be seen from the kinetics curves for h (t) and c_0 (t) of the two experiments (see Fig. 1), for the first several hours the thickness of the porous layer actually does increase at a constant rate. Then the rate of the process, as was to be expected, decreases. It is interesting to mention that the first semitransparent layer ("stratum") appears at the moment the linear regime ceases and is linked to this decrease in the rate. In accordance with (10), the rate of leaching by a linear regime increases in direct proportion to the square root of the rate of increase in the concentration.

The experimentally observed ratio of the layer thicknesses, worked out in accordance with a linear regime (h_2 lin/h_1 lin = 1.20-1.33), is in quite good agreement with the value 1.37, calculated from the approximate ratio h_2 lin/h_1 lin $\approx$ A_2B_1/A_1B_2, deriving from Equation (12) with some simplification of the assumptions.

The author wishes to thank O. M. Todes for his valuable advice and criticism in writing this paper.

LITERATURE CITED

[1] L. A. Vulis, J. Tech. Phys. (USSR) 10, 1959 (1940).

[2] G. Tammann, Zs. anorg. u. allgem. Chem. 111, 78 (1920).

[3] I. V. Grebenshchikov and O. S. Molchanova, J. Gen. Chem. 12, 588 (1942).

[4] O. S. Molchanova, Dissertation (Leningrad, 1943).*

Received November 14, 1957.

* In Russian.

ADSORPTION OF SULFUR BY IRON FROM ACID HYDROGEN SULFIDE SOLUTIONS

Z. A. Iofa

(Presented by Academician A. N. Frumkin, December 12, 1957)

The study of the mechanism by which hydrogen sulfide promotes or inhibits the corrosion of iron in acid solutions in the presence of some organic compounds [1] leads us to consider the problem of measuring the amount of sulfur adsorbed by iron from these solutions.

The amount of adsorbed material was measured by using the method of radioactive isotopes. Iron sulfide was prepared from radioactive sulfur (S^{35}) and iron powder; it was then decomposed by H_2SO_4, and the resulting radioactive H_2S was transferred into a 0.1 N NaOH solution by a current of hydrogen. We thus obtained a 0.05 to 0.7 N Na_2S^* solution. Plates of chemically pure (Hilger) or Armco iron were degreased and placed for a given period of time into an $H_2SO_4 + Na_2S^*$ solution, then taken out, washed with distilled water and dried. The experiments showed that the corroding solution is completely removed after three minutes washing; the washing was continued for 5 minutes in all cases. The radioactivity of the plates was determined with an end-type radiation counter. The specific activity of the solution was measured by the number of impulses given off by the samples prepared in the following way: a small drop of the solution was placed on a silver or copper plate, weighed on a precision balance, diluted and dried on an electric hot plate. The irregularity factor of the surface of the plates was determined by comparing the number of impulses given off by a given plate and by a well polished plate after adsorption of sulfur under identical conditions; the irregularity factor in the case of the polished plate was taken as equal to 1.2.

TABLE 1

Adsorption From A 0.1 $H_2SO_4^+$ Solution

Conc. of Na_2S, in N	Duration of absorption, in min.	Γ (g-equiv/cm^2)$\cdot 10^{10}$
$1{,}5\cdot10^{-5}$	3	10
	15	32
	30	36
$1{,}5\cdot10^{-4}$	1	20
	3	36
	15	44
$1{,}5\cdot10^{-3}$	1	33
	5	43
	150	110

TABLE 2

Conc. in N			Duration of absorption (min)	Γ (g-equiv/cm^2)$\cdot10^{10}$
Na_2S	H_2SO_4	$N(C_4H_9)_4^+$		
$1{,}5\cdot10^{-5}$	0,1	none	15	40
$1{,}0\cdot10^{-3}$	1,0	$1{,}4\cdot10^{-3}$	1	32
			15	45
$1{,}5\cdot10^{-3}$	0,1	10^{-3}	5	43
	1,4		5	42
	6,0		5	38

Table 1 represents the average results (in gram-equivalents) obtained in the case of adsorption by 1 cm^2 of real surface of chemically pure iron at $t = 20°$ C. Analogous results were obtained for Armco iron.

The addition of the inhibitor $N(C_4H_9)_4^+$ does not change the amount of sulfur adsorbed (see Table 2).

The increase of the amount of adsorbed material with time in the case of acid solutions containing more than 10^{-4} N Na_2S and which do not contain inhibitors is apparently due to the increase of the total surface resulting from etching. Furthermore, after 6-10 minutes the surface of the plate becomes covered with protruding bubbles, whose number and size increase with etching time. In the presence of an inhibitor the plates remain smooth and brilliant and adsorption increases but little with time.

In the case of prolonged exposure of the plates, the measured increase of the adsorbed material with time can be due to the radiation coming from the sulfur which has penetrated into the body of the metal. This penetration was determined by measuring the radioactivity of the iron plates after adsorption from a 1 N H_2SO_4 + + $4.6 \cdot 10^{-4}$ N Na_2S* solution, removal of the surface layer with sandpaper (No. 000), and weighing on a precision balance. Penetration of SO_4^{2-}, and also I^- and Br^- into the plate was reported earlier by N. A. Balashova [3].

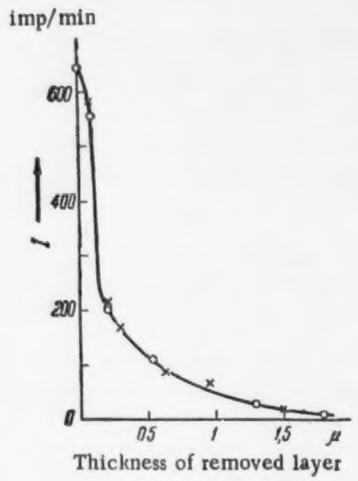

Figure 1 represents the variation of the activity of a plate with successive removal of metal layers; it shows that a certain amount of sulfur (about 10%) penetrates into the body of the metal to a depth greater than 1.5μ.* The adsorption of electrons released by S^{35}, by a layer of iron 1μ thick does not exceed 10-12% (determined from the adsorption curve corresponding to aluminum foil; we consider that the adsorption for 1 mg/cm² is the same for Al and Fe).

Table 3 shows that the solution rate of iron in sulfuric acid containing H_2S is practically unaltered by the addition of KI; however, the solution rate increases sharply when Na_2S is added to the mixture of H_2SO_4 + KI.

One can conclude that the adsorbed sulfur adheres to iron much more strongly than iodine and that iodine is displaced from the surface of the metal during the adsorption of sulfur, since the inhibiting effect of KI disappears almost completely when Na_2S is added to the solution (Table 3, lines 3 and 4), while the addition of KI to the H_2SO_4 + Na_2S solution has almost no effect on the amount of sulfur adsorbed (Table 4).

TABLE 3

Solution Rate of Iron in 1 N $H_2SO_4^+$

Conc. in N			Solution rate in g/cm².hr
Na_2S	KI	$N(C_4H_9)_4^+$	
none	none	none	$4 \cdot 10^{-4}$
0,001	none	none	$9 \cdot 10^{-4}$
0,001	0,001	none	$7,8 \cdot 10^{-4}$
none	0,001	none	$2,2 \cdot 10^{-5}$
0,001	0,001	0,001	$7,2 \cdot 10^{-6}$
0,001	none	0,001	$1,2 \cdot 10^{-5}$

The strong inhibitive action of $N(C_4H_9)_4^+$ ions in the solution containing Na_2S and KI as compared to that in the acid solution containing only Na_2S (Table 3, lines 5 and 6) indicates the presence of a considerable amount of iodine on the surface [1, 2]. In fact, measurements of the amount of iodine ions adsorbed by iron from the solution containing H_2SO_4 + KI, using KI^{131} as a tracer, show that in the presence of Na_2S the adsorption of iodine decreases only by 20-25%.

Experimentally obtained polarization curves showed that the addition of Na_2S to an H_2SO_4 solution decreases the hydrogen overpotential. However, the addition of an organic inhibitor (for example, tetrabutylammonium sulfate) to a solution containing Na_2S considerably increases the value of the overpotential.

It must be noted that the addition of the inhibitor to the H_2SO_4 + H_2S solution prevents hydrogen embrittlement of iron during etching. Thus, for example, a steel wire 0.2 mm in diameter undergoing cathodic polarization in a 1 N H_2SO_4 + 10^{-3} N Na_2S solution (with a current density of 0.01 amp/cm²) under a load of one kilogram, breaks after 2-3 minutes, while it takes 4-5 hours before breaking occurs when 10^{-3} mole/liter of tetrabutylammonium sulfate is added to the solution. In pure 1.0 N H_2SO_4 the wire does not break even after 4-5 hours of exposure.

TABLE 4

Composition of the solution, in N				Duration of absorption, in min	Γ (g-equiv/cm² · 10^{10})
H_2SO_4	Na_2S	KI	$N(C_4H_9)_4^+$		
1,0	$1,2 \cdot 10^{-3}$	none	none	5	44
0,1	$1,2 \cdot 10^{-3}$	$0,5 \cdot 10^{-3}$	none	5	42
1,0	10^{-3}	$0,5 \cdot 10^{-3}$	$1,4 \cdot 10^{-3}$	20	46
1,0	10^{-3}	none	10^{-3}	20	45

*

* The small initial retardation in the fall of radioactivity corresponding to the removal of very thin layers of metal is apparently due to the fact that the grains of abrasive on the sandpaper is of the order of 0.2-0.3 μ.

Adsorption of sulfur by iron is an irreversible process. This can be seen from the fact that even after prolonged washing the plate retains almost all of the adsorbed sulfur. Washing of the plate with 1 N H_2SO_4 for 10 minutes reduces the amount of adsorbed material only from $35 \cdot 10^{-10}$ to $27 \cdot 10^{-10}$ g-equiv/cm^2.

The average amount of sulfur adsorbed during 5 minutes from a 1 N H_2SO_4 + 0.001 N Na_2S solution is equal to $42 \cdot 10^{-10}$ g-equiv/cm^2 or $21 \cdot 10^{-10}$ g-atom sulfur per one cm^2. This amount is slightly lower than that necessary for the formation of a two-atom layer of S^{2-} ions ($r = 1.84$ A, $\Gamma = 12.3 \cdot 10^{-10}$ g-equiv/cm^2 for a single layer). These values correspond to the binding of slightly less than one atom of sulfur with one atom of iron (for $\alpha-Fe$, $r = 1.238$ A on the surface of $27 \cdot 10^{-10}$ g-atom/cm^2). However, it is impossible to determine exactly the amount of sulfur adsorbed because some of the sulfur penetrates into the body of the metal.

Comparison of these data with those concerning the amount of iodine adsorbed by iron [4] shows, however, that sulfur covers a considerably greater part of the iron surface than iodine.

The stimulating effect of hydrogen sulfide on the solution rate of iron in acids, controlled essentially by the anodic process [5], is apparently due to the weakening of the interatomic bonds between iron atoms (which renders their ionization easier) as the result of the formation of a strong bond between the iron and the sulfur atoms.*

It is also necessary to explain the disappearance of the stimulating action of hydrogen sulfide in the presence of some inhibitors, and the increased inhibiting action of the inhibitors on corrosion in the presence of H_2S as compared with the effect of the same inhibitors in the absence of H_2S. Experiments showed that for a given concentration of the inhibitor in the solution there exists an optimum concentration of H_2S for a maximum inhibiting effect. The concentration of H_2S can be increased up to 10^{-2} N without reducing the inhibitive effect on corrosion when the concentration of the inhibitor (for example tribenzylamine) is increased.

It must be noted that H_2S considerably increases the inhibitive action only in the case of such organic compounds as organic acids and alcohols (for example, caproic acid or hexylalcohol), while the stimulating action of H_2S is increased by sulfoacids.

These facts allow us to assume that the cations of inhibitors form (by electrostatic forces) strongly bonded pairs, with the formation of dipoles $Fe \overline{-} S$ on the iron surface. The number of these pairs per unit surface is determined by the concentration of the inhibitor in the solution. When the concentration of the inhibitor is sufficient, the stimulating effect of H_2S is preserved. This assumption is confirmed by the previously stated fact that hydrogen overpotential is increased in acid solutions when H_2S and the inhibitor are present simultaneously, and as a result the corrosion rate of iron is reduced. It is probable that the surface concentration of the adsorbed atoms of hydrogen $[H]_s$ is decreased, an assumption borne out by the fact that the hydrogen embrittlement is decreased in the $H_2SO_4 + H_2S$ solution (if i = const) when an organic base is added to it. The decrease of embrittlement due to the decrease of the diffusion rate of atomic hydrogen into the metal is promoted because the cathodic potential becomes higher with the addition of the inhibitor and the increase of the rate of removal of hydrogen (according to the electrochemical mechanism), in the same way as in the case of the simultaneous action of halogen ions and organic compounds in the presence of As_2O_3 [7].

LITERATURE CITED

[1] Z. A. Iofa, Bulletin of the Moscow State University, 2, 139 (1956).

[2] Z. A. Iofa, E. I. Liakhovtskaia, and K. Sharifov, Proc. Acad. Sci. USSR 84, 543 (1952).

[3] N. A. Balashova Proc. Acad. Sci. USSR 103, 639 (1955).

[4] Z. A. Iofa and G. B. Rozhdestvenskaia, Proc. Acad. Sci. USSR 91, 1159 (1953).

[5] V. A. Kuznetzov, and Z. A. Iofa, J. Phys. Chem. USSR 21, 201 (1947).

* A somewhat different mechanism of the stimulating action of hydrogen sulfide was proposed by Makrides and Hackerman [6].

[6] A. Makrides and N. Hackerman, Ind. and Eng. Chem. 47, 1773 (1955).

[7] Z. A. Iofa and E. I. Liakhovetskaia, Proc. Acad. Sci. USSR 86, 577 (1952).

M. V. Lomonosov
Moscow State University

Received December 6, 1957

DIFFUSION IN CRITICAL REGION OF TERNARY SOLUTIONS

I. R. Krichevskii, N. E. Khazanova, and L. R. Linshits

(Presented by Academician A. N. Frumkin, December 24, 1957)

The diffusion rate in solutions is determined by the gradients of the chemical potentials [1]. At the critical point of a binary solution the derivative of the chemical potential of a component with respect to the composition is equal to zero [2]. Consequently, at the critical point of a binary solution the gradient of the chemical potential of a component is equal to zero at a concentration gradient of the component different from zero.

That diffusion ceases near the critical region of a binary solution, first predicted by D. P. Konovalov, has found experimental confirmation only recently [3, 4]. The fact that diffusion ceases almost completely in the critical region is of extreme theoretical interest, and it also assumes great importance in practice since it places special emphasis on the kinetics of the processes taking place in this region [4].

At the critical point of a ternary solution none of the derivatives of the chemical potentials of the components with respect to composition, in contrast to binary systems, is converted to zero [2]. Consequently, in the general case, the diffusion rate of the components of a ternary solution near the critical point will not fall to a very small value. However, if the solution is dilute in the third component, then the theory of binary systems can be applied with a closer degree of approximation to the main components. Then, in such systems the diffusion rate of the two main components near the critical point remains close to zero, since the derivatives of the chemical potentials of the components with respect to the composition will differ very little from zero at the critical point (they will be smaller the smaller the amount of third component). The derivative of the chemical potential of the third component will be different from zero, and its diffusion should proceed at a finite rate.

The utilization of such a phenomenon should permit enrichment with a third component (or purification from a third component) if the component in question could be made to diffuse across a boundary at a relatively much faster rate than would hold for the main components. The utilization of such a phenomenon would also permit carrying out selective heterogenous chemical reactions, which would proceed by the chemical kinetics valid for the third component, whereas for the two main components these reactions can proceed only by diffusion or by a mixed kinetics [4]. Consequently, an investigation of the diffusion rate of the components in the critical region of such ternary mixtures is of great interest.

The objective in the present investigation was limited to solving the main problem, namely, to clearly determine whether as the result of molecular diffusion in the critical region there is substantial enrichment of the solution in the third component, functioning as a small addition to the binary system.

For a number of reasons the system triethylamine – water with the addition of a small amount of butylamine was selected as a good example for studying diffusion in ternary solutions. We used the capillary method in making the study. For our work we used a capillary with a diameter of about 2 mm and a length of about 40 mm. The experiments were run for periods ranging from 50 to 90 hours. The temperature of the thermostat was controlled with an accuracy of $\pm$ 0.05°. The experimental technique used was the same as that employed to study diffusion in the critical region of two-component systems [3, 4].

The minimum amount of butylamine added was limited by the accuracy of the analysis method (Van Slyke) used. The construction of the apparatus and the method of analysis, both worked out specially for the present

case,* made it possible to determine as little as 1 mg of butylamine in approximately 10 ml of liquid with an accuracy of 3-5 weight percent.

TABLE 1

Diffusion Coefficient of Butylamine in Ternary Mixture at 18°

Conc. in the capillary, g/cm^3 initial	final	Duration of experiment, hrs	D($\times 10^{-5} cm^2/sec$)
Concentration of triethylamine in beaker 36.3, and in capillary 17.6 wt. %			
0,0115	0,0140	45,25	0,17
0,0114	0,0130	45,9	0,14
0,0114	0,0130	45,9	0,14
0,0114	0,0137	69,9	0,19
0,0114	0,0127	69,9	0,06
0,0108	0,0130	95,3	0,12
0,0108	0,0136	71,4	0,25
0,0108	0,0131	71,4	0,17
		Average. . .	0,16±0,01
Concentration of triethylamine in beaker 19.3 wt. %, and in capillary 0.0			
0,0000	0,0055	65,5	0,50
0,0000	0,0037	65,5	0,23
0,0000	0,00405	69,1	0,41
0,0000	0,00343	69,1	0,29
		Average. . .	0,35±0,04

In our investigation of diffusion in a three-component mixture we always used solutions in which a constant ratio of butylamine to triethylamine was maintained (~ 1:14). We also always used a constant temperature of 18° (the critical temperature of the investigated ternary mixture is 21.8°).

To obtain clearer results (limited by the sensitivity of the analysis method for butylamine) we selected a large concentration gradient of the diffusing component for investigation. The difference in the concentrations of the original solutions in the beaker and in the capillary were of the order of 0.2 g/cm^3 for triethylamine and of the order of 0.013 g/cm^3 for butylamine.

TABLE 2

Diffusion Coefficient of Triethylamine in Ternary Mixture at 18°

Conc. in the capillary g/cm^3 initial	final	Duration of experiment, hours	D($\times 10^{-7} cm^2/sec$)
Concentration of triethylamine in beaker 36.3 wt. %			
0,157	0,166	45,25	2,3
0,157	0,164	45,25	1,4
0,169	0,180	45,9	5,2
0,169	0,182	45,9	3,7
0,169	0,184	69,9	4,7
0,158	0,178	95,3	5,3
0,158	0,169	71,4	2,2
0,158	0,169	71,4	2,2
		Average . .	3,4±0,4
Concentration of triethylamine in beaker 19.3 wt, %			
0,000	0,0302	65,5	15,9
0,000	0,0326	65,5	18,4
0,000	0,0370	69,1	18,6
0,000	0,0379	69,1	19,7
		Average . . .	18,1±0,5

* The analysis method will be described in a separate communication.

From the data presented in Tables 1 and 2 it can be seen that the diffusion coefficient of butylamine is of the same order in the critical region and in dilute solutions. The somewhat higher values of D for butylamine in dilute solutions is explained by the lower viscosity of the latter when compared with concentrated solutions. As a result, the diffusion rate of butylamine, present as a small addition to the binary mixture triethylamine—water, does not stop in the critical region, which is different from triethylamine (Table 2), the diffusion rate of which is sharply lowered in this region. In dilute solutions the diffusion coefficient of triethylamine is of the same order as the diffusion coefficient of butylamine. It is interesting to note that the values of D for triethylamine in dilute solutions, both for three-component and for binary solutions [4], lie close to each other.

In accord with theoretical considerations the system became richer in butylamine. The ratio of butylamine to triethylamine in the diffusion stream was approximately 1:6, whereas in the original solution is was 1:14.

As a result, the first investigation made of the diffusion rate in the critical region of three-component solutions revealed, in agreement with theory, that it is possible to enrich the solution in the third component as the result of the molecular diffusion of the latter.

LITERATURE CITED

[1] L. Onsager and R. M. Fuoss, J. Phys. Chem. 36, 2689 (1932).

[2] J. W. Gibbs, Thermodynamic Studies [Russian Translation] (Moscow-Leningrad, 1950).

[3] I. R. Krichevskii, N. E. Khazanova, and L. R. Linshits, Proc. Acad. Sci. USSR 99, 113 (1954).

[4] I. R. Krichevskii and Iu. V. Tsekhanskaia, J. Phys. Chem. (USSR) 30, 2315 (1956).

State Scientific and Planning Institute
of the Nitrogen Industry

Received December 21, 1957

METASTABLE STATE DIAGRAM OF THE IRON — CHROMIUM SYSTEM

A. G. Lesnik

(Presented by Academician G. V. Kurdiumov, December 7, 1957)

This article describes a quantitative study of the energy of interatomic reaction in alloys of the iron-chromium system; the study was based on the data previously obtained [1] and on the results of experiments devised especially for the determination of curves representing the alpha-gamma phase equilibrium in this system.

According to our previous work when the distribution of atoms on the faces of the lattices has a random character the alpha and gamma equilibrium curves are described by the following equations:

$$RT\ln\frac{C_{A\alpha}}{C_{A\gamma}} = \Delta G_A + \frac{z_\alpha\varepsilon_\alpha}{2}C^2_{B\alpha} - \frac{z_\gamma\varepsilon_\gamma}{2}C^2_{B\gamma};$$

$$RT\ln\frac{C_{B\alpha}}{C_{B\gamma}} = \Delta G_B + \frac{z_\alpha\varepsilon_\alpha}{2}C^2_{A\alpha} - \frac{z_\gamma\varepsilon_\gamma}{2}C^2_{A\gamma}; \qquad (1)$$

Here $C_{A\alpha}$, $C_{B\alpha}$, $C_{A\gamma}$, and $C_{B\gamma}$, represent, correspondingly, the concentration of A (iron) and B (chromium) atoms in the α and γ phases; z_α and z_γ are the lattice coordination numbers of the α and the γ phases; $\varepsilon_\alpha = \varepsilon^\alpha_{AA} + \varepsilon^\alpha_{BB} - 2\varepsilon^\alpha_{AB}$ & $\varepsilon_\gamma = \varepsilon^\gamma_{AA} + \varepsilon^\gamma_{BB} - 2\varepsilon^\gamma_{AB}$ are the parameters characterizing the interatomic reaction in the alpha and the gamma phases; the magnitude $\Delta G_A = G^\gamma_A - G^\alpha_A$ represents the difference between the free energies of the α and the γ phases in pure iron; ΔG_B is the theoretical parameter, depending only on the temperature.

In our previous work we have shown that these equations (1) allow us to explain the presence of a minimum on the equilibrium curves of the α and γ phases of certain systems; in particular, in the case of the Fe—Cr system, these Equations (1) were compared to the averaged experimental results obtained by various authors. It became apparent then that it is possible to determine the difference $\frac{z_\gamma\epsilon_\gamma}{2} - \frac{z_\alpha\epsilon_\alpha}{2}$ and also the parameter ΔG_β, which was found to increase linearly with temperature within the whole existing region of the loop. The values $\frac{z_\gamma\epsilon_\gamma}{2}$ and γ $\frac{z_\alpha\epsilon_\alpha}{2}$ were not determined separately because in order to obtain reliable results one needs more precise data on the position of the loop than those available in the literature.

In the literature one finds data for technically pure alloys; furthermore these data are calculated without taking into account the possible effect of high-temperature treatment of the alloys, prior to the experiment, on the position of the equilibrium curves. We have shown that a "homogenizing" treatment of alloys may considerably displace the equilibrium curves; this is apparently due to the creation of close order in phases submitted to prolonged heating.

In order to calculate ϵ_γ and ϵ_α by these equations (1) we have performed new experiments allowing us to determine the position of the equilibrium curves of alpha and gamma phases in the iron— chromium system.*

* The experiments were performed in collaboration with G. B. Khar'kova.

The materials used for the experiment were the following: electrolytic chromium, refined in a stream of hydrogen (it contained 0.003% O_2, 0.0266% N_2, 0.03% Si) and electrolytic iron (in the form of little scales) originally containing 0.02% C, 0.0009% Mn, 0.017% Si, 0.003% P; it was degassed in high vacuum at 1400-1500° C for 13 hours, melted and maintained in the molten state for about 2 hours. After this treatment only traces of carbon (< 0.003%) remained in iron. The $\alpha \rightarrow \gamma$ transformation temperature of the alloys was determined by the sharp break in the curves representing the variation of the electrical resistance as the function of temperature. Figure 1 represents the curves obtained for the beginning and the end of the $\alpha \rightarrow \gamma$ transformation for the alloys investigated. It must be noted that the end of the transformation was registered with a certain delay; this is seen from the fact that the curves representing the beginning and the end of the transformation do not touch each other at the minimum point. Therefore, to determine the magnitudes we were interested in, we used only the data relative to the beginning of the transformation. It must be noted that our data are relative to alloys which were not submitted to prolonged high-temperature treatment, i.e., in our experiments we maintained conditions ensuring random distribution of atoms on the lattice faces [2].

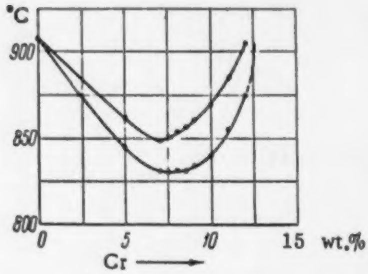

Fig. 1. Curves of the beginning and end of the transformations (during heating) of the Fe–Cr system.

For the comparison of Equation (1) with the experimental data we used values taken from a previous work [3] for ΔG_A.

Since ΔG_A and ΔG_B are independent of the composition of the alloy we found (graphically) by applying Equations (1) that this equation is valid only when $\frac{z_\gamma \epsilon_\gamma}{2} - \frac{z_\alpha \epsilon_\alpha}{2} = 2570$ cal/g-atom. Furthermore, at the minimum point ($C_{B_\alpha} = C_{B_\gamma}$) the following conditions must be fulfilled:

$$\Delta G_A(T_{min}) = \left(\frac{z_\gamma \varepsilon_\gamma}{2} - \frac{z_\alpha \varepsilon_\alpha}{2}\right) C^2_{min}$$

$$\Delta G_B(T_{min}) = \left(\frac{z_\gamma \varepsilon_\gamma}{2} - \frac{z_\alpha \varepsilon_\alpha}{2}\right)(1 - C_{min})^2. \qquad (2)$$

According to our data $T_{min} = 830$ °C; according to the data of a previous work [3], ΔG_A (830° C) = 19 cal/g-atom; thus, using Equation (2) we obtained $C_{min} = 8.6$ atom percent (or about 8% by weight), ΔG_B (830° C) = = 2147 cal/g-atom. It would be simpler to operate in reverse: take the value of C_{min} from the experimental curve of the beginning of the transformation and determine the difference $\frac{z_\gamma \epsilon_\gamma}{2} - \frac{z_\alpha \epsilon_\alpha}{2}$ from Equation (2). In this way, however, a considerable error could be introduced in the determination of $\frac{z_\gamma \epsilon_\gamma}{2} - \frac{z_\alpha \epsilon_\alpha}{2}$ since the position of the minimum on the curve (Fig. 1) cannot be determined with sufficient precision. Furthermore, Equations (1) are used for the determination of $\frac{z_\gamma \epsilon_\gamma}{2}$ and $\frac{z_\alpha \epsilon_\alpha}{2}$ separately. For this it would suffice to use data relative to some other temperature, 840° C, for example. According to Shmit [3], ΔG_A (840° C) = = 16 cal/g-atom; according to our data the straight line T = 840° C intersects the curve of the beginning of the transformation at two points: $C'_{B\alpha} = 10.67$ atom percent and gives $C''_{B\alpha} = 5.88$ atom percent. Under these conditions the graphic solution of Equations (1) gives us:

$$\frac{z_\alpha \varepsilon_\alpha}{2} = -3530 \text{ cal/g-atom}$$

$$\frac{z_\gamma \varepsilon_\gamma}{2} = -960 \text{ cal/g-atom} \qquad (3)$$

and ΔG_B (840° C) becomes equal to 2165 cal/g-atom, i.e., it increases with temperature as was previously shown [1].

The negative sign of ϵ_{α} and ϵ_{γ} indicates that both phases belong to Becker type disintegrating solid solutions. In reality however, we should observe only the decomposition of the α phase, since the γ phase exists only within a very limited region of concentrations. The theoretical curve of the decomposition of the solid solution of the γ phase, drawn according to the equation published elsewhere [4] and using Relationship (3), is represented in Fig. 2.

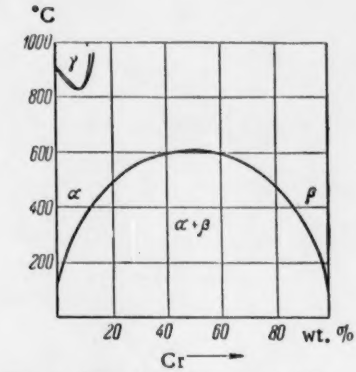

Fig. 2. Diagram of a metastable Fe– Cr system.

The results obtained allow us to understand the nature of the so-called 475° C-fragility – a well known phenomenon – only recently investigated in detail [5]; in this work it was proven by direct experiments that the 475° C-fragility is due to the decomposition of the initial solid solution (Fig. 2).

The diagram drawn on Fig. 2 represents a very stable metastable state. In fact, as we have seen before, the conditions of the experiment eliminated the possibility of close ordering in alloys, necessary for the formation of a metal compound (σ-phase) during equilibrium decomposition.

The negative values of $\epsilon = \epsilon_{AA} + \epsilon_{BB} - 2\epsilon_{AB}$ (positive displacement energy $-\frac{1}{2} C_A C_B z\epsilon$) show that the absolute value of the reaction energy of atoms of the same kind is greater than the reaction energy of a pair of atoms of different kinds. In the case of equilibrium, close order must be created in this type of solid solution so that atoms of different kinds repel each other and each atom tends to surround itself with atoms of the same kind. Yet chromium ferrite is decomposed under equilibrium conditions with the formation of a metallic compound; one could therefore expect close order in the original solid solution and the tendency of each atom to surround itself with an atom of a different kind.

The described contradiction indicates that in the case of the Fe–Cr system the interatomic reaction cannot be completely described by the value of ϵ we have determined. During close ordering in the alloy, there must appear some additional forces in the form of an additional energy carrying a negative sign, which fully compensates the positive displacement energy of the alloy in the random state, $-\frac{1}{2} C_A C_B z\epsilon_{\alpha}$, so that it becomes thermodynamically advantageous for the atoms to surround themselves with atoms of a different kind.

According to our previous work such a possibility occurs in systems in which there exists, outside the ordinary metallic bond, an additional interatomic bond, ionic in character, which results from the redistribution of the electronic charges between atoms of different kinds in the alloy.

LITERATURE CITED

[1] V. N. Svechnikov and A. G. Lesnik, Physics of Metals and Metallography 3,1,87 (1956).

[2] A. G. Lesnik, Series of Scientific Reports, Laboratory of Physics of Metals (Acad. Sci. USSR Press, 1954), p. 118.*

[3] M. Kohen, Phase Transformation in Solids (1951), p. 588.

[4] Ya. S. Umanskii et al., Physical Basis of the Study of Metals (Moscow, 1955), p. 131.*

[5] R. O. Williams and H. W. Paxton, J. Iron and Steel Inst. 185, Part 3, 358 (1957).

Institute for Physics of Metals of the
Academy of Sciences of the USSR

Received December 2, 1957

* In Russian.

INVESTIGATION OF THE COPOLYMERIZATION OF ISOPRENE AND DIVINYL BY BUTYLLITHIUM

G. V. Rakova and A. A. Korotkov

(Presented by Academician A. V. Topchiev December 16, 1957)

Up to now catalytic copolymerization with basic catalysts has hardly been studied. Only a few papers have been published which give quantitative data [1-5]. Judging by the values of the copolymerization constants, monomers differ very considerably in their reactivities. Monomers in which the double bond of the vinyl group is conjugated with the multiple bond of a nitrile or a carboxyl group have the greatest activity. The copolymerization of diene hydrocarbons under the action of basic catalysts has not been investigated as yet. It is known that in free radical (emulsion) polymerization these hydrocarbons have relatively similar activities [6].

It seemed interesting to establish the relative reactivity of the diethylene hydrocarbons, isoprene and divinyl, which differ by only a methyl group, in alkali-catalyzed copolymerization. Labeled atoms were used for determining the composition of the copolymers. For this we synthesized isoprene containing radioactive carbon, C^{14} (from acetylene-C^{14}, prepared from $BaC^{14}O_3$) by a modification of Favorskii's method [7].

Copolymerization and separate polymerizations of isoprene and divinyl were carried out in hexane solution with butyllithium at 50°, with a total monomer concentration of 2 moles/liter and a catalyst concentration of 0.0025 mole/liter. Butyllithium was synthesized by the known method [8]. The butyllithium solution was analyzed by the usual method with a double titration [8].

Thoroughly purified and dried monomers and solvent were used for the polymerization. All operations of measuring out the products into the reaction ampules were carried out in a current of dry nitrogen and in vacuum with a distributing comb (T. N. Presumably an apparatus similar to a vacuum fractionation "pig."). The reaction ampules consisted of two sections, separated by a wall and connected with a graduated tube. The solvent and monomers were placed in one section and the catalyst, a solution of butyllithium in hexane, in the other.

The wall in the ampule was broken with a glass plunger and the contents of the ampule mixed together rapidly. Polymerization was performed in a water thermostat at 50°. The polymerization rate was determined from the decrease in volume of the reaction solution.

The polymerization was stopped at different degrees of reaction by cooling the reaction ampule rapidly, then opening it and adding a small amount of ethyl alcohol (2 ml) to decompose the catalyst. The unreacted monomers and solvent were distilled from the ampule and the degree of reaction was determined by the weight of the polymer, dried at 60-80° (p = 2 mm Hg).

The copolymer compositions were determined by the radioactivity of the samples: as the standard we used polyisoprene-C^{14}, whose relative activity was expressed as the number of standard units in a sample of $BaC^{14}O_3$. The polymer samples were collected in small brass vessels (2 cm in diameter and 0.5 cm high), whose geometric position was fixed under the window of an end-window counter. The experimental results are given in Table 1. The data obtained made it possible to calculate the copolymerization constants by the exact Mayo-Lewis integral Equation [9], $\alpha = 0.47 \pm 0.03$ (for isoprene) and $\beta = 3.38 \pm 0.14$ (for divinyl). Figures 1 and 2 give the curves calculated for the copolymer compositions and also the experimental points.

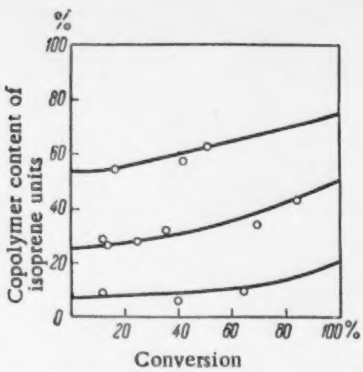

Fig. 1. Calculated integral curves of the isoprene–divinyl system ($\alpha = 0.47$; $\beta = 3.38$).

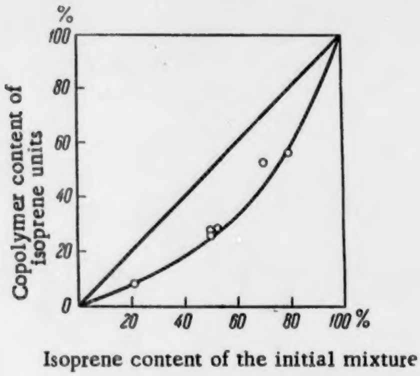

Fig. 2. Copolymerization curve of the isoprene–divinyl system.

TABLE 1

The Relation of Copolymer Compositions to the Composition of the Initial Mixture and the Degree of Reaction

Composition initial mixture (mole %)		Copolymer comp. by radio-activity (mole %)		Reaction degree (%)	Composition initial mixture (mole %)		Copolymer comp. by radio-activity (mole %)		Reaction degree (%)
iso-prene	divinyl	iso-prene	divinyl		iso-prene	divinyl	iso-prene	divinyl	
51,1	48,9	43,7	56,3	84,6	20,7	79,3	6,6	93,4	40,2
49,0	51,0	27,0	73,0	14,5	19,8	80,2	9,5	90,5	64,5
48,7	51,3	28,3	71,7	25,2	20,9	79,1	8,0	92,0	11,9
52,2	47,8	28,7	71,3	12,4	78,9	21,1	57,5	42,5	42,3
51,1	48,8	31,9	68,1	35,4	69,7	30,3	54,4	45,6	16,8
49,0	51,0	34,5	65,5	69,5	78,0	22,0	63,0	37,0	50,8

With the given initial monomer ratios, the copolymer compositions were calculated graphically by the known integral equation for copolymerization

$$\beta = \frac{\log\frac{B_0}{B} - \frac{1}{p}\log\dfrac{1 - p\frac{A}{B}}{1 - p\frac{A_0}{B_0}}}{\log\frac{A_0}{A} + \log\dfrac{1 - p\frac{A}{B}}{1 - p\frac{A_0}{B_0}}}, \tag{1}$$

where $p = \dfrac{1-\alpha}{1-\beta}$, may be expressed as:

$$\log\frac{B_0}{B_0} = \frac{\alpha\beta - 1}{(\beta - 1)(\alpha - 1)}\log\frac{\frac{A}{B} - \frac{1}{p}}{\frac{A_0}{B_0} - \frac{1}{p}} - \frac{\beta}{\beta - 1}\log\frac{\frac{A}{B}}{\frac{A_0}{B_0}}. \tag{2}$$

If the following criterion is introduced

$$\frac{A}{A_0} = x;\ \frac{B}{B_0} = y;\ \frac{\alpha\beta - 1}{(\beta - 1)(\alpha - 1)} = k_1;\ \frac{\beta}{\beta - 1} = k_2;\ \frac{B_0}{A_0}\cdot\frac{1}{p} = k_3;\ k_4 = k_1 \ln\,(1 - k_3,).$$

where A_0 and B_0 are the monomer concentrations at the initial moment and A and B are the monomer concentrations at the moment of terminating polymerization, then Equation (2) will appear as:

$$\log y + k_1 = k_1 \log\left(\frac{x}{y} - k_3\right) - k_2 \log\frac{x}{y} \quad (3)$$

A graphic resolution of Equation (3) makes it possible to determine the magnitude $z = \frac{x}{y}$ for various values of $\underline{y}$, i.e., to determine the required values A and B.

The experimental points lie quite well on the calculated curves, when one considers the permissible errors in measuring the monomers volumetrically.

Figure 3 gives the kinetic curves for the separate polymerization of isoprene and divinyl and the copolymerization at a monomer ratio of 1:1.

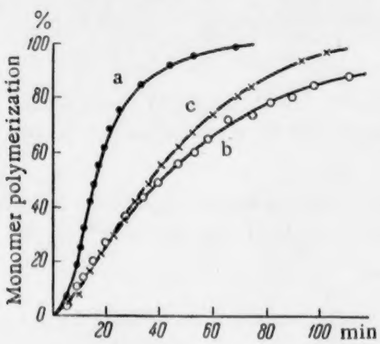

Fig. 3. Kinetic polymerization curves C_{mon} = 2 moles/liter; C_{cat} = = 0.0025 mole/liter. a) Isoprene, b) divinyl, c) isoprene–divinyl (1:1).

It follows from the experimental data given that:

1. Divinyl is the more active monomer in copolymerization ($\beta > 1$; $\alpha < 1$).

2. In separate polymerization, isoprene is more active as it polymerizes at a rate approximately 3 times greater than divinyl.

3. In copolymerization, the rate of the reaction in the first stage corresponds to the rate of separate divinyl polymerization.

An analogous phenomenon was observed in the copolymerization of styrene with divinyl under the effect of butyllithium [5]. In separate polymerization, styrene was polymerized many times more rapidly than divinyl. In copolymerization, first divinyl was polymerized at the rate of its separate polymerization and, after it was practically all exhausted, styrene started polymerizing, also at the rate of its separate polymerization.

The higher reactivity of isoprene in comparison with that of divinyl in separate polymerization is due, apparently, to the presence of a constant dipole moment in an isoprene molecule caused by the positive induction effect of the methyl group.

The phenomenon of the "inversion" of the monomer's activity in copolymerization cannot be explained on the basis of the ideas on the step mechanism of polymerization [10]. Regardless of the end unit in the growing polymer chain:

$$\sim CH_2-CH=CH-CH_2Li \quad \text{or} \quad \sim CH_2-CH=\underset{\displaystyle CH_3}{\underset{|}{C}}-CH_2Li$$

the probability of addition of each monomer molecule must be controlled by the activity of the monomer and its concentration in the solution. Thus, in our case the copolymer must be enriched in isoprene.

In order to explain the phenomenon of the "inversion" of the monomer's activity, the course of the reaction may be expressed as follows. In catalytic polymerization the active center is a dipole which reacts with the surrounding medium; if the rate at which the monomer reacts with the dipole, which could also be a metallo-organic compound, is relatively low, then the dipole would be surrounded by an envelope of polarized monomer molecules. The copolymer composition and the polymerization rate would be determined by the monomer concentration in this envelope. In the copolymerization of isoprene with divinyl, due to the relatively greater lability of the electron cloud and smaller steric hindrances of divinyl molecules, the monomer envelope would apparently consist mainly of divinyl molecules. Therefore, the total rate corresponds to the separate polymerization

rate of divinyl and the copolymer composition is enriched in the latter. As in radical polymerization the active center has no charge and is not dipolar, no such envelope forms and the addition order of monomer molecules depends only on the concentration and relative activity of the monomers and free radicals at the ends of the growing chains and therefore the phenomenon of "inversion" does not occur.

LITERATURE CITED

[1] J. Landler, Comptes rend. 230, 539 (1950).

[2] J. Landler, J. Pol. Sci. 8, 64 (1952).

[3] F. C. Foster, J. Am. Chem. Soc. 72, 1370 (1950).

[4] F. C. Foster, J. Am. Chem. Soc. 74, 2299 (1952).

[5] N. N. Chesnokova and A. A. Korotkov, Theses of Repts. to the Ninth Conference on the General Problems of Chemistry and Physics of High Molecular Compounds (Moscow, 1956), p. 32.*

[6] R. J. Orr and H. L. Williams, Canad. J. Chem. 30, 108 (1952).

[7] A. E. Favorskii, Trans. Sess. Acad. Sci. USSR on Organic Chemistry (Acad. Sci. USSR Press, 1939), p. 38. A. A. Korotkov, S. P. Mitsengendler, and G. V. Rakova, Coll. Repts. All-Soviet Conf. on the Use of Isotopes in Science and Industry (Moscow, 1957). *

[8] K. A. Kocheshkov and T. V. Talalaeva, Synthetic Methods in the Field of Metalloorganic Compounds of Lithium, Sodium, Potassium, Rubidium, and Cesium (Acad. Sci. USSR Press, 1949), pp. 26, 352. *

[9] F. R. Mayo and F. M. Lewis, J. Am. Chem. Soc. 66, 1594 (1944).

[10] K. Ziegler and K. Bahr, Ber. 61, 253 (1928); S. S. Medvedev and A. Abkin, Trans. Farad. Soc. 32, 286 (1936).

Institute of High Molecular Compounds
Academy of Sciences of the USSR

Received December 16, 1957

* In Russian.

PASSIVATING PROPERTIES OF SULFATE IONS

I. L. Rozenfel'd and V. P. Maksimchuk

(Presented by Academician A. N. Frumkin, December 23, 1957)

The passive state of iron alloys with chromium and nickel (stainless steels) is destroyed in the presence of chlorine ions and consequently these alloys undergo corrosion in chloride solutions. Up to the present it was known that the activating actions of chlorine ions can be completely excluded or suppressed by the introduction of passivating agents into the electrolyte [1].

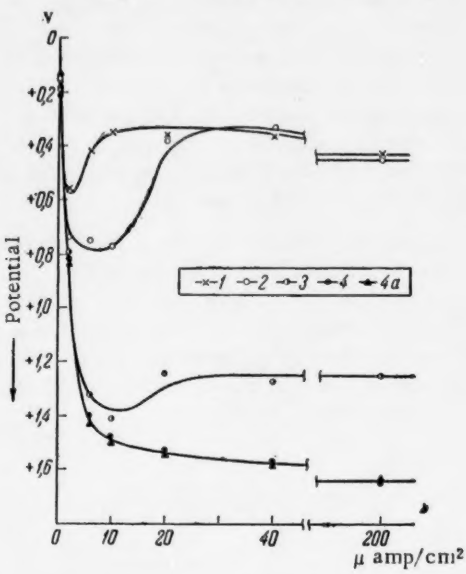

Fig. 1. Anode polarization curves for 1Cr18N9T Steel. 1) In a 0.1 N NaCl solution; 2) in a 0.1 N NaCl + 0.1 N Na_2SO_4 solution; 3) in a 0.1 N NaCl + 0.5 N Na_2SO_4 solution; 4) in a 0.1 N NaCl + 1.0 N Na_2SO_4 solution; 4a) in a 1.0 N Na_2SO_4 solution.

We have discovered and subsequently investigated a new phenomenon which demonstrates that sulfate ions possess properties analogous to passivating agents with respect to chlorine ions.

Figure 1 represents anode polarization curves relative to 1Cr18N9T steel in 0.1 N NaCl solution containing different amounts of sulfate. In a 0.1 N NaCl solution the polarization curve has a characteristic bend which indicates that the electrode has lost its passivity and become active. Therefore, the values of the potentials corresponding to the minimum points of such curves characterize the stability of the passive state.

Figure 1 shows clearly that the stability of the passive state increases in the presence of sulfates. As the concentration of the sulfate increases, the activation potential shifts rapidly toward the area of more positive potentials. Finally, when $C_{NaCl} : C_{Na_2SO_4} \leq 1:10$ no activation takes place. For the majority of stainless steels the polarization curves obtained in electrolytes of this type coincide with the curves obtained in pure sulfate solutions.

When the amount of sulfate is sufficient, stainless steel behaves as a passive electrode; it can be polarized up to relatively high potentials without the appearance of the active state.

There exists a significant difference in the corrosion character of the electrodes. The electrodes submitted to anodic polarization in NaCl + Na_2SO_4 solution undergo much less pitting corrosion than the electrodes polarized in NaCl solution. The electrode remains unattacked if $C_{NaCl} : C_{Na_2SO_4} \leq 1:10$.

In order to clarify the electrochemical behavior of the different components of stainless steels we have drawn anode polarization curves with iron, nickel, molybdenum, chromium, and, for comparison, with Cr28 chromium steel (Fig. 2).

With iron, whose potential was about − 0.3 volt, the sulfate ions' effect is absent. Furthermore, the introduction of sulfate into the electrolyte displaces the stationary potential toward more negative values and favors the process of anodic dissolution of iron.

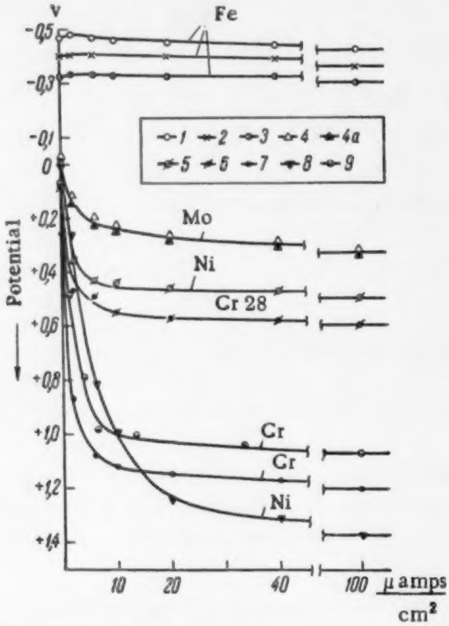

Fig. 2. Anode polarization curves. 1) Fe in 0.1 N NaCl + 1.0 N Na_2SO_4; 2) Fe in 0.1 N Na_2SO_4; 3) Fe in 0.1 N NaCl; 4) Mo in 0.1 N NaCl; 4a) Mo in 0.1 N NaCl + 1.0 N Na_2SO_4; 5) Ni in 0.01 N NaCl; 6) Cr28 in 0.1 N NaCl; 7) Cr28 in 0.1 N NaCl + 1.0 N Na_2SO_4; 8) Ni in 0.01 N NaCl + 1.0 N Na_2SO_4; 9) Cr in 0.1 N NaCl.

Chlorine ions have no activating effect on chromium; during anodic polarization chromium is easily passivated even in chloride solutions and therefore the effect of SO_4^{--} cannot be put in evidence. Sulfate ions do not affect the molybdenum electrode in the presence of chlorides. The passivating effect of sulfate ions is clearly manifest in the case of iron − chromium solid solution (the Cr28 steel); compare curves 6 and 7 of Fig. 2. In pure chloride solutions this steel can be polarized only up to the potential equal to + 0.6 volt; beyond this value the steel passes into the active state. In the presence of sulfate ions, however, this steel can be polarized up to + 1.2 volt. This effect is analogous to that observed with 1Cr18N9T steel.

Sulfate ions also prevent the activation of nickel by chloride ions. However, when $C_{NaCl} : C_{Na_2SO_4} = 1:10$, nickel is in an active−passive state; during anodic polarization in this solution the potential of nickel is very unstable; it varies within a wide range limited by curves 5 and 8 (Fig. 2). The passive state becomes stable only when $C_{NaCl} : C_{Na_2SO_4} \leq 1:100$; nickel can then be polarized without any oscillation of potential up to relatively high potentials.

Thus, one may conclude that the passivating action of SO_4^{--} ions on stainless steel is determined to a great extent by chromium and to a lesser extent by nickel. The passivating property of sulfate ions can be studied and demonstrated directly by the variation of the potential as the function of time during polarization of steel at constant current density.

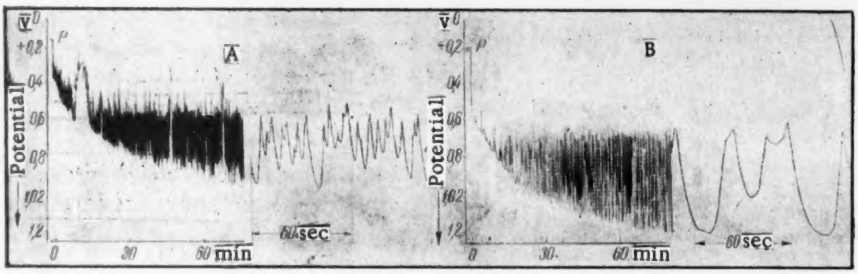

Fig. 3. Variation of the potential of 1Cr18N9T steel as the function of time with current density equal to 2μ amp/cm². A) In a 0.1 N NaCl solution; B) in a 0.1 N NaCl + 0.1 N Na_2SO_4 solution. Initial rate of feed of the band was 120 mm/hr; final rate of feed 4800 mm/hr.

The diagrams represented in Figs. 2 and 4 were obtained with an automatically registering potentiometer connected to a direct current amplifier. In pure chloride solutions the surface of steel is in an active−passive state and its potential oscillates, as is shown by the diagram (Fig. 3, A). The frequency of oscillations of the

potential and the limits within which it varies (which can be determined directly on the diagram when input is large; see the right side of the diagram) characterize the degree of stability of the passive state. The diagram shows distinctly that the introduction of sulfate into the electrolyte sharply decreases the frequency of oscillations of the potential. In a 0.1 N NaCl solution with the density of current equal to 2μ amp/cm^2 one observes 12 oscillations per minute on the average, after a period of 1.5 hours; the value of the potential oscillates between + 0.55 and + 0.95 volt; in a 0.1 N NaCl + 0.1 N Na_2SO_4 solution the values of the potential experience 2 to 3 oscillations within the limits of + 0.65 and + 1.25 volts. When the concentration of sulfate is ten times greater than that of the chloride the frequency of potential oscillations is reduced to zero: then steel undergoes anodic polarization without variation of its potential (Fig. 4).

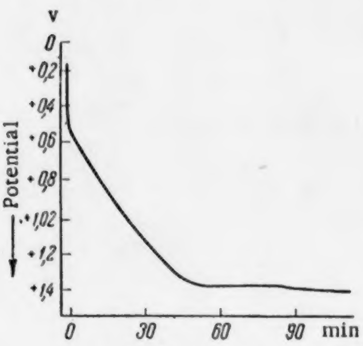

Fig. 4. Variation of the potential of 1Cr18N9T steel as the function of time in a 0.1 N NaCl + 1.0 N Na_2SO_4 solution with the current density equal to 2μ amp/cm^2. The graph paper band was fed in at the rate of 120 mm/hour.

According to the surface film theory of passivity the activating effect of chlorine ions is explained in the following way: because of their small radius, chlorine ions can easily penetrate the protecting surface film and destroy it. The function of the passivating agent is reduced to the mending of the defects occurring as the result of the action of chlorine ions. One cannot expect this type of action from sulfate ions since they do not possess an oxidation power and do not form insoluble compounds with the components entering into the composition of stainless steel.

The effect we discovered can be explained satisfactorily by assuming that the processes taking place at the surface of the electrode in the presence of chlorine and sulfate ions are adsorption processes. According to this mechanism the stability of the passive state must therefore be determined by the adsorption of anions from the solution.

There exists sufficient evidence that the passivating property of sulfate ions is determined primarily by their adsorption by the metal surface, the adsorbed sulfate ions displace the chlorine ions from the surface.

As the result of this exchange of adsorbed ions, the chlorine ions are either completely removed from the metal surface or their concentration becomes so insignificant that they are incapable of activating the metal.

The process of adsorption of ions from electrolytes was studied in detail by A. N. Frumkin and his students [2]. They have studied the relationship between the adsorption capacity and the charge of the surface and have shown that for given potentials strong adsorption of anions takes place even on an oxidized surface. This result was proven by N. A. Balashova [3] in the case of SO_4^{--} by the method of radioactive tracers.

Adsorption of ions by chromium from electrolytes containing SO_4^{--} and Cl^- was studied by Hackerman and Powers. These authors showed that the adsorbed SO_4^{--} and Cl^- ions exchange with the adsorbed CrO_4^{--} ions and remove them from the metal's surface. It is important to underline that the SO_4^{--} ions are revealed as much more active than the Cl^- ions: equal displacement of CrO_4^{--} is achieved by SO_4^{--} and by Cl^- when the concentration of Cl^- is 500 times higher than that of SO_4^{--}. It can be concluded therefore that the SO_4^{--} ions are much more easily adsorbed by the metal surface than the Cl^- ions and consequently can displace the Cl^- ions.

The results obtained reflect favorably the adsorptional mechanism of action of chlorine ions; the theory of this mechanism was worked out by B. N. Kabanov and his collaborators [5]; according to this theory the activation of the metal by the anions is explained by the adsorption and displacement from the surface of oxygen responsible for passivity.

LITERATURE CITED

[1] G. V. Akimov, Theory and Investigation Methods of Corrosion of Metals (1945), p. 162;* U. R. Evans, J. Chem. Soc. 2476 (1932).

* In Russian.

[2] A. N. Frumkin, V. S. Bagotskii, Z. A. Iofa, and B. N. Kabanov, Kinetics of Electrode Reactions (1952), p. 33;* A. Shlygin, A. Frumkin, and V. Medvedovskii, Acta Physicochim USSR 4, 911 (1936).

[3] N. A. Balashova, Proc. Acad. Sci. USSR 103, 4, 639 (1955).

[4] N. Hackerman and R. A. Powers, J. Phys. Chem. 57, 139 (1953).

[5] L. V. Vaniukova and B. N. Kabanov, Proc. Acad. Sci. USSR 59, 917 (1948); J. Phys. Chem. USSR 28, 1025 (1954).

Institute for Physical Chemistry
Academy of Sciences, USSR

Received December 21, 1957

* In Russian.

DEOXIDIZING CAPACITY OF CARBON IN VACUUM

A. M. Samarin, Corresponding Member of the Academy of Sciences, USSR,

and R. A. Karasev

The reactions between carbon and oxygen in liquid iron, described by the following equations:

$$[C] + x[O] = CO_{x\,(g)} \tag{1}$$

$$k = \frac{P_{CO_x}}{[a_C]\,[a_O]^x}, \tag{1a}$$

are the fundamental reactions involved in steel manufacturing.

The coefficient x in Equation (1) is determined by the ratio of CO to CO_2 in the reaction. The value of x increases from 1 to 2 when the composition of the reaction products passes from pure carbon monoxide to pure carbon dioxide [1].

The determination of the equilibrium constant of the reaction showed that the deoxidizing capacity of carbon, fixed by the product [% C]·[% O], depends on the pressure, and for a pressure of one atmosphere it can be represented by curve I of Fig. 1 [2].

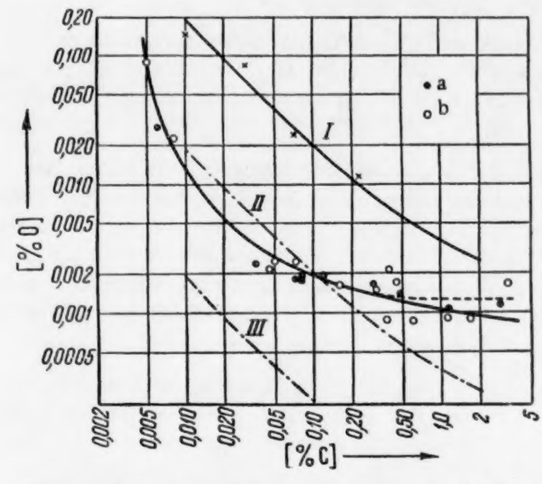

Fig. 1. I) Pressure of 1 atm; II) pressure of 0.1 atm; III) pressure of 0.01 atm. a) Vacuum of (1-5)·10^{-2} mm Hg; b) vacuum of (5-7)·10^{-6} mm Hg.

Insofar as in Equation (1) the variation of the number of moles of gaseous substances is equal to unity, the equilibrium constant is a single function of temperature. Consequently, the deoxidizing capacity of carbon is inversely proportional to the pressure of the gaseous phase, i.e., a decrease in pressure from 1 atm to 0.1 atm or

0.01 atm must correspondingly increase the deoxidizing capacity of carbon 10 or 100 times. Assuming this mechanism of the reaction, one may conclude that under the conditions of modern vacuum technique the deoxidizing capacity of carbon should be raised up to values exceeding the deoxidizing capacity of strong deoxidizing agents such as aluminum and zirconium [3-6].

Experiments on fusion of carbon-iron alloys contradict this conclusion however, because when the pressure of the gaseous phase is below one mm Hg the deoxidizing capacity of carbon becomes, for practical purposes, independent of pressure.

We have performed a series of experiments to determine the variation of the deoxidizing capacity of carbon as the function of pressure; in these experiments liquid iron, containing different concentrations of carbon, was maintained at a given temperature in high vacuum until the attainment of equilibrium conditions between carbon and oxygen dissolved in liquid iron.

The experimental method was based on the assumption that when equilibrium is being reached by deoxidation the composition of the gaseous phase above the liquid metal has no appreciable effect on the equilibrium state. This assumption was verified in the case of fusions performed in an atmosphere of argon under a pressure of 1 atm. The results of these preliminary fusions are represented in Fig. 1. The comparison of these results with those illustrated by curve I, corresponding to the equilibrium with the gaseous phase composed of CO and CO_2, shows that the results obtained by deoxidation in the atmosphere of argon confirm our assumption.

Experimental fusions under the pressure of $(5-7) \cdot 10^{-6}$ mm Hg were performed in a resistance furnace evacuated with the aid of the VA-0.5-1 installation. The heating element was a molybdenum coil fixed in a special ceramic holder of beryllium oxide. Experimental fusions under the pressure of $(1-5) \cdot 10^{-2}$ mm Hg were performed in a high-frequency furnace connected to a 15 kw generator. In both cases the temperature was measured with a Pt–PtRh thermocouple. The temperature was measured to a precision of ± 5° in the case of the resistance heating and ± 15° in the case of high-frequency heating.

We tried the MgO, Al_2O_3, ThO_2, ZrO_2, and BeO crucibles in our experiments. Spectral analysis showed that the crucible material reacts with the liquid metal so that it becomes impossible to determine the real deoxidation power of carbon in liquid iron. In the case of corundum, however, it was found that if the same crucible is used over and over again, the amount of aluminum dissolved in liquid iron decreases sharply after the first fusion. After 3-4 fusions in the same crucible the material of the crucible becomes practically inert with respect to liquid iron containing up to 0.8-1.0% C.

Consequently, all the results reported in Table 1 are relative to experiments performed in crucibles which underwent the treatment mentioned above. The presence of aluminum was checked in samples 15, 17, 19, 114, 115, 118, 119, 212, 214, 218, and 219; spectral analysis revealed the presence of small amounts of aluminum only in samples 114, 115, 118, and 218.

The results presented in Table 1 show that the deoxidizing power of carbon, determined experimentally at 1590°, is considerably lower than that calculated on the basis of the reaction equilibrium constant. Furthermore, the positions of the experimental points on Fig. 1 indicate that the results obtained under pressures of 10^{-2} and 10^{-6} mm Hg fall satisfactorily on the same curve. In other words, within this range of pressures a 10^4-fold change of pressure does not affect the deoxidizing power of carbon in liquid iron. It is important to note another fact, namely that the effect of vacuum on the increase of the deoxidizing power of carbon is not the same for different concentrations of carbon in liquid iron.

The results obtained are quite satisfactory for a reaction taking place in a liquid metal solution with the formation of a new gaseous phase. The divergence between the calculated and the experimental values of the deoxidizing power of carbon in vacuum is due to the incorrect interpretation of the parameter P_{CO_x} in Equation (1a). During the reaction between carbon and oxygen in liquid iron the value of P_{CO} is determined by three factors: barometric pressure above the metal; pressure due to the column of liquid metal at a given depth of the bath; and pressure induced by the forces of surface tension on the surface of the gas bubble of radius r :

$$P_{CO_x} = P_b + \gamma h + \frac{2\sigma}{r}. \tag{2}$$

Here P_b represents the barometric pressure above the metal; γ is the density of the liquid metal; $\underline{h}$ is the depth of the metal bath at the level at which the gas bubbles are formed; σ is the surface tension of the liquid metal; $\underline{r}$ is the radius of the gas bubble embryo.

TABLE 1

Effect of Pressure on the Equilibrium Between Carbon and Oxygen Dissolved in Liquid Iron (1590°)

Sample No.	Pressure (mm Hg)	Duration of expt. (min)	[%C]	[% O]		
				I	II	average
11 Ar	760 Ar	20	0,24	0,0113	0,0107	0,0110
12 Ar	760 Ar	30	0,03	0,0800	0,0780	0,079
13 Ar	760 Ar	40	0,07	0,0236	0,0252	0,0244
14 Ar	760 Ar	60	0,01	0,1272	0,1278	0,1275
15	$(5-7)\cdot10^{-6}$	60	0,31	0,0012	0,0017	0,0015
16	$(5-7)\cdot10^{-6}$	60	0,005	0,0860	0,0910	0,0880
28	$(1-5)\cdot10^{-2}$	60	0,07	0,0017	0,0019	0,0018
29	$(1-5)\cdot10^{-2}$	60	0,08	0,0018	0,0018	0,0018
210	$(1-5)\cdot10^{-2}$	20	0,006	0,0294	0,0286	0,0290
211	$(1-5)\cdot10^{-2}$	60	0,035	0,0021	0,0025	0,0023
212	$(1-5)\cdot10^{-2}$	60	0,30	0,0015	0,0017	0,0016
213	$(1-5)\cdot10^{-2}$	60	0,08	000017	0,0017	0,0017
214	$(1-5)\cdot10^{-2}$	60	0,12	0,0019	0,0020	0,0019
215	$(1-5)\cdot10^{-2}$	90	0,49	0,0014	0,0013	0,0014
218	$(1-5)\cdot10^{-2}$	60	2,95	0,0011	0,0011	0,0011
219	$(1-5)\cdot10^{-2}$	60	1,15	0,0010	0,0010	0,0010
17	$(5-7)\cdot10^{-6}$	60	0,008	0,0230	0,0230	0,0230
18	$(5-7)\cdot10^{-6}$	90	0,045	0,0020	0,0022	0,0021
19	$(5-7)\cdot10^{-6}$	90	0,45	0,0015	0,0018	0,0016
110	$(5-7)\cdot10^{-6}$	60	0,61	0,0008	0,0009	0,0008
111	$(5-7)\cdot10^{-6}$	60	0,37	0,0009	0,0009	0,0009
112	$(5-7)\cdot10^{-6}$	90	0,05	0,0024	0,0025	0,0024
113	$(5-7)\cdot10^{-6}$	60	0,072	0,0020	0,0028	0,0024
114	$(5-7)\cdot10^{-6}$	60	1,13	0,0009	0,0009	0,0009
115	$(5-7)\cdot10^{-6}$	60	3,43	0,0016	0,0016	0,0016
116	$(5-7)\cdot10^{-6}$	60	0,165	0,0014	0,0018	0,0016
118	$(5-7)\cdot10^{-6}$	60	1,75	0,0008	0,0010	0,0009
119	$(5-7)\cdot10^{-6}$	60	0,40	0,0019	0,0022	0,0020

Equation (2) shows that P_{CO_x} becomes equal to $2\sigma/r$ when P_b and $\underline{h}$ tend toward zero, i.e., the deoxidizing power of carbon in vacuum is determined by the magnitude of the surface tension of the liquid metal and by the size of the gaseous embryo formed within the liquid metal.

From Equation (2) it follows that the effect of vacuum on the deoxidizing capacity of carbon is determined by the relationship between the values of P_b and $\gamma h + \frac{2\sigma}{r}$. When $\gamma h + \frac{2\sigma}{r} \gg P_b$, no further decrease of the barometric pressure above the metal can change the value of P_{CO_x} and therefore it cannot affect further increase of deoxidation power of carbon in liquid metal. For the practice of deoxidation of steel by carbon in vacuum it is of interest to determine the maximum rarefication in the furnace for which further increase of vacuum becomes irrational from the point of view of deoxidation.

The results represented in Fig. 1 show that within the range of carbon concentrations investigated the minimum value [% C]·[% O] is located in the vicinity of 0.1 atm. Considering the value of P_{CO_x} corresponding to this pressure one can conclude that for complete deoxidation of liquid iron by the carbon dissolved in it, the pressure in the furnace must be 1-2 mm Hg, a diminishingly small value as compared to 0.1 atm.

LITERATURE CITED

[1] A. M. Samarin and R. A. Karasev, Bull. Acad. Sci. USSR, Div. Techn. Sci. 8, 1130 (1953).

[2] S. Marshall and J. Chipman, Trans. ASM. 30, 695 (1942).

[3] L. Columbier, Rev. Metallurg. 44, 11-12, 374 (1947).

[4] A. M. Samarin, L. M. Novik, N. I. Goncharenko, and A. F. Tregubenko, Steel 8, 700 (1956).

[5] F. Handers, H. Knuppel, and K. Brotmann, Stahl und Eisen, 26, 1721 (1956).

[6] K. Bungardt and H. Sychrovsky, Stahl und Eisen 16, 1040 (1956).

A. A. Baikov Institute of Metallurgy
Academy of Sciences, USSR

Received May 5, 1957.

THE STRUCTURE AND STRENGTHENING EFFECT OF COLLODIAL SILICIC ACID AS A FILLER FOR SYNTHETIC CAOUTCHOUC

B. Dogadkin, K. Pechkovskaia, and E. Gol'dman

(Presented by Academician P. A. Rebinder, December 25, 1957)

The problem of the reaction of caoutchouc and filler has been studied in great detail. In spite of this many essential sides of this process remain unclarified. In particular, the effect of the filler's structure and the character of its distribution on the strengthening factor has hardly been studied.

It was shown [1] that active carbon blacks, capable of strengthening caoutchouc, form thixotropic structures in which the carbon black particles come into contact with each other to a certain degree (lattice structures). The non-strengthening carbon blacks form systems in which the carbon black is relatively evenly distributed in the form of primary or secondary particles in the caoutchouc medium. Therefore, there is an interrelation between the character of carbon black distribution and the strengthening effect.

TABLE 1

Characteristics of filler samples	Tensile strength, kg/cm^2	Relative elongation, %	Residual elongation, %	Resistance to tearing, kg/cm
Active	115.7	527	34.6	43.3
Average activity	69.0	452	37.0	34.0
Inactive	39.4	300	16.0	27.0

This investigation was aimed at studying the character of the distribution of colloidal silicic acid in sodium-butadiene caoutchouc as the former is an example of the new class of fillers which have recently acquired practical value.

The choice of the substance to be investigated was also determined in this case by the fact that the same raw material and the same method, changing only the conditions of the technological process, gave samples of colloidal silicic acid that had considerably different strengthening effects. This made it possible to compare active and inactive fillers which were much more similar to each other than all the samples of carbon blacks investigated earlier.

For the investigation we prepared a series of collodial silicic acid samples, with high, medium, and low strengthening effect in rubbers of sodium-butadiene caoutchouc (Table 1). The chemical composition of these samples was practically identical. They also differed very little in specific surface, pH and a series of adsorption characteristics (toluene, stearic acid, caoutchouc adsorption) (Table 2).

However, the rubber mixtures prepared from the sodium-butadiene caoutchouc and containing the samples investigated, were very different in structure and in the physicomechanical properties of the vulcanizates.

The high solubility of colloidal silicic acid in dilute sodium hydroxide solution, in contrast to caoutchouc, which is insoluble in it, was used for studying the structure of the mixture. After boiling a mixture in such a

solution, we then measured the amount of filler that had passed into solution. It was found that the more active a colloidal silicic acid the more rapidly and fully it was removed from the mixture with caoutchouc. In analogy with bentonite [2] and carbon black [3] mixtures, one can assume that the particles of the more active colloidal silicic acid are capable of forming chain structures which allow the solvent to penetrate the mixture readily and the solution of silicate to be removed from it, just as readily. When there was no solution it was assumed that a

TABLE 2

Characteristics of filler samples	Sp. surface, m^2/g	Toluene ads., mmole/g	Stearic acid ads., mmole/g	Caoutchouc ads., g/g	pH
Active	61.8	9.4	0.47	0.13	8.7
Average activity	–	8.8	–	–	8.4
Inactive	50.3	7.7	0.56	0.108	10.0

more or less thick caoutchouc layer between the isolated silicic acid particles hindered the diffusion of the solvent to the filler particles. It should be noted that the degree of solution in an aqueous medium of NaOH is the same for active and inactive samples.

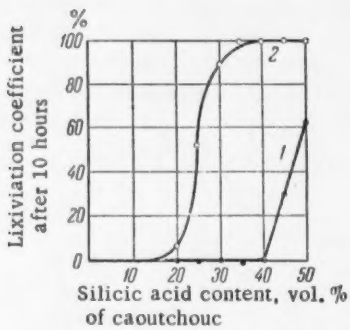

Fig. 1. The relation between the filler and lixiviation coefficient of active and inactive silicic acid from three component mixtures containing inactive (1) and active (2) silicic acid.

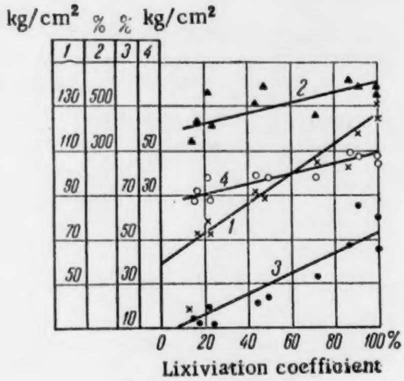

Fig. 2. Relation between lixiviation coefficient and physicomechanical properties of vulcanizates. 1) Tensile strength; 2) relative elongation; 3) residual elongation; 4) resistance to tearing.

To characterize the degree of filler participation in the structure of the mixture, we used a "lixiviation coefficient," which specified the fraction of the total filler content of the mixture passing into an alkali solution.

Figure 1 shows the relation of the lixiviation coefficient to the amount of filler for colloidal silicic acid samples with the greatest strengthening capacity (active sample) and the least strengthening capacity (inactive sample). As can be seen, the active silicic acid was lixiviated completely with a degree of filling (about 35 volumes per 100 weight parts of caoutchouc) at which the inactive sample, under the same conditions, remained practically insoluble. This confirmed the difference in the character of the distribution of the two silicic acid samples investigated in sodium-butadiene caoutchouc.

It is interesting to note that after removing the active silicic acid with alkali, the residual sample of crude rubber mixture remained as insoluble in an organic solvent as before alkali treatment.

The fact that an active sample was removed much more readily from the mixture with alkali than an inactive one cannot be explained by the formation of a different amount of caoutchouc – filler gel as then one would have to assume that the active sample bonded the caoutchouc to a lesser degree than the inactive one, but this would contradict the existing concepts on the interaction of caoutchouc and filler.

It appears to us that the data obtained, as well as the results of earlier papers [1, 4, 5], indicate that, besides the bonds between caoutchouc and filler [6, 7] in the structure of the insoluble caoutchouc – filler gel, the cross-links between the polymer molecules themselves have a considerable effect.

TABLE 3

Heating temperature, °C	Ignition loss, %	Lixiviation coefficient after 10 hrs., %	Tensile strength, kg/cm^2	Relative elongation, %	Residual elongation, %	Resistance to tearing, kg/cm
–	–	100	111.5	448	30.8	39.3
400	10.5	91.0	115.6	626	54.0	50.9
600	12.4	12.5	52.8	494	17.0	17.7

A study of the physicomechanical properties of vulcanizates, containing the colloidal silicic acid samples being investigated, showed that the higher the lixiviation coefficient of a filler from the given system, the higher the stability characteristics of the vulcanizate. These data are shown in Fig. 2.

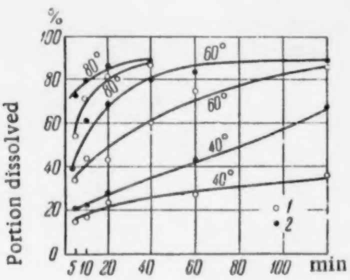

Fig. 3. Solution kinetics of technical silicic acid: 1) Active, 2) inactive.

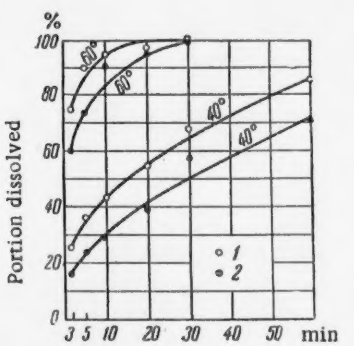

Fig. 4. Solution kinetics of dialyzed silicic acid. 1) Active, 2) inactive.

All the samples tested may be divided into three groups by degree of activity: a) inactive samples, whose lixiviation coefficient is less than 25%; b) samples of average activity, whose lixiviation coefficient is 40-50% and c) active samples, whose lixiviation coefficient reaches 70-100%. A considerable majority of the samples investigated are distributed in the same order by the physicomechanical indexes of the corresponding vulcanizates.

The activity of a colloidal silicic acid sample may be considerably decreased by heating it at 600°. These results are shown in Table 3.

The relatively low temperature at which the observed changes occurred indicates the known instability of the crystal lattice of silicic acid, that is probably connected with precipitation conditions. Apparently at 600° recrystallization occurs and as a result the elementary crystals making up the lattice change into another, more stable crystalline form: this change is accompanied by a loss in activity of the material as a caoutchouc strengthener.

The unstable state of the crystal lattice of the active sample must be reflected in a series of properties of the material and, in particular, in its behavior to solvents. With this in mind we investigated the solution kinetics of technical (active and inactive) and dialyzed (active and inactive) colloidal silicic acid in an aqueous sodium hydroxide solution at various temperatures.

As Figs. 3 and 4 show, a technical, active sample in a 1% NaOH solution dissolved at a slower rate than the inactive sample at all the temperatures investigated. On the contrary, an active sample, purified electrodialitically, dissolved more rapidly than an inactive sample subjected to the same purification. Thus, impurities adsorbed on the surface of silicic acid retarded the solution of an active modification more than an inactive one. After these impurities had been removed electrodialitically, the active sample dissolved, as we had expected, at a greater rate than the inactive sample.

This difference in the solution rates of dialyzed substances of the same chemical composition indicates a difference in the structure of the elementary cell, which is less stable in the case of the active sample. The latter may be due to the presence of deformation or defects caused by foreign atoms or ions caught in the precipitation of silicic acid from solution.

LITERATURE CITED

[1] B. Dogadkin and M. Fel'dshtein, Caoutchouc and Rubber 12 (1939).

[2] B. Dogadkin, K. Pechkovskaia, and L. Chernikina, Coll. J. 8, 1-2, 31 (1946).

[3] B. Dogadkin, K. Pechkovskaia, and M. Dashevskii, Coll. J. 10, 5, 357 (1958).*

[4] F. Menadue, India-Rubb. J. 85, 689 (1933).

[5] F. Endter, Kautschuk u. Gummi 5, 2, 17 (1952).

[6] S. Polinchak et al., Rubb. Age 70, 6, 754 (1952).

[7] V. Garten, Nature 173, 997, 4412 (1954).

Research Institute of the Tire Industry

Received December 12, 1957

* Original Russian pagination. See C. B. Translation.

THE AFFINITY OF HYDROGEN AND SATURATED HYDROCARBONS FOR PROTONS

E. L. Frankevich and V. L. Tal'roze

(Presented by Academician V. N. Kondrat'ev, October 24, 1957)

The affinity of molecules for a proton, P, is a very important thermochemical constant. However, direct experimental data on the affinity for protons, obtained by electron collision, were known only for unsaturated compounds until recently.

The existence of a positive affinity of hydrogen and methane for a proton is due to the existence of the stable ions H_3^+ [1] and CH_5^+ [2]. There is no information in the literature on "onium" ions of methane homologs. A paper by one of the authors [3] reported that when molecular ions of ethane, propane and butane collided with the molecules of these substances, the corresponding "onium" ions were not formed. This paper, as well as the one by Stevenson and Schissler [13] gave an evaluation of the lower limit of P_{H_2}. Hirschfelder [4] and Barker and Eyring [5] calculated theoretically the energy of the H_3^+ ion. Simons et al. [6] obtained the value of P_{H_2} using Hirschfelder's calculations from the relations governing the interaction between H^+ and H_2, found in experiments on the scattering of protons in hydrogen [6]. In this paper we give the results of experiments on the determination of the affinity of hydrogen, methane, ethane and propane for protons, using the method of ion collision developed by the authors [7].

The experiments for detecting the reactions that lead to the formation of secondary H_3^+ ions were carried out on a MS-1a mass-spectrometer [8]. The energy of the ionizing electrons was equal to 50 ev. In experiments with different gas pressures in the ion source we investigated the following reactions:

$$(1)\ H_2^+ + H_2 \rightarrow H_3^+ + H; \quad (2)\ H_2^+ + C_2H_2 \rightarrow H_3^+ + C_2H; \quad (3)\ H_2 + C_2H_2^+ \rightarrow H_3^+ + C_2H;$$
$$(4)\ H_2^+ + C_2H_6 \rightarrow H_3^+ + C_2H_5; \quad (5)\ H_2 + C_2H_6^+ \rightarrow H_3^+ + C_2H_5.$$

It was shown that the addition of acetylene to the ion source, containing hydrogen at a pressure of approximately 10^{-4} mm Hg did not increase the yield of H_3^+ ions. Under these conditions H_3^+ ions were formed only by Process (1). However, the addition of ethane to the ion source under similar conditions, increased the H_3^+ ion current; this indicated that besides (1), at least one of the two processes, (4) and (5), also occurred. To evaluate the maximum values of the H_2 molecules affinity for protons, the authors used the following values for the dissociation energy and ionization potentials of the molecules: $D(H_2) = 103.2$ kcal/mole, $D(C_2H_5 - H) = 96$ kcal/mole [9], $D(C_2H - H) = 121$ kcal/mole [9], $I(H_2) = 15.43$ ev, $I(C_2H_2) = 11.43$ ev [10], $I(C_2H_6) = 11.76$ ev [10].

As, in accordance with the laws governing the ion collision method, the heat effect of the ion-molecule reactions, detected mass-spectrometrically, is either positive or equal to zero, and that of the undetected ones is negative, then using experimental data on Reactions (1) - (5) and the energy magnitudes given above, we may write the following series of inequalities, which determine the limits of the permissible values for proton affinity: 1) $P_{H_2} \geq 61$ kcal/mole; 2) $P_{H_2} < 79$ kcal/mole; 3) $P_{H_2} < 171$ kcal/mole; 4) $P_{H_2} \geq 54$ kcal/mole.

The inequalities 1) and 2) determine the narrowest range of possible values of P_{H_2}: 61 kcal/mole $\leq P_{H_2} < 79$ kcal/mole. Taking the average of the two possible limiting values, we obtain $P_{H_2} = 70 \pm 9$ kcal/mole. It is interesting that this value, calculated from data in [4] and [5], and the experimental value of $D(H_2)$ is 81 and 77 kcal/mole, while Simons gives 69.2 kcal/mole from his experiments.

All further experiments were carried out on a special high sensitivity mass-spectrometer which made it possible to measure accurately the appearance potentials of the ions [11]. To determine the affinity of a methane molecule for a proton, we investigated the following processes, in which CH_5^+ ions may be formed:

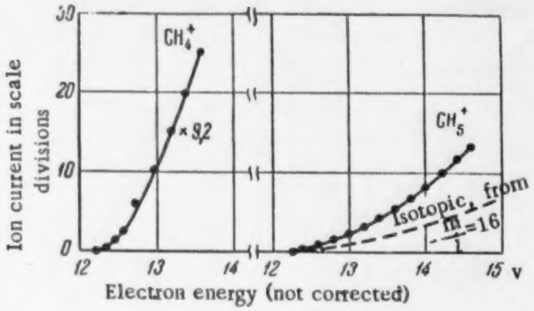

Fig. 1. Curves of CH_4^+ and CH_5^+ ion appearance from methane. The number beside the curve of CH_4^+ appearance is a coefficient, by which the appropriate coordinates should be multiplied so as to compare the appearance curves. $P_{source\, CH_4} = 10^{-4}$ mm Hg. $P_{source\, C_2H_6} = 2 \cdot 10^{-4}$ mm Hg.

$$(6)\quad CH_4^+ + CH_4 \rightarrow CH_5^+ + CH_3;$$
$$(7)\quad CH_4 + C_2H_6^+ \rightarrow CH_5^+ + C_2H_5;$$
$$(8)\quad CH_4 + H_3O^+ \rightarrow CH_5^+ + OH;$$
$$(9)\quad CH_4^+ + H_2O \rightarrow CH_5^+ + OH;$$
$$(10)\quad CH_4 + H_2^+ \rightarrow CH_5^+ + H;$$
$$(11)\quad CH_4^+ + H_2 \rightarrow CH_5^+ + H;$$
$$(12)\quad C_3H_6^+ + CH_4 \rightarrow CH_5^+ + C_3H_5;$$
$$(13)\quad C_3H_6 + CH_4^+ \rightarrow CH_5^+ + C_3H_5.$$

Reaction (6) was identified by comparing the appearance potentials of CH_4^+ and CH_5^+ ions. The corresponding appearance curves are shown in Fig. 1. On adding ethane to the ion source, the appearance potential of the CH_5^+ ion did not change. This meant that Process (7) was endothermal.

Processes (8) and (9) were checked experimentally with an increased water vapor pressure in the ion source. Ionization was carried out with 14 ev electrons. Under these conditions the only primary ions in the ionization chamber were CH_4^+ and H_2O^+. An increased water vapor pressure did not increase the yield of CH_5^+ ions. The 17 amu ion current remained constant and was due to isotopic methane ions and secondary CH_5^+ ions, formed during Process (6). The addition of hydrogen to the ion source, containing methane, increased the yield of CH_5^+ ions (Fig. 2). This increase, apparently, was due to at least one of the two processes (10) and (11). An analogous experiment was carried out with propylene added to the ion source (Fig. 3). The increase in the CH_5^+ ion current was in this case due to at least one of the two processes, (12) and (13).*

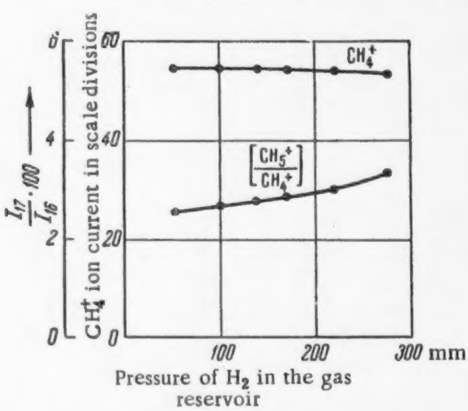

Fig. 2. The relation of the yield of CH_5^+ ions to hydrogen pressure. The ion source contained a mixture of CH_4-H_2. The gas pressure in the ion source was a factor of approximately 10^6 less than the pressure in the gas reservoir.

The limiting values of the affinity of methane for a proton, P_{CH_4}, calculated on the basis of data

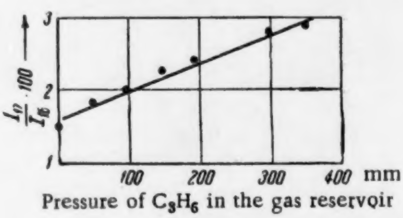

Fig. 3. The relation of the yield of CH_5^+ ions to propylene pressure. The ion source contained a mixture of $CH_4-C_3H_6$; $P_{res.\, CH_4} = 50$ mm Hg.

obtained for the processes of CH_5^+ ion formation, gave the following inequalities: 6) $P_{CH_4} \geq 114$ kcal/mole; 7) $P_{CH_4} < 139$ kcal/mole; 8) $P_{CH_4} < 129$ kcal/mole; 9) $P_{CH_4} < 139$ kcal/mole; 10) $P_{CH_4} \geq 61.2$ kcal/mole; 11) $P_{CH_4} \geq 91$ kcal/mole.

* As Processes (10), (11), (12), and (13) were not investigated separately, we can only attribute the increase in the secondary ion current to that process which gives the least value for P_{CH_4}.

Inequalities 6) and 8) determined the narrowest limits: 114 kcal/mole $\leq P_{CH_4}$ < 129 kcal/mole.

In the calculations, besides the values given above for $D(H_2)$, $D(C_2H_5-H)$, $I(H_2)$, $I(C_2H_6)$, we used the following magnitudes: $D(CH_3-H) = 101$ kcal/mole [9], $D(HO-H) = 116$ kcal/mole [9], $D(C_3H_5-H) = 77$ kcal/mole [12], $I(CH_4) = 13.04$ ev [10], $I(H_2O) = 12.62$ ev [10], $I(C_3H_6) = 9.84$ ev [10].

We looked for the "weighted" $C_2H_7^+$ ions during the collisions of ions or ethane molecules with the molecules and ions of various hydrocarbons, as well as hydrogen. The following collision processes were investigated:

$$C_2H_6^+ + H_2;\ C_2H_6 + H_2^+;\ C_2H_6^+ + CH_4;$$
$$C_2H_6 + CH_4^+;\ C_2H_6 + C_3H_8^+;\quad C_2H_6^+ +$$
$$+ C_3H_8;\quad C_2H_6 + nCH_{10}^+;\ C_2H_6^+ +$$
$$+ nC_4H_{10};\ C_2H_6 + iso\text{-}C_4H_{10}^+;\ C_2H_6^+ +$$
$$+ iso\text{-}C_4H_{10};\ C_2H_6^+ + C_2H_6.$$

The addition of any of the gases mentioned to the ion source, containing ethane, did not increase the ratio of the ion currents at 31 and 30 a m u and the latter remained equal to the ratio of the corresponding isotopic ethane ion currents (2.3%). Consequently, no $C_2H_7^+$ ions were formed in any of the processes. The $C_2H_6 + H_2^+$ process gave the least possible value for the upper limit of an ethane molecule's affinity for a proton. This gave $P_{C_2H_6}$ < 61 kcal/mole.

We looked for $C_3H_9^+$ ions during the ionization of propane and of a mixture of propane with hydrogen, with methane and with ethane. It was found that $C_3H_9^+$ ions were not among the products of the processes:

$$C_3H_8^+ + H_2,\ C_3H_8 + H_2^+,\ C_3H_8^+ +$$
$$+ CH_4,\quad C_3H_8 + CH_4^+,\quad C_3H_8^+ + C_2H_6,$$
$$C_3H_8 + C_2H_6^+,\ C_3H_8 + C_3H_8^+.$$

The process $C_3H_8 + H_2^+$ gave the least possible value for the upper limit of $P_{C_3H_8}$. Thus, $P_{C_3H_8}$ < 61 kcal/mole.

Strictly speaking, detection of all the ion-molecule processes mentioned in this article is possible, in the apparatus used by the authors, not only in the cases when these processes were thermoneutral or exothermal but also when the processes were endothermal by 1-2 kcal/mole. This results in a decrease in the values found by 1-2 kcal/mole.

The great difference found between the affinity of methane and its homologs for protons was extremely unexpected and requires a theoretical explanation.

LITERATURE CITED

[1] H. D. Smyth, Rev. Mod. Phys. 3, 347 (1931).

[2] V. L. Tal'roze and A. K. Liubimova, Proc. Acad. Sci. USSR 86, 909 (1952).

[3] V. L. Tal'roze, Thesis, Inst. Chem. Phys. Acad. Sci. USSR (1952).*

[4] J. O. Hirschfelder, J. Chem. Phys. 6, 795 (1938).

[5] R. S. Barker and H. Eyring, J. Chem. Phys. 22, 2072 (1954).

[6] J. H. Simons et al., J. Chem. Phys. 11, 312 (1943).

[7] V. L. Tal'roze and E. L. Frankevich, Proc. Acad. Sci. USSR 111, 376 (1956).**

[8] V. L. Tal'roze, G. D. Tantsyrev, and Ia. A. Iukhvidin, Factory Labs. 10, 1147 (1955).

[9] T. Cottrell, The Stability of Chemical Bonds (Foreign Lit. Press, 1956) [Russian Translation].

* In Russian.

** Original Russian pagination. See C. B. Translation.

[10] R. E. Honig, J. Chem. Phys. 16, 105 (1948).

[11] E. L. Frankevich and V. L. Tal'roze, Pribory i Tekhn. Eksperim. 2, 48 (1957).

[12] E. Steacie, Atomic and Free Radical Reactions (New York, 1954).

[13] D. P. Stevenson and D. O. Schissler, J. Chem. Phys. 23, 1353 (1955).

Institute of Chemical Physics of the
Academy of Sciences, USSR

Received October 21, 1957.

THERMOPHORESIS IN MOVING AEROSOLS

N. A. Fuks and S. S. Iankovskii

(Presented by Academician A. N. Frumkin, January 2, 1958)

The problem concerning the magnitude of the forces acting upon the aerosol particles in a nonuniformly heated medium was solved for two limit cases: for very large and for very small values of d/λ, where d represents the size of the particles and λ the mean free path of the gas molecules. When $d \ll \lambda$ the presence of particles does not disturb the distribution of the molecular velocities, the temperature gradient within the particle is small and can be neglected. The force acting upon a particle results from the difference in the mean velocities of the gas molecules bombarding the particle from all sides. In the case of a spherical particle of diameter d the resulting force, independent of the nature of the particle (if one neglects the small effect due to the differences in the accommodation coefficients of the molecules and one considers it as equal to unity), is equal to:

$$F = -\frac{\pi d^2 p \lambda G}{8T}, \tag{1}$$

where p is the pressure of the gas, T is the absolute temperature, and G is the temperature gradient in the gas [1, 2].

When $d \gg \lambda$, the temperature gradient plays the most important role on the surface of the particle, inducing (according to Maxwell) a sliding of the gas along the surface. According to Epstein [3] the force resulting from friction between the particle and the gas is equal to:

$$F = -\frac{9\pi\beta\eta^2 dG}{2\gamma T}, \tag{2}$$

where η is the viscosity of the gas and γ is the density of the gas, $\beta = \chi_a / (2\chi_a + \chi_i)$, χ_a and χ_i are the thermal conductivity of the gas and of the particle.

When $d \gg \lambda$, F is equal to the resistance of the medium and the velocity of thermophoresis, i.e., the motion of particles in the field of the temperature gradient, will be expressed by the following relationship:

$$V = -\frac{3\beta\nu G}{2T}, \tag{3}$$

where ν is the kinematic viscosity of the gas. When $d \ll \lambda$ the resistance of the medium is equal to $-\pi/_3 \varkappa\gamma\bar{c}d^2V$, where $\bar{c}$ is the average absolute velocity of the gas molecules, κ a coefficient whose value varies from 1.0 to 1.44 [4]. Consequently:

$$V = -\frac{3p\lambda G}{8\varkappa\gamma\bar{c}T}. \tag{4}$$

Assuming $p = \pi/_8 \cdot \gamma(\bar{c})^2$, $\eta = \vartheta\gamma\bar{c}\lambda$ (ϑ is a numerical coefficient varying from 0.3 to 0.5), we obtain:

$$V = -\frac{3\pi\nu G}{64\vartheta\varkappa T}. \tag{5}$$

Thus, in the two limit cases the velocity of thermophoresis is independent of the particle size. Since in the majority of cases $\beta \ll 1$, the velocity of thermophoresis, except in the case of particles of very poor heat conductors, must be considerably higher for $d \ll \lambda$ than for $d \gg \lambda$. For $d \approx \lambda$ the theory of the phenomenon is very complex; no work has been done in this direction.

For our experimental study of thermophoresis we used the Milliken condenser in which the upper wrapping was at a higher temperature than the lower [5, 6], i.e., the experiments were performed in still medium. We measured the velocity of thermophoresis with drops of nonvolatile organic liquids 0.8-4.0 μ in diameter. The results obtained were in good agreement with those provided by Formula (3); when the diameter of the drops was smaller than 1μ ($d < 1\,\mu$) it became necessary to introduce the Cunningham correction factor into the formula.

Thermophoretic precipitation of aerosols from circulating gases has a great importance in technology; dust deposited on the walls of refrigerating units, boiler pipes, etc., from the circulating hot dusty gases usually has low thermal conductivity and is difficult to eliminate. The functioning of one of the most important apparatuses for the investigation of aerosols — the thermoprecipitator — is based on the thermophoresis in gas currents; in this apparatus the aerosol is passed through a narrow slit located between massive metal blocks in the middle of which is stretched a heated metal thread or ribbon perpendicular to the direction of the current. The aerosol precipitates on transparent underplates, in the form of narrow strips, located on the surface of the blocks.

In studying the functioning of this apparatus with a number of polydispersion aerosols we observed that the smallest particles are deposited mainly at the front edge of the strips (directed against the current), while the largest particles are deposited mainly at the back edge of the strips. The dispersional composition of the deposit varies continuously between the front and the back edge so that the ratio of the number of particles belonging to neighboring fractions changes in favor of the larger fractions (see Fig. 1). This phenomenon was observed for all particles whose diameter was between 0.05 and 6 μ, with the following substances: aerosols obtained by pulverizing NaCl or India ink solutions with subsequent drying of the drops, or by blowing air over a quartz powder, and PbO fumes obtained by distilling galenite in an air current. The conditions for precipitation were the following: the cross section of the slit = 0.6 × 9 mm, the thickness of the nickel wire = 0.2 mm, the heating current = 1.2 - 1.5 amp, the sucking rate = 5 - 10 ml/sec, which corresponds to an average linear speed of 2-4 cm/sec. The aerosol was sucked directly into the slit and moved vertically upward. The precipitation was done either on cover glasses (for optical microscopy) or on screens with colloidal films (for electron microscopy). It must be noted that the sucking velocity used in the apparatus allowed 20-30 μ particles to be sucked in, however, the maximum size of the particles in the deposit did not exceed 6-7 μ. It is well known that the efficiency of precipitation in the thermoprecipitator drops rapidly with the increase of the particle size, starting with $d \approx 5\,\mu$.

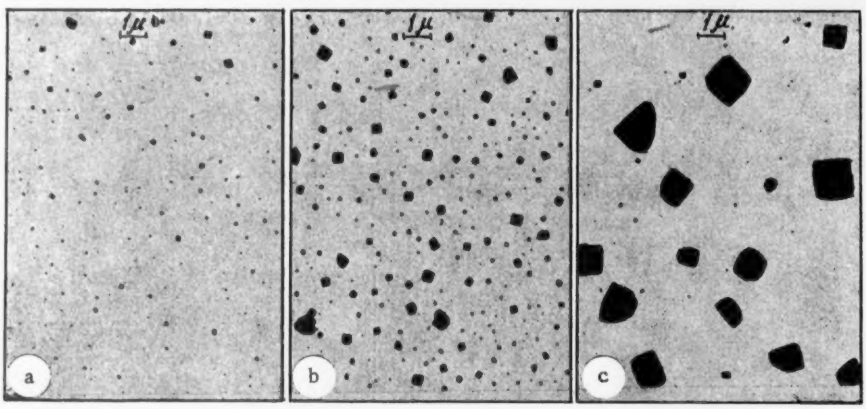

Fig. 1. Electron-microscope photographs of the NaCl aerosol precipitate in the thermoprecipitator. a) At the front edge, b) in the middle of the precipitate, c) at the back edge.

The phenomenon described, showing that in a moving medium the thermophoresis rate drops with increase in particle size even in the area where Formula (3) is applicable, could not remain unnoticed by the many re-

searchers working with this apparatus; but strange as it may seem one finds in the literature only side remarks that the distribution of particle sizes in the precipitate of the thermoprecipitator is not completely uniform. The same contradiction with the Epstein theory was found in the recently published work by Schadt and Cadle [7]; these authors studied the precipitation of aerosols of very different heat conductivity in the thermoprecipitator and found that the effect of thermal conductivity on the precipitation is considerably smaller than that predicted by Formula (3). Since in the case of a still medium this formula is confirmed by experiment, the cause of the contradiction must lie in some effects relative to the motion of the aerosol. Let us investigate a few of these effects.

Inertia of the particles opposes their precipitation. However, the magnitude of the "inertial path" of the particles [8], characterizing the deviation from the trajectories of the particles due to inertia, was equal in our experiments to 1-2 μ for 4μ NaCl particles. Such deviation is insignificant when the region of the temperature gradient is equal to a few hundreds of microns. The rotation of particles induced by the velocity gradient of the current opposes the creation of a temperature gradient within the particle. In our experiments the maximum values of Γ were of the order of 1000 sec^{-1}, which corresponds [9] to a rotation period of approximately 0.01 sec; while the time of the temperature relaxation of NaCl particles of $d = 4\mu$ is equal to $3 \cdot 10^{-7}$ sec [10]. The value of the Brownian motion of the particles is even smaller. When the particles move parallel to the walls, at a small distance from the wall, a repulsion force from the wall equal to $F = {}^{9}/_{64} \cdot \pi\gamma\, d^2V^2$ [11] is created if the Re numbers are low. In the case of NaCl particles described above, this force, induced by sedimentation of particles, is equal to $8 \cdot 10^{-13}$ dynes. Under ordinary conditions of functioning of the thermoprecipitator, G has a value of the order of 5000 degree/cm while the thermophoretic force is, according to Formula (2), of the order of 10^{-8} dynes. Thus, none of the effects investigated explains the phenomenon described above. It also contradicts the experiments performed by Kogan and Repina [12], who investigated the upward motion of aerosols in a vertical capillary tube, i.e., in the absence of thermophoresis; they observed that the precipitation of aerosols on the walls of the capillary tube increases with the particle size (beginning with $d = 0.5\ \mu$).

LITERATURE CITED

[1] A. Einstein, Zs. Phys. 27, 1 (1924).

[2] W. Cawood, Trans. Farad. Soc. 32, 1068 (1936).

[3] P. Epstein, Zs. Phys. 54, 537 (1929).

[4] P. Epstein, Phys. Rev. 23, 710 (1924).

[5] P. Rosenblatt and V. La Mer, Phys. Rev. 70, 385 (1946).

[6] R. Saxton and W. Ranz, J. Appl. Phys. 23, 917 (1952).

[7] C. Schadt and R. D. Cadle, Anal. Chem. 29, 864 (1957).

[8] N. A. Fuks, Mechanics of Aerosols (Acad. Sci. USSR Press, 1955), pp. 80 and 165.*

[9] N. A. Fuks, Mechanics of Aerosols (Acad. Sci. USSR Press, 1955), p. 47.*

[10] N. A. Fuks, Mechanics of Aerosols (Acad. Sci. USSR Press, 1955), p. 74.*

[11] N. A. Fuks, Mechanics of Aerosols (Acad. Sci. USSR Press, 1955), p. 100.*

[12] Ia. I. Kogan and R. S. Repina, Proc. Acad. Sci. USSR 111, 851 (1956). **

State Science Research Institute
for Nonferrous Metals

Received December 28, 1957.

* In Russian.

** Original Russian pagination. See C. B. Translation.

THE SYNTHESIS OF SUBSTANCES IN WATER, SATURATED WITH THE GASES OF A REDUCING ATMOSPHERE, UNDER THE EFFECT OF ULTRASONIC WAVES

I. E. El'piner and A. V. Sokol'skaia

(Presented by Academician A. I. Oparin, December 19, 1957)

In this article we present data showing that the propagation of high intensity ultrasonic waves in water, even in the absence of oxygen, produces chemical processes accompanied by the synthesis of a series of new substances.

In accordance with the widely accepted, so-called cavitation, electrochemical theory [1-3], as a result of the high electrical voltages arising electronic disruption occurs in the cavity [4] and this produces ionization of the water molecules, which are present here in the vapor state. The ionized water particles almost immediately decompose into free radicals with unsaturated valences and atomic hydrogen ($H_2O \rightarrow H + OH$) as occurs in the interaction of ionizing radiations with water.

If in the cavity there are actually moving charges, capable of ionizing water molecules, then we are justified in expecting that molecules of gas diffusing there are also able to undergo this process. Starting from these premises, in 1950 one of us [5] conducted special experiments which showed that the dissociation of iodine occurred in water saturated with gaseous hydrogen and molecular iodine, under the effect of ultrasonic waves. This process was apparently brought about in the cavity, into which molecules of iodine diffused, together with gaseous hydrogen. The ionization (or dissociation) of iodine was closely connected with the parallel ionization (or dissociation) of hydrogen. Later Henglein [6] also observed that iodine was reduced in water saturated with hydrogen and molecular iodine under the action of ultrasonic waves.

Recently, we showed that other gases also were activated (dissociated) in water by ultrasonic waves. For example, we found that in the presence of ultrasonically treated water, hydrogen and nitrogen formed ammonia.

The treatment of water with ultrasonics in the presence of nitrogen and hydrogen was carried out in glass vessels with an ultrasonic wave intensity of 6-7 watts per cm^2 of the irradiated surface (oscillation frequency of 380 380 and 750 kHz). The volume of distilled water treated was 10 ml. The water studied was first saturated simultaneously with gaseous nitrogen and hydrogen, carefully freed from traces of oxygen.

For thorough purification of the nitrogen to remove oxygen, we used the method developed by L. M. Kantorovich and F. M. Rapoport [7], in which dried, heated gas is passed through a column with a preparation consisting of copper precipitated on silica gel. The hydrogen, which was prepared in a Kipp's apparatus, was purified by passing it through an alkaline solution of pyrogallol. As a result of this treatment the water saturated with the gases did not contain sufficient oxygen to be detected polarographically.

The ammonia content of the water before and after ultrasonic treatment was determined quantitatively with Nessler's reagent (see Table 1).

As Table 1 shows, the amount of ammonia formed increased with an increase in the time of ultrasonic treatment. With the water saturated with only nitrogen it was only after prolonged ultrasonic treatment (120 min) that ammonia appeared in extremely small amounts. Extremely small amounts of ammonia were also formed during prolonged ultrasonic treatment of water in the presence of oxygen and nitrogen, which also agrees with some literature data [8]. Oxides of nitrogen were formed predominantly during ultrasonic treatment of water, saturated with nitrogen, in the presence of oxygen.

It is important to note that the presence of carbon monoxide in the gas mixture of nitrogen and hydrogen did did not inhibit the formation of ammonia in ultrasonically treated water. We added carbon monoxide by decomposing oxalic or formic acid with gentle heating in the presence of sulfuric acid.

TABLE 1

Synthesis of Ammonia in an Ultrasonic Wave Field

Length of ultrasonic treatment (min)	Amt. of ammonia formed in γ per ml of water				
	with H_2	with N_2	with H_2+N_2	with H_2+ $+N_2+CO$	with air
50	—	—	0,85	—	—
60	0	0	1,26	—	0,04
120	—	0,62	2,6	—	—
180	—	—	8,7	—	0,62
180	—	—	—	7,8	—
180	—	—	—	7,1	—
180	—	—	—	8,5 *	—
180	—	—	9,0 **	6,5 **	—
360	—	—	12,5	—	—

* The ultrasonic treatment was performed in 0.1 N HCl.

** The ultrasonic treatment was performed in 1% succinic acid.

TABLE 2

Synthesis of Formaldehyde in an Ultrasonic Wave Field

Length of ultrasonic treatment (min)	Amt. of formaldehyde formed in γ (10^{-6} g) per ml of water				
	with H_2	with H_2+CO	with H_2+ $+CO+N_2$	with air	with CO
0	—	—	0	0	0
60	—	5,6	1,8	—	4,0
120	0,2	16,0	6,0	0,4	6,4
180	—	24	15,0	0,1	7,4
180	—	26,4	—	—	—

It was then discovered that on adding carbon monoxide to the $N_2 + H_2$ gas mixture in the ultrasonically treated water, hydrocyanic acid (as well as ammonia) was formed and this was determined by Gin'iar* method [9], which is based on the conversion of picric into purpuric acid in the presence of the vapor of hydrocyanic acid.

Many investigations showed that ultrasonic treatment of water (3 hours treatment) in the presence of N_2, CO, and H_2 produced from 1 to 10 γ of HCN. Hydrocyanic acid was not observed in water treated with ultrasonics in the presence of oxygen or nitrogen alone or a gas mixture of N_2 and H_2.

Hydrocyanic acid was also synthesized in an ultrasonic wave field when the carbon monoxide was substituted by methane in the gas mixture used, i.e., in the presence of N_2, H_2, and CH_4.

Later we were able to establish that formaldehyde was formed in water treated with ultrasonics if the water contained hydrogen and carbon monoxide. The method we used for determining the formaldehyde was based on the reaction of the latter with phenylhydrazine in an alkaline solution of $K_3Fe(CN)_6$ [10]. The amount of formaldehyde formed was determined quantitatively with an SF-4 spectrophotometer at $\lambda = 520$ mμ.

As Table 2 shows, 26 γ of formaldehyde is formed per ml of water in water treated with ultrasonics for 180 minutes in the presence of H_2 and CO; almost no formaldehyde was found in water treated with ultrasonics in the presence of air. Formaldehyde was also formed under the effect of ultrasonic waves in the presence of H_2, CO, and N_2. Under these conditions NH_3 and HCN were synthesized simultaneously with the formaldehyde, and the amounts of these increased as the time of ultrasonic treatment increased. The appearance of these products may lead to further synthesis of substances of biological importance as occurs under the effect of electrical discharges and ultraviolet irradiation [11, 12].

The data we obtained indicate that acoustic and ultraacoustic oscillations, together with other physical agents (ultraviolet rays, electrical discharges and radioactive decay) may provide a source of energy for the synthesis of the basic products used as materials for the construction of living organisms in the primordial period of existence of our planet. This proposition agrees completely with the theory of A. I. Oparin [13] on the origination of life on earth. A quantitative evaluation of the acoustic energy, which was produced and is being produced at the present time under natural conditions (electrical discharges, waterfalls, seaquakes, etc.) is of very great importance.

LITERATURE CITED

[1] R. O. Prudhomme and P. Grabar, J. Chim. Phys. 46, 323 (1949).

[2] N. Miller, Trans. Farad. Soc. 46, 546 (1950).

* Transliteration of Russian — Publisher's note.

[3] I. E. El'piner, J. Tech. Phys. 21, 1205 (1951).

[4] Ia. I. Frenkel', Acta Physiochim. USSR 12, 317 (1940).

[5] I. E. El'piner, Acoust. J. 2, 217 (1956).

[6] A. Henglein, Naturwiss 43, 277 (1956).

[7] L. M. Kantorovich and F. M. Rapoport, Trans. State Sci. Research and Planning Inst. of the Nitrogen Industry 1 (1952).

[8] I. G. Polotskii, J. Gen. Chem. 9, 885 (1940).

[9] N. N. Ivanov, Methods of Plant Physiology and Biochemistry (1946).*

[10] M. Tannenbaum and C. E. Bricker, Anal. Chem. 23, 354 (1951).

[11] S. Miller, J. Am. Chem. Soc. 77, 2351 (1955).

[12] T. E. Pavlovskaia and A. G. Pasynskii, Coll. Repts. to the Initl. Conf. on the Origin of Life on Earth,* (Acad. Sci. USSR Press, 1957), p. 102.

[13] A. I. Oparin, Origin of Life on Earth *(Acad. Sci. USSR Press, 1957).

Received November 21, 1958

* In Russian.

INITIATING EFFECT OF RADON RADIATION IN THE OXIDATION OF ISODECANE (2,7-DIMETHYLOCTANE)

N. M. Emanuel', E. A. Bliumberg, D. M. Ziv, and V. L. Pikaeva

(Presented by Academician V. N. Kondrat'ev December 28, 1957)

One of us proposed the use of the radiation of radioactive inert gases for initiating reaction chains as a logical consequence of the principle of gaseous initiation by chemically active gases [1] and the stimulating action of penetrating radiations [2].

Nowadays, the experimental chemist has at his disposal Xe^{133}, Kr^{85}, and Ar^{41} as well as the radioactive emanations – radon, thoron, and actinon. The three former radioactive gases may be prepared from the corresponding inactive inert gases by an (n,γ)- reaction. In addition, Xe^{133} and Kr^{85} are products of U^{235} and Pu^{239} fission and are isolated during the purification of blocks of nuclear fuel, poisoned with fission products.

The application of radioactive inert gases makes it possible to use for initiation all types of radiation; α, β and γ at various radiation energy values. In addition, α and β particles emitted by the particular radioactive atoms pass directly into the reacting system and exert their effect uniformly throughout the whole of the liquid mass. This is very important as the introduction of these particles into a reaction vessel from an external source involves enormous difficulties or is completely impossible due to strong absorption of them by the wall of the vessel or the material of the window.

The application of radiation from radioactive gases for initiation must be extremely effective and not only in the case of the slow chains in liquid phase reactions. It is also certain that the application of radioactive gases will make interesting experiments with gas phase chain reactions possible.

In the present work we set out to investigate the oxidation of isodecane (2,7-dimethyloctane) under the effect of the α-particles of radon. We proceeded from the fact that oxidation processes in hydrocarbons in the liquid phase are degenerate branched chain reactions. This implies that the stimulation of these processes may be realized in only the initial period of branching of the process.

The action of radon radiation leads to the production of active particles – free radicals and atoms in the system, i.e., to an increase in the initial rate of chain production w_0. The value of w_0 under the effect of radioactive gases may be calculated readily from the energy of the ionizing radiation and the energy required to break a bond in the original hydrocarbon. This is one of the advantages of using radioactive inert gases as initiators in comparison with chemically active gases.

The experiments were performed in a glass apparatus (Fig. 1), which included the oxidation cell used in our work on liquid phase oxidation [3].

A mixture of radon and oxygen was prepared in the flask 1, fitted with outlets and with a double ground glass joint; the upper joint was intended for turning the rod R, to break an ampule of radon placed in the tube, and the lower one to fix the tube in the flask.

To avoid losses of radon into the surrounding atmosphere, the system was used under slight vacuum (~ 700 mm Hg). The oxygen, containing radon, was drawn with a water pump from the flask 1 through the oxidation cell, placed in an air thermostat at a temperature of 120°, and then through three successive U-traps, filled with active charcoal and cooled to – 80°. The unreacted oxygen was freed from radon by adsorption of the latter on the charcoal and then ejected into the atmosphere.

At the end of the initiating action of the radon (1 hour after the beginning of the experiment) the flask was shut off and the oxidation carried out with pure oxygen from a tank. Under the conditions of our experiments,

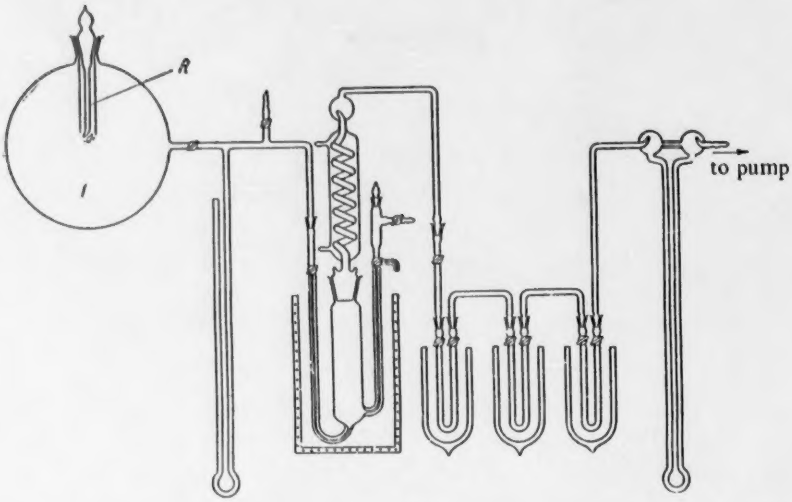

Fig. 1. Scheme of experimental apparatus.

the reaction was affected by the radon bubbling through the liquid, dissolved radon and radon in the gas phase over the surface of the liquid. In addition, the daughter products of Rn decay played an important role. In calculating the integral dose we allowed for all these sources of radioactive action on the isodecane. With a starting radon activity of 12 mC in the ampule, the total dose received by the system during the one hour initiation, was 615 rads. It is interesting to note that under the conditions of our experiments the main effect was produced by radon dissolved in the isodecane (165 rads) and the daughter radioactive decay products (437 rads). The effect of the radioactive decay products, which amounted to a considerable part of the radiation dose, continued for some time after the initiation period, i.e. after the radon had been completely flushed from the liquid by the stream of pure oxygen. However, this period of the after-effect of the active residue did not exceed 1-1.5 hours, and during this time the activity of the residue fell rapidly (after 20 minutes there remained only a total of 30% of the activity at the end of the initiation period). Thus, under the conditions of our experiments (with a starting radon activity of 12 mC) the initiating effect of the radon lasted at the most for 2.5 hours.

We should note that in using chemically active gaseous initiators in the liquid phase oxidation of hydrocarbons (NO_2, Cl_2, O_3, etc.) we confined ourselves to much shorter initiation times. However, relative to the oxidation reaction of isodecane at 120°, a radiation treatment time of 2.5 hours is not too great as the uninitiated formation of acids under these conditions has an induction period of the order of 20 hours.

The kinetic curves for the accumulation of peroxides and acids during isodecane oxidation, initiated by the α-radiation of radon (and also α- and β-radiation of the Rn decay products) are shown in Figs. 2 and 3. On the same diagrams dotted curves show the change in the total activity with time, when the starting activity of radon in the ampule was 12 mC.

Figure 2 shows that the short stimulating effect of the radon radiation is sufficient for a significant decrease in the induction period with the formation of peroxides. There is also an increase in the maximal yield of peroxide compounds.

A comparison of the kinetic curves of acid accumulation (2 and 3) with curve 1 for the uninitiated oxidation (Fig. 3) also shows extremely clearly the effect of the short stimulating action. While the process of acid formation under normal conditions during autooxidation begins only 20 hours after the addition of oxygen, with 12 mC of Rn added to the oxygen and this passed through the isodecane at 120° for 1 hour (curve 3), a significant amount of acids appears in the reaction mixture after only 5-6 hours, i.e., the induction period of the oxidation is reduced by a factor of more than three. This result agrees with the change in the initial rate of chain production

under the effect of the ionizing radiation. The value of w_0 for the uninitiated reaction, calculated in the hypothesis of the thermal reaction of a hydrocarbon with an O_2 molecule, equals 10^2-10^3 radicals/cm^3·sec. In the case of initiation using 12 mC of Rn, w_0 equals 10^{12} radicals/cm^3·sec.

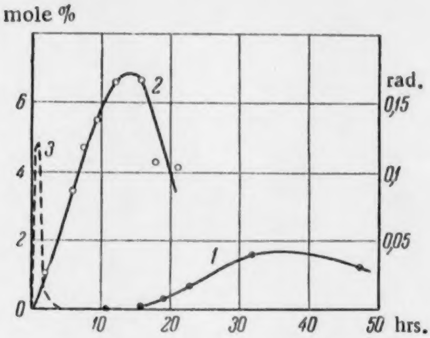

Fig. 2. Kinetic curves of hydroperoxide accumulation during the oxidation of isodecane at 120°. 1) Uninitiated reaction; 2) action of Rn (starting activity of 12 mC) for 1 hour; 3) change in the total activity during the reaction (right hand scale).

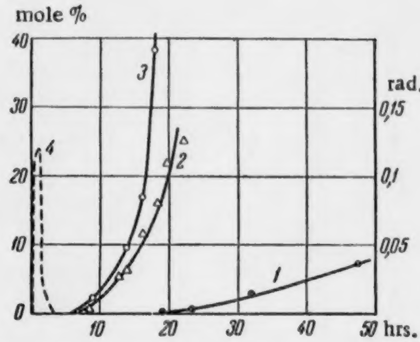

Fig. 3. Kinetic curves of acid accumulation during the oxidation of isodecane at 120°. 1) Uninitiated oxidation; 2) oxidation with Rn treatment (starting activity 7 mC) for 1 hour; 3) the same with a starting activity of 12 mC; 4) change in total activity during the reaction.

This strong increase in the rate of active center production must lead to a significant reduction in the induction period as was observed in the experiment.

The action of Rn α-radiation has an even bigger effect on the reaction rate after the induction period. After the induction period, the uninitiated oxidation of isodecane proceeds at a relatively low rate, which remains practically constant up to a high degree of conversion (32 mole %). The kinetic curve of acid formation with treatment by 12 mC of Rn is a curve with a sharply expressed autocatalytic character. In this case, the rate of oxidation after the induction period increases sharply and its maximum value is more than 10 times greater than the rate of uninitiated oxidation. Experiments with other activities (different from 12 mC) were only approximate. It was shown that increasing the dose (above 615 rads) did not produce additional effects causing an increase in the reaction rate.

From the data on the initiating action of 7 mC of radon (Fig. 3) it is obvious that doses of less than 615 rads are also able to produce clear accelerations of the oxidation process. When 7 mC of radon was used, the total dose was approximately 400 rads but the acceleration effect obtained was practically the same as when 12 mC of radioactive emanation was used.

The authors would like to thank V. M. Vdovenko for his interest in the work and also V. M. Permiakov and his co-workers for preparing the radon samples used in this work.

LITERATURE CITED

[1] N. M. Emanuel', J. Phys. Chem. 30, 847 (1956).

[2] N. M. Emanuel', Proc. Acad. Sci. USSR 111, 1286 (1956).*

[3] D. G. Knorre, Z. K. Maizus, and N. M. Emanuel', J. Phys. Chem. 29, 710 (1955).

Institute of Chemical Physics of the
Academy of Sciences of the USSR

Received December 25, 1957

Radium Institute of the
Academy of Sciences of the USSR

* Original Russian pagination. See C. B. Translation.

SIGNIFICANCE OF ABBREVIATIONS MOST FREQUENTLY ENCOUNTERED IN SOVIET PERIODICALS

FIAN	Phys. Inst. Acad. Sci. USSR.
GDI	Water Power Inst.
GITI	State Sci.-Tech. Press
GITTL	State Tech. and Theor. Lit. Press
GONTI	State United Sci.-Tech. Press
Gosenergoizdat	State Power Press
Goskhimizdat	State Chem. Press
GOST	All-Union State Standard
GTTI	State Tech. and Theor. Lit. Press
IL	Foreign Lit. Press
ISN (Izd. Sov. Nauk)	Soviet Science Press
Izd. AN SSSR	Acad. Sci. USSR Press
Izd. MGU	Moscow State Univ. Press
LEIIZhT	Leningrad Power Inst. of Railroad Engineering
LET	Leningrad Elec. Engr. School
LETI	Leningrad Electrotechnical Inst.
LETIIZhT	Leningrad Electrical Engineering Research Inst. of Railroad Engr.
Mashgiz	State Sci.-Tech. Press for Machine Construction Lit.
MEP	Ministry of Electrical Industry
MES	Ministry of Electrical Power Plants
MESEP	Ministry of Electrical Power Plants and the Electrical Industry
MGU	Moscow State Univ.
MKhTI	Moscow Inst. Chem. Tech.
MOPI	Moscow Regional Pedagogical Inst.
MSP	Ministry of Industrial Construction
NII ZVUKSZAPIOI	Scientific Research Inst. of Sound Recording
NIKFI	Sci. Inst. of Modern Motion Picture Photography
ONTI	United Sci.-Tech. Press
OTI	Division of Technical Information
OTN	Div. Tech. Sci.
Stroiizdat	Construction Press
TOE	Association of Power Engineers
TsKTI	Central Research Inst. for Boilers and Turbines
TsNIEL	Central Scientific Research Elec. Engr. Lab.
TsNIEL-MES	Central Scientific Research Elec. Engr. Lab.—Ministry of Electric Power Plants
TsVTI	Central Office of Economic Information
UF	Ural Branch
VIESKh	All-Union Inst. of Rural Elec. Power Stations
VNIIM	All-Union Scientific Research Inst. of Meteorology
VNIIZhDT	All-Union Scientific Research Inst. of Railroad Engineering
VTI	All-Union Thermotech. Inst.
VZEI	All-Union Power Correspondence Inst.

Note: Abbreviations not on this list and not explained in the translation have been transliterated, no further information about their significance being available to us. — Publisher.